

## Steady State and transient behavior of underground cables in 380 kV transmission grids

Hoogendorp, Gerben

**DOI**

[10.4233/uuid:2ecf0e07-58c8-42b9-bbf1-67878a3f6018](https://doi.org/10.4233/uuid:2ecf0e07-58c8-42b9-bbf1-67878a3f6018)

**Publication date**

2016

**Document Version**

Final published version

**Citation (APA)**

Hoogendorp, G. (2016). *Steady State and transient behavior of underground cables in 380 kV transmission grids*. [Dissertation (TU Delft), Delft University of Technology]. <https://doi.org/10.4233/uuid:2ecf0e07-58c8-42b9-bbf1-67878a3f6018>

**Important note**

To cite this publication, please use the final published version (if applicable).  
Please check the document version above.

**Copyright**

Other than for strictly personal use, it is not permitted to download, forward or distribute the text or part of it, without the consent of the author(s) and/or copyright holder(s), unless the work is under an open content license such as Creative Commons.

**Takedown policy**

Please contact us and provide details if you believe this document breaches copyrights.  
We will remove access to the work immediately and investigate your claim.

# **Steady State and transient behavior of underground cables in 380 kV transmission grids**

PROEFSCHRIFT

ter verkrijging van de graad van doctor  
aan de Technische Universiteit Delft  
op gezag van de Rector Magnificus, prof. ir. K.C.A.M. Luyben,  
voorzitter van het College voor Promoties,  
in het openbaar te verdedigen op 3 oktober 2016 om 12:30

door

Gerben HOOGENDORP

Elektrotechnisch ingenieur  
geboren te Den Haag, Nederland

Dit proefschrift is goedgekeurd door de

promotor: Prof.ir. L. van der Sluis

copromotor: Dr.ir. M. Popov

Samenstelling promotiecommissie bestaat uit:

Rector magnificus

Prof.ir. L. van der Sluis

Dr.ir. M. Popov

voorzitter

promotor

copromotor

Onafhankelijke leden:

Prof.ir. M.A.M.M. van der Meijden

Prof.dr. P. Palensky

Prof.dr. J.J. Smit

Prof.dr.ing.habil. L. Hoffman

Dr. G.R. Kuik

EWI, TU Delft

EWI, TU Delft

EWI, TU Delft

Leibniz University of Hannover

TenneT TSO B.V.

Reservelid:

Prof. dr. R. Ross

EWI, TU Delft

This research was financially supported by TenneT TSO B.V. within the scope of the monitoring program of the Randstad380 cable project.

ISBN: 978-90-73077-81-2

Copyright © 2016 Gerben Hoogendorp, Delft, the Netherlands

# CONTENTS

<b>SUMMARY</b>	<b>1</b>
<b>SAMENVATTING</b>	<b>4</b>
<b>1 INTRODUCTION</b>	<b>7</b>
1.1 BACKGROUND	7
1.2 STATE OF ART	8
1.3 THE RANDSTAD 380 KV PROJECT	13
1.4 SHORT OVERVIEW OF RELATED CABLE PROJECTS	14
1.5 GOAL OF THE WORK	15
1.5 THESIS OUTLINE	15
<b>2 SYSTEM BEHAVIOR OF UNDERGROUND CABLES</b>	<b>18</b>
2.1 INTRODUCTION	18
2.2 TRANSMISSION LINE THEORY	19
2.3 STEADY STATE OPERATION OF POWER SYSTEMS	31
2.4 CABLE LENGTH AND TRANSMISSION CAPACITY	32
2.5 SHUNT REACTOR SIZING AND VOLTAGE PROFILE	35
2.6 CONCLUSION	37
<b>3 CABLE MODELING ISSUES AND SYSTEM PERFORMANCE</b>	<b>39</b>
3.1 INTRODUCTION	39
3.2 MUTUAL COUPLING IN AN UNDERGROUND CABLE SYSTEM	39
3.3 GROUNDING AND CROSS BONDING OF THE CABLE SCREEN CONDUCTOR	44

3.4	CABLE CONFIGURATIONS	47
3.5	CABLE GROUND RETURN IMPEDANCE	48
3.6	TEMPORARY OVERVOLTAGES (TOV)	50
3.7	ZERO MISSING PHENOMENA	52
3.8	CONCLUSION	53
<b>4</b>	<b>STEADY STATE ANALYSIS OF MIXED 380 KV OVERHEAD-LINE UNDERGROUND CABLE</b>	<b>54</b>
4.1	INTRODUCTION	54
4.2	EARLY LOAD FLOW AND CONTINGENCY STUDY ON THE 380 KV GRID	55
4.3	RESULTS OF THE CONTINGENCY STUDY	63
4.4	INFLUENCE OF SHUNT COMPENSATION ON THE VOLTAGE PROFILE	66
4.5	CONCLUSION	70
<b>5</b>	<b>TRANSIENT MODEL FOR 380 KV MIXED LINE-CABLE-LINE SYSTEMS</b>	<b>71</b>
5.1	INTRODUCTION	71
5.2	TRANSIENT CABLE MODELS	71
5.3	SIMULATION MODEL FOR THE RANDSTAD 380 KV CABLE CIRCUITS	72
5.4	MODEL FOR THE CABLE CROSS-BONDING CONFIGURATION	81
5.5	CONCLUSION	90
<b>6</b>	<b>SWITCHING OF MIXED 380 KV LINE-CABLE-LINE SECTIONS</b>	<b>92</b>
6.1	INTRODUCTION	92
6.2	TRANSFORMER AND CIRCUIT BREAKER MODELING	93
6.3	CABLE SWITCHING-IN STUDY (ENERGIZATION)	95
6.4	SWITCHING OF CHARGED CABLES	104
6.5	CABLE DISCHARGE CURRENTS	107
6.6	CONCLUSION	111

<b>7</b>	<b>LIGHTNING INDUCED OVERVOLTAGES IN MIXED LINE-CABLE-LINE CIRCUITS</b>	<b>112</b>
7.1	INTRODUCTION	112
7.2	THE MECHANISM OF LIGHTNING DISCHARGES CURRENTS	113
7.3	LIGHTNING OVERVOLTAGE ANALYSIS FOR 380 KV MIXED LINE-CABLE-LINE CIRCUITS	114
7.4	LIGHTNING OVERVOLTAGES VERSUS CABLE LENGTH	124
7.5	BEWLEY LATTICE DIAGRAMS	128
7.6	CONCLUSION	132
<b>8</b>	<b>FIELD MEASUREMENTS FOR CABLE AND OVERHEAD LINE MODEL VALIDATION</b>	<b>134</b>
8.1	INTRODUCTION	134
8.2	PULSE INJECTION MEASUREMENTS ON THE 380 KV CABLE	135
8.3	STEP VOLTAGE MEASUREMENTS ON THE 380 KV CABLE	144
8.4	PULSE INJECTION MEASUREMENTS ON THE OVERHEAD-LINE SECTIONS	148
8.5	CONCLUSION	153
<b>9</b>	<b>CONCLUSIONS, RECOMMENDATIONS AND FUTURE WORK</b>	<b>154</b>
9.1	CONCLUSIONS	154
9.2	RECOMMENDATIONS	156
9.3	FUTURE WORK	157
<b>APPENDIX A</b>	<b>CABLE MATRIX IMPEDANCE ELEMENTS APPROXIMATED BY BESSEL FUNCTIONS</b>	<b>158</b>
<b>APPENDIX B</b>	<b>THE FREQUENCY DEPENDENT PHASE MODEL</b>	<b>161</b>
<b>APPENDIX C</b>	<b>LIGHTNING OVERVOLTAGES AT HIGH VOLTAGE TOWER TOP</b>	<b>164</b>
<b>BIBLIOGRAPHY</b>		<b>167</b>
<b>ACKNOWLEDGMENT</b>		<b>175</b>
<b>CURRICULUM VITAE</b>		<b>177</b>
<b>LIST OF PUBLICATIONS</b>		<b>178</b>

# SUMMARY

The extension of the Dutch 380 kV high voltage grid is necessary in order to guarantee security of electricity supply to the consumers. To achieve this extension, there are two new 380 kV connections under construction in the Randstad area, a densely populated area in the western part of the Netherlands. In these 380 kV connections, underground cables are applied.

The work described in this thesis forms a part of a monitoring program that is managed by the Dutch transmission grid operator TenneT. In this program, the behavior of the two new underground cable connections in the Dutch 380 kV grid is being investigated and the work described in this thesis contributes to this program.

Unlike the common overhead transmission line, which has an inductive behavior, a cable acts as a capacitance when it is in operation. This difference in electrical behavior makes research on the grid behavior necessary.

The research is divided into two parts: steady state behavior and transient behavior. The steady state behavior mainly deals with the observation of the power flows and the voltage levels in the grid when cables are applied. This is important since the cable capacitance produces reactive power, for which compensation might be necessary and shunt reactors should be installed so that it influences the power flows in the grid. Searching for overloads in 380 kV connections is of importance as well, and also the monitoring of the voltage levels since they need to be kept within their range as prescribed by the grid operator (342 kV - 418 kV).

The study on transient behavior mainly focuses on observing voltage and current transients that occur in the new 380 kV connections, during switching actions on the shunt compensated cable system and during the injection of lightning discharge currents into the overhead line section close to the cable after a lightning stroke. Transient phenomena can

produce steep wave fronts propagating as travelling waves throughout the power system and can stress vulnerable parts of power system components as the insulating material of transformer windings. In this work, the severity of transient overvoltages is investigated by observing the peak overvoltages that occur in the 380 kV mixed line-cable connections during switching actions and lightning currents.

In order to perform research on grid behavior, appropriate models for the 380 kV cables, the overhead lines, the 380/150 kV transformers including the shunt reactors connected to the tertiary winding, are necessary. In this thesis, the electromagnetic field theory is used as a starting point for the modeling work of underground cables, which describes the important issues that play a role in cable modeling. When the grid is in steady state condition, cable and overhead line sections can be modeled as lumped circuit elements. As the power frequency is 50 Hz, this means that the wavelength is large compared to the physical dimensions of the mixed overhead line – cable connection. Therefore, PI sections are used to perform load flow studies and to investigate the steady state behavior of the 380 kV grid. To investigate the influence of shunt compensated cables in the grid, both the power flows and the voltage levels are compared for the situation with cables and with overhead lines only. Cable clearly cause a change in both the active and the reactive power flows in the network and for the steady state voltage level close to the cable location. However, the 380 kV grid still satisfy the  $n-2$  criterion, as it can be learned.

Transients cause high frequency oscillations and this means that the circuit parameters have to be taken to be uniformly distributed along the transmission line. The widely applied Frequency Dependent Phase Model (FDPM), which is a transmission line model that takes into account the frequency dependency of cable and line parameters, is used to model the cable and overhead line section. Based on measurements performed on the cross-bonding cable, suitable models are developed for cross-bonding cables. Energization studies for the 380 kV connection between the substations Weteringen and Bleiswijk are done to analyze the impact of the cables on the oscillation period and on the transient peak voltage, in comparison with a connection with overhead lines. Lightning impact studies confirmed that the cable length in mixed line-cable-line configurations is an important parameter and has large influence on the peak voltage appearing at the line-cable junctions, when a lightning surge current is injected into the overhead line conductor close to the line-cable junction point after a lightning stroke.

Field measurements are performed for both the 380 kV cross-bonded cable and the overhead line sections and the results are used for transient cable model verification. For the overhead line, the measured waveforms matches the simulated results nicely, which confirms the validity of the line model. A step voltage was applied to the 380 kV cable core conductor and measured voltage response meet the simulated results, meaning that the cable model is validated, but a small deviation was observed with the simulated waveform. Parameter sensitivity analysis was carried out to find the origin of this deviation. The specific ground resistance has an important effect on the measured results, and should be subject for further research.

The scientific contribution of this work is the determination of the parameters for the 380 kV cross bonding system by using reflection measurements and the validation of the FDPM



transmission line model by using field measurements on the actual cross bonded 380 kV cable system.

# **SAMENVATTING**

Uitbreiding van het Nederlandse 380 kV hoogspanningsnet is noodzakelijk om de levering van elektriciteit aan de afnemers te kunnen blijven garanderen. Ter uitbreiding van dit net zijn in de Randstad, een dicht bevolkt gebied in het westen van Nederland, twee nieuwe 380 kV verbindingen in aanbouw, waarin gedeeltelijk ondergrondse kabels worden toegepast.

Het werk dat in dit proefschrift is beschreven maakt deel uit van een monitoringsprogramma dat wordt uitgevoerd door TenneT, de beheerder van het Nederlandse hoogspanningsnet. In dit programma wordt het gedrag van de twee nieuwe ondergrondse kabelverbindingen in het Nederlandse 380 kV net onderzocht, waaraan dit proefschrift een bijdrage levert.

In tegenstelling tot de gebruikelijke bovengrondse hoogspanningslijnen, die inductief zijn, gedraagt een kabel zich als een capaciteit. Dit verschil maakt het onderzoek naar het gedrag van het 380 kV net, wanneer gemengde lijn-kabel-lijn netten worden toegepast, noodzakelijk.

Het werk in dit proefschrift kan worden onderverdeeld in twee onderzoeksgebieden: het stationair gedrag en het transiënte gedrag. Het onderzoek naar het stationaire gedrag omvat vooral het observeren van de vermogensstromen en de spanningsniveaus in het net wanneer er kabels worden toegepast. Dit onderzoek is van belang vanwege het feit dat een kabel zich als een capaciteit gedraagt en dus reactief vermogen levert, waarvoor compensatie nodig kan zijn d.m.v. het plaatsen van shunt spoelen. Daarom is het belangrijk om eventuele overbelastingen in de 380 kV verbindingen op te sporen en om de spanningsniveaus, die binnen de door de netbeheerder voorgeschreven grenzen dienen te blijven (342 kV - 418 kV), in de gaten te kunnen houden.

Het onderzoek naar het transiënte gedrag richt zich vooral op het observeren van transiënte spanningen en stromen die optreden in de nieuwe 380 kV verbindingen, tijdens zowel

schakelhandelingen in de gecompenseerde kabelverbindingen als tijdens bliksemstromen in de bovengrondse lijnen vlakbij de kabel. Transiënte verschijnselen kunnen golfvormen met steile flanken produceren die zich vervolgens als een lopende golf door het elektriciteitsvoorzieningssysteem voortplanten, waardoor kwetsbare onderdelen van componenten in het net, zoals bijvoorbeeld de isolatie van transformator wikkelingen, extra zwaar worden belast. In dit proefschrift wordt de ernst van transiënte overspanningen onderzocht door de piekspanningen in kaart te brengen die optreden in de nieuwe gemixte 380 kV lijn-kabel-lijn netten als gevolg van schakelhandelingen en bliksemstromen.

Om onderzoek te kunnen doen naar het gedrag van het net, zijn modellen nodig voor de toegepaste 380 kV kabelstukken, de bovengrondse lijnstukken, de 380/150 kV transformatoren en de shunt compensatiespoelen die op de tertiaire transformatorwikkelingen zijn aangebracht. In dit proefschrift is de elektromagnetische veldtheorie gebruikt als startpunt voor zowel het modelleren van kabelverbindingen als het beschrijven van aspecten die bij het modeleren van kabels een rol spelen. Wanneer het net zich in stationaire toestand bevindt, kunnen kabels en lijnen worden gemodelleerd met spoelen, weerstanden en condensatoren omdat de frequentie 50 Hz bedraagt en de golflengte lang is t.o.v. de fysieke afmetingen van de beschouwde 380 kV verbinding. Daarom worden PI secties in dit werk gebruikt voor het modeleren van alle 380 kV verbindingen, waarmee load flow berekeningen worden uitgevoerd om het stationaire gedrag van het 380 kV net in kaart te brengen. Om de impact van de met shunt spoelen gecompenseerde kabels in het net te kunnen onderzoeken, worden de vermogensstromen en spanningen voor de situaties met en zonder kabels in het net, met elkaar vergeleken. De aanwezigheid van kabels laat een verandering zien in zowel de actieve en reactieve vermogensstromen in het net als in de spanningsniveaus dichtbij de kabelverbindingen. Uit de studie blijkt dat het 380 kV net voldoet aan het ' $n-2$ ' criterium.

Transiënte verschijnselen kunnen hoogfrequente oscillaties veroorzaken, hetgeen voor het model van een transmissielijn betekent dat de parameters van die lijn als uniform verdeeld moeten worden beschouwd over de lengte van die lijn. Het hedendaags veelgebruikte Frequency Dependent Phase Model (FDPM), een transmissielijn model dat de frequentieafhankelijkheid van de kabel en lijnparameters meeneemt, wordt in dit onderzoek gebruikt voor het modeleren van zowel de kabels als de bovengrondse lijnen. Met dit model zijn in dit werk simulatie modellen gemaakt van de nieuwe gemixte 380 kV verbindingen, waarin het aardscherm van de kabelgedeelten kruisverbindingen bevat. Op basis van metingen die zijn uitgevoerd aan de kabel met kruisverbindingen, zijn voor de in deze verbindingen toegepaste kruisverbindingen passende modellen gemaakt.

Onderzoek naar het op spanning brengen van de 380 kV verbinding tussen de stations Wateringen en Bleiswijk laat het effect zien van de aanwezigheid van kabels op zowel de periode als de piek van de transiënte spanning, wanneer deze worden vergeleken met de situatie van bovengrondse lijnen.

Onderzoek naar het effect van blikseminslag op een 380 kV lijn vlakbij een overgang van lijn naar kabel, bevestigt dat de lengte van de toegepaste kabel in gemengde lijn-kabel-lijn configuraties een grote invloed heeft op de piekspanning die optreedt bij de kabel-lijn overgangen.

Er zijn in dit onderzoek veldmetingen gedaan aan zowel de 380 kV kabel met kruisverbindingen in het aardscherm als aan de bovengrondse lijn. De resultaten van deze metingen zijn gebruikt ter verificatie van het toegepaste FDPM transmissielijn model. Voor de bovengrondse lijn is gebleken dat de meetresultaten volledig overeenkomen met de gesimuleerde resultaten, hetgeen de geldigheid van het gebruikte model bevestigt. Een stapspanning is geïnjecteerd in de 380 kV kabel en de gemeten golfvorm aan het einde van de 10.8 km lange kabel kwam overeen met de gesimuleerde golfvorm. Er is echter een klein verschil te zien tussen de gemeten en de gesimuleerde resultaten. Analyse naar de gevoeligheid van de kabel parameters is uitgevoerd om de oorzaak van het verschil te verduidelijken. De specifieke grondweerstand heeft een belangrijke invloed op de gemeten resultaten en daarmee kan een deel van het verschil tussen gemeten en gesimuleerde resultaten worden verklaard.

De wetenschappelijke bijdrage van dit werk is de bepaling van de parameters van de cross bonding componenten van de 380 kV kabel en de verificatie van het FDPM transmissielijn model door gebruik te maken van uitgevoerde veldmetingen aan het complete 380 kV cross bonded kabelsysteem.

# CHAPTER 1

## INTRODUCTION

### 1.1 BACKGROUND

Overhead transmission lines are a common way of energy transportation at high voltage levels. An increasing population density over the years leads to higher energy demand. As a consequence, the extension of existing power systems is unavoidable in order to guarantee the electric power supply in the future. Currently, the application of extra high voltage (EHV) cables in power grids is popular for the extension of existing grids. People who live nearby overhead lines are reluctant to the construction of new high voltage overhead lines. The appearance of high voltage towers and lines in the landscape can have a large visual and ecological impact. Besides, in terms of an aesthetic component in this opinion, some people are concerned about electromagnetic field effects from the high voltage overhead lines to their health, because of the continuous exposure to (low frequency) electromagnetic fields (EM fields) from overhead lines. There is no hard evidence of adverse health effects resulting from long term exposure to the EM fields produced by overhead lines.

The highest electrical field strength is located at the conductor surface of the overhead line. Directly under 400 kV overhead lines, the electric field strength lies between 7 kV/m and 10 kV/m. At a distance of about 25 m from away the overhead line, the electric field strength is lower than 5 kV/m. This field strength is an admissible level for human exposure. In underground cable systems, there exists only an electric field between the inner conductor and the screen conductor. Since the screen conductor is usually connected at ground potential, there is no electric field outside the cable. This means that the electric field is enclosed between the cable core conductor and the screen conductor. The magnetic field strength around a current carrying underground cable is higher compared with overhead lines, but the strength decreases more rapidly with the distance. There are exposure limits for the magnetic flux density: in the Netherlands this limit is 0,4  $\mu\text{T}$  [1]. This chapter starts with an overview of existing work and a summary of their results that are related to the application of underground cables. Thereafter, a description of the

Randstad 380 kV is presented. The Randstad 380 kV project forms an important motivation for the work presented in this thesis and therefore, a short overview of related cable projects in the world will be given. The last section of this chapter describes the outline of this thesis.

## 1.2 STATE OF ART

Several transmission utilities in the world are now studying the effect of application of EHV AC cable lines in their power grids. Energinet (Denmark) plans to apply underground cabling of the existing 132 kV and 150 kV grids by 2030. Underground cables can be applied to extend the power grid but also to replace existing overhead transmission lines. For the lower voltage levels in distribution grids, cables are widely used. In 2005, a total length of almost 33000 km of AC land and sea cables was in service [2] in the world. At voltage levels below 220 kV, more than 90% of the cables installed in the period between 2001 and 2005 are of the XLPE insulated type and above 220 kV, more than 40% are of the self-contained oil-filled type. At this moment, network planners and transmission system operators have little experience with the behavior of power grids in which long high voltage AC cables are integrated. At this moment, the longest EHV cable connection is in use in Japan; a length of 40 km at 500 kV [3]. In Denmark, a 150 kV connection to the offshore wind farm Horns Rev 2 is being installed and has a length of 100 km [4]. The Danish system operator Energinet.dk has performed several studies in relation to the application of very long EHV AC cables. These studies have shown that further analysis is needed to answer questions and to provide insight in the behavior of a power system with integrated cables. The stability of the grid and the security of supply are important issues in these studies.

The application of underground cables and mixed line-cable-line configurations in power grids will have impact on the behavior of the power system as such in several aspects. The steady state, transient and dynamic responses of cables differ significantly from overhead lines when considering both small and large disturbances and this has implications for the operation of the power system in terms of grid stability and security of supply. Therefore, steady state and transient phenomena should be a subject to study before the integration of cables is realized in practice.

From the installation point of view, high voltage cables longer than 1-2 km require cross-bonding schemes to reduce induced sheath currents. For shorter lengths, single-point bonding is generally applied. From the electrical point of view, cables cannot simply be replaced by overhead lines. The electrical behavior of cables differs from that of overhead lines. An overhead line is a transmission line surrounded by air, that gives the insulation and has a dominant inductive behavior. A cable consists of an inner and a screen conductor with an insulating material with semiconductor layers in between and this causes a dominant capacitive behavior. The values of the cable capacitance and inductance per unit length differ from overhead lines. The series inductance of a cable is five times smaller and the shunt capacitance 20 times larger than that of an overhead line. As a result, the characteristic impedance of cables is 10 times lower and the traveling wave velocity approximately two times smaller. So, the cable characteristic impedance value lies roughly

between 30 and 70  $\Omega$ . This means that the characteristic impedance loading (SIL) for a cable is several times larger than lines and is determined by the characteristic impedance and the applied voltage. Hence, a cable loaded below its SIL, behaves like a shunt capacitor. The cable loading above its SIL behaves as a shunt reactor. A large SIL can even exceed the cable ampacity. When the cable load equals its SIL, there is no net reactive power flow. In this situation, there is a flat voltage profile along the cable.

A capacitance can be regarded as a source of reactive power. This means that an energized cable injects reactive power to the power grid. The magnitude of the capacitive current of a cable depends on the applied power voltage and on the cable reactance which means that this current depends on the capacitance per unit length. When the cable ampacity is completely consumed by the capacitive charging current, no active power can be transferred through the cable. This occurs at the so-called critical cable length and therefore the capacitive current forms an important limitation in the application of AC cables for long distances. The Maximum Operable Cable Length at Thermal Limit (MCLTL) is used as a steady state operational design criterion of cables [5-7]. The large capacitive current has also consequences for the cable life time and therefore it is an important issue when applying long EHV AC cables. High voltage equipment in the grid, like transformers and motors, is inductive because it creates magnetic fields and therefore reactive power is required. Application of long cables in the system can lead to an unbalance between produced and required reactive power.

A surplus of reactive power causes power-frequency voltage rise at the cable terminations and at adjacent nodes in the power grid. A sudden voltage change of 3% is usually allowed when connecting or disconnecting a cable [8]. The allowable voltage change during switching of cables is prescribed in the net code of the grid operator. Compensation of reactive power by shunt inductors is necessary in order to keep these stationary overvoltages in the grid below an acceptable level. These shunt coils are usually installed at both cable ends but they can also be located at the transformer tertiary winding to achieve compensation of reactive power. When there is symmetry in the line-cable-line section, meaning that the two sections of the overhead line are of equal length, fixed shunt reactors can be applied. Variable shunt reactors are installed when one overhead line section is much longer than the other. Algorithms are described to find the optimal taps of the variable shunt reactor [5]. Shunt reactors need to be designed according to steady state operating constraints. Important criteria for shunt reactor sizing are the voltage rise at the supply node, receiving end overvoltages and rated line-charging breaking current [5].

Switching of shunt reactors may result in oscillations caused by the interchange of reactive power between system inductances and the cable capacitance. These oscillations are superimposed to the natural frequency of the system and can result in a temporary voltage rise in the power grid. Therefore, switching actions in shunt compensated mixed line-cable-line configurations may also result in temporary overvoltages. In [9], switching-off simulations were performed on a Danish operating 400 kV system for the connection between Aarhus and Aalborg which has a length of 90 km. An overvoltage level of 132 % was observed compared to the voltage level before switching-off. This overvoltage was caused by resonances that occurred between the shunt reactor and the cable. In another

study that was performed for a planned 60 kV cable connection of 18,5 km between Albaek and Hedebo (Denmark), there were no remarkable overvoltages observed after switching off [10].

The amount of compensation influences the cable charging current and therefore on the voltage profile along the cable. A study performed on a 400 kV underground cable system has shown that a reduction of the charging current to half of the largest value can be achieved when shunt reactors are placed at both cable ends. Installation of shunt reactors reduces this current to 25%, four reactors to 16% and five reactors to 12,5% of the largest value [1]. System studies for long cables recommend applying shunt reactors with a distance of 15 km to 40 km between them [11]. In a feasibility study [12], the influence of shunt compensation on the voltage profile along a 400 kV cable connection was investigated. The lowest compensation rate was 93,3% and it was shown that the voltage along the cable stayed below 420 kV. For the highest compensation rate of 111,9%, it turned out that the voltage level along the line was less than 415 kV.

In a study that was carried out by the Cigre Working Group B1.05, a cable end termination was placed at the cable-overhead line joint. It was demonstrated that for an incoming wave with a front rise time of 2  $\mu$ s, the cable voltage was raised by 2%. For a front time of 1  $\mu$ s, the increase of the voltage was 1% [13]. The wave propagation velocity along a cable is about 50% of the velocity of overhead lines. In a cable, the voltage and current waves propagate between the core conductor and the sheath.

In Denmark, a 150 kV connection to the offshore wind farm Horns Rev 2 is installed and has a length of 100 km. This cable forms the connection between the wind farm and 400 kV grid. A study to line-to-line overvoltages during energization of the 150 kV cable is reported in [4] for different short circuit power in the 400 kV grid. This study shows that in some cases, overvoltages are higher than the maximum allowable values.

Investigating the behavior of mixed line-cable-line configurations during lightning events is of importance in power system transient studies since lightning currents can cause high overvoltages that can affect equipment insulation. This means that overvoltage protection devices like surge arresters must be applied. The results of a study on a mixed overhead-cable system at 380 kV level have shown that shielding failure does not represent a critical event [14]. Furthermore, it was shown that installing surge arresters at both cable ends reduces tower foot voltage by 10 to 15%.

Another issue, related to shunt compensated cables, is the zero-missing phenomenon that normally occurs for shunt compensated cables during the energization process of the cables. The decay of the current DC component depends on the cable- and reactor-resistances that are in general small. This results in the current not crossing zero for several cycles, meaning that the opening of the circuit-breaker could be delayed. To avoid the failure of circuit-breakers, methods have been proposed to minimize the occurrence of the zero-missing phenomenon by applying a pre-insertion resistor [15, 16].

Cables and overhead lines can lead to parallel paths. The lower impedance of cables gives an inequality in power flow, which even could result in overloading the cable connections.



This implies that during steady state operation, compensation is required in two different ways: as compensation for the reactive power surplus and for the difference in impedance to control the flow of power. The larger capacitance of a cable has also consequences for the system resonance frequencies. A parallel resonance circuit consisting of the cable capacitance and the shunt reactor inductance is formed by compensated cable circuits. The cable capacitance and the transformer leakage inductance form series resonance circuit in the system. Series and parallel resonances can result in temporary power frequency overvoltages.

Apart of influencing the steady state operation, there are also consequences for transient situations when using cables in the system. First of all, transients cause slow-front, fast-front and very-fast-front overvoltages, which depend on their origin. Slow-front overvoltages occur for instance during the cable (de)-energization period, line switching and fault clearing. Fast-front surges caused by lightning current injections in overhead lines can result in high overvoltages.

Characteristic impedances of cables, cable joints and overhead lines differ significantly from each other and this means that there are impedance mismatches at line-cable-line junctions. As a consequence, reflections of traveling voltage and current waves will occur at these transition points and result in high voltage peaks. Characteristic impedances of cables and overhead lines are frequency dependent and that means that reflection coefficients at cable-line junctions are also frequency dependent. At high frequencies, reflections at those junctions can lead to doubling of the voltage amplitude. This can also occur at the coupling point of a transformer and a cable and this results in overstress of the transformer insulation. This overstress leads to accelerated aging of the transformer insulation.

When the cable length increases, attenuation and distortion effects increase and the maximum voltage at cable reduces. This maximum voltage reduction depends on the core, the insulation material and the sheath conductor. Calculations were performed to study the influence of material dimensions at maximum voltage [13]. A square pulse of 10  $\mu$ s duration applied to a 145 kV cable with a copper core and 17 mm insulation thickness, and it was found that reducing the cable lead sheath from 4 mm to 2 mm resulted in a substantial reduction of the cables maximum voltage. Furthermore, it was shown that the reduction of the maximum voltage, increases by increasing cable length. In the same study, it is shown that, when frequency dependent insulation losses were taken into account in the calculations, paper oil insulation results in significantly more reduction of the maximum voltage than XPLE insulation.

Simulation studies of transient phenomena in cables are of major importance when performing system studies with cables. A detailed cable model is required for accurate calculation of transients. Transients in power systems can result in steep voltage wave fronts and steep voltages contain high frequency oscillations. For accuracy, a transient cable model should take into account the frequency dependence of cable parameters. The calculation of the parameters for transient studies is a rather complex task caused by the different frequency dependent parameters and the influence of the ground return path. For

cable modeling, the total series impedance and shunt admittance of a cable has to be determined. The shunt admittance is formed by the insulating and semiconducting layers. The material properties of the admittances are modeled by complex permittivities.

In general, the accuracy of modeling an underground cable depends on the type of phenomenon that is considered. Several cable models have been developed over years, both for planning and for system studies. The available cable models can be divided into two main classes: lumped parameter models (also called PI-section models) and distributed parameter models (also called travelling wave models). For power system steady state analysis like planning studies,  $\pi$ -sections have been used with sufficient accuracy. For these cases, it is usually not necessary to take account for full frequency dependency of the cable parameters. The exact  $\pi$ -model is accurate for power frequency studies.

Distributed wave models can be subdivided into Frequency Dependent Mode Models (FDMM) and Frequency Dependent Phase Models (FDPM). Frequency Dependent Mode Models use a constant (frequency independent) transformation matrix. This approach splits a multi-phase system into mutually exclusive modes meaning that each mode is treated as a single-phase circuit. The Frequency Dependent Phase Models are frequency dependent in all parameters. These models have been implemented in EMTP-based simulation software tools.

The FDMM, developed by J.R. Marti [17], uses a frequency independent transformation matrix to separate multiple coupled phases into single-phase circuits. An improvement of this model was made by taking into account the frequency dependency of the transformation matrix, developed by L. Marti [18]. To overcome the complexity with the modal transformation matrix, a Frequency Dependent Phase Model was developed [19]. This method minimizes the computation time by using the ARMA model. A widely used cable model nowadays, is an FDPM model using the s-domain. This model is implemented in EMTDC-based simulation programs [20]. The difficulty with the transformation matrix is circumvented when the cable model is split into a constant ideal line section and a frequency dependent loss section [21].

For accurate cable modeling, the total series impedance and shunt admittance have to be determined. A fundamental description of the cables' impedance, its admittance and the semiconducting layer is described by Ametani [22, 23]. This formulation has been widely used for the calculation of cable parameters for transient studies. The evaluation of frequency dependent impedances of underground cables can be done in different ways, for example by using the finite element method is also performed [24].

In order to perform accurate cable modeling for transient studies, the frequency dependency of cable parameters needs to be taken into account and therefore, cable parameter determination over a wide frequency range is an important topic. A method to calculate the frequency dependent parameters of power cables, based on spatial discretization of their cross-sections, is described in [25]. Simplifications have often to be made, such as assuming constant permeability, neglectation of dielectric losses, ignoring the proximity effects and assuming coaxial arrangement of the conducting and insulation layers. Next to that, an accurate model for the earth impedance is rather complicated and requires specific data. Evaluation for cable earth impedances can be done, by applying

Pollaczek's integral [26], [27]. In general, considerable approximations have to be made while calculating the earth impedance [28].

The best way to verify models is to compare calculated values with field measurements. And for verification, a measurement set up should be made. For validation of high frequency models, a voltage with the shape of a step-function is applied at the cable termination and measurements are carried out to verify the transient cable models implemented in software like PSCAD (Power Systems Computer Aided Design). This is how the 400 kV Gistrup-Skudshale cross bonded cable system in Denmark was studied. The comparison of transient cable models with field measurements has been reported for cross bonded cables in [29].

### **1.3 THE RANDSTAD 380 KV PROJECT**

The Randstad380 project deals with the integration of a heavily loaded cable circuit as a part of the meshed Dutch 380 kV grid. The goal of this project is to study the behavior of 380 kV systems in which cable sections have been integrated. It should give insight and provide experience in the behavior of underground cables in 380 kV power systems. At 380 kV level, there is limited experience with underground cable systems yet but this experience is absolutely necessary for future power system planning studies. The use of cables influences the system behavior in several aspects and the items of interest in this project are the steady state, the transient and the dynamic behavior of 380 kV power systems with mixed line-cable-line sections. The length of cables applied in this project is limited to 20 km in total, 10 km for the Northern trajectory (Bleiswijk-Beverwijk) and 10 km for the Southern trajectory (Wateringen-Bleiswijk). In Figure 1.1, the 380 kV connections in the Randstad area are shown. The central research question that needs to be answered is whether it is possible to include longer cable sections in the future without violating to security of supply and the voltage stability.

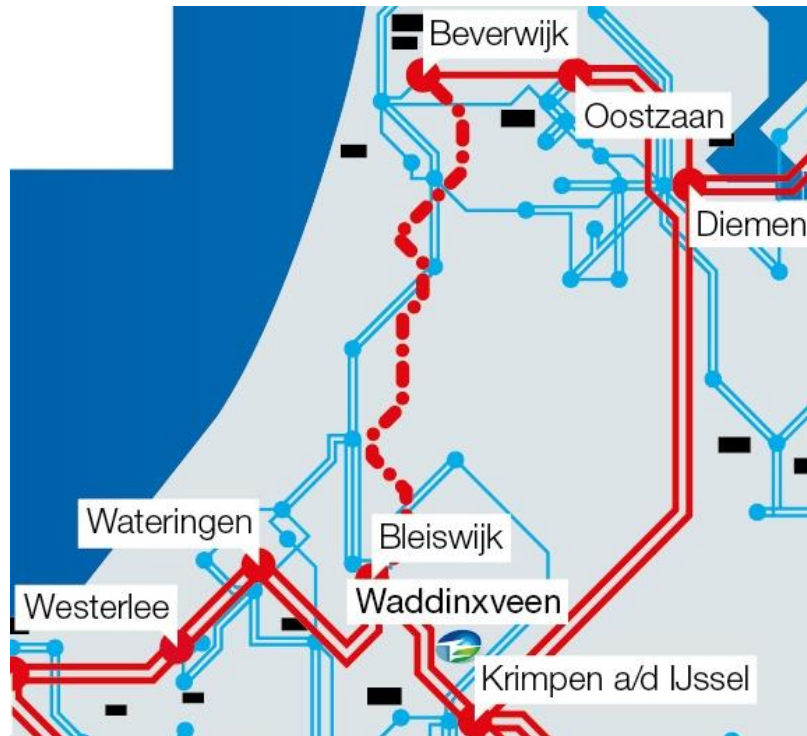


Figure 1.1 Randstad area with new 380 kV connections under construction.

## 1.4 SHORT OVERVIEW OF RELATED CABLE PROJECTS

Worldwide, similar studies for underground cable projects have been carried out. These projects can be distinguished with respect to the total cable length, the transmission capacity and the number of circuits in the particular system. In Table 1.1, a short overview of high voltage underground cable projects similar to the Randstad 380 kV project, is listed. It can be seen that the Randstad 380 kV project is a unique project in terms of cable circuit transmission capacity and total cable length.

Table 1.1. Related high voltage underground cable projects.

<b>Country</b>	<b>Number of circuits</b>	<b>Transmission capacity (MW)</b>	<b>Cable length per circuit (km)</b>	<b>Total cable length (km)</b>
Denmark	1	975	66	66
Germany	2	1150	12	72
Japan	2	1200	40	240
Spain	2	1720	13	156
Netherlands	2	2640	120	240
Italy	2	2000	114	228

## 1.5 GOAL OF THE WORK

The overall goal of the work in this thesis can be divided into two parts. The first goal is investigating the steady state power flows and voltage levels in mixed 380 kV line-cable grids, in order to evaluate whether overload and steady state overvoltage occur in the connections of the grid. The second goal is investigating transient behavior in mixed line-cable grids in order to evaluate whether transient overvoltages in the 380 kV grid stay below the prescribed limits during switching actions and lightning.

## 1.6 THESIS OUTLINE

The details of the research approach are further described by chapter as follows:

Chapter 2 deals with the fundamentals of steady state operation of cables. The Maxwell equations, that describe the fundamentals of electromagnetism, are taken as a starting point for cable modeling. Thereafter, the concept of reactive power compensation and the influence of compensation on the voltage profile are explained. This theoretic basis for the modeling work of both overhead and underground transmission lines is important as it forms the base in all studies where appropriate transmission line models are required.

Chapter 3 deals with cable modeling issues and system performance. Cable related modeling issues are presented, like mutual coupling between cable conductors in a system, the ground return impedance and the concept of cable screen cross-bonding are discussed. Furthermore, temporary overvoltages and the zero miss phenomenon are explained. The

modeling work for an underground transmission system starts in general with describing the system by its impedance matrix. This chapter explains the elements of the impedance matrix of an underground transmission system and simultaneously it describes the theory of mutual coupling between cables in an underground system, cable grounding, cable cross bonding and the cable ground return impedance. The content of this chapter therefore forms an important base for the modeling work for a particular underground system.

Chapter 4 deals with the impact of cables on the steady state behavior of the Dutch 380 kV grid. The steady state behavior is analyzed by means of load flow studies and contingency analysis, that provides insight in voltage levels and power flows in the grid. The work that is described in this chapter is performed by using a transmission line model for representing the connections in the Dutch 380 kV grid in order to investigate the steady state behavior of the 380 kV grid as a whole. Such a transmission line model is necessary for investigating the impact of both the reactive power production by the cables and the shunt compensation coils on the steady state power voltage level in the grid and on the active and reactive power flows in the 380 kV grid. The transmission line models used for this particular 380 kV system and method of the analysis can also be used in other 380 kV grids in which mixed line-cable-line connections are applied.

Chapter 5 deals with the transient modeling of the 380 kV mixed line-cable-line circuits including the cross-bonding (CB) of the 380 kV cable screen. Furthermore, models for the cross-bonding (CB-cable, CB-box and CB-joint) are developed by using the results of measurements that are performed on the cross-bonding cable. The cross bonding model that is developed enables us to study the transient behavior of mixed line-cable configurations including the effect of the cross-bonding cable. The innovative aspect is that pulse injection measurements were performed on the actual cross bonding cable system and analysis of the measurement data resulted in a model for the cross bonding cable, the cross bonding box and the cross bonding joint of the 380 kV system.

Chapter 6 deals with the analysis of switching actions in mixed line-cable-line circuits. Switching simulation studies are performed on the 380 kV circuits under different conditions in order to study the oscillation that occurs during switching transients. The focus of the work in this chapter lays on investigating the peak overvoltages after switching the mixed line-cable connection, by making use of the transient cable model that is developed in Chapter 5. The work in this chapter enables us to figure out when the largest peak overvoltage can be expected when switching a 380 kV cable in a mixed line-cable-line circuit, for different initial cable charging conditions.

Chapter 7 deals with lightning overvoltage analysis for mixed line-cable-line circuits. Studies on lightning overvoltages in the particular mixed 380 kV grid are done and the impact of cables is analyzed. The transient model for the mixed line-cable configuration that is described in Chapter 5 is applied for analyzing overvoltages that appear in the system

after the injection of lightning discharge currents. The focus of this work is to analyze the peak voltages at the line-cable junction points when the cable length is varied, in order to find at which applied cable length the peak voltage exceeds the allowable limit. The goal of this work is to show the relation between the expected peak voltage in the 380 kV system and the applied cable length. The results of this work can be used for predicting the overvoltages that appear at cable terminals after fast transient phenomena and this is important for making decisions in the protection strategy.

Chapter 8 deals with verification of the used transient transmission line model by means of a comparison of the simulation results with the field measurements that are performed on the actual 380 kV cable. Such a validation of the cable and line model enables us to check whether the Frequency Dependent Phase Model that is used in this work is an appropriate model for studying transient behavior of transmission systems in which underground parts are integrated. Furthermore, the goal of the verification of the FDPM model is also to confirm the validity of the model for transient studies.

Chapter 9 describes the conclusions of the work in this thesis, pays attention to ongoing PhD work and gives recommendations for future work.

## **CHAPTER 2**

# **SYSTEM BEHAVIOUR OF UNDERGROUND CABLES**

### **2.1 INTRODUCTION**

Installing EHVAC underground cables in the power systems can have important influence on the system performance. Reactive power generation is an important issue when cables are applied. Because of the capacitive behavior of cables, charging currents are present when cables are put into service. The magnitudes of capacitive charging currents are proportional to the applied cable length, the longer the cable, the higher the current. Above 30 km, it is necessary to compensate for these charging currents [6]. In general, it can be stated that compensation for underground cables is required when the length of the cable is 20 to 30 times shorter than an overhead line with equal length [30], [31]. The compensation is done by installing shunt reactors in parallel with the cable circuit. Shunt reactors are inductive and therefore they absorb the capacitive reactive power currents. This chapter deals with the cable theory in order to explain the theory of reactive power compensation in 380 kV mixed line-cable-line circuits. The electromagnetic field theory is taken as starting point and the steady-state operational modeling aspects are treated. Next, the concept of reactive power generation and compensation is explained and both the relation between cable length and transmission capacity as well as the influence of the shunt compensation on the voltage profile are interpreted.



## 2.2 TRANSMISSION LINE THEORY

The electromagnetic field theory is the base for the practical application of electrical engineering as electromagnetic fields play a major role in transportation of electrical energy. The term “field” refers to a state of the space and this term is used when speaking about the electromagnetic field. The field theory is the starting point for accurate modeling of transmission lines for the steady-state and transient mode of operation and is described by Maxwell’s equations. These equations show how time varying electric- and magnetic fields are related to each other. An electric current through a conductor is defined as the amount of moving electrical charge carriers per unit of time.

First of all, it is important to explain the base of electromagnetic forces in a simple way by considering static electric point charges for a certain position in space. In case of an electrostatic charge, an electrical force is acting on that particular charge and the strength of that force decreases inversely with the square of the distance between the charges (Coulomb’s law), given by equation 2.1.

$$\mathbf{F} = k_e \frac{q_1 q_2}{r^2} \quad (2.1)$$

where:

$q_1$  and  $q_2$  are the point charges [C];  
 $r$  is the distance between those charges [m]; and

$k_e$  is Coulomb’s constant:  $k_e = \frac{1}{4\pi\epsilon_0}$

where:

$\epsilon_0$  is the dielectric permittivity ( $8.85 \cdot 10^{-12}$  F/m).

When the charges are moving, the total force acting on the charge depends also on the charge motions. We know that the force acting on a charge depends on its position, velocity and on the amount of charge. In case of moving charges, the total force acting on a particular charge is given by equation (2.2). The total force is composed by the electric field  $\mathbf{E}$  and the magnetic field  $\mathbf{B}$  at charge location. Electric fields are visualized by lines that start at the positive charge and end at the negative charge (Figure 2.1a).

$$\mathbf{F} = q(\mathbf{E} + \mathbf{v} \times \mathbf{B}) \quad (2.2)$$

An electrical current flowing *through* a conductor induces a magnetic field *around* the conductor. The magnetic field visualized by concentric circles around that conductors (Figure 2.1b). Electric and magnetic field lines are perpendicular to each other. According to Faraday's induction law, a time varying magnetic field induces a voltage in a closed loop. A time varying electric field causes a flow of current in a conducting loop, that on its turn induces a magnetic field that opposes the original magnetic field (Lenz law). Maxwell's equations are general and they are from the mathematical point of view not easy to solve.

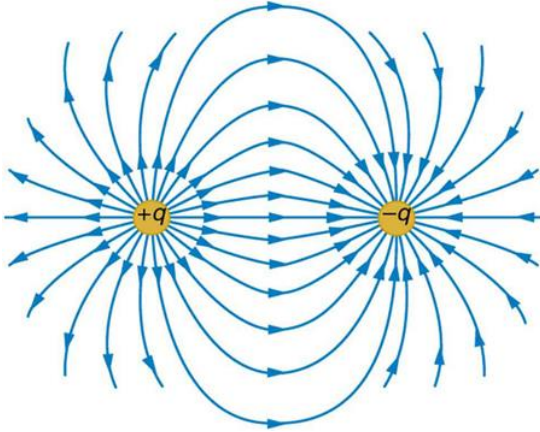


Figure 2.1a. Electric field lines.

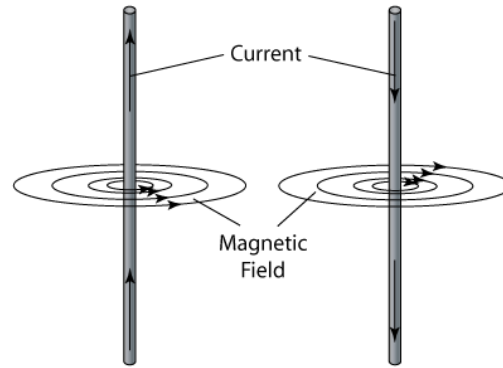


Figure 2.1b. Magnetic field lines.

Simplifications of the equations are often feasible for power system modeling purposes as it will be explained in the next section. Basic relationships, like Ohms law and the voltage-current relation for reactors and capacitors, result after simplifications of the Maxwell equations. The fundamental relations described by Maxwell can be written in local (or differential) and in global (or integral) form. The four equations in differential form are given by formula (2.3)-(2.6). The first equation relates the dielectric flux density  $\mathbf{D}$  to the amount of free charge carriers present in a defined closed surface. It describes the electric field caused by a charge distribution. This relation is referred to as Gauss's law for the electric field. The second equation is called Gauss's law for magnetism and describes the continuity of magnetic flux lines. It states that the number of magnetic field lines entering a volume is equal to the number of magnetic field lines leaving that volume. This equation describes in fact that there is no such a thing as a magnetic monopole. The third equation relates the variation in time of the magnetic flux to the induced voltage and it is also known as the Faraday's law of induction. It states that a time varying magnetic field induces an electric field at a certain point in space that causes motion of charge. The fourth equation is also known as Ampere's law and states that the curl (infinitesimal rotation) of the magnetic field is equal to the total current density. A motion of charge can induce a magnetic field in space. The term  $\mathbf{J}$  in this equation denotes the current density and can be regarded as the source of that field. This equation shows that the total current flowing through a certain loop  $S$ , is equal to the sum of the electric current through the conducting wire and the time derivative of the electric flux density  $\mathbf{D}$ . The second term of the right

side of this equation denotes the rate of change of the electric flux density and is also referred to as Maxwell's displacement current.

$$\nabla \cdot \mathbf{D} = \rho \quad (2.3)$$

$$\nabla \cdot \mathbf{B} = 0 \quad (2.4)$$

$$\nabla \times \mathbf{E} = - \frac{\partial \mathbf{B}}{\partial t} \quad (2.5)$$

$$\nabla \times \mathbf{H} = \mathbf{J} + \frac{\partial \mathbf{D}}{\partial t} \quad (2.6)$$

The field quantities  $\mathbf{E}$  and  $\mathbf{H}$  in Maxwell's equations, which are in general vector quantities, are recursively related to each other, since a variation in time of one field component causes a variation in space of the other field component. The electric- and magnetic field vectors both depend on time and have three dimensions in space, meaning that on every location in space, there exists an electric and a magnetic field vector that can have three special coordinates and a time dependence. Maxwell's equations provide the most complete description of electric- and magnetic fields.

When considering Maxwell's equations in more detail, the current density  $\mathbf{J}$  and the electric field  $\mathbf{E}$  are related to each other by the material conductivity  $\sigma$ . The electric field components  $\mathbf{D}$  and  $\mathbf{E}$  are related to each other by the permittivity  $\varepsilon$ . The electric flux  $\mathbf{D}$  density also depends on the polarization  $\mathbf{P}$  of the material, which is a superposition of a field-dependent part and a field-independent part (permanent part). The magnetic flux density  $\mathbf{B}$  and the magnetic field  $\mathbf{H}$  are related to each other by the permeability  $\mu$  of the material. Moreover, the field density depends on the magnetization  $\mathbf{M}$  of the material, which is also a superposition of a field dependent part and a permanent part. The so-called constitutive relations between the field components are expressed by (2.7)-(2.9).

$$\mathbf{J} = \sigma \mathbf{E} \quad (2.7)$$

$$\mathbf{D} = \varepsilon_0 \mathbf{E} + \mathbf{P}_i(\mathbf{E}) + \mathbf{P}_p \quad (2.8)$$

$$\mathbf{B} = \mu_0 \mathbf{H} + \mu_0 \mathbf{M}_i + \mu_0 \mathbf{M}_p \quad (2.9)$$

Maxwell's equations can be shown in schematic in order to explain the recursive relationship between the electric- and magnetic field, without the need for considering the vector notation of these fields. In Figure 2.2, a schematic overview is shown, in which the

field quantities and the constitutive relations between the field quantities are made visible in a block diagram [32]. When integrating the electric flux density  $\mathbf{D}$  over a surface  $S$ , the total amount of free charge is found can be computed. The integration of the magnetic flux density  $\mathbf{B}$  over that surface results in total magnetic flux. From this overview, it can be seen that the relations between the electric and the magnetic field quantities have a recursive character:

$$\mathbf{J}_E + \partial_t \mathbf{D} \longrightarrow \mathbf{H} \longrightarrow \partial_t \mathbf{B} \longrightarrow \mathbf{E} \longrightarrow \mathbf{J}_E \longrightarrow \partial_t \mathbf{D}$$

The strength of recursion in Maxwell's equations is determined by both the spatial derivatives and the time derivatives of the field quantities. When the mathematical 'product' of both derivatives is small, the recursive effect can be neglected.

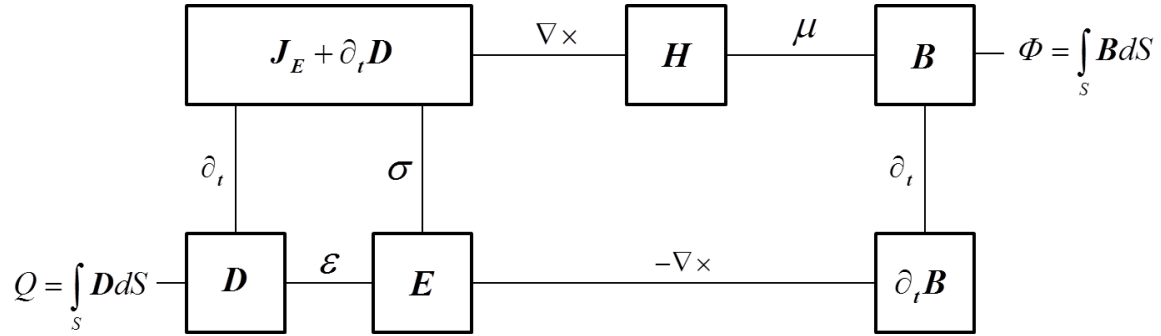


Figure 2.2. Schematic overview of Maxwell's equations.

Electric energy is transported to the consumers via electromagnetic fields around a conductor by a propagating electromagnetic wave, in which the  $\mathbf{E}$ -component and the  $\mathbf{H}$ -component of the field are perpendicular to each other. During the propagation of this electromagnetic wave, the amount of energy is equally divided over the electric- and the magnetic field. Neglecting the recursive relation in Maxwell's equations is allowed in cases when the "electric distance" is small. This means that the wavelength of the EM wave is large compared to the dimension of the system. In case of a small electric distance, the wavelength and the dimensions of the network are in the same order of magnitude, meaning that the values of the wave are equal along the distance of the network. A consequence of neglecting the recursive relation, is that the  $\mathbf{E}$ - and  $\mathbf{H}$ -field can be treated separately.

There are several types of wave propagation with respect to the number of dimensions of propagation. A special case of an electromagnetic wave propagation are the so-called plane waves. For every point in space, the electric- and magnetic field components are laying in a plane and for all points in space these planes are in parallel. This means that in one of the three dimensions of space, the field components are equal to zero. Such a wave propagates in one dimension of space. In this situation, the  $\mathbf{H}$ -component in the direction of propagation is zero and thus is the closed-loop integral of the  $\mathbf{E}$ -component in a plane perpendicular to the direction of propagation equal to zero. This enables the introduction

of simplified calculations with “potentials” and this reduces the complexity of the modeling work [32].

When considering plane waves in more detail, a distinction has to be made between uniform plane waves, in which the field components in the plane perpendicular to the direction of propagation are equal at all locations in the plane. The second type is non-uniform plane waves, in which the field components in the plane can have different values at all locations in that plane. In Figure 2.3, an example is shown of an propagating electromagnetic plane wave. It can be seen that the  $\mathbf{E}$ -component and the  $\mathbf{H}$ -component are varying sinusoidal in time and are perpendicular to each other and to the direction of propagation. Moreover, the figure shows that the  $\mathbf{E}$ - and  $\mathbf{H}$ -field only have non-zero values perpendicular to the direction of propagation. Furthermore, there is only propagation in one direction in space. This type of waves are called transversal electromagnetic (TEM) waves and these mainly occur in transmission lines. Since the field components in the direction of propagation are zero, Maxwell’s equations need to be analyzed only in that particular plane.

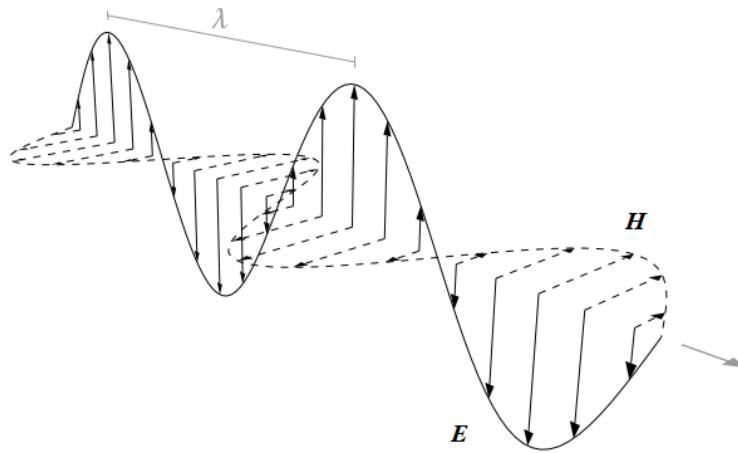


Figure 2.3. Propagating electromagnetic plane wave.

Based on this theory, it can be concluded that electric energy is transported to the consumers by EM-wave propagation, as happens with transmission lines. There are several types of transmission lines in practice that differ from each other with respect to the configuration of the lines and the number of conductors. A transmission line consists of two or more parallel conductors and the electromagnetic wave propagates along these conductors. When using the term “transmission line”, it is assumed that the distance between the conductors is relatively small. In case of relative large distances between the conductors, the analysis of the EM-field becomes more complex and then the term “waveguide” is used [32].

This analysis leads to two important conclusions [32]. Because the magnetic field strength in the direction of propagation is zero, its time derivative is zero, which implies that the surface integral is zero. As a consequence, the magnetic flux through a certain area perpendicular to the conductors is also zero and this means that no electromagnetic force

is induced in the plane. In this case, closed loop integral of the electric field strength in that plane is equal to zero. Now, the potential difference between two points of the conductors can be calculated by taking the integral of the electric field over a certain path in that plane. Since the electric field strength in the direction of propagation is zero, its time derivative is zero and this results in the fact that the closed-loop integral of the magnetic field strength over a certain loop around a conductor in the plane is equal to the surface integral of the current density  $\mathbf{J}$  through that surface. In this way, this surface integral equals the current through the conductors. As a result of this analysis, the quantities voltages and currents can be introduced for every point on the transmission line. Moreover, it can be concluded that the three dimensional time dependent field quantities in Maxwell's equations are reduced to a one dimensional time dependent problem, because the wave propagates along the line in only one direction.

In this section, the theory and the analysis of a two-conductor transmission line is treated, based on the electromagnetic field theory. The considered transmission line consists of a core conductor and a screen. The electrical energy transmitted by a conductor, is stored in the electromagnetic field (EM field) around that conductor. The electric field component of the EM field stems from charges in the conductor, and can be modeled by a capacitive element in a transmission line conductor. The capacitance  $C$  between the conductors of a two wire transmission line is related to the charge  $q$  and to the potential difference between the conductors  $v$ , given by (2.10).

$$C = \frac{q}{v} \quad (2.10)$$

The magnetic field component of the EM field is created by the moving charges in the line, the current as we call it. The term 'electromagnetic' implies that the electric- and the magnetic field components are interlinked and that is described by the Maxwell equations. The electric field  $\mathbf{E}$  and the magnetic field  $\mathbf{H}$ , are vector quantities and are generally dependent from time. It can be proven that both the  $\mathbf{E}$  and the  $\mathbf{H}$ -field satisfy the wave equation. The energy stored in the electromagnetic field propagates along the transmission line in the form of an electromagnetic wave, with a certain velocity. Furthermore, electromagnetic waves exhibit polarization. The  $\mathbf{E}$  and the  $\mathbf{H}$ -field oscillate with the same frequency but perpendicular to each other and also perpendicular to the direction of propagation.

The travelling wave velocity, also called propagation speed, depends on the permeability and permittivity of the medium in which the wave propagates. The propagation characteristic of a transmission line is governed by its passive electrical circuit parameters. These parameters are the four frequency dependent parameters of the transmission line:  $R$ ,  $L$ ,  $C$  and  $G$ . The conductor losses are associated with the resistivity of the conductor and can be represented by a resistive element  $R$ . The self-inductance  $L$  of the transmission line conductor accounts for the magnetic field component of the EM wave. The amount of charge divided by the potential difference present between the conductors is equal to the line capacitance  $C$  and accounts for the electric field component. There are also small

resistive losses caused by the conductivity of the dielectric material between the line conductors.

The wavelength of an electromagnetic wave depends on the frequency and the propagation speed. Switching actions in power systems, result in high frequency oscillations and the corresponding EM waves experience attenuation and a phase shift when travelling along the transmission line. The attenuation and phase shift can be expressed by a complex number, that is called the propagation constant. The propagation constant is an important characteristic parameter of the transmission line. Both the attenuation and the phase shift are completely determined by the transmission line parameters. When the travelling time of the voltage and current waves are taken into consideration, it is necessary to consider the line parameters to be uniformly distributed along the line. This means that a transmission line with a finite length should be considered by an infinite amount of line sections with length  $\Delta x$ . If a two conductor transmission line is modeled in this way, each differential line section contains the four elements  $R$ ,  $L$ ,  $C$  and  $G$  to account for the electric and magnetic field component and the Ohmic losses. A line section of a differential length is depicted in Figure 2.4 [33]. The lumped elements indicated in the figure have values in per unit length.

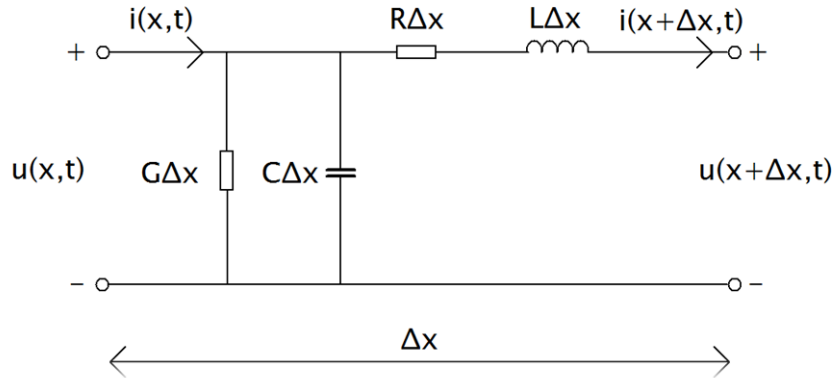


Figure 2.4. Equivalent circuit of a two conductor transmission line section with length  $\Delta x$ .

When the equivalent circuit of the transmission line is considered, the expressions (2.11) and (2.12) for the electric flux and the magnetic flux can be applied in order to find the expressions for the voltage  $u(x, t)$  and current  $i(x, t)$ .

$$d\Psi(t) = u(x,t)C\Delta x \quad (2.11)$$

$$d\Phi(t) = i(x,t)L\Delta x \quad (2.12)$$

When Kirchhoff's voltage and current law are applied over the distance  $\Delta x$  of the transmission line section, equations for the voltage and current can be found. When considering  $\Delta x \rightarrow 0$ , the voltage and current equations become [33]:

$$\frac{\partial u(x,t)}{\partial x} = -L \frac{\partial i(x,t)}{\partial t} - Ri(x,t) \quad (2.13)$$

$$\frac{\partial i(x,t)}{\partial x} = -C \frac{\partial u(x,t)}{\partial t} - Gu(x,t) \quad (2.14)$$

The electric and magnetic flux produced by the EM wave are represented by a capacitive and inductive element respectively and therefore Kirchhoff's laws can be applied to this line section, since voltages and currents are already defined. Because of the frequency dependency of the inductance and capacitance, it is convenient to transform the equations to the Laplace domain. When the substitutions (2.15) and (2.16) for the series impedance and the shunt admittance are used, the equations are expressed in the Laplace domain [33].

$$Z = R + sL \quad (2.15)$$

$$Y = G + sC \quad (2.16)$$

This substitution results in two first order partial differential equations, given by (2.17) and (2.18).

$$-\frac{\partial u(x,s)}{\partial x} = (R + sL)i(x,s) \quad (2.17)$$

$$-\frac{\partial i(x,s)}{\partial x} = (G + sC)u(x,s) \quad (2.18)$$

When these equations are differentiated once more with respect to  $x$ , two second-order partial differential equations are obtained, given by (2.19) and (2.20).

$$\frac{\partial^2 u(x,s)}{\partial x^2} = -Z \frac{\partial i(x,s)}{\partial x} = ZYu(x,s) = \gamma^2 u(x,s) \quad (2.19)$$

$$\frac{\partial^2 i(x,s)}{\partial x^2} = -Y \frac{\partial u(x,s)}{\partial x} = YZi(x,s) = \gamma^2 i(x,s) \quad (2.20)$$



This set of equations can be solved in the time domain and the characteristic impedance of the transmission line and the propagation constant can be expressed in terms of R, L, C and G. In these equations, the symbol  $\gamma$  denotes the propagation constant of the travelling wave and is equal to [33]:

$$\gamma = \sqrt{RG + (RC + GL)s + LCs^2} \quad (2.21)$$

Because the propagation constant is a complex number having a real and an imaginary part, it is convenient to write it in Cartesian coordinates. To achieve this, an intermediate step is taken by writing (2.21) in Polar notation. This equation is equal to:

$$\gamma = \sqrt[4]{(R^2 + \omega^2 L^2)(G^2 + \omega^2 C^2)} \exp j \left[ \frac{\arctan \left\{ \frac{\omega L}{R} \right\}}{2} + \frac{\arctan \left\{ \frac{\omega C}{G} \right\}}{2} \right] \quad (2.22)$$

The real part of (2.22) represents the attenuation and the imaginary part describes the phase shift of the travelling wave. The real and imaginary part of (2.22) are given by (2.23) and (2.24) respectively.

$$\text{Re}\{\Gamma\} = \alpha = \sqrt[4]{(R^2 + \omega^2 L^2)(G^2 + \omega^2 C^2)} \cos \theta \quad (2.23)$$

$$\text{Im}\{\Gamma\} = \beta = \sqrt[4]{(R^2 + \omega^2 L^2)(G^2 + \omega^2 C^2)} \sin \theta \quad (2.24)$$

The above expression for the propagation constant is the most general and comprehensive form. When analyzing and modeling transmission lines, it is often allowed to make assumptions regarding the amount of attenuation present in the line. This assumption results in a simplified expression for the propagation constant. When the attenuation in the transmission line is small, which is the case in many practical situations, (2.23) and (2.24) can respectively be approximated by (2.25) and (2.26) [34]:

$$\alpha \approx \frac{1}{2} \frac{R}{|Z_0|} + \frac{1}{2} G |Z_0| \quad (2.25)$$

$$\beta \approx \omega \sqrt{LC} \left[ 1 + \frac{1}{2} \left( \frac{R}{2\omega L} - \frac{G}{2\omega C} \right)^2 \right] \quad (2.26)$$

where,  $Z_0$  is the characteristic impedance of the transmission line and is equal to (2.27).

$$Z_0 = \sqrt{\frac{R + j\omega L}{G + j\omega C}} \quad (2.27)$$

The characteristic impedance of a line is the terminal line impedance, which when terminating an arbitrary length of line at its output will produce an input impedance equal to the characteristic impedance. When a line with finite length is terminated by its characteristic impedance, it will act as an infinitely long line. It is equal to the ratio of voltage wave and current wave. As it can be seen from (2.27), the characteristic impedance is determined by the four circuit parameters. The length of the transmission line does not influence the characteristic impedance. For an overhead transmission line, the characteristic impedance is between 300  $\Omega$  and 400  $\Omega$ . For an underground cable, the characteristic impedance is about ten times smaller. For short transmission systems, it is allowed to ignore the losses, meaning that the characteristic impedance is mainly determined by  $L$  and  $C$ . Knowing the phase shift, the propagation speed of the travelling wave can be derived. The relation between the frequency  $f$ , the wave length  $\lambda$ , the phase constant  $\beta$  and the propagation velocity is:

$$v = f\lambda = \frac{\omega}{\beta} \quad (2.28)$$

When assuming a lossless transmission line, the series resistance  $R$  and the shunt conductance  $G$  can be neglected. For a distortionless line, the shape of the wave does not change during its propagation along the line and the propagation velocity is constant. In both cases, the propagation velocity becomes equal to:

$$v = \frac{1}{\sqrt{LC}} \quad (2.29)$$

Finally, the time domain solutions for the second order partial differential equations (2.19) and (2.20) for the voltage and current wave are:

$$u(x, t) = e^{\gamma x} f_1(t) + e^{-\gamma x} f_2(t) \quad (2.30)$$

$$i(x, t) = -\frac{1}{Z_0} [e^{\gamma x} f_1(t) - e^{-\gamma x} f_2(t)] \quad (2.31)$$

These expressions show that the travelling voltage and current waves contain a forward and a backward wave because they propagate in positive and negative x-direction respectively. The time dependent functions  $f_1$  and  $f_2$  are arbitrary. For a short overhead line section for instance, the dielectric losses are usually neglected, because the air insulation in between the conductors has a very low conductivity, meaning that the losses are negligible. Moreover, the resistive losses of the line conductor are small for short line sections. This means that the parameters  $R$  and  $G$  can be omitted and the expressions for the characteristic impedance and the propagation constant simplifies considerably.

The propagation of electromagnetic waves along a transmission line is affected when discontinuities occur in the characteristic impedance of the transmission path. A transmission path may consist of different types of transmission lines, each with different impedances. This is the case when for instance an overhead line is connected to a cable, or when a cable is connected to a substation transformer. At the line-cable joint, voltages and currents are continuous. This means that (2.32) and (2.33) describe the voltage and current at the line-cable joint when an incident wave reaches the discontinuity at location  $x_0$  at time instant  $t = t_0$ .

$$v_{line}(x_0, t) = v_{cable}(x_0, t) \quad (2.32)$$

$$i_{line}(x_0, t) = i_{cable}(x_0, t) \quad (2.33)$$

At the line-cable joint, a difference in characteristic impedance is seen and as a result, a part of the energy in the electromagnetic wave will be reflected while the remaining part of the energy is let through. At the joint, the sum of the incident wave and the reflected wave is equal to the wave that is let through. When the incident wave, the reflected wave and the wave that is let through have subscript 1, 2 and 3 respectively, the voltages and currents at the discontinuity  $x_0$  can be expressed by (2.34) and (2.35).

$$v_{1line}(x_0, t) + v_{2line}(x_0, t) = v_{3cable}(x_0, t) \quad (2.34)$$

$$\frac{v_{1line}(x_0, t)}{Z_{line}} - \frac{v_{2line}(x_0, t)}{Z_{line}} = \frac{v_{3cable}(x_0, t)}{Z_{cable}} \quad (2.35)$$

Based on these equations, expressions (2.36) and (2.37) are found for the voltage and current wave that is let through.

$$v_{3cable}(x_0, t) = \left\{ \frac{2Z_{cable}}{Z_{line} + Z_{cable}} \right\} v_{1line}(x_0, t) \quad (2.36)$$

$$i_{3cable}(x_0, t) = \left\{ \frac{2Z_{line}}{Z_{line} + Z_{cable}} \right\} i_{1line}(x_0, t) \quad (2.37)$$

For the reflected voltage and current wave, expressions (2.38) and (2.39) are found.

$$v_{2line}(x_0, t) = \left\{ \frac{Z_{cable} - Z_{line}}{Z_{line} + Z_{cable}} \right\} v_{1line}(x_0, t) \quad (2.38)$$

$$i_{2line}(x_0, t) = \left\{ \frac{Z_{line} - Z_{cable}}{Z_{line} + Z_{cable}} \right\} i_{1line}(x_0, t) \quad (2.39)$$

From the previous section, it can be concluded that the reflection is the result of the difference in characteristic impedances. Therefore, the amount of reflections can be expressed in terms of characteristic impedances, by the reflection coefficient  $r$ . When a transmission line with characteristic impedance  $Z_o$  is terminated with a load impedance  $Z_L$ , the reflection coefficient is equal to (2.40).

$$r = \frac{Z_L - Z_o}{Z_L + Z_o} \quad (2.40)$$

The part of the travelling voltage wave that is let through is equal to the sum of the incident and the reflected wave. The consequences of voltage reflections will be discussed in more detail in the Chapters 5 and 7.

## 2.3 STEADY STATE OPERATION OF POWER SYSTEMS

The normal day to day operation of the power systems is called the steady state condition. The voltages and currents throughout the system vary with power frequency, which is either 50 Hz or 60 Hz. At 50 Hz, the wavelength of the voltages and currents is 6000 km when the wave speed equals the speed of light. An overhead line is in fact an aluminum conductor with air insulation. The relative permeability and a relative permittivity of an air insulation is close to one. This means that the propagation speed for overhead lines is close to the speed of light. A wavelength of 6000 km is in many cases large compared to the physical dimensions of the whole system and electric- and magnetic fields are quasi static. When the wavelength is large compared to the dimensions of the considered system, electric and magnetic fields may be considered separately because low frequencies cause slow variations in both the electric- and magnetic fields. A slow variation of the electric field does not contribute significantly to the magnitude of the magnetic field and vice versa. When the physical dimension of the considered system is smaller than 1/10 of the wave length of the travelling waves, this assumption is justified [35], [36]. This means that the recursive relation, presented in Maxwell's equations, between electric- and magnetic fields can be ignored for low frequency signals. Therefore, electric- and magnetic fields can be treated independent from each other. This simplification of Maxwell's equations brings advantages for modeling a transmission line at power frequency.

This means that  $E$ -field and the  $H$ -field can be stored in a capacitance and an inductance respectively and overhead lines and cables operating in steady state condition can be modeled by lumped elements  $R$ ,  $L$ ,  $C$  and  $G$  and it is no longer necessary to use distributed parameters.

A resistance with a series inductance represents the self-inductance and conductive losses of the aluminum core conductor of the line. The electric field is stored in lumped parallel capacitors being the capacitance between the conductor and the ground. For overhead lines, the capacitance is formed by the conductor and the ground, with air insulation in between. The parallel resistive losses, corona losses for instance, are negligible. An underground cable has a more complicated design. The copper core conductor is built from strands and is divided into segments. Segments are applied to reduce the influence of skin effect and proximity effect. The skin effect can be regarded as the tendency of the current distribution of an AC current in such a way that the current density is largest near the conductor surface, while it decreases with larger depth in the conductor. The proximity effect is the phenomenon that when currents are flowing through one or more conductors close to each other, the current distribution in the first conductor will be constrained to smaller regions. The core conductor is surrounded by a semi conductive layer and insulation material. Cross-linked polyethylene (XLPE) is often used as cable insulation material. In order to enable the insulation from locally high electric field strengths, it is absolutely necessary to have an insulation layer free of cavities and inclusions. A screen in combination with a metallic sheath forms the electrostatic shield of the cable. This shield serves also as return path for cable charging currents and line to ground faults in the system. The metallic sheath

is made of aluminum or lead and provides also protection against moisture and serves as armour as well. A cross section of a high voltage cable is shown in Figure 2.5.



Figure 2.5. Cross section of a high voltage cable.

A commonly used lumped-element model to represent overhead lines and cables in a steady state condition, is the so-called PI-section as is shown in Figure 2.6 [8]. The shunt capacitance is equally divided between the line ends because a line is symmetric. When an overhead line is short, this capacitance can be neglected without affecting the model accuracy significantly. In this case, the PI-section reduces to a series resistance and an inductance and the dielectric losses are ignored.

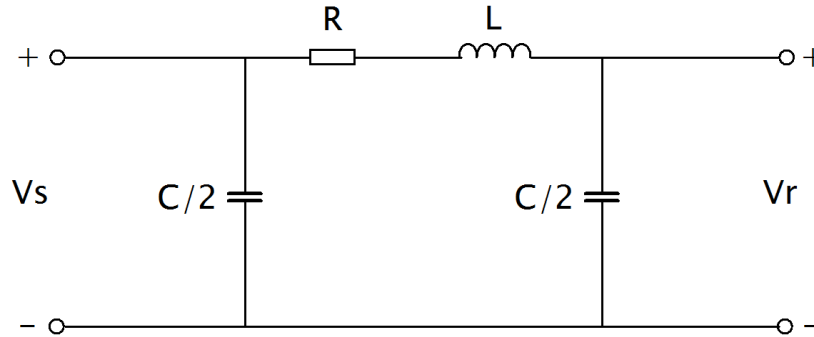


Figure 2.6. Equivalent PI section.

## 2.4 CABLE LENGTH AND TRANSMISSION CAPACITY

During operation, there is a maximum to the amount of power that can be transferred through the cable, as the maximum current is related to the thermal limit or cable ampacity. The total apparent power that flows into the cable during steady state operation, should not exceed this thermal limit. A part of this maximum allowable current is necessary for the supply of reactive power, that is responsible for the capacitive charging current of the cable.

When electric energy is transmitted by cables, it is obvious that the major part of the transmission capacity should be available for the transfer of active power and to achieve this, compensation of reactive power by shunt reactors is often required. Shunt compensation is done by installing reactors parallel to the cable. The lumped capacitors present in the PI section model are a measure for the cable charging current.

In order to enable the maximum possible active power transfer for a given cable length, the operating criterion for a long EHV cable is the equality of reactive power flows at the two terminals of the cable. The active and reactive power at the transmitted and receiving end can be calculated by (2.41)-(2.43) [6].

$$P_R = P_T = \rho S_Z \quad (2.41)$$

$$Q_R = \sigma S_Z \sqrt{1 - \rho^2} \quad (2.42)$$

$$Q_T = S_Z \sqrt{1 - \rho^2} \quad (2.43)$$

In these equations,  $P_R$  and  $Q_R$  are respectively the active power and reactive power at the receiving cable end.  $P_T$  and  $Q_T$  are respectively the active and reactive power at the transmitted end,  $\rho$  is the per unit utilization of the line. The per unit utilization is the amount of active power relative to the apparent power, described by (2.44).

$$\rho = \frac{P_R}{S_Z} \quad (2.44)$$

When  $\sigma=0$ , no reactive power is injected in the receiving network, while if  $\sigma=1$ , the amount of reactive power delivered at the receiving end is such that the cable is operating at thermal limit.

An important operational issue for AC cables is the occupation of the cable transmission capacity by its own charging current. The desired steady state operation condition of the equal reactive power flows at both cable terminals, means a unity power factor at the cable midpoint. It can be shown that the apparent power increases at the cable terminations, caused by the rising amount of reactive power. As a consequence, the power factor at the cable ends will be lower than in the middle. The operation condition and the power factor derating define the maximum cable length, which is called the maximum cable length at thermal limit, or *mcltl*. The *mcltl* is the maximum operable cable length without a shunt compensation. This number can be expressed in terms of the apparent power at thermal limit and the characteristic impedance loading (SIL) of the cable. To arrive at this expression, the expressions regarding the voltages and currents along the transmission line have to be resumed. The magnitudes of the lossless transmission constants (2.45) and

(2.46) can be used to find an expression that describes the relation between the cable power flow and its length [5].

$$A = \cos(kL) \quad (2.45)$$

$$B = Z_c \sin(kL) \quad (2.46)$$

The final expression is:

$$\frac{P_c^2 - S_z^2}{2P_c S_z} \tan(kL) = \sqrt{1 - \rho^2} \quad (2.47)$$

$S_z$  is the apparent power at rated voltage and at the thermal limit [VA];  
 $P_c$  is the characteristic impedance loading (SIL) of the cable. [W];  
 $k$  is the propagation constant of the cable;  
 $Z_c$  is the characteristic impedance of the cable [ $\Omega$ ]; and  
 $L$  is the length of the transmission line [m].

The *mcltl* is equal to:

$$mcltl = \frac{1}{k} \arctan \left[ \frac{2P_c S_z \sqrt{1 - \rho^2}}{P_c^2 - S_z^2} \right] \quad (2.48)$$

To illustrate the voltage profile and the reactive power consumption at both cable ends, a lossless cable is considered. In Figure 2.7a, a single-line diagram is shown for a lossless cable. In Figure 2.7b [6], [37], the voltage and power profiles along the cable are illustrated for a cable length equal to the *mcltl*. The maximum voltage is present in the middle of the cable. The active power flow is equal at all locations along the cable and the reactive power flow decreases when the voltage increases. When the maximum voltage across the cable is present at the sending end, the amount of active power transmission would be limited by the reactive power flow at the receiving end. The installation of shunt reactors, at both ends of the cable, makes it possible to create the desired operation condition. Shunt reactors can be designed as fixed or with a switching possibility. Switchable shunt reactors can be versatile, because by making the reactances variable, the reactive power flow along the cable can be controlled and the voltage profile of Figure 2.7b can be obtained [6], [37].



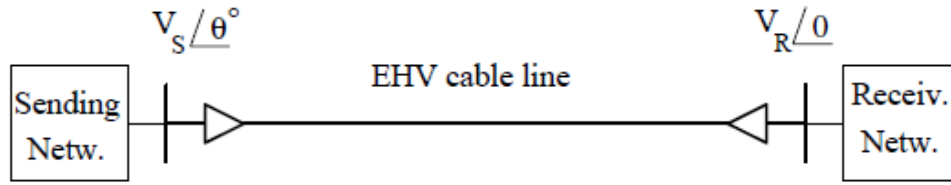


Figure 2.7a. Single-line diagram of a EHV lossless cable.

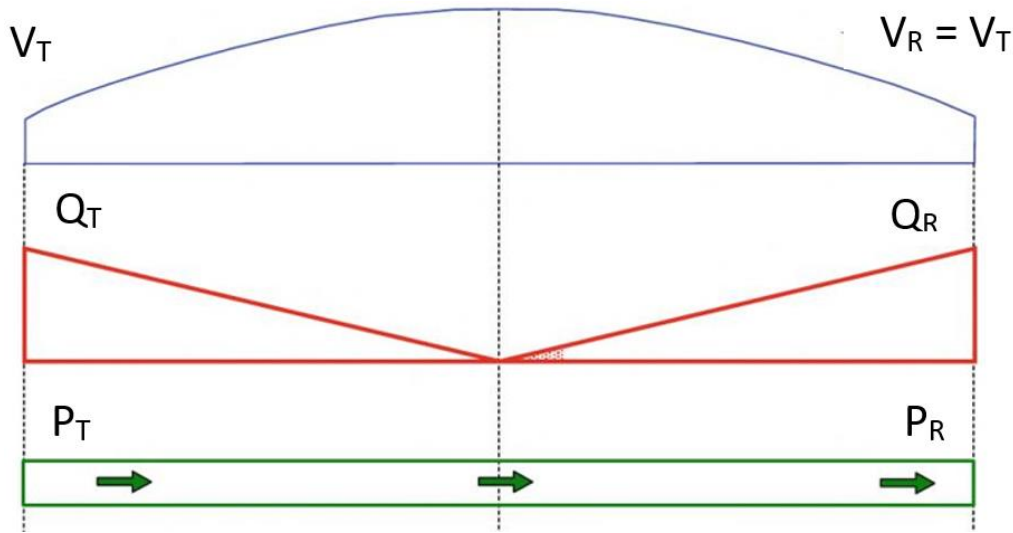


Figure 2.7b. Voltage profile along a lossless EHV cable.

## 2.5 SHUNT REACTOR SIZING AND VOLTAGE PROFILE

Applying shunt reactors in underground cable circuits influences the steady state operation and there are operational constraints when dimensioning shunt reactors for a given specific cable system [8]. A sudden voltage rise at the supply side of a mixed line-cable-line circuit, caused by no-load line energization is one of these constraints. In general, a sudden change in voltage of 3% is within the limits, but it depends of course on the netcode of the grid operator.

Another constraint is the open end overvoltage at the receiving end. Protection equipment like surge arrestors must be checked in terms of temporary overvoltage (TOV) capability. This is necessary in situations of load rejection with large power flows. When large TOV's occur, line fast switching-off at the energizing end is an option, under the condition that the breaking capability of the circuit breaker is sufficient. When shunt compensation is applied, it must be certain that the no-load current of the mixed line-cable-line circuit is

not higher than the rated line-charging breaking current of the circuit breaker. This is an important requirement in order to avoid circuit-breaker failures.

In mixed line-cable-line circuits, the current at the sending end could also be an issue. In cases where the length of the mixed circuit exceeds the critical length of the cable, shunt compensation should be applied to avoid that the current at the sending end stays below the thermal limit (ampacity) of the cable.

From the system planning point of view, some issues have to be considered regarding shunt compensation. The degree of shunt compensation is important. When a circuit consists of overhead lines only, there is a capacitive coupling between phases. During an open-phase condition, there exists capacitive coupling between the disconnected phase and the remaining energized phases. Under these conditions, line resonances can occur and can cause overvoltages throughout the system. To reduce this risk, the compensation rate of such a network, is limited to 60% to 80%. For underground cable circuits, capacitive coupling between phases can be neglected, because the cable sheath is in most cases connected to the ground. The current carrying conductors are positioned close to each other and this means that inductive coupling cannot be neglected. Compensation rates up to 100% are quite common for underground cable systems.

In this section, an example of the voltages for different shunt compensation is provided, to show the influence of the amount of compensation on the voltage profile. This example is the 400 kV cable connection between Endrup and Idomlund in Denmark [12]. To observe the voltage profile along the connection, the 400 kV cable is divided into nine sections. A schematic view of this cable connection is shown in Figure 2.8. A power flow calculation was performed for this network under N-0 condition. The voltage level at the Endrup side of the connection is fixed at 415 kV. The starting-point is a voltage level along the cable that is lower than 420 kV. The compensation rates of all eight considered scenarios are between 93.3% and 111.9%, as it can be observed from Figure 2.9 [12]. It is observed from the figure that for all compensation rates, the voltage stays below 420 kV.

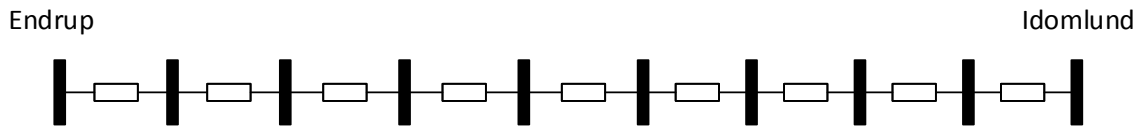


Figure 2.8. 400 kV cable connection Endrup-Idomlund.

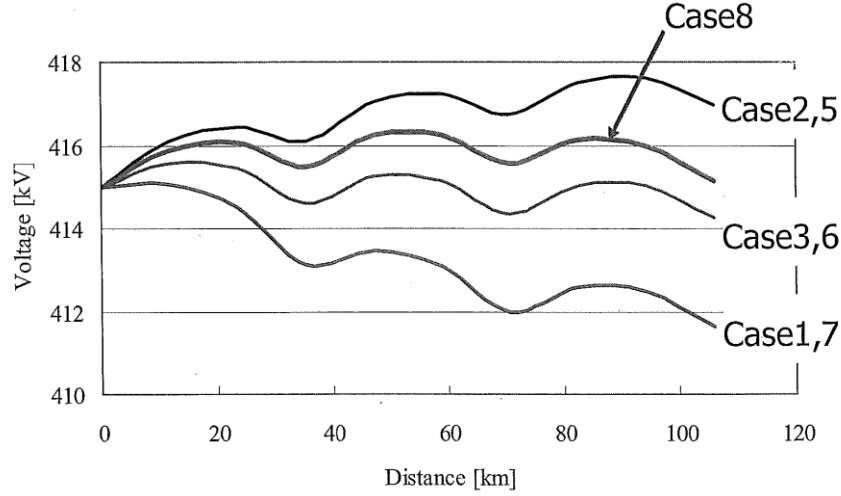


Figure 2.9. Voltage profiles along the Endrup-Idomlund for the N-0 condition [11].

The computation was done in the case of failure of one of the shunt reactors at the open end of the cable. It was observed that in this N-1 situation, not every compensation scheme was able to maintain the voltage level within the specified limit. The best way of compensation is case 8, as shown in figure 2.10 [12]. The compensation rate in this case equals 99.5%. The voltage profiles for the shunt compensated cable system in the Dutch Randstad 380 kV project, are discussed in detail in Chapter 4.

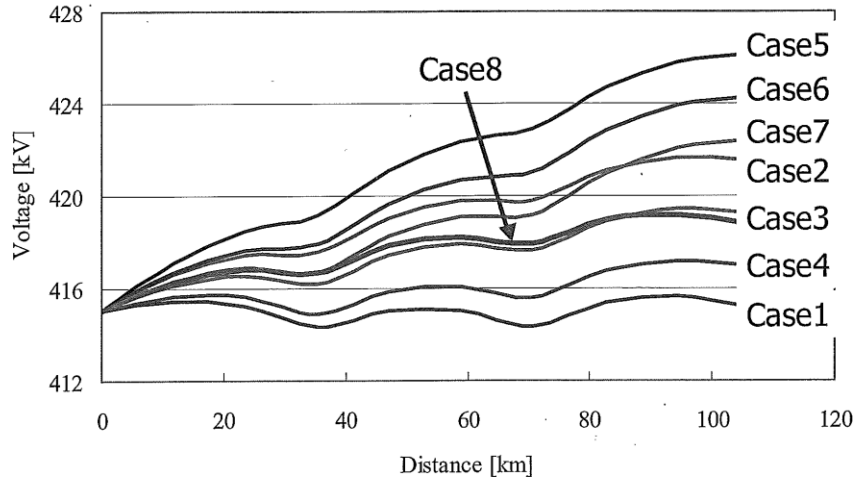


Figure 2.10. Voltage profiles of the along the Endrup-Idomlund for the N-1 condition [11].

## 2.6 CONCLUSION

This chapter gave a description of the electromagnetic field theory and this was used as a base for the modeling work of transmission lines during steady state and transient

phenomena. Maxwell's equations are used as a base for deriving suitable transmission line models. For slow variations of the  $\mathbf{E}$ - and  $\mathbf{H}$ -field, Maxwell's equations can be simplified and this means that the PI model is a suitable representation of a cable and an overhead line when it is considered at the 50 Hz power frequency. Therefore, the PI model will be used for investigating the steady state behavior of both the overhead and underground sections in the Randstad 380 kV (Chapter 4). For transient studies, higher frequencies are involved and this means that using a travelling wave model that accounts for the frequency dependency of the transmission line parameters is necessary. The results from [12], showed that the amount of shunt compensation has a large impact on the steady state voltage level along the 380 kV cable connection. Therefore, it can be concluded that reactor sizing and monitoring the voltage level in the grid are important when applying cables. The transmission line modeling approach based on the simplification of Maxwell's equations, is applied in this thesis for a particular 380 kV transmission system, but it can be used for system impact studies where transmission line modeling forms an important part of the work.

## **CHAPTER 3**

# **CABLE MODELING ISSUES AND SYSTEM PERFORMANCE**

### **3.1 INTRODUCTION**

An accurate simulation model for an underground cable system is necessary for transient studies. In this chapter, the theory behind cable modeling is outlined and attention is paid to the underlying phenomena and their origins. The modeling approach for the Randstad 380 kV cable connection is described in more detail in chapter 5. In section 3.2, the mutual coupling between the conductors in an underground system is analyzed. Another issue with respect to the grounding of a cable system is the cross-bonding of the cable screen conductor. Different grounding principles and cross-bonding of the cable screen conductor are explained in section 3.3. The configuration of the cable system with respect to the cable's sheath and its core material is discussed in section 3.4 and the impact of the cable earth return impedance on the mutual coupling is outlined in section 3.5. Section 3.6 describes the origins of temporary overvoltages in shunt compensated cable systems. Another issue related to switching in shunt compensated cable systems, is the zero-missing phenomenon. This is treated in section 3.7.

### **3.2 MUTUAL COUPLING IN AN UNDERGROUND CABLE SYSTEM**

An important aspect that influences the system performance of an underground cable connection is the mutual coupling between the conductors which are inductive or capacitive. When two or more cable conductors are close to each other, there is a noticeable coupling between the conductors when they carry a large current. The currents produce a strong magnetic field close around the conductor. This magnetic field induces voltages in adjacent cable conductors. The origin of the magnetic coupling stems from the fact that

magnetic fields lines are circular, as it follows from the fourth equation of Maxwell (Chapter 2). The continuity of magnetic fields lines means that the field lines have no starting and no end points and conductors in the vicinity of the current carrying conductor, cannot be screened from the magnetic field lines created by the power current.

The strength of this mutual inductive coupling is described in terms of the mutual inductance present between the conductors. The strength of the magnetic coupling depends on the arrangement of the conductors and is determined by the magnetic flux that passes through the other conductor. The shorter the distance between two conductors, the stronger the inductive coupling. With a transmission capacity of 2600 MVA of a circuit in the Randstad 380 kV connection, currents up to 2 kA flow through the cable core conductors, as the circuit consists of 2 cables per phase. This results in a strong magnetic field around the conductor when the cable system is in service. The strength of this magnetic field decreases with the distance, but induces voltages in neighboring cables. The magnitude of the induced voltages in a conductor depends on the frequency of the alternating magnetic fields (Faraday's law). The higher the frequency, the larger the induced voltage. The frequency dependency means that the magnitude of the induced voltage is larger for higher frequencies. For instance, when fast transients are present after a lightning stroke on an overhead line, high frequency oscillations are generated as a result from reflecting and refracting travelling waves. When a steep lightning current front reaches the cable, a large voltage is induced in the adjacent cable conductors. In the Randstad 380 kV underground cable system, the average distance between the cable conductors is relatively small and attention must be paid to the magnetic coupling, when modelling the cable.

Insulating material between two conductors creates a capacitor. Capacitive coupling is the result of a potential difference between two or more conductors, separated by material that acts as a dielectric. For cables, different materials play a role in forming the dielectric. For overhead lines, the insulating "material" is the air.

For underground cables, there are insulation layers from the cable itself, the semi-conductive cable layers and the soil that contribute to the dielectric permittivity. In practice, the screen conductor of the high-voltage cable is usually connected to the ground to bring the cable at earth potential. In this way, the electric field is kept inside the cable and electrostatic screening is achieved because by grounding the screen conductor, a starting point and an end point for the electric field lines is created. The source of the electric field arises from the core conductor potential and the end point is at earth potential. As a consequence, the cable is electrically isolated from its surroundings. This avoids capacitive coupling, as there is no potential difference among the different cable screens. For power cable applications, grounding of screen conductors is the solution to avoid capacitive coupling between the conductors.

For accurate cable modeling, it is necessary to take the mutual coupling between cable conductors into account and this increases the complexity of cable system modeling work. Mathematical expressions can be derived for both the self and mutual impedance of the

cables in an underground system [38], [39]. The calculations taking into account the mutual coupling is illustrated in this section for a cable system containing two-layer coaxial cables without ground return path. The ground return path in an underground cable system will be treated in paragraph 3.5. Figure 3.1 shows one of the two cable circuits of the Randstad 380 kV connection under construction, with 6 cables in parallel.



Figure 3.1. Cable circuit of the Randstad 380 kV connection.

A cable system is fully characterized by its  $Z$  and  $Y$  parameters. For Telegrapher's equations (Chapter 2) applied to a multi-conductor transmission line system, the impedance  $Z$  and the admittance  $Y$  are square matrices and  $V$  and  $I$  are vectors. The elements of both the  $Z$  and  $Y$  matrices are different for overhead lines and underground cables, because of the mutual coupling between the adjacent conductors and the ground return. Solving these matrices for underground cables is more cumbersome than for overhead lines, since there is a mutual coupling between the different conducting layers for instance. Let us first look at the  $Z$  matrix of an underground cable. Figure 3.2a [40] shows the cross-section of a two-conducting layer single-core cable, having a core with two conductors and two insulation layers. The impedance of such a cable is represented with matrix elements that are shown in Figure 3.2b [40].

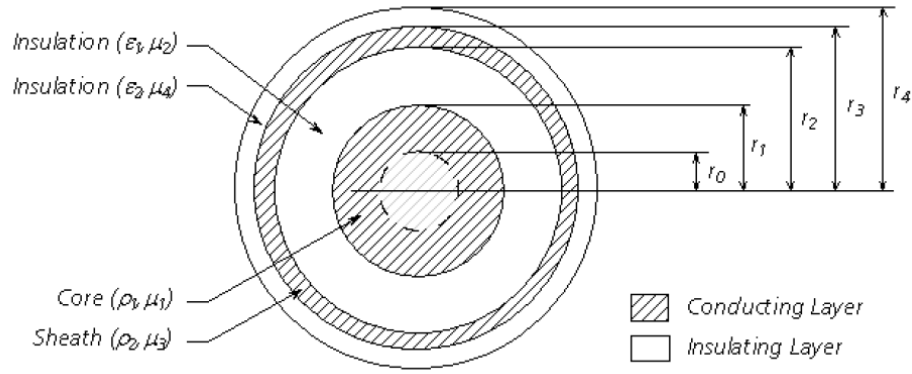


Figure 3.2a. Cross-section of a two-layer coaxial cable.

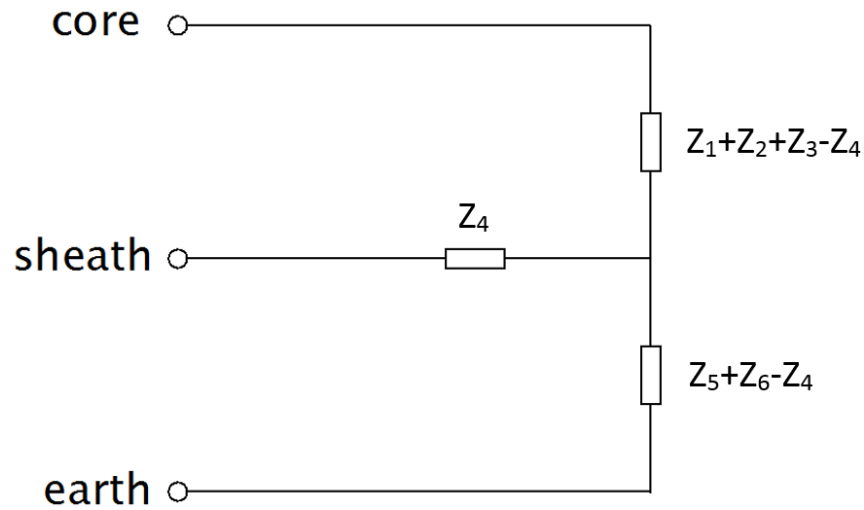


Figure 3.2b. Impedance elements of a two-layer coaxial cable.

The series impedance matrix  $\mathbf{Z}$  of an underground cable system is built with these impedances. In general, this impedance matrix consists of two parts:

$$\mathbf{Z} = \mathbf{Z}_{\text{in}} + \mathbf{Z}_{\text{r}} \quad (3.1)$$

In (3.1),  $\mathbf{Z}_{\text{in}}$  contains the internal impedance elements of the cable system and  $\mathbf{Z}_{\text{r}}$  contains the return impedances from the earth. When the underground connection system consists of  $n$  single core cables, these matrices are of the size  $n \times n$  with the impedance elements from (3.2).



$$\mathbf{Z} = \begin{bmatrix} \mathbf{Z}_{in_1} & \cdots & \mathbf{0} \\ \vdots & \ddots & \vdots \\ \mathbf{0} & \cdots & \mathbf{Z}_{in_n} \end{bmatrix} + \begin{bmatrix} \mathbf{Z}_{r_{11}} & \cdots & \mathbf{Z}_{r_{1n}} \\ \vdots & \ddots & \vdots \\ \mathbf{Z}_{r_{1n}} & \cdots & \mathbf{Z}_{r_{nn}} \end{bmatrix} \quad (3.2)$$

The elements of the matrices of (3.2) are the single core cable internal impedances and are in general sub-matrices. In general, the elements of (3.2) are written as a sub-matrix with the self and mutual impedances of the cable:

$$\mathbf{Z}_{in_i} = \begin{bmatrix} Z_{cc_i} & Z_{cs_i} \\ Z_{cs_i} & Z_{ss_i} \end{bmatrix} \quad (3.3)$$

The matrix elements in (3.3) are the impedance elements shown in Figure 3.2b:

$$Z_{cc_i} = Z_1 + Z_2 + Z_3 + Z_5 + Z_6 - 2Z_4$$

$$Z_{cs_i} = Z_5 + Z_6 - Z_4$$

$$Z_{ss_i} = Z_5 + Z_6$$

where:

$Z_{cc_i}$  - Cable core self-impedance [ $\Omega$ ]

$Z_{cs_i}$  - Impedance between cable core and sheath [ $\Omega$ ]

$Z_{ss_i}$  - Cable sheath self-impedance [ $\Omega$ ]

An exact evaluation of the internal impedances is a complex task. A method to calculate the internal impedances  $Z_1$  to  $Z_6$  requires the use of Bessel functions [40]. The Bessel function approach is an accurate way to express the impedances, since these equations use the characteristics of the conductor impedances. The Bessel function based expressions for the impedances  $Z_1$  to  $Z_6$  are in Appendix A.

The elements of  $\mathbf{Z}_r$  are the cable earth return impedances and these are generally also sub-matrices. The elements of the earth return sub-matrix  $\mathbf{Z}_{r_{ij}}$  are the earth return mutual impedances between cables  $i$  and  $j$ :

$$\mathbf{Z}_{r_{ij}} = \begin{bmatrix} Z_{r_{ij}} & Z_{r_{ij}} \\ Z_{r_{ij}} & Z_{r_{ij}} \end{bmatrix} \quad (3.4)$$

The shunt admittance matrix  $\mathbf{Y}$  for a single-core cable system with  $n$  cables is based on the potential coefficient matrix  $\mathbf{P}_{\text{in}}$ , given by (3.5).

$$\mathbf{P}_{\text{in}} = \begin{bmatrix} \mathbf{P}_{\text{in}_1} & \cdots & \mathbf{0} \\ \vdots & \ddots & \vdots \\ \mathbf{0} & \cdots & \mathbf{P}_{\text{in}_n} \end{bmatrix} \quad (3.5)$$

The elements of this diagonal matrix  $\mathbf{P}_{\text{in}}$  are generally matrices with the internal potential coefficients. The submatrix  $\mathbf{P}_{\text{in}_1}$  is equal to:

$$\mathbf{P}_{\text{in}_1} = \begin{bmatrix} P_{c_j} + P_{s_j} & P_{s_j} \\ P_{s_j} & P_{s_j} \end{bmatrix} \quad (3.6)$$

The elements in this submatrix (3.6) are:

$P_{c_j}$  - core potential coefficient

$P_{s_j}$  - sheath potential coefficient

The mathematical expressions for the potential coefficients of (3.6) are given in Appendix A. Using  $\mathbf{P}_{\text{in}}$ , the shunt admittance matrix  $\mathbf{Y}$  is equal to (3.7). Since the considered system is an underground system,  $\mathbf{Y}$  has null off-diagonal elements since the surrounding earth acts as an electrostatic shield [40].

$$\mathbf{Y} = j\omega\mathbf{P}_{\text{in}}^{-1} \quad (3.7)$$

### 3.3 GROUNDING AND CROSS BONDING OF THE CABLE SCREEN CONDUCTOR

When the power system operates in a steady state, the system is assumed to be balanced, meaning that the load is equally divided over the three phases. The cable screen conductor is in practice at earth potential, so the screen forms a return path for the charging current of the cable and a path for fault currents. Fault currents can have large values and when the cable screen is grounded at one cable end only, large voltage can appear at the ungrounded cable end. During steady state operation, a 50 Hz current is flows through the core of the

cable. This creates an alternating magnetic field around that cable and also currents are induced in the cable screen conductor. The induced screen currents cause resistive losses and has a negative impact on the performance of the cable system as a whole. The way of grounding of the screen conductor has influence on these losses [4].

A possible method of grounding is when the screen conductors of the three cables are connected to each other and grounded at one cable. The losses in the screen are reduced but a high voltage proportional to the cable length is induced at the screen open end. To avoid these induced voltages at the screen end, this grounding method is only used for short cable lengths [41]. Another way of grounding is connecting the screens together and grounding them at both cable ends. There is no large reduction in losses for this configuration, because there remains still a closed loop for the current to flow. The induced voltage at the screen is, however, canceled.

Basically, there are three ways for grounding the cable screen. The first method is to ground the screen at both cable terminals, see Figure 3.3 [42]. The screen can also be grounded at one side of the cable only, see Figure 3.4 [42].  $I_{cc}$  is the current in the cable core conductor and  $I_{cs}$  is the cable screen current. Several parameters are affected by the way of grounding of an underground cable system [42]:

- The current rating of the cable circuit itself;
- The earth impedance of substations;
- The return currents through the earth and
- The positive and zero sequence impedance.

When the screen is grounded at both cable terminals, a circulating current flows through the screen conductor, induced by the magnetic field of the conductor and the closed loop that is formed by the cable screen. A circulating current is creates additional losses in the cable system. Due to these extra screen losses, the current rating of the cable is changed.

In the situation of both side grounding, there is no induced voltage in the cable screen loop, since this is compensated by the circulating current. The values for the zero-sequence impedance are normally lower compared to the situation with one side grounding.

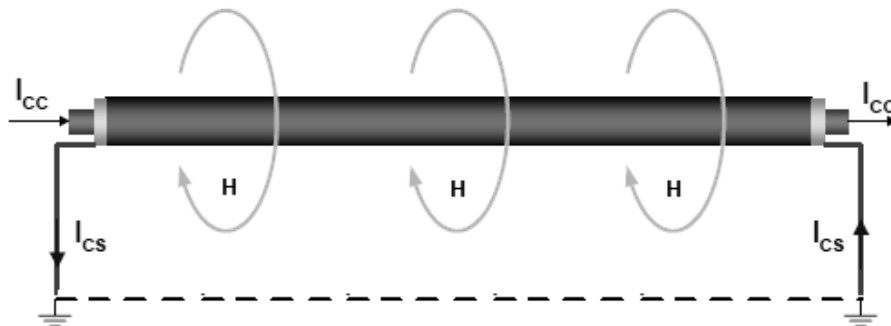


Figure 3.3. Grounding at both cable sides.

When the screen is grounded at only one side, no circulating currents can flow as the screen is open, but an induced voltage appears at the open cable screen end. In this situation, the cable ampacity is larger compared with the case when both sides are grounded, since the losses are much less. The zero-sequence impedance is larger than for the case with both sides grounded. The reason for this is that the average return distance of the current in the earth is in the range of 1000 m. [42] and this gives a larger value for the inductive component of the zero-sequence impedance.

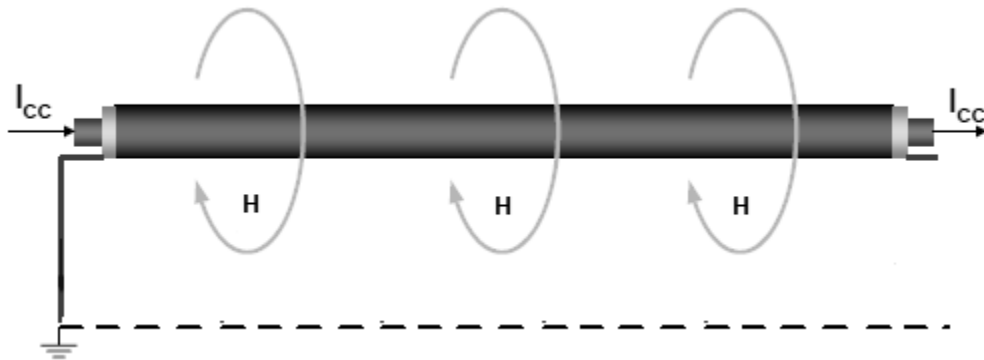


Figure 3.4. Grounding at only one cable side.

The third method is cross bonding of the cable screen conductor. Cross bonding of screen conductors is a widely applied method of grounding of underground cable systems. When using cross bonding, also grounding of the screen conductors at both cable ends is necessary to reduce the screen overvoltages. Reduction of the screen overvoltages can be achieved in this way, since the grounding impedance is small. Cross bonding is done for long cable sections and the cable needs to be divided into major and minor parts. In Figure 3.5, the principle of cross-bonding of the cable screen conductor is drawn for a three phase underground cable system that has three cables. The figure shows a major part of a cross-bonded cable system, having three minor sections and as it can be seen, cross-bonding of the screen conductor is done for every smaller section. For each major section, the screen conductors are connected to ground. This way of bonding the screen conductors is done along the complete cable length. In practice, special cables are used for cross-bonding the screen conductor of the high-voltage cable. This makes cross-bonding an important issue for cable system modeling work, that is discussed in more detail in Chapter 5.

In the Randstad380 project, cross-bonding of the screen is also applied to the 10.8 km high-voltage cable. To do this, the cable is divided into four major sections of 2.7 km each. Each major section has three minor sections and this means that cross bonding is done every 0.9 km.

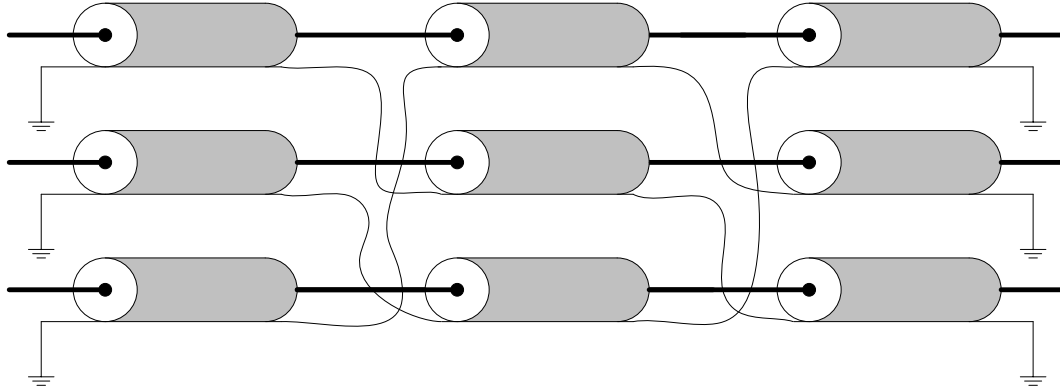


Figure 3.5 Cable screen cross bonding principle.

The induced screen currents in a three phase cable system are 120 degrees out of phase from each other and for a balanced three phase situation, the sum of the screen currents equals zero. But in practice, there is always an unbalance in voltages and currents also caused by imperfections of the cable layout. Cross-bonding of the screen conductor and transposition of the core conductor are sometimes applied to balance the cable system as such. Dividing the cable length into sections creates the possibility for transposition of the core conductors similar as transposition of the phase conductors of overhead lines. Some countries practice cross-bonding of the phase conductors as well.

### 3.4 CABLE CONFIGURATIONS

Another important issue for the modeling work in an underground cable system, is the cable configuration itself. Cables are manufactured in different ways with respect to the core, conductor material and sheath. Depending on the voltage level, cables are manufactured as single-core and three-core configuration [43]. The electric field strength is an important parameter in high-voltage equipment since it is the stress parameter for the insulation that influences the lifetime of the material. In order to reduce the electric field strength at the surface of the cable core conductor, cables at a high-voltage level, must have a thicker core conductor compared to cables for a low voltage level and for high voltages, a thicker insulation layer is necessary. Cables applied in high-voltage systems are usually manufactured as single-core cables for a practical reason: transportation. In the new 10.8 km underground cable section of the Randstad380 project, single-core cables are used. As already mentioned, the cables are buried in soil and are positioned in a horizontal flat arrangement. This will be discussed in more detail in Chapter 5.

At lower voltage levels, two types of cables are generally used. At distribution voltage levels, from 10-20 kV, belted cables are common with three core conductors in a triangular form in one sheath. Another possible construction is with three conductors positioned in triangular form and each conductor having its own sheath. This is comparable to the configuration of three single core cables. For both cable types, the three cables are inside a metallic pipe or inside an insulating pipe. In the case of a metallic pipe, the cable can be

modeled as a so called pipe-type cable [44], [45]. In this configuration, the steel pipe is filled with a pressurized oil or gas. In another Dutch 380 kV connection, a water crossing is the barrier to be crossed and the cables are laid in a steel pipe. The representation and modeling of a pipe-type cable is nowadays available in simulation software. Apart from different configuration with respect to the cable sheath, there are also different possible constructions of the core conductor. The cable core conductor can be made from copper or from aluminum and can be stranded, segmented or solid. Aluminum has a lower density, resulting in less weight for a given cable length compared to copper. The advantage of copper is that it has a lower specific  $\Omega$ ic resistance as aluminum. In case of a lower specific resistance, a smaller conductor thickness is required for a specified maximum current capacity of the cable.

### 3.5 CABLE GROUND RETURN IMPEDANCE

The electromagnetic field theory is the base for transmission line modeling. The EM-field around a transmission line is not only affected by the electric and magnetic properties of the line itself, but also by the condition of the conducting ground. In both overhead lines and underground cable systems, impedances exist between the conductive layers of the transmission lines and between cables and ground conductor. In general, the electrical parameters of underground cables are frequency dependent, because of the skin effect of the conductors and relaxation phenomena in the dielectric materials. The transient behavior of an underground cable system is influenced by the electrical properties of the ground. In this paragraph, an underground cable system is considered with the ground return path taken into account. The ground return impedance depends on the material and geometric properties. For the calculation of the ground return impedance for overhead lines, equations were given by J.R. Carson in 1926 [40], [46]. These equations contain infinite integrals with complex arguments, which are not easy to be solved [47]. Evaluation of the mutual coupling between conductors including the earth return impedance is therefore a difficult task. In most situations, an exact evaluation of the earth return impedance is even impossible. Therefore, numerical approximation techniques have been developed and widely used for overhead transmission line modeling. An expression for the earth return impedance is obtained by numerical integration of Carson's integral, as described in [40]. Similar as for overhead lines, evaluation of the ground return impedance for underground cable systems is also a complicated affaire. A calculation method is developed by Pollaczek in 1931 [48]. This calculation contains integrals that define an electric field vector at a point within a homogeneous ground. The problem with the Pollaczek integral is that it is formulated in the form of an infinite integral. Several numerical approximations have been made for solving the Pollaczek integral. A widely applied approximation of the Pollaczek integral was described by Wedepohl and Wilcox [49]. The result of this work is an expression for the self and mutual impedance of the cables including the ground return path. These approximations for the mutual coupling including the earth return impedance have been implemented in EMTP simulation programs. In this paragraph, the mutual impedance of an underground system with ground return is considered. The equation for the mutual impedance with earth return in an underground system is described by the Pollaczek integral, which is given by (3.8).

$$Z_{r_{ij}} = \frac{\rho m^2}{2\pi} \int_{-\infty}^{\infty} e^{j\alpha x_j} \left[ \frac{e^{-(h_i+y_i)\sqrt{\alpha^2+m^2}}}{|\alpha| + \sqrt{\alpha^2+m^2}} + \frac{e^{-(y_j-h_j)\sqrt{\alpha^2+m^2}} - e^{-(y_j+h_j)\sqrt{\alpha^2+m^2}}}{2\sqrt{\alpha^2+m^2}} \right] d\alpha \quad (3.8)$$

An analytical approximation for the Pollaczek integral was developed by Wedepohl and Wilcox [12]. The approximations for both the self and mutual parts of the earth return impedance  $Z_{r_{ii}}$  and  $Z_{r_{ij}}$  between the cables  $i$  and  $j$  is given by respectively (3.9) and (3.10).

$$Z_{r_{ii}} = j\omega \frac{\mu}{2\pi} \left( -\ln \left( \frac{\gamma m r_i}{2} \right) + \frac{1}{2} - \frac{4}{3} m h_i \right) \quad (3.9)$$

$$Z_{r_{ij}} = j\omega \frac{\mu}{2\pi} \left( -\ln \left( \frac{\gamma m d_{ij}}{2} \right) + \frac{1}{2} - \frac{2}{3} m \sum h \right) \quad (3.10)$$

In (3.9) and (3.10):

$\mu$  - Ground return relative permeability [H/m];

$\gamma$  - 1.7811 Eulers's constant;

$r_i$  - Outer radius of the  $i^{\text{th}}$  cable [m];

$d_{ij}$  - Distance between the center points between the  $i^{\text{th}}$  and the  $j^{\text{th}}$  cable [m];

$h_i$  - Depth of the  $i^{\text{th}}$  cable (center point) below the ground surface [m];

$m = \sqrt{\frac{j\omega\mu}{\rho}}$  - inverse depth of penetration;

$\sum h$  - sum of the depths of  $i^{\text{th}}$  and  $j^{\text{th}}$  cable; and

$\alpha$  - integration variable [50].

### 3.6 TEMPORARY OVERVOLTAGES (TOV)

Transients in power systems can result in large overvoltages at different locations in the network. Depending on the origin of the transient, overvoltages are divided into switching overvoltages, lightning overvoltages and temporary overvoltages. During switching actions, a part of the network is connected to or disconnected from another part by closing or opening of a circuit breaker. The origin of switching overvoltages in a shunt compensated cable system is the oscillation between the inductive shunt reactor and the capacitive cable [51]. Switching overvoltages will occur for instance during the energization time of an unloaded cable or when the shunt reactors are switched on or off. The amplitude of the resulting overvoltages depends on the instant of switching and will decrease rapidly over time. The decaying time depends on the damping in the system. Simulation results of switching actions performed on cable systems will be discussed in Chapter 6. Lightning overvoltages result from lightning discharge currents that are injected into the power system. The impact of lightning discharge currents on the voltages in the power system is discussed in Chapter 7.

Temporary overvoltages (TOV) exist for a longer period of time than switching transients (up to a few seconds). TOV are caused by resonances and ferro resonances in the system, by single phase to ground faults or by the Ferranti phenomenon. Fault disconnection can result in oscillatory overvoltages in the circuit in case of a three phase fault [12]. In such a situation, the resulting overvoltage is caused by two overvoltages with different frequencies. The principle of this situation is illustrated by a simplified circuit, shown in Figure 3.6. A single phase representation is given of a three phase to ground fault that exists at the cable end. The cable and the shunt reactor are represented by a lumped capacitance  $C$  and  $L$  respectively. The power supply side is represented by the voltage source  $V_s$  and the inductance  $L_0$ . When the circuit breaker opens, oscillations occur between cable capacitance and shunt reactor. The frequency of this oscillation is determined by  $L$  and  $C$ . There is also an oscillation at another frequency, caused by  $L_0$  and  $C$ . The overvoltages that appear in the system are the result of superposition of these two oscillations.

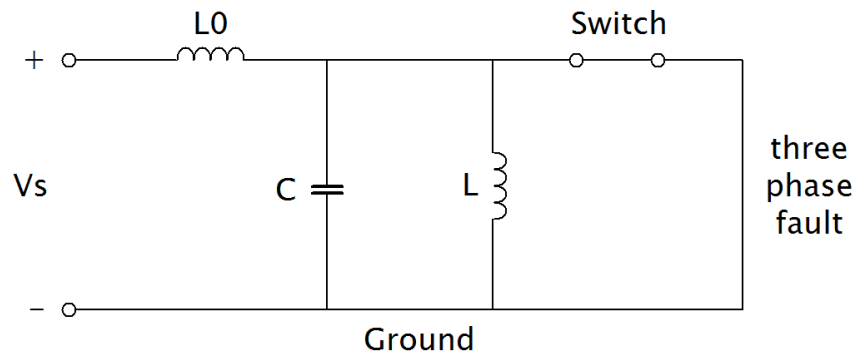


Figure 3.6. Scheme to illustrate a three phase to ground fault.



The Ferranti phenomenon is the voltage rise at the receiving end of a long unloaded or lightly loaded transmission line. This voltage rise is due to the capacitive cable charging current that causes a voltage drop across the line inductance. In case of a small load current, the current drawn by the cable is mainly formed by the cables charging current and the magnitude of the charging current is proportional with both the cable length and the applied power voltage. The voltage rise observed at the receiving cable end is a phenomenon occurring mainly with long cables at a high-voltage level. Since the Ferranti effect shows up at steady state condition, only the power system frequency is involved meaning that the voltage rise can be illustrated by representing the unloaded cable by a PI-section model, as is shown in Figure 3.7. At the sending cable end, a power voltage is applied. For the calculation of the receiving cable end voltage, the series resistance and the shunt conductance can be neglected since they are much smaller than the reactance. The voltage at the receiving cable end is equal to:

$$V_s = V_r \left( 1 - \frac{1}{2} \omega^2 LC \right) \quad (3.11)$$

where:

$V_s$  - transmission line sending end voltage (V);

$V_r$  - transmission line receiving end voltage (V);

$L$  - transmission line self-inductance (H/m); and

$C$  - transmission line capacitance (F/m).

From (3.5), it can be seen that the receiving cable end voltage is larger than the sending end voltage, since the frequency, the inductance and the capacitance have a positive value. In Chapter 4, steady state voltage rise in cables will be discussed in more detail.

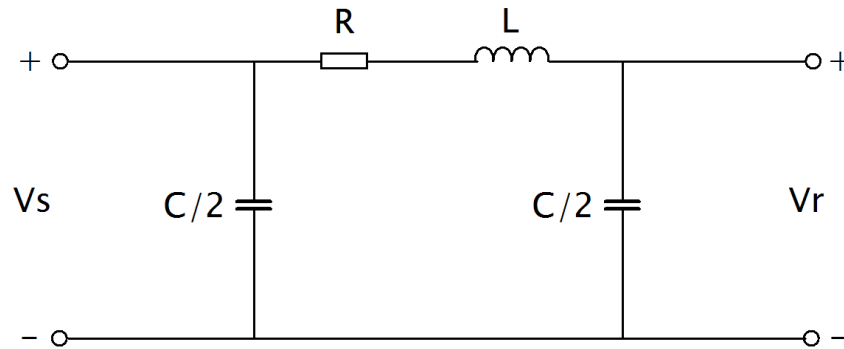


Figure 3.7 PI-section to illustrate the Ferranti effect.

### 3.7 ZERO MISSING PHENOMENA

The zero-missing phenomenon is an important issue for switching in a cable system with shunt compensation coils. The zero-missing means that the AC current is not crossing zero for several cycles of the power current, caused by the DC component in the current. This may occur for instance when an unloaded shunt compensated cable connection is energized. When the current is not passing zero, it is not possible to open the circuit breaker without risk of damage during the energization period of the cable. To understand the origin of the zero-missing phenomenon, a simple representation of a shunt compensated cable system is considered, modeled with lumped circuit elements. The cable is modeled as a lumped capacitance and the shunt reactor coil as a lumped inductance with a small resistance in series to account for the losses. The shunt compensated cable system is modeled by the capacitance in parallel with the inductance, according to Figure 3.8 [15], [16]. During the energization period, the currents in the capacitor and the inductor are in phase opposition. Moreover, the peak of the DC component depends on the instant of switching. The phase shift between the inductor voltage and the current is 90 degree. The inductor current is continuous in time and can have a DC component with an amplitude equal to the amplitude of the AC component when connected at zero voltage. When the cable is switched in at a peak voltage, there is no DC component, but there can occur large switching overvoltages. The value of the DC component decreases over time and depends on the amount of attenuation in the circuit. Since the small series resistance of the shunt reactor forms the only attenuation in the system, it takes several cycles before the DC component has disappeared. This DC component prevents the current through the breaker from crossing zero until the DC component is less than the AC component.

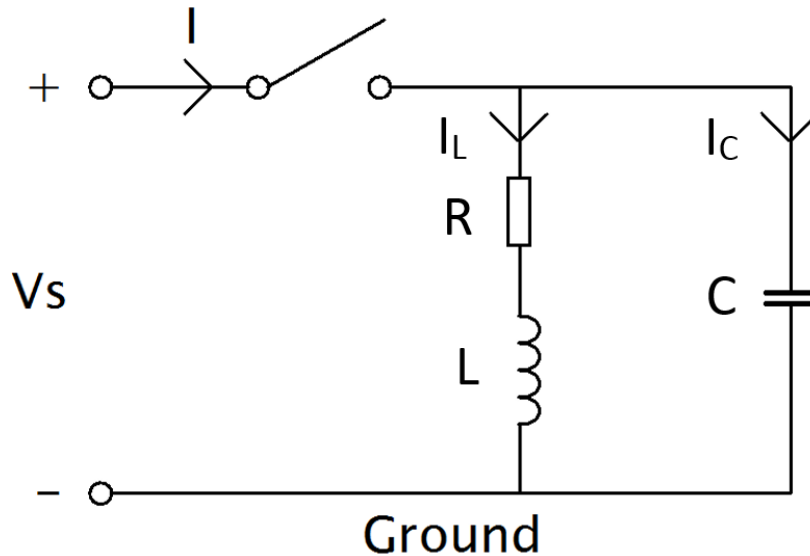


Figure 3.8. Scheme to illustrate the zero-missing phenomenon [4].

Several countermeasures are available to reduce or to eliminate the zero-missing phenomenon [15]. A possibility to reduce the initial current DC component is to connect

and disconnect the shunt reactor by a circuit breaker when the voltage is at a peak value [52]. When the shunt reactor is connected directly to the cable, the insertion of a resistor is another way to reduce the zero-missing phenomenon. This resistor can be considered as a resistance that is placed in parallel to the breaking chamber of the circuit breaker. In [16], method is described to find an optimal value for this resistor. By placing such a resistor, the circuit is able to attenuate the DC component within 10 ms. This countermeasure forms a compromise between reduction of the zero-missing phenomenon and switching overvoltages.

### 3.8 CONCLUSION

In this chapter, it was outlined that an underground cable system can be described by its impedance and admittance matrices,  $\mathbf{Z}$  and  $\mathbf{Y}$  respectively, including both the mutual coupling between the conductors and the ground return impedance, which is not easy to determine. All elements of the cable impedance matrix should be determined in order to model an underground cable system with a ground return. Having a cable system that contains two circuits with 6 cables each, as it is the case in the Randstad 380 kV project, the modeling work is of such a system is complicated because of the mutual coupling (Chapter 5). Grounding the cable screen conductor is an important issue since it has impact on several parameters that influences the performance of the cable system. Different ways of grounding a cable screen conductor were described and for long cables, such as in the Randstad 380 kV project, cross-bonding of the screen conductor is applied in order to equalize the screen voltages. For applying cross-bonding, the 10.8 km cable system must be divided into parts. Applying cross-bonding has an impact on the modeling work, since special cables are used for interconnecting the cable screen conductors on every 0.9 km (Figure 3.5). The way to find the elements of both the impedance and the admittance matrix of the particular underground transmission system and the description of the grounding and cross-bonding configurations is not restricted to the particular mixed line-cable-line circuits in the Randstad 380 kV project, but can be seen as general issues that play when modeling an underground transmission system.

## **CHAPTER 4**

# **STEADY STATE ANALYSIS OF 380 KV MIXED OVERHEAD-LINE UNDERGROUND CABLE**

### **4.1 INTRODUCTION**

The presence of long underground cables in the Dutch 380 kV grid has impact on the steady state system behavior, as it is already mentioned in Chapter 2. The generation of reactive power by the cables itself is one of the major issues. Reactive power produced by cables can result in a voltage rise at the adjacent substations. When the Transmission System Operator (TSO) make the decision to have cable sections in their grid, it is important to know in advance whether this voltage rise will stay within allowable limits. The permissible range for steady state voltages is laid down in the net code of the TSO. For the Dutch 380 kV grid, the steady state voltage level may vary from 90% to 110% of the nominal rated voltage; so between 342 kV to 418 kV for 380 kV. In this chapter, the steady state voltage levels are studied at the Dutch 380 kV substations, when cable sections are integrated in the Randstad network. We want to learn the voltage rise stemming from the reactive power generation of the cables. In section 4.2, the calculation setup and the used input data is discussed. Section 4.3 gives the results obtained and in section 4.4, the influence of the installed shunt compensation reactors on the steady state voltage profile and on the actual power flow in the grid is outlined.

## 4.2 EARLY LOAD FLOW AND CONTINGENCY STUDY ON THE 380 KV GRID

Before the Randstad 380 kV project started, an early study was done on the Dutch 380 kV grid to know the reliability of the grid with both cables and overhead lines. In spite that only on a very limited number of studies are available, it is common knowledge that the reliability of cable circuits is less than that of circuits with overhead lines only. The mean time to repair (MTTR) for instance for a cable circuit is much longer compared to an overhead line. This has important consequences with respect to the unavailability of power to be supplied and this makes the reliability analysis of a mixed cable OHL system of vital importance [54]. In this chapter we look at the impact on the reliability of power supply for 20 km underground cable. The Dutch TSO TenneT made, together with the minister of economic affairs, the decision to limit the cable length to 20 km in order to avoid an unacceptable risk for the security of power supply in the Netherlands [53]. The steady state behavior analysis of the Randstad 380 kV grid is done by means of load flow and contingency studies.

Load flow calculations and a contingency analysis give the TSO insight in the steady state voltage and the flow of power in their network and enables them to monitor overloading of transformers, lines and cables. A contingency study gives insight in power flows and voltage levels during  $n-1$  and  $n-2$  conditions. In this work, the  $n-1$  condition during maintenance is tested. Although the  $n-1$  condition during maintenance is strictly speaking not the same as the  $n-2$  condition, it is called  $n-2$  in this work for convenience.

A load flow calculation gives the voltages (in magnitude and in angle) and also the active and reactive power flowing towards and from the network nodes. For each node of the system 4 variables describe the actual state.

1	Voltage magnitude $ V_i $	[V]
2	Phase angle of the voltage $\delta_i$	[°]
3	Active power $P$	[W]
4	Reactive power $Q$	[VAr]

The voltage at node  $i$  of a network consisting of  $N$  nodes, is written by (4.1) [43], [58].

$$V_i = |V_i| \angle \delta_i = |V_i| (\cos \delta_i + j \sin \delta_i) \quad (4.1)$$

The total current injected into the grid at node  $i$  can be written in terms of the elements of the admittance matrix  $\mathbf{Y}$  of the grid. The admittance between node  $i$  and  $j$  can be expressed in polar form as well as in Cartesian-coordinates:

$$Y_{ij} = |Y_{ij}| \angle \theta_{ij} = |Y_{ij}| (\cos \theta_{ij} + j \sin \theta_{ij}) = G_{ij} + jB_{ij} \quad (4.2)$$

In (4.2),  $\theta$  is the admittance phase angle. Combining the admittance elements for each branch in the network with the voltages at the nodes, gives the total current injected at node  $i$ :

$$I_i = Y_{i1}V_1 + Y_{i2}V_2 + \dots + Y_{iN}V_N = \sum_{n=1}^N Y_{in}V_n \quad (4.3)$$

The active power  $P_i$  and reactive power  $Q_i$  entering the network at node  $i$ , and the complex conjugate of that power equals:

$$P_i - jQ_i = V_i^* \sum_{n=1}^N Y_{in}V_n \quad (4.4)$$

When (4.2) and (4.3) are substituted into (4.4), the real and imaginary part of the power at node  $i$  can be written as (4.5) and (4.6), being a set of non-linear equations that are called the load flow equations.

$$P_i = \sum_{n=1}^N |Y_{in}V_iV_n| \cos(\theta_{in} + \delta_n - \delta_i) \quad (4.5)$$

$$Q_i = -\sum_{n=1}^N |Y_{in}V_iV_n| \sin(\theta_{in} + \delta_n - \delta_i) \quad (4.6)$$

In a load flow problem, three types of busses are distinguished with respect to the known quantities at those busses:

For a *Load bus*; the active power  $P$  and the reactive power  $Q$  are known.

For a *Voltage-controlled bus*; where the voltage is kept constant, the voltage magnitude and the active power  $P$  are specified.

The *Swing bus*: The bus serves as a reference for the voltage angles of all other voltages. It is common practice to set the voltage angle of this bus equal to zero. This bus enables the load flow computation to balance the active and reactive power in the network.

There are different computational methods to solve the set of load flow equations, that are implemented in software programs (e.g. Power System Simulator for Engineering (PSS/E program), developed by Siemens [57]). With the amount of generated active power  $P_{gi}$  and the amount of active power demand of the load  $P_{di}$ , we have the real power losses in the network. The total losses in the system can be written by:

$$\sum_{i=1}^N P_i = \sum_{i=1}^N P_{gi} - \sum_{i=1}^N P_{di} \quad (4.7)$$

The difference between the amount of reactive power  $Q_{gi}$  that is supplied by the power plants and the amount  $Q_{di}$  that is consumed by the loads, equals the reactive power  $Q_i$  required to maintain the Electromagnetic field. The total amount of  $Q_i$  can be written by:

$$\sum_{i=1}^N Q_i = \sum_{i=1}^N Q_{gi} - \sum_{i=1}^N Q_{di} \quad (4.8)$$

Since cables and overhead lines have a different impedance, cable in the network do influence the distribution of power flow in the system. This difference in impedance is compensated by series inductors in the connection between the substations Maasvlakte and Westerlee. The series inductors have an impedance of  $8 \Omega$  and give a more efficient power flow distribution in the network. For planning studies, it is of importance to know whether cable integration leads to poor distributed flows of power or result even in overload situations in adjacent 380 kV connections.

To obtain a representative result, the Dutch 380 kV grid has to be suitable modeled for a steady state power flow analysis. The components that play a role are the 380 kV overhead transmission lines, the 20 km underground cable sections, the power plants and the loads. TenneT TSO supplied the requested data for the power production plant and the load scenarios in line with the network situation in 2014 [55]. To perform load flow studies, suitable models for the cables and overhead lines have to be chosen. In Chapter 2, it was already mentioned that for power frequency studies, transmission lines as such can be modeled, with sufficient accuracy, by lumped circuit elements and therefore, PI-sections represent the cable sections and the overhead lines. Overhead lines, cables and high voltage towers are represented as a lumped resistance, a lumped inductance and a lumped capacitance. The component values came from TenneT.

Figure 4.1 shows the Dutch 380 kV network on the level of 380 kV substations and the interconnections with neighboring countries [56]. Particular attention is paid to the Randstad area, because of the new 380 kV underground cable sections this region. The Randstad nodes are in the figure red colored. Most 380 kV connections are double circuits,

indicated by parallel black lines in the figure. The names of the grid nodes correspond with the names of the 380 kV substations in the field. Table 4.1 gives the names of these substations. The 380 kV interconnections are listed in Table 4.2.

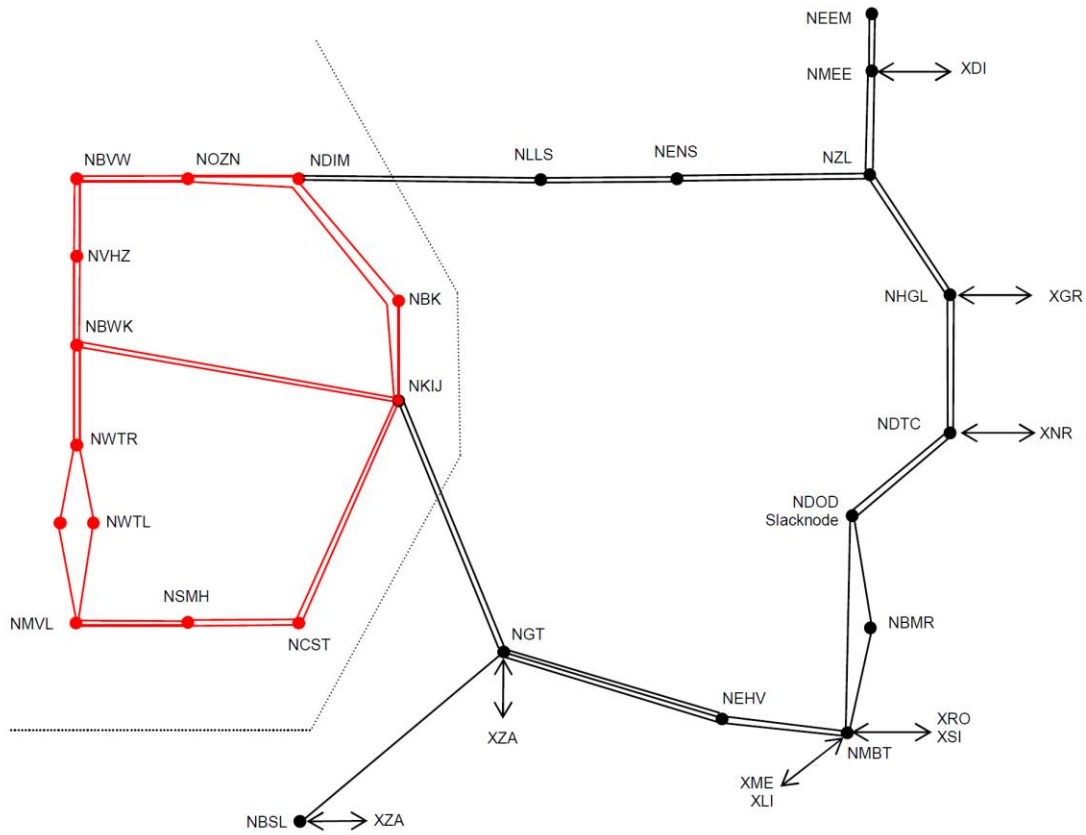


Figure 4.1. Dutch 380 kV substations and the interconnections with the neighboring countries.



Table 4.1. 380 kV substations names.

Abbreviation node	Name of 380 kV substation
NMVL	Maasvlakte
NWTL	Westerlee
NWTR	Wateringen
NBWK	Bleiswijk
NVHZ	Vijfhuizen
NBVW	Beverwijk
NOZN	Oostzaan
NDIM	Diemen
NBK	Breukelen
NKIJ	Krimpen a/d IJssel
NCST	Crayestein
NSMH	Simonshaven
NGT	Geertruidenberg
NBSL	Borssele
NEHV	Eindhoven
NMBT	Maasbracht
NBMR	Boxmeer
NDOD	Dodewaard
NDTC	Doetinchem
NHGL	Hengelo
NZL	Zwolle
NENS	Ens
NLLS	Lelystad
NMEE	Meeden
NEEM	Eemshaven

Table 4.2. Names of the 380 kV interconnections with neighboring countries.

Abbreviation node	Connection to
XZA	Zandvliet
XME	Meerhout
XLI	Van Eyck
XSI	Siersdorf
XRO	Rommerskirchen
XNR	Wesel
XGR	Gronau
XDI	Diele

Load flow calculations with PI sections requires accurate values for the  $R$ ,  $X$ ,  $C$  and  $G$  of all transmission lines in the Dutch 380 kV grid. The shunt losses are small, so the shunt conductance  $G$  can be neglected. Determining the values of these parameters is important in order to get reliable calculation results. In order to demonstrate the impact of the underground cable sections in the Randstad area on the system behaviour, a comparison is made between a particular situation with cables and with overhead lines instead of cables and that means that for both cases, the values for  $R$ ,  $X$  and  $C$  are necessary. In Table 4.3, the values for  $R$ ,  $X$  and  $C$  are listed for the 22 km 380 kV connection between the substations Wieringen and Bleiswijk, where 11 km underground cable is used [56]. The two overhead line sections of this connection have different values for  $R$ ,  $X$  and  $C$ , because of the difference in tower construction. Table 4.5 gives the values for the connection between Bleiswijk and Beverwijk. Between Bleiswijk and Beverwijk lies substation Vijfhuizen. The underground part is divided into three sections with a total length of 9 km. The load flow calculation and the contingency analysis were done with the Power System Simulator for Engineering (PSS/E Software), originally developed by PTI in the United States and now owned by Siemens [57]. In the Tables 4.4 and 4.6, the values of the parameters are listed when overhead lines instead of cables make the connection [56].

Table 4.3. Parameters for the connection WTR-BWK with cables.

Transmission line type	Construction type	Length (km)	R ( $\Omega$ )	X ( $\Omega$ )	C ( $\mu$ F)
OHL	Wintrack 4 bundel, 4 circuits	6	0.074	1.455	0.093
Cable	Flat arrangement 2*2500 mm <sup>2</sup>	10	0.046	1.162	4.640
OHL	Wintrack 4 bundel, 2 circuits	6	0.095	1.446	0.092
<b>Sum</b>		<b>22</b>	<b>0.235</b>	<b>4.063</b>	<b>4.825</b>

Table 4.4. Parameters for the connection WTR-BWK without cables.

Transmission line type	Construction type	Length (km)	R ( $\Omega$ )	X ( $\Omega$ )	C ( $\mu$ F)
OHL	Wintrack 4 bundel, 4 circuits	6	0.074	1.455	0.093
OHL	Wintrack 4 bundel, 2 circuits	16	0.253	3.856	0.246
<b>Sum</b>		<b>22</b>	<b>0.327</b>	<b>5.311</b>	<b>0.339</b>

At each 380 kV substation, power transformers transform the voltage from 380 kV to 150 kV. At 150 kV, the electricity is transported further to different regions in the country. The focus is on the reliability of the 380 kV grid, meaning that for the calculations only the power components at 380 kV level have to be taken into account. The influence of the 380 kV cable section on the system performance at the 150 kV side of the transformer is not considered and the 380 kV/150 kV transformers left out of our scope. In practice, reactive power generated by the cables is compensated by shunt reactors connected to the 50 kV tertiary winding of the power transformers. In substations Wateringen and Bleiswijk, shunt reactors are placed each of 300 MVA, making the total amount of compensation 600 MVA for this connection. Also 600 MVA of compensation will be installed for the connection from Bleiswijk to Beverwijk. To see the influence of the shunt reactors on the steady state voltage level, the shunt reactors are modeled at 380 kV level. The major power production is located at Maasvlakte and the voltages at the units are kept constantly at 1.05 pu (380 kV being the per unit base voltage). Since the 150 kV networks are not taken into account, the  $P$  and  $Q$  loads for the networks are represented (in the substations) as fixed loads at 380 kV level. The interconnections to the neighboring countries are in a similar way treated as fixed  $P$  and  $Q$  loads.

Table 4.5. Parameters for the connection BWK-BVW with cables.

<b>Transmission line type</b>	<b>Construction type</b>	<b>Length (km)</b>	<b>R (<math>\Omega</math>)</b>	<b>X (<math>\Omega</math>)</b>	<b>C (<math>\mu</math>F)</b>
OHL	Wintrack 3 bundel, 2 circuits	5	0.104	1.333	0.069
OHL	Wintrack 3 bundel, 4 circuits	9.6	0.199	2.573	0.134
OHL	Wintrack 3 bundel, 2 circuits	5	0.104	1.333	0.069
Cable	Flat arrangement 2*2500 mm <sup>2</sup>	5.1	0.023	0.592	2.366
OHL	Wintrack 3 bundel, 2 circuits	10	0.208	2.665	0.139
Cable	Flat arrangement 2*2500 mm <sup>2</sup>	3.1	0.014	0.360	1.438
OHL	Wintrack 3 bundel, 2 circuits	9.5	0.198	2.532	0.132
OHL	Wintrack 3 bundel, 2 circuits	9.8	0.204	2.612	0.136
Cable	Triangle arrangement 2*2500 mm <sup>2</sup>	0.8	0.004	0.095	0.371
OHL	Wintrack 3 bundel, 2 circuits	1.5	0.031	0.400	0.021
<b>Sum</b>		<b>59.4</b>	<b>1.089</b>	<b>14.495</b>	<b>4.892</b>

Table 4.6. Parameters for the connection BWK-BVW with overhead lines only.

<b>Transmission line type</b>	<b>Construction type</b>	<b>Length (km)</b>	<b>R (<math>\Omega</math>)</b>	<b>X (<math>\Omega</math>)</b>	<b>C (<math>\mu</math>F)</b>
OHL	Wintrack 3 bundel, 2 circuits	5	0.104	1.333	0.069
OHL	Wintrack 3 bundel, 4 circuits	9.6	0.199	2.573	0.134
OHL	Wintrack 3 bundel, 2 circuits	44.8	0.931	11.93	0.619
<b>Sum</b>		<b>59.4</b>	<b>1.234</b>	<b>15.836</b>	<b>0.822</b>

### 4.3 RESULTS OF THE CONTINGENCY STUDY

A transmission and distribution network must be designed such that the outage of one element does not cause an interruption of the power supply for the customer. This is named the  $(n-1)$  criterion. During the (scheduled) maintenance of a network component, the outage of another component should not lead to a loss of supply. This is called the  $(n-2)$  criterion. Both conditions are prescribed in the grid code for the TSO. In order to analyze the 380 kV grid during  $(n-2)$  contingencies, two types of contingency studies are done. First, one 380 kV connection is taken out of service, subsequently, another connection is taken out of service and the loading percentages of the other 380 kV connections are calculated. This is repeatedly done for all 380 kV connections, in order to analyze all possible combinations of contingencies and to determine whether the system is capable to remain in normal operation during  $(n-2)$  contingencies. Limits are established for the amount of apparent power that can be drawn from the 380 kV connections. The maximum allowable loading of the connections is taken to be 110% [56]. The voltages should stay between 342 kV and 418 kV.

Table 4.7 gives the calculation results for those situations for a loading exceeding 100% with only overhead lines in the grid. The connections for which the overload appeared are labeled by their percentage of overload for that particular connection. Table 4.8 gives the loadings when there is 20 km cable in the Randstad connection. We see that there are small differences in loadings between both situations, caused by the difference in impedance of an overhead line and a cable and this gives a difference in power flow. The highest loading is in the connection between Crayestein and Simonshaven, but there is no unacceptable overload during  $n-2$  contingencies.

Table 4.7. Results of  $n-2$  contingencies for line outages in the case of overhead lines only.

Outage 1	Outage 2	Overload in circuit	Loading percentage (%)
SMH-CST wit	WTR-WTL wit	SMH-CST zwart	108
	WTR-WTL zwart	SMH-CST zwart	109
	WTL-MVL wit	SMH-CST zwart	110
	WTL-MVL zwart	SMH-CST zwart	110
	SMH-CST zwart	WTL-MVL zwart	101
SMH-CST zwart	WTR-WTL wit	SMH-CST wit	108
	WTR-WTL zwart	SMH-CST wit	109
	WTL-MVL wit	SMH-CST wit	109
	WTL-MVL zwart	SMH-CST wit	110
MVL-SMH wit	WTR-WTL zwart	MVL-SMH zwart	101
	WTL-MVL-zwart	MVL-SMH zwart	101
	WTL-MVL-zwart	MVL-SMH zwart	102
MVL-SMH zwart	WTR-WTL wit	MVL-SMH wit	100
	WTR-WTL zwart	MVL-SMH wit	102
	WTL-MVL wit	MVL-SMH wit	102
	WTL-MVL zwart	MVL-SMH wit	102

Table 4.8. Results of  $n-2$  contingencies for line outages in the case of cables and overhead lines.

Outage 1	Outage 2	Overload in circuit	Loading percentage (%)
SMH-CST wit	WTR-WTL wit	SMH-CST zwart	104
	WTR-WTL zwart	SMH-CST zwart	105
	WTL-MVL wit	SMH-CST zwart	106
	WTL-MVL zwart	SMH-CST zwart	106
	SMH-CST zwart	WTL-MVL zwart	100
SMH-CST zwart	WTR-WTL wit	SMH-CST wit	108
	WTR-WTL zwart	SMH-CST wit	109
	WTL-MVL wit	SMH-CST wit	109
	WTL-MVL zwart	SMH-CST wit	110

In the second part of the contingency study, the loadings of the 380 kV connections are monitored when a rail is under maintenance. In this situation, one of the connections is taken out of service. This procedure is repeated for all possible combinations of bus bars and connections. The results are listed in Table 4.9 for the cases that resulted in more than 100% loading of the connections. It turned out that there is no unacceptable overload observed.

Table 4.9. Results of  $n-2$  contingencies for bus bar and line outages with and without cables.

			With cables	Only OHL
Bus bar under maintenance	Circuit in failure	Overload in circuit	Load %	Load %
KIJ A	OZN-BVW wit	OZN-BVW zwart	106	101
	OZN-BVW zwart	OZN-BVW wit	107	102
KIJ B	DIM-OZN-grijs	BK-KIJ wit	101	101
	WTL-MVL wit	KIJ-CST wit	100	97
CST A	KIJ-CST wit	KIJ-BWK wit	102	105
	WTR-WTL-wit	SMH-CST wit	103	99
	WTR-WTL zwart	SMH-CST wit	104	100
	WTL-MVL zwart	SMH-CST wit	104	100
	WTL-MVL wit	SMH-CST wit	105	101
CST B	SMH-CST wit	WTL-MVL wit	101	101
	WTR-WTL zwart	SMH-CST wit	101	97
	WTL-MVL-zwart	SMH-CST wit	101	98
	WTL-MVL wit	SMH-CST wit	102	98
	SMH-CST wit	WTL-MVL wit	101	100
WTL A	WTL-MVL wit	WTL-MVL zwart	96	100
	WTL-MVL zwart	WTL-MVL wit	97	101
	MVL-SMH wit	MVL-SMH zwart	101	97
	MVL-SMH zwart	MVL-SMH wit	102	98
	SMH-CST zwart	SMH-CST zwart	110	106
WTL B	SMH-CST wit	MVL-SMH zwart	110	106
	MVL-SMH wit	MVL-SMH zwart	102	98
	MVL-SMH zwart	MVL-SMH wit	102	99
	SMH-CST zwart	SMH-CST wit	110	107
	SMH-CST wit	SMH-CST zwart	110	106

The steady state voltage levels at the substations from MVL to BWK are calculated for 5 different scenarios, and are given in Table 4.10. As can be seen, the voltages for case 1 are almost the same as for case 3. This was to be expected because the reactive power generated by the cable is being compensated for by the shunt reactors at the four substations, and this gives the same voltage profile. In all 5 cases, the voltage levels remain within the prescribed range, from 342 kV to 418 kV.

- Case 1: The base case with only OHL in the network
- Case 2: Two circuits WTR-BWK are out of service
- Case 3: The base case with OHL and cables and reactive power compensation
- Case 4: Two circuits WTR-BWK are out of service, but the shunt reactors are still connected.
- Case 5: Case 4, but without shunt reactors being connected at WTR and BWK.

Table 4.10. Steady state voltages for different cases.

Substation	Voltages (kV)				
	Case 1	Case 2	Case 3	Case 4	Case 5
BWK	394.6	395.1	394.7	394.2	396.5
WTR	393.4	394.5	393.2	387.6	393.8
WTL	396.5	395.5	396.1	389.4	394.8
MVL	398.9	398.9	398.9	398.7	398.9

Based on the calculations, one can conclude that no large circuit overloadings occurred in the 380 kV transmission network during line and rail failures. In some cases, small overloads were present, but the percentages are small in both cases. Some remarks have to be made with respect to the grid model being used and the results obtained. The high load grid profile was the outcome when using fixed  $P$  and  $Q$  loads connected at 380 kV level. When more accurate results are desired, the calculations have to be repeated by modelling a stochastic load or by calculating different fixed load profiles.

#### 4.4 INFLUENCE OF SHUNT COMPENSATION ON THE VOLTAGE PROFILE

Reactive power compensation by means of shunt reactors is an important issue for longer underground cable circuits. The objective of shunt reactors is to compensate for the reactive power produced by the cables in order to keep the voltage level within the prescribed limits. In Chapter 2, we saw already for an example cable configuration that the steady state voltage profile in the network depends on the amount of shunt compensation applied. Reactive power surplus in the grid can result in a high voltage rise and that is why the influence of shunt reactor presence on the voltage profile is further analyzed. In order to do this, the same 380 kV network representation is used as in the previous section. In practice, the shunt reactors are connected to the 50 kV tertiary winding of the power transformer, but for the calculation the reactive power drawn by the shunt reactors is calculated at 380 kV.

Shunt reactors are installed at the substations Weteringen (WTR), Bleiswijk (BWK), Vijhuizen (VHZ) and Beverwijk (BVW), the total amount of installed reactive power for compensation is 300 MVar. The connection WTR-BWK has a total length of 22 km, in which the cable part is 10.8 km long. The amount of reactive power generated by this connection can be calculated, from the capacitance per unit length for the cable, which is 0.23  $\mu\text{F}/\text{km}$ . The phase to ground operating voltage is 230 kV. The capacitance of the overhead lines is approximately 10 times lower than that of the cable, so the reactive power generated by the overhead line is also 10 times lower. The total length of the line section for this circuit is about 11 km. The amount of reactive power generated by the lines and the cables of the whole connection can be calculated by (4.9) and (4.10).



$$Q_{cable} = \frac{V_{LG}^2}{X_{cable}} = V_{LG}^2 2\pi C_{cable} \quad (4.9)$$

$$= 230kV^2 2\pi \times 0.23\mu F / km = 3.8 \text{ MVar/ km}$$

$$Q_{OHL} \approx 0.1 \cdot Q_{cable} = 0.38 \text{ MVar/ km} \quad (4.10)$$

Since the underground part has 12 cables, the total amount of reactive power produced by the cable section in the connection WTR-BWK is 520 MVA. The overhead line section produces 25 MVar. For the connection BWK-BVW, the cable length is approximately 9 km, meaning that 410 MVar is coming from the cable and 111 MVar from the overhead lines. Having 300 MVar reactive power compensation installed at both sides of the connection, the amount of compensation that can be achieved is more than 100 %.

The impact of the shunt compensation coils on the voltage level is calculated for three different scenarios with different load profiles. To obtain an overview of the possible voltage profiles, various load scenarios should be looked at since the load is not constant during the day. A stochastic load flow calculation is an option for analyzing variations in load profiles, but this has not been done.

The first scenario is calculated with the network model as we used for the contingency analysis. The load profile was relatively high and therefore, we take this scenario as being 100% load. In the second scenario, the loads are brought to 50% of the value and in the third scenario, the load is brought back to 25%. For each of the three scenario's, the load flow is made with and without the shunt compensation.

To investigate the impact of shunt compensation, attention should be paid to the connected power plants because they control the amount of reactive power over a certain range. For a load flow calculation, the surplus of reactive power is leveled by the generator. Since a surplus of reactive power in the grid influences the voltage levels mainly locally, it is of importance to look at the settings of the control of the generator that are installed near by the cable sections. For the Randstad area most power plants are located at Maasvlakte. In order to make the impact of the reactive power on the voltage level visible, the generators should not absorb the reactive power from the cables. The reactive power control range of the generators is set to zero in the load flow calculation.

Apart from the steady state voltage levels, it is also worthwhile to observe the reactive power flows outside the Randstad area in the case that the amount of compensation changes. The installed shunt reactors can be switched on and off manually, depending on the load conditions. As a result of disconnecting the shunt reactors from the connections WTR-BWK and BWK-BVW, the amount of reactive power increases and it can be expected that this results in a local voltage rise at the adjacent substations. The reactive power flows in the connections around these substations also changes as a result of the absence of the reactors. The reactors consume reactive power generated by the cables and when the reactors are disconnected, it can be expected that the flows in the network are adjusted. For a correct analysis of the load flow results in the Randstad area, it is important that the power flow to the swing bus has no impact on the area under study and for that reason, the swing bus is made at substation Dodewaard, far away from the Randstad area.

In the Tables 4.11 and 4.12, the voltage levels are listed for the 380 kV substations in the Randstad, inside the red area shown from Figure 4.1. The voltages are calculated running a load flow on the 380 kV with and without shunt reactors connected. The results in this table make clear that there is a difference in voltage level for the situations with and without shunt reactor, but this difference is not significant. For all substations, the voltage will not surpass the upper limit of 418 kV, as stipulated in the grid code for TenneT.

A remark should be made here concerning base voltage value for the calculation. A base voltage 380 kV is taken. In the TenneT grid, the base voltage level is usually taken as 400 kV, so the voltage levels can be 20 kV higher for this base value. Another thing to note is the range of reactive power for the generators. For the generators, the voltage level and the active power are kept constant and the reactive power can vary. Therefore, the generators will level the difference in the reactive power balance of the grid, in case the shunt reactors are taken out of service. In that case, the voltage change will be considerable and in order to observe the effect of the change in reactive power flow on the voltage profile, the control range of the excitation of the synchronous generators nearby the Randstad area is kept at zero for this computation, but there is still a small difference in voltage between the situations with and without shunt reactors connected, as it can be seen from the calculation results.

The voltage levels increase when the load is reduced. Reduction of the loads means, in this case, that both the  $P$  and  $Q$  of the load at the 380 kV substation are proportionally reduced in order to keep the power factor at that particular bus unchanged. When the total system load is reduced, the power to be delivered by the power plants is reduced as well. Current reduction in the grid results in less voltage drop and therefore in less losses for the transmission lines of the system. The voltage levels will be higher as the voltage and the active power of the power plants have a fixed value.

Table 4.11. Steady state voltages with shunt reactors connected.

Load	Voltage (pu)											
	BV W	VHZ	BW K	WT R	WTL	MV L	SMH	CST	NKIJ	NBK	DIM	OZN
<b>100 %</b>	1.020	1.021	1.028	1.026	1.035	1.050	1.048	1.034	1.033	1.018	1.025	1.023
<b>50%</b>	1.024	1.025	1.033	1.032	1.040	1.050	1.049	1.038	1.037	1.029	1.032	1.027
<b>25%</b>	1.028	1.029	1.036	1.035	1.043	1.055	1.049	1.041	1.040	1.035	1.036	1.031

Table 4.12. Steady state voltages with shunt reactors disconnected.

Load	Voltage (pu)											
	BV W	VHZ	BW K	WT R	WTL	MV L	SMH	CST	NKIJ	NBK	DIM	OZN
<b>100 %</b>	1.045	1.047	1.046	1.044	1.051	1.050	1.049	1.042	1.044	1.030	1.037	1.042
<b>50%</b>	1.047	1.050	1.052	1.050	1.056	1.050	1.049	1.046	1.048	1.040	1.044	1.046
<b>25%</b>	1.058	1.059	1.057	1.055	1.061	1.050	1.049	1.049	1.052	1.048	1.050	1.055

From Figure 4.1, we can see that there are two connections from the Randstad area to the rest of the Dutch 380 kV grid: from Diemen to Lelystad and from Krimpen a/d IJssel to Geertruidenberg.

These are the connections for which both the active and reactive power flow is influenced by the shunt reactors in the connections Wateringen-Bleiswijk and Bleiswijk-Beverwijk. Tables 4.13 and 4.14 show the voltage levels, the active power  $P$  and the reactive power  $Q$ , from the substations Diemen and Krimpen a/d IJssel.

The first column of Table 4.13 lists the substations connected to Diemen while Table 4.14 gives the names of the substations connected to Krimpen a/d IJssel. From these calculated results, we learn that the shunt reactors have no great impact on the active power flow in the neighboring grid. This was to be expected since the reactors taken as pure inductive loads and therefore, they do not influence the active power flow in the network. As expected, the change in reactive power is more significant, since the shunt reactors causes a redistribution of the reactive power flow in the grid.

Table 4.13. Steady state power flows from substation Diemen.

Station Dim	Voltage (pu)		P (MW)		Q (MVar)	
	Shunt	No shunt	Shunt	No shunt	Shunt	No shunt
LLS	1.048	1.049	-509.2	-506.0	-479.1	-245.1
NBK	1.018	1.030	-111.5	-106.5	213.6	222.0
OZN	1.023	1.042	-379.2	-387.4	105.3	-137.1

Table 4.14. Steady state power flows from substation Krimpen a/d IJssel.

Station NKIJ	Voltage (pu)		P (MW)		Q (MVar)	
	Shunt	No shunt	Shunt	No shunt	Shunt	No shunt
NBK	1.018	1.030	715.1	710.0	131.3	120.6
BWK	1.028	1.046	-602.5	-605.1	313.7	-174.7
CST	1.034	1.042	-2149.9	-2137.5	27.2	254.5
NGT	1.050	1.050	1374.3	1372.6	-654.3	-320.9

## 4.5 CONCLUSION

Load flow calculations and contingency analysis were done to investigate the impact of cables in the Randstad area on the power flow and the voltages in the 380 kV grid. The calculated results proves that cables in the Randstad area do not lead to significant overloads in the adjacent (overhead line) connections. Furthermore, the calculations made clear that the voltage remains below the upper limit for the considered scenario's (418 kV). From the calculations, the influence of the shunt reactors on the voltages in the grid was proven and it turned out that the voltage rise is small when these reactors are disconnected. The small voltage rise shows that the impact of the shunt coils is relatively small in spite of the large difference in the amount of reactive power in the grid. This small voltage rise and the fact that no overloads are identified, mean that no additional measures are needed by the grid operator to keep the voltage within the allowable limits and to control the power flow in the network. The results in this chapter are strongly related to the cable and line configurations in the Randstad 380 kV project, but a similar computation approach can be followed for analyzing the power flows and voltage levels in 380 kV grids with other dimensions for the lines, the cables and the shunt reactors. This means that for future cable projects, the same computation can be done. For a complete overview with respect to the observed load scenario's, it is worthwhile to do the computations by a stochastic load flow, but the results in this chapter give a representative first impressions of the impact of cables on the steady state grid behavior.

## **CHAPTER 5**

# **TRANSIENT MODEL FOR 380 KV MIXED LINE-CABLE-LINE SYSTEMS**

### **5.1 INTRODUCTION**

Cable sections in the 380 kV overhead-line network have impact on the behavior of the system as a whole during transients, so it is important to look at the effect of different transient phenomena more closely. A large part of this thesis focusses on the behavior of the Dutch 380 kV mixed line-cable-line sections in the Randstad connection during the transient period by computer calculations. To obtain representative results, an accurate model of the 380 kV cable section is a necessity and this requires data about cable dimensions and material properties. Detailed transmission line models for both the overhead and underground sections are required as well. In section 5.2, the transmission line model as used in the simulation studies is described. The modeling work for the cable, overhead-line sections and the shunt reactor in the Randstad 380 kV connections is presented in paragraph 5.3. The cross-bonding of the cable screen conductor plays an important role and special attention is paid to the cross-bonding of the cable. In section 5.4, the modeling work for this is described and the cross-bonding scheme as applied in the Randstad 380 kV cable connection is outlined.

### **5.2 TRANSIENT CABLE MODELS**

Chapter 1 gave short overview of different cable models that have been developed over years. In Chapter 2, the difference between lumped element models and distributed element models was discussed with respect to their validity. Over the years, several cable models

have been published for transient studies. For transient studies, high frequencies play a dominant role and this requires a distributed parameter model based on travelling wave theory [59], [60]. A distributed transmission line model takes the frequency dependency of all line parameters into account. In the simulation studies in this work, the EMTDC based program PSCAD is used. In the PSCAD software library there are several implemented transmission line models available. We have used the Frequency Dependent Phase Model (FDPM) [20]. This model is also referred to as the Universal Line Model and is often used for transient calculations. An underground or an overhead transmission line is fully characterized by its propagation matrix  $\mathbf{H}$  and its admittance matrix  $\mathbf{Y}$  [29]. These matrices are frequency dependent (because the parameters of the transmission line are frequency dependent) and therefore it is convenient to express the elements of the matrices in the frequency domain. The inverse Fourier transform is used to give the time-domain values. In the Universal Line Model, the transmission line parameters are directly fitted in the phase domain in order to reduce complexity and save computation time. The least square fitting routine Vector Fitting (VF) is applied to fit the elements of both the propagation matrix  $\mathbf{H}$  and the admittance matrix  $\mathbf{Y}$  in the phase domain [29], [61]. Afterwards, the computed results in the frequency domain are transformed back to the time domain. The FDPM is explained in Appendix B.

### 5.3 SIMULATION MODEL FOR THE RANDSTAD 380 KV CABLE CIRCUITS

Transient calculations have been carried out on the two mixed line-cable-line circuits that are part of the Randstad 380-connection. In September 2013, the southern part between the 380 kV substations Wateringen and Bleiswijk is brought into service. The Northern part between Bleiswijk and Beverwijk is still under construction and will be completed in 2017. For both connections, simulations have been carried out for several transient phenomena. In Figure 5.1a, a block scheme shows the Southern part of the Randstad 380 kV connection, from Maasvlakte to substation Krimpen a/d IJssel. The lengths of the overhead-line and cable sections are shown. Between Maasvlakte and substation Westerlee, the series reactance is connected (see Chapter 4).

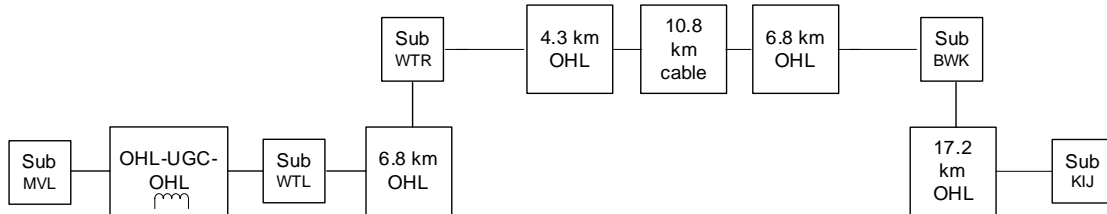


Figure 5.1a. Southern connection of the Randstad 380 kV grid.

Figure 5.1b shows the Northern part of the Randstad 380 connection, from substation Bleiswijk towards Beverwijk. 380 kV substation Vijfhuizen is in the middle. Four cable

sections make part of this connection. The total cable length in the Maasvlakte - Beverwijk is 19.8 km.

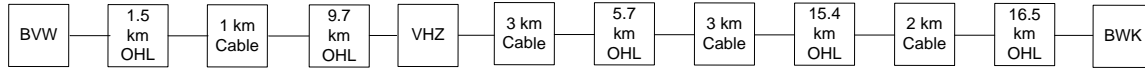


Figure 5.1b. Northern connection of the Randstad 380 kV grid.

For the 380 kV connection from Maasvlakte to Bleiswijk and as well as for the connection Bleiswijk - Beverwijk, a transient simulation model is built in PSCAD. To be able to do so, accurate cable and overhead-line data are necessary. For the overhead lines, this means that the material data and the dimensions of the high voltage towers are required, and for the cable sections, the insulation material parameters, burial and the inside arrangement of the cables are necessary. The overhead line calculations are straight forward, because there is no shielding and no semiconductor material. A cable has two conductive layers (the core conductor and the screen) with insulation material in between. The cable has also semi-conductive layers which complicate the modeling of the physical behavior of the cable. A cross section of the cable being used in the Randstad 380 project, is depicted in Figure 5.2.

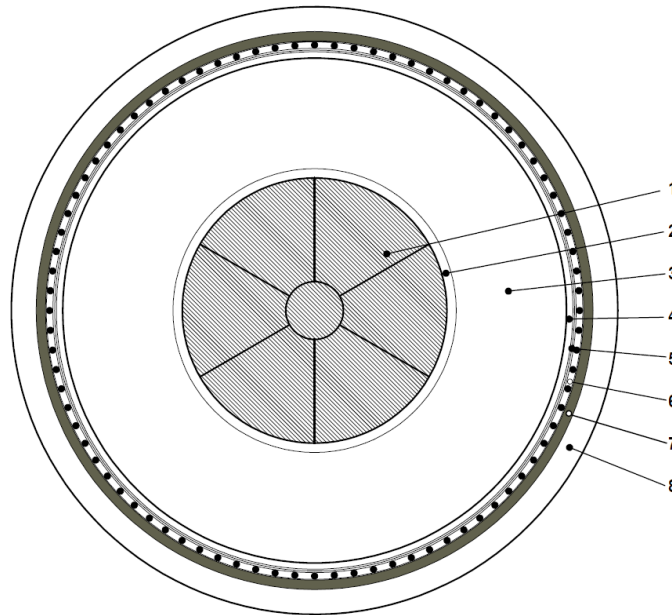


Figure 5.2. Cross section of the 380 kV cable in the Randstad 380 project.

The cable dimensions are:

1	<i>Copper conductor</i>	<i>(2500 mm<sup>2</sup>)</i>
2	<i>Semi-conducting layer</i>	<i>(2.2 mm)</i>
3	<i>XLPE insulation</i>	<i>(26 mm)</i>
4	<i>Semi-conducting layer</i>	<i>(1.5 mm)</i>
5	<i>Bedding (semi-conductor and swelling tape)</i>	
6	<i>Copper screen</i>	<i>(155 mm<sup>2</sup>)</i>
7	<i>Lead sheath</i>	<i>(2 mm)</i>
8	<i>PE sheath</i>	<i>(5.1 mm)</i>

The cable core consists of a copper conductor, segmented in order to minimize skin- and proximity-effects. The solid main insulation material between the core conductor and the metallic screen is so-called cross-linked polyethylene (XLPE) and a semi-conducting layer is put on the inner and on the outer surface of the XLPE layer. The semi-conductive layers reduce gradually the electric field strength inside the insulating material. By the copper screen, that is connected to ground potential, the electric field is locked inside the cable. The copper screen forms a return path for the cable charging current and consists of copper wires, placed along the bedding of the swelling tape. The cable screen conductor gives also a return path for fault currents. A lead sheath forms a radial water barrier and is extruded at the outside of the metallic screen and acts as an extra cable screen. The protection of the cable against outside damages is taken care off by an outer sheath layer, made of high density polyethylene (HDPE).

The Frequency Dependent Phase Model from the PSCAD software library needs rather precise geometric dimensions and precise material parameters for the overhead lines and cables. Most of the required data are available from the cable and line manufacturer and the grid operator, as given in Figure 5.2. To construct a model for the cable section, the number of layers needs to be defined in the cable interface of the PSCAD software and the parameters for the core conductor, the screen, the inside cable configuration, the thickness, the conductivity and the permeability must be specified. The XLPE insulation layer is specified by its thickness, its permeability and its permittivity.

In the PSCAD cable model, it is not possible to add a specific semi conductive layer. The cable capacitance is mainly formed by the insulation material between core conductor and the screen. This capacitance per unit length is specified by the manufacturer and can be calculated by (5.1). The constant capacitance, being the capacitance between core conductor and cable screen, includes the semiconducting layers. This is done by enlarging the thickness and the permittivity of the insulation layer [29].

$$C = \varepsilon_0 \varepsilon_r \frac{2\pi}{\ln\left(\frac{r_2}{r_1}\right)} \quad (5.1)$$



where

$\epsilon_r$  is the known relative permittivity of the XLPE insulation; and

$r_1$  and  $r_2$  are respectively the inner and outer radius of the insulation layer [m].

The relative permittivity of XLPE is 2.3, specified by the cable manufacturer. When the thickness of the insulation layer increases, the permittivity of the insulation changes and the value of the permittivity has to be adjusted, in order to keep the total cable capacitance at its original value [62]. The adjusted permittivity for the insulation, with the semi conductive layers included, is formed by (5.2), giving a value of 2.65.

$$\epsilon_{corrected} = \epsilon_0 \epsilon_r \frac{\ln\left(\frac{b}{a}\right)}{\ln\left(\frac{r_2}{r_1}\right)} \quad (5.2)$$

where

$\epsilon_{corrected}$  is the corrected relative permittivity of the insulation layer; and

$a$  and  $b$  are respectively the outer radius of the core conductor and the inner radius of the screen in meters.

The second modeling issue concerns the round cable conductors. In PSCAD, it is only possible to model the core and the screen of the cable either as a solid or a hollow conductor. Because the cable core conductor is segmented, the resistivity will be slightly higher since the effective area is less compared to the solid conductor. The copper resistivity equals  $1.68 \cdot 10^{-8} \Omega \cdot m$ . In practice, the metallic screen is formed by wires that are helically stranded around the outer semiconductive layer. This has an influence on the inductance while the magnetic field will follow a solenoid shaped path dictated by the helical structure of the screen and that increases the inductance [29]. This inductance can be taken into account by making a correction to the permeability of the material. The magnetic flux density and the self-inductance of a solenoid effect are [29]:

$$B = \mu NI \quad (5.3)$$

$$L = \mu N^2 \pi (r_2^2 - r_1^2) \quad (5.4)$$

The corrected permeability leads to the third adjustment to be made: according to Equation 5.5, a value of 1.07 is found.

$$\mu_{corrected} = \mu + \frac{\mu}{\ln\left(\frac{r_2}{r_1}\right)} 2\pi^2 N^2 (r_2^2 - r_1^2) \quad (5.5)$$

where

$r_1$  and  $r_2$  are the radius of the conductor and the outer semi conductive layer respectively [m];

$\mu$  is the permeability of the insulation ( $4\pi \cdot 10^{-7}$  F/m); and

$N$  is the number of turns of the cable per meter

When all cable data is available, the cable network can be built in PSCAD. For the cable connection between Weteringen and Bleiswijk, there are two underground three phase cable circuits connected in parallel. The cables are laid in a flat configuration (see Figure 5.3). Each circuit has a maximum transmission capacity of 2600 MVA. Each cable circuit is a three-phase system with two cables per phase. This means that a set of 12 cables in total has to be treated as one system. The section with 12 cables, each having a core conductor and a sheath, contains 24 conductors in total and is buried at a depth of 1.25 m. The horizontal spacing between two cables in a circuit is 0.75m, while the spacing between the centers of both parallel circuits is 6.75 m.

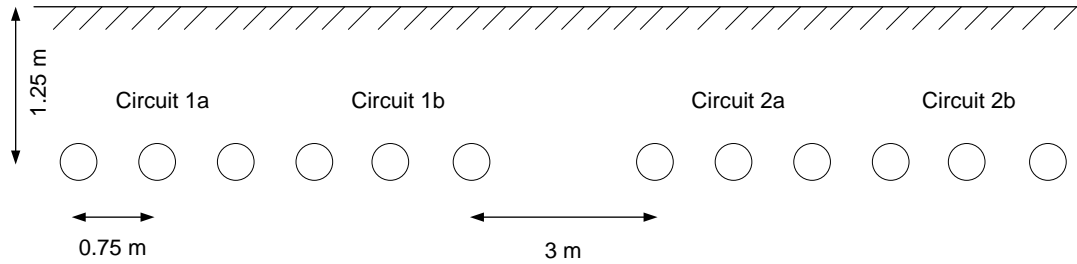


Figure 5.3. Flat configuration of the 380 kV cable system.

In practice, the burial depth and the distance between the cables varies slightly along the whole length of 10.8 km. To keep the modeling work in PSCAD manageable, the distances and depth are taken to be constant. In Figure 5.4, a cross section of a cable circuit that is built in PSCAD and the dimensions of the configuration is shown.

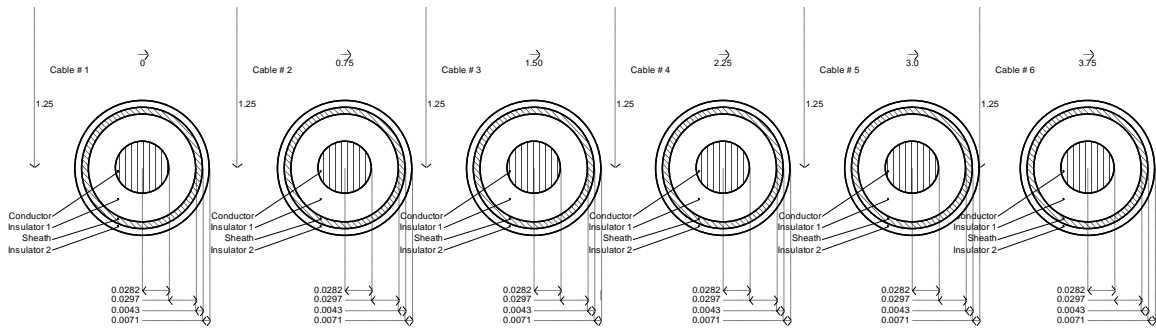


Figure 5.4. Cable circuit as modeled in PSCAD.

For the connection between Maasvlakte and Westerlee, there is also a short cable because of a water crossing. This cable section has two circuits and a total length of 2.1 km. Unlike the circuit between Wieringen and Bleiswijk, the cables in this section are in the trench positioned in a triangular configuration and therefore the elements of the impedance matrix  $\mathbf{Z}$  differ from the ones for the section between Wieringen and Bleiswijk.

As already explained earlier (in Chapter 3), an important modeling issue for underground cables, is the mutual coupling between the conductors. Because of the relative small physical distance amongst the conductors, the mutual inductive coupling between *all* conductors of the cable circuit must be taken into account. The capacitive coupling is neglected because the screen conductor of each cable is at ground potential. Using the data from the cable positions, the cable system shown in Figure 5.4 is transferred into a lumped element model and the mutual inductive coupling is calculated by the PSCAD software. The mutual coupling for one circuit of 6 cables has to be extended to 12 cables, but the size of the admittance and propagation matrix, and thus the complexity of the calculation process increases considerable when the number of cables increases. This is a problem for PSCAD in relation to large cable systems: the number of cables that can be mutually coupled to a single cable interface is limited to 8. The software gives a possibility to couple two identical parallel cable systems. This means that in theory 24 cable conductors can be mutually coupled to each other when two parallel systems of 6 cables are to be modelled.

In order to be able to look at a complete cable section having 12 cables, a simplification is made in the modeling process when it comes to mutual coupling. As explained earlier in Chapter 3, the coupling between two cables becomes less when the distance increases. The spacing between two cables in one circuit is 0.75 m, while the horizontal spacing between the parallel circuits is 3 m. In line with this is relatively large distance, the assumption can be made that the coupling amongst the circuits themselves can be neglected. This means that the total cable system is considered as two separate systems with 6 cables each. To verify whether this assumption is correct, a calculation has been done on a simplified cable system of 10.8 km length containing two identical parallel circuits of three cables. These two cable circuits are modelled in PSCAD and have a mutually coupling. The two circuits are drawn in Figure 5.5. A step voltage function with a rise time of 100 ns and an amplitude

of 1 kV is switched on to the circuit. A step voltage has a very steep front and is therefore representative for a fast transient. The step voltage is switched-on to the sending end of one cable at time instant  $t = 100 \mu s$ . The location of the voltage injection is at  $V_{in}$  (Figure 5.5). In the other circuit, the induced response voltage to the incident step function is measured at the receiving cable end that is closest to the injected cable, at  $V_{out}$  in Figure 5.5.

The calculation is done for different distances between the two cable circuits in order to see the effect of the distance on the coupling. In Figure 5.6, the measured receiving end voltage waveforms are plotted for four distances  $D$  between the parallel cable circuits. We see from the results that the highest peak value of the measured waveform is slightly above 50 mV for a distance of 6 m between the two circuits. We also see note that the peak value decreases with the distance as expected. For the connection Wateringen-Bleiswijk, the distance between both cable circuits is 6.75 m so we can conclude that the induced voltage in the neighboring circuit is quite small during steep wave voltage surges. We can translate this as that there is only a weak coupling between the two circuits and that they do not have a large influence on each other. Based on this, we can conclude that the two cable systems can be considered as having no mutual coupling. The cable terminals were left open for this calculation. In practice, the terminals will be grounded when a circuit is taken out of service. This is done for safety and security.

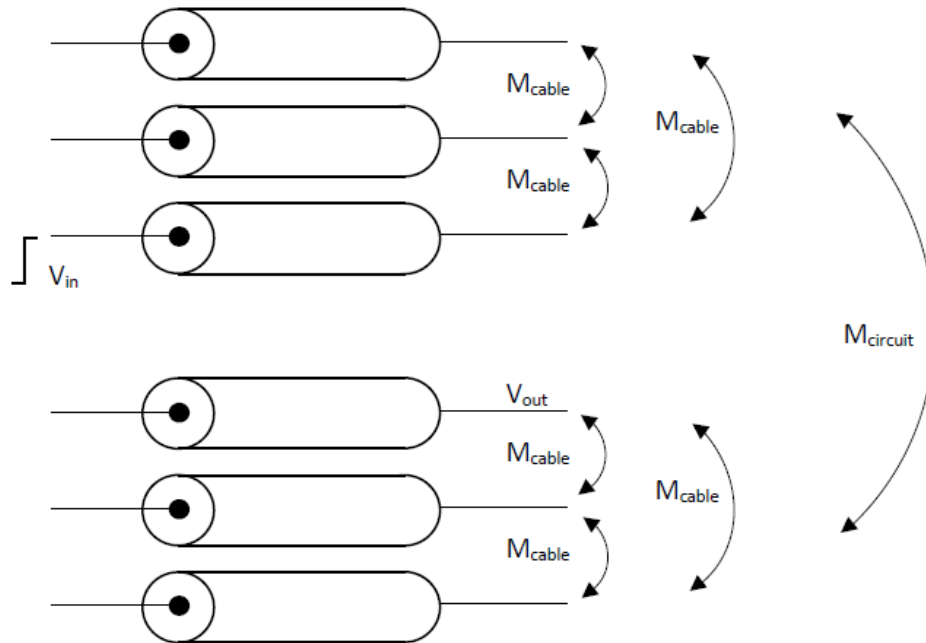


Figure 5.5 Two mutually coupled identical cable circuits.

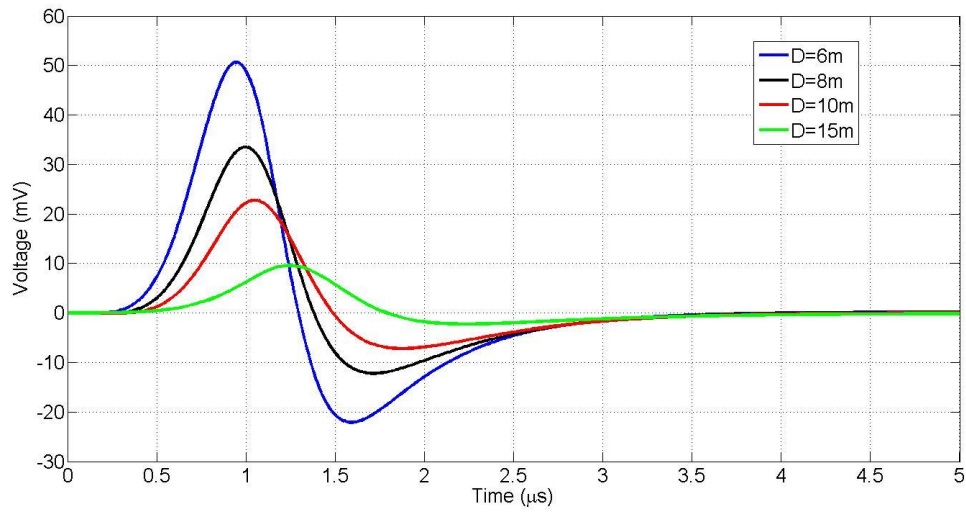


Figure 5.6 Simulated cable receiving end voltages for different distances between the cable circuits.

The connection Wateringen-Bleiswijk has 4.3 km overhead line, 10.8 km underground cable and 6.8 km overhead line. In the connection Bleiswijk-Beverwijk, there are five overhead line sections, see Figure 5.1b. The line sections in this connection have an aluminum conductor with an overall diameter of 32.4 mm. The line section has one conductor per phase, making 6 phase conductors in total. Also, a new high voltage tower design (the Wintrack) is made in order to mitigate the magnetic field strength and to reduce the environmental impact of high voltage towers on the country side. The Wintrack tower, has two cross arms, separated 16 m from each other with the phase conductors are positioned in a vertical plane. Above the phase conductors, there are two ground wires for protection against lightning (see Chapter 7). A cross section of the phase and ground wire configuration as built in PSCAD is shown in Figure 5.7, where C1 to C6 are the phase conductors and G1 and G2 are the grounding conductors.

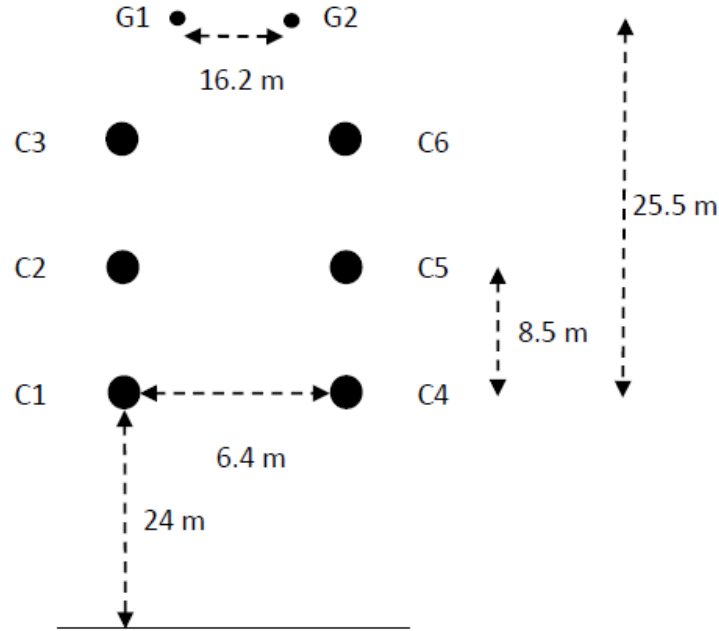


Figure 5.7 Cross section of the overhead line section for a Wintrack tower.

As it can be seen from Figure 5.1, a series reactor is connected between Maasvlakte and substation westerlee. The purpose of this reactor is to control the active power flow in the network by compensating for the difference in impedance between a cable and an overhead line. The reactor itself will have an influence on the system behavior, since it is an additional inductive component. To quantify the influence on the transient behavior, an appropriate reactor model is required. The reactor in the Randstad 380 project has a nominal operating voltage of 420 kV and the nominal impedance is approximately  $8 \Omega$ . The reactor model is shown in Figure 5.8 [63]. The magnetic circuit of the reactor consists of an air path and an iron path. The air path is modeled by a linear inductance of 22.68 mH. To take the saturation of the iron core into account, a non-linear inductance of 4.35 mH is placed in series with the linear inductance. The capacitance between the windings of the reactor plays an important role for transients. This capacitance is modeled as a lumped element,  $C_s$  in Figure 5.8. The equivalent reactor capacitance  $C_e$  is equally divided between the two terminals as two lumped capacitors.

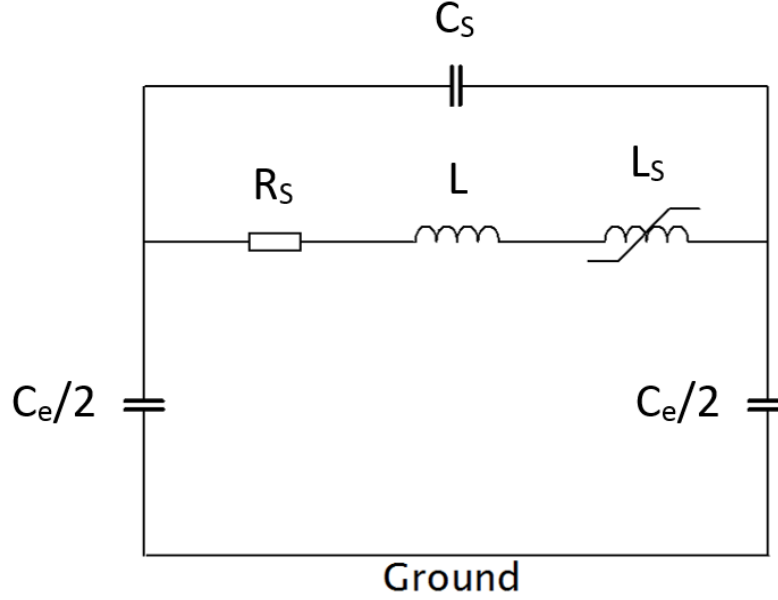


Figure 5.8 Applied model for the series reactor.

The values for the lumped reactor elements are:

$$C_s = 500 \text{ pF}$$

$$C_e = 1830 \text{ pF}$$

$$R_s = 26.15 \text{ } \Omega$$

$$L = 22.68 \text{ mH}$$

$$L_s = 4.35 \text{ mH}$$

#### 5.4 MODEL FOR THE CABLE CROSS-BONDING CONFIGURATION

The cross-bonding of cable screen conductors is done in order to reduce the screen voltages and currents. This is important to reduce the losses in the cable (Chapter 3). In the 10.8 km cable section of the Randstad 380 connection, the cable screen conductors are interconnected by means of cross-bonding cables (CB cables). The connection between the screen of the 380 kV cable and the CB cable is at a cross-bonding joint (CB joint). The actual cross-bonding is done in a cross-bonding box (CB box). Special attention is given to the modeling of the cross-bonding of the 380 kV cable screen conductor [64], because for cross-bonding, the cable is divided in sections: the 10.8 km 380 kV cable into four sections. For each section cross-bonding is done as drawn in Figure 5.9. The 380 kV section is divided in three smaller sections. The numbers labels phases. In this paragraph, lumped element models are derived for the CB cable, the CB box and the CB joint [65]. These models play a role in the transient simulation studies in Chapter 6 and Chapter 7. A cross-bonding scheme has traditionally been modeled with lumped circuit elements [29], but for

fast transients, the lumped element approach is not accurate enough and the circuit elements must be considered to be uniformly distributed along the CB cable.

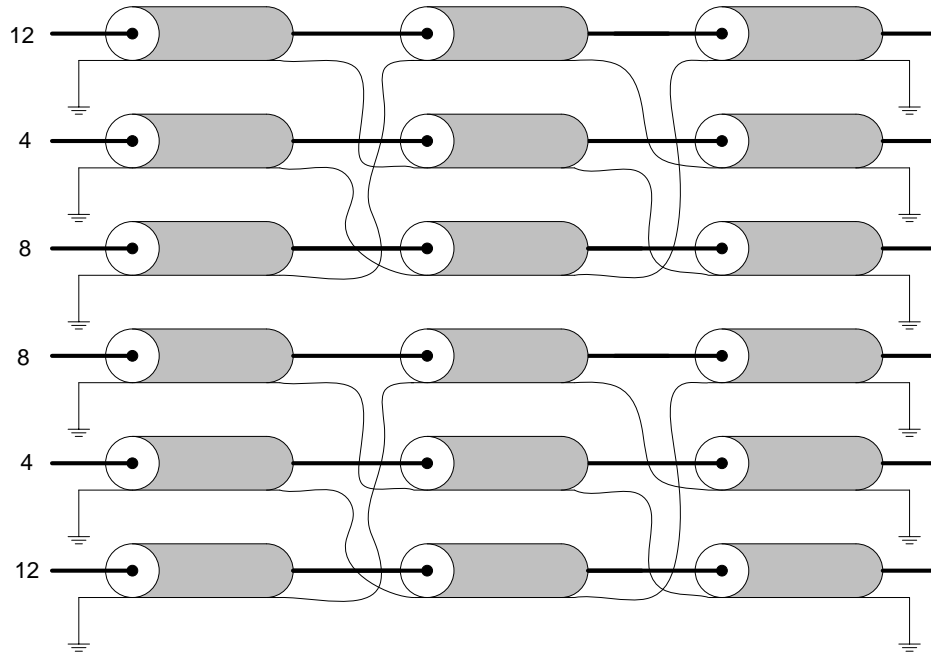


Figure 5.9 Major section of the 380 kV cable circuit. The phases are labeled (by the numbers 4, 8 and 12) and this shows the arrangement of the three phases in the cable section.

### *CB cable*

Figure 5.10a shows how the CB-cable is connected with the CB-joint: the core conductor of the CB-cable is connected to the screen of the 380 kV cable (left cable part). The screen conductor is connected to the screen of the 380 kV cable that continues (right cable part). Figure 5.10b illustrates the cross section of the applied cross-bonding cable with its dimensions. The construction of the CB-cable is different from a high-voltage cable. XLPE is the cable insulation material, but semi-conductive layers are not present. The absence of the semi-conductive layers gives a lower attenuation for the high frequencies [66].

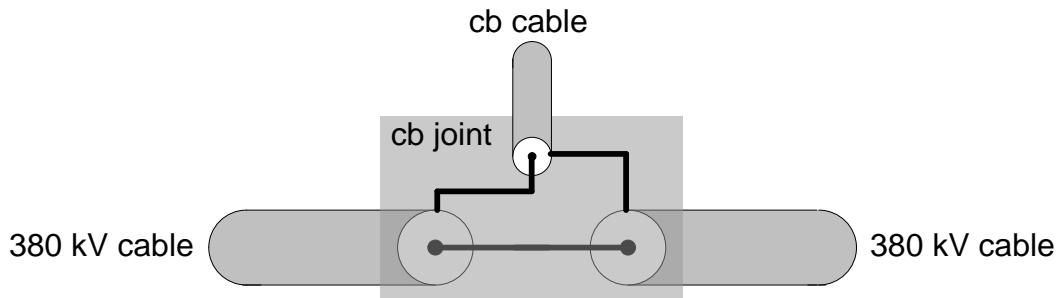




Figure 5.10a Connection of CB-cable to CB-joint.

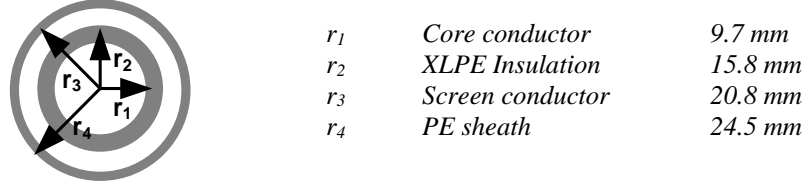


Figure 5.10b Cross section of the CB-cable and dimensions.

For fast transients, the CB-cable must be treated as a transmission line and it can be described by a characteristic impedance and a propagation constant. The characteristic impedance  $Z_{ccb}$  of the CB-cable can be calculated with (5.6), the known material properties and the physical dimensions. For the CB-cable used in the Randstad 380 connection, the characteristic impedance is 19.2  $\Omega$ .

$$Z_{ccb} = \frac{1}{2\pi} \sqrt{\frac{\mu_0}{\epsilon_0 \epsilon_{XLPE}}} \ln \left( \frac{r_1}{r_2} \right) \quad (5.6)$$

The attenuation and the phase shift of the propagation constant can be estimated from the shunt conductance and the propagation velocity. For the higher frequencies, a more accurate determination of the characteristic impedance and the propagation constant is required and to determine the parameters of the cross bonding cable, pulse injection measurements are done [66]. After the measurement, the obtained time domain results are transformed to the frequency domain and a transfer function can be assigned to the CB-cable. Figure 5.11 shows the measurement setup used for the pulse injection into the cb cable is shown. The CB-cable is connected to a pulse generator via a coaxial injection cable. An adapter is placed between the injection cable and the CB-cable in order to avoid reflections. The length of the CB-cable is 12.3 m and the receiving end of the CB-cable is left open.

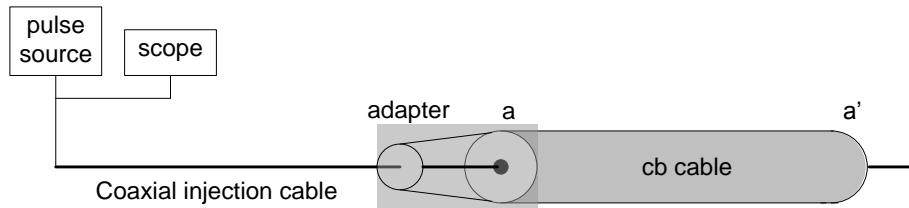


Figure 5.11 Measurement layout for pulse injection in CB-cable.

The coaxial injection cable, having a length of 50 m, and the adapter influence the pulse injection measurement and therefore, a calibration measurement is necessary for both the injection cable and the adapter. The injection cable calibration is done by injecting a short pulse to the sending end and the receiving end being short circuited. At the sending end, the injected and reflected signals are measured and the transfer function of the injection cable is calculated. The adapter is calibrated by injecting a pulse at the sending end of the injection cable, while the receiving end is connected to the short-circuited adapter. From the measured reflection signals and the injected pulse, the transfer function can be calculated and the impedance of the adapter can be calculated [66].

After these calibration exercises, the pulse measurement for determining the parameters of the CB-cable can be carried out. A pulse of 8 ns width is injected via the coaxial measuring cable to the CB-cable core conductor. A part of the injected pulse reflects at the junction point between measuring cable and CB-cable. The refracted part propagates through the CB-cable and reflects at the open end. At the terminal where the pulse is injected, the reflected signals are measured. The results are plotted in Figure 5.12. The green line is the injected pulse. The negative red pulse is the reflection at location *a*, in Figure 5.11. The blue pulses are the reflections at the receiving open CB-cable end *a*'.

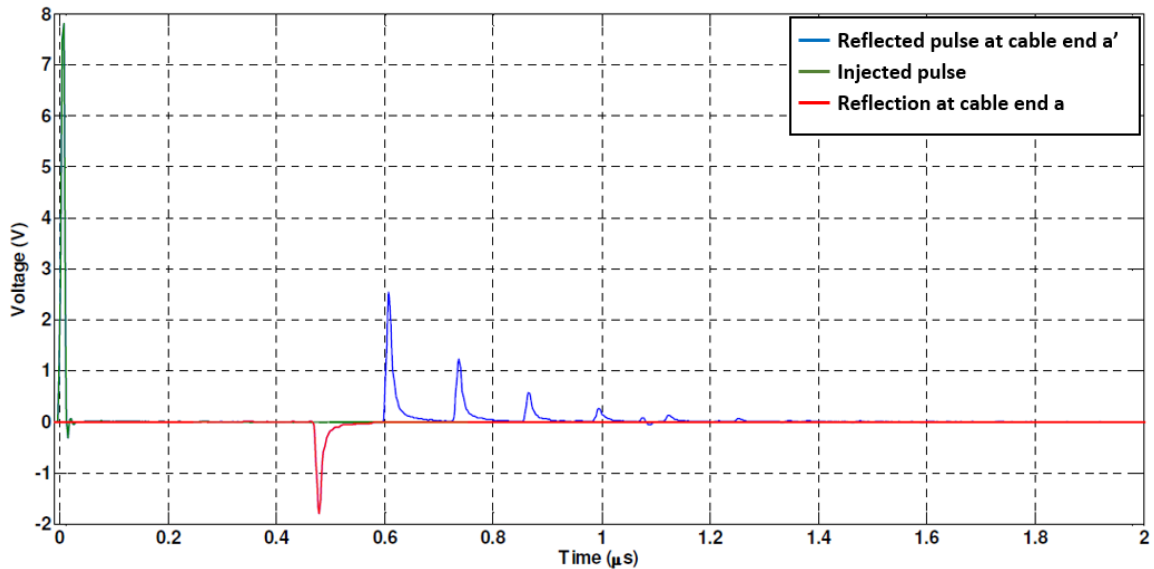


Figure 5.12 Reflection pattern measured at the sending end.

The reflection pattern in the time domain, is transformed to the frequency domain and the CB-cable parameters can be estimated from the transfer function. The transfer function  $H_I$ , relating the injected pulse  $Y_{inj}$  to the reflected pulse at the junction between the injection cable and the CB-cable  $Y_a$ , is given by (5.7). The transfer function of the injection cable is described in [66], [67]. With these two transfer functions, the characteristic impedance of the CB-cable can be calculated with Equation (5.8). In Equation 5.8,  $Z_o$  is the characteristic impedance of the measuring cable and  $Z_s$  is the impedance of the adapter. The average value for the characteristic impedance, for frequencies up to 10 MHz, is 17  $\Omega$ .

$$H_1 = \frac{Y_a}{Y_{inj}} \quad (5.7)$$

$$Z_{ccb} = Z_0 \frac{H_{inj} + H_1}{H_{inj} - H_1} - Z_s \quad (5.8)$$

The propagation constant of the CB-cable is calculated from the refracted pulse  $Y_{aa'}$  at the cable's open end. The transfer function  $H_2$ , of this reflection is expressed by (5.9). The transmission coefficient  $\tau_{c-i}$  denoting the part of the pulse being transmitted from the injection cable to the CB-cable, can be calculated from the characteristic impedances of both cables. For the reflected pulse propagating back to the injection cable, the transmission coefficient  $\tau_{i-c}$  is calculated in the same way. The propagation constant  $\gamma_{cb}$ , including attenuation and phase shift, is calculated with Equation (5.10). Because of the short length of the measured CB-cable, the attenuation is rather small and can be neglected. From the calculated phase shift, the propagation velocity is found, being 190 m/ $\mu$ s.

$$H_2 = \frac{Y_{aa'}}{Y_{inj}} = H_{inj} \tau_{c-i} \tau_{i-c} e^{-\gamma_{cb} 2l_{cb}} \quad (5.9)$$

$$\gamma_{cb} = \frac{1}{2l_{cb}} \ln \left( \frac{H_{inj} \tau_{c-i} \tau_{i-c}}{H_2} \right) \quad (5.10)$$

### *CB box*

In the CB-box, the connections between the CB cables are physically made. The coaxial structure of the CB-cables is affected by the copper bars inside the box. The result of this is that an inductive loop is created that has to be modeled by the impedance of the CB- box [68]. Figure 5.13 gives an inside view of the CB-box and shows the copper bars that create the inductive loops. The values for the box inductances are calculated from a pulse reflection measurement. The setup for such a measurement and the impedances are shown in Figure 5.14.

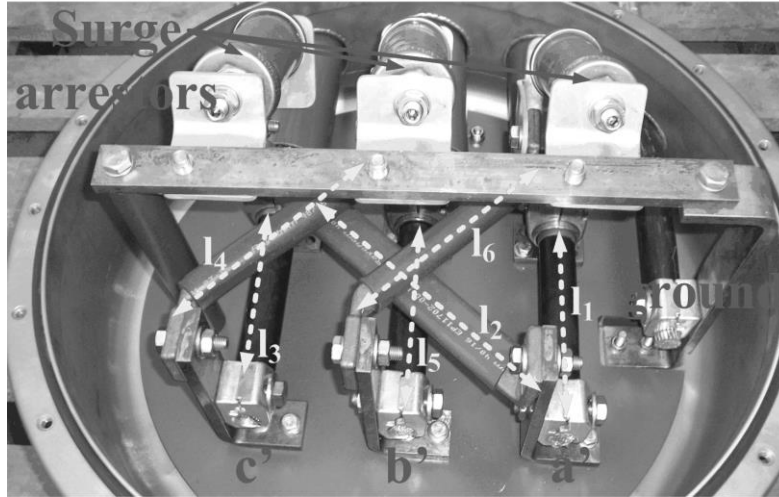


Figure 5.13 Inside view of the CB-box.

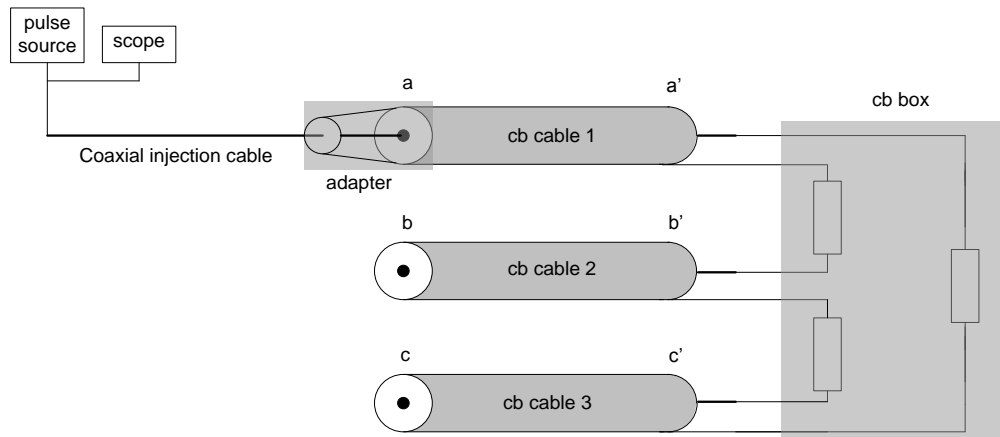


Figure 5.14 CB-cables connected to the CB-box.

A pulse of 8 ns width is injected via, the coaxial injection cable, into CB-cable 1 (Figure 5.14). The sending ends of the two other CB-cables are open. The injected pulse propagates along the injection cable and reflection and refraction takes place at location a. The reflected part propagates back to the sending end while the refracted part propagates along the CB-cable and reflects at location a'. The reflected pulses are measured at the sending end of the injected CB-cable. Also, the pulses transmitted to CB cables 2 and 3 are recorded. The pulse injection measurement is also done for CB-cables 2 and 3. In Figures 5.15 to 5.17, the measured pulses are plotted for all three measurements.

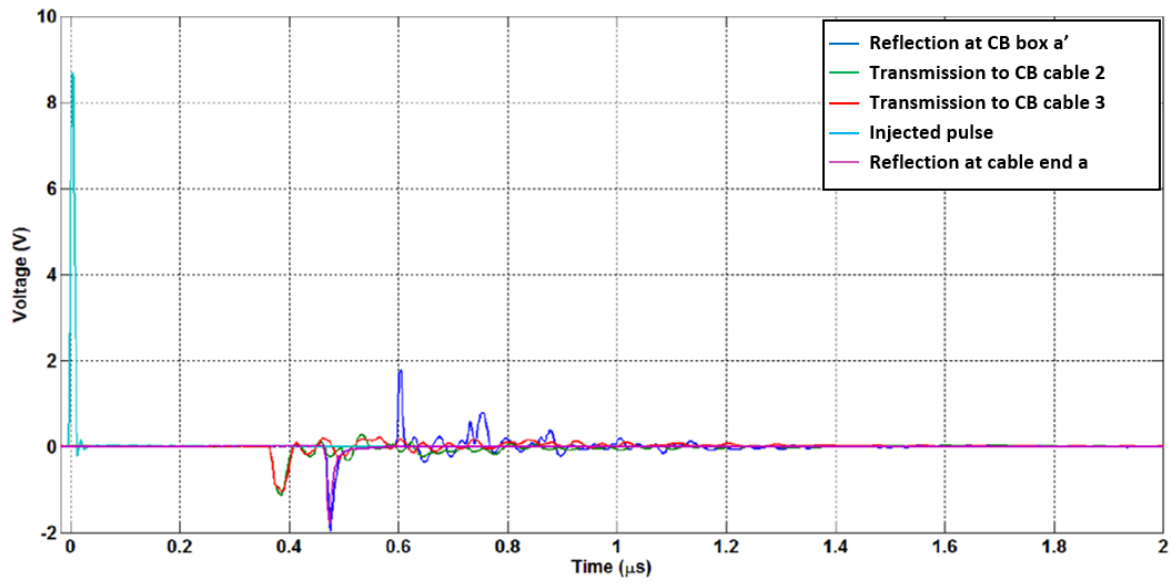


Figure 5.15 Measured signals after a pulse injection at CB-cable 1.

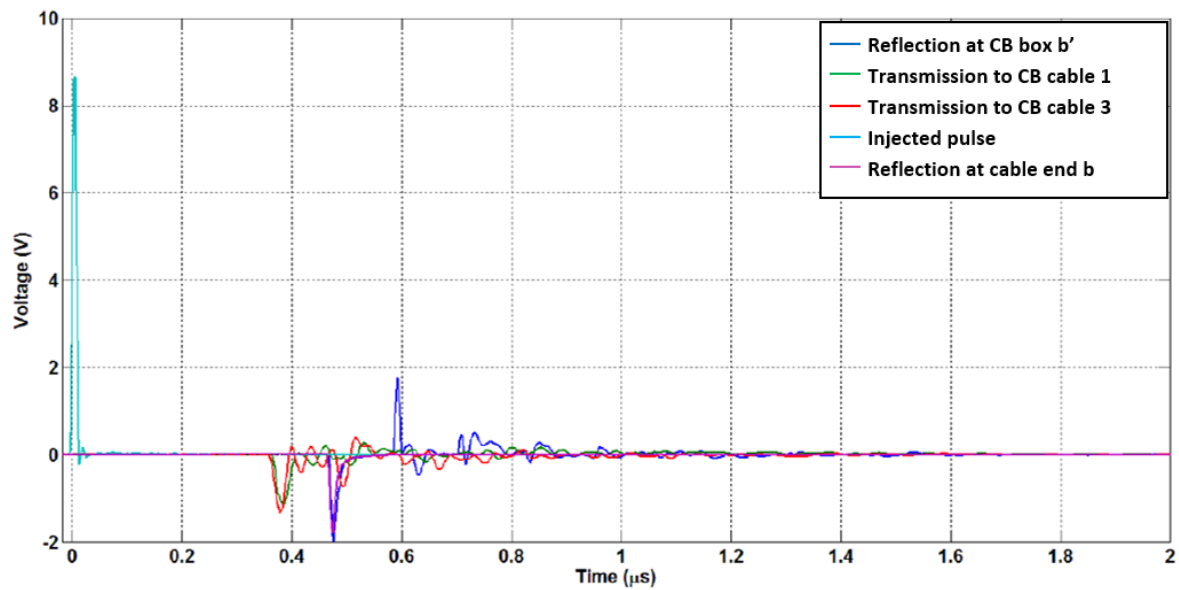


Figure 5.16 Measured signals after a pulse injection at CB-cable 2.

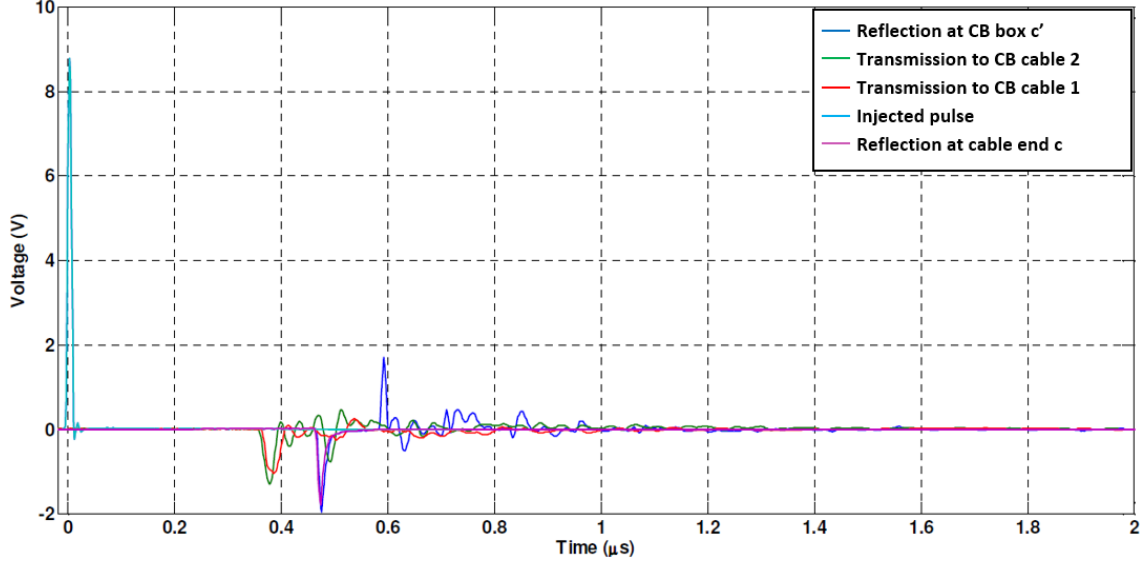


Figure 5.17 Measured signals after a pulse injection at CB-cable 3.

The cyan colored line in the graphs is the pulse injected into the coaxial measuring cable and partly reflected at the CB-cable end. This is the purple pulse in the figures. The other part of the pulse refracts and propagates through CB-cables 1 (red) and 2 (green). For all three measurements, the reflected pulse at the CB-box is  $Y_{cbbox}$ . From the injected pulse and the reflected signals, the CB-box transfer function is calculated with Equation (5.11). Also, the reflection coefficient  $r_{cbbox}$  at the CB-box, at location  $a'$ , can be calculated (Equation 5.12) and also  $Z_{cbbox}$  can be found [65].

$$H = \frac{Y_{cbbox}}{Y_{inj}} = H_{inj} \tau_{c-i} \tau_{i-c} r_{cbbox} e^{-\gamma_{cb} 2l_{cb}} \quad (5.11)$$

$$r_{cbbox} = \frac{Z_{ccb} + Z_{cbbox}}{3Z_{ccb} + Z_{cbbox}} \quad (5.12)$$

Frequency analysis as published in [65] gives us the following values for the three lumped inductances:

$$\begin{aligned} L_{cbbox1} &= 443 \text{ nH} \\ L_{cbbox2} &= 427 \text{ nH} \\ L_{cbbox3} &= 430 \text{ nH} \end{aligned}$$

## CB-joint

The cb joint forms the connection between the CB-cable and the screen conductor of the 380 kV cable. Figure 5.18 gives a view on the cross section of the CB-joint where the screen conductor of the CB-joint is interrupted. This interruption gives an inductive loop within the CB-joint [68], [69] and this loop is modeled as a rectangular current loop. The value of the corresponding inductance can be calculated from the pulse reflection measurements performed on a section of the 380 kV cable system, in which the CB-joint is installed.

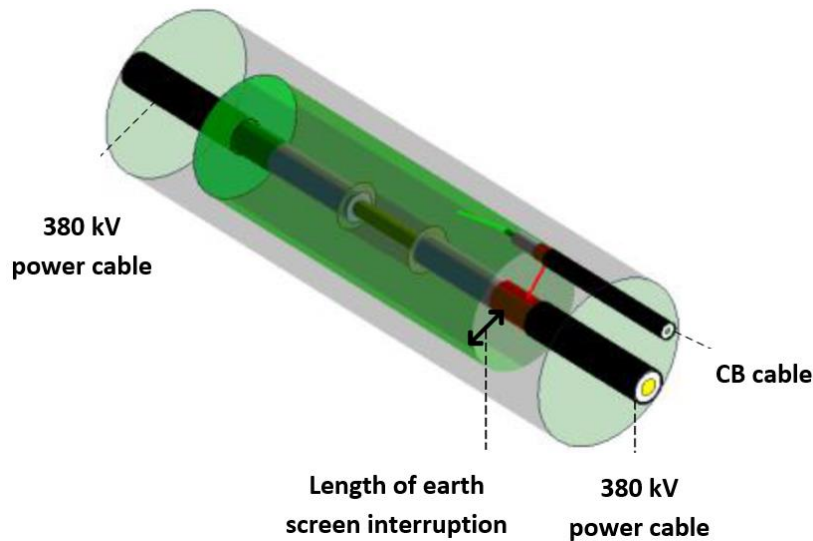


Figure 5.18 Cross section of the CB-joint.

The measurement setup is shown in Figure 5.19. A pulse of 100 ns width is injected via the coaxial injection cable into the 380 kV cable. The receiving CB-cable end is left open at location b. The pulse will partially reflect at CB-joint location a'. The measured reflected pulse at this location is denoted as  $Y_I$ . From these two pulses, the transfer function, describing the propagation from the location of injection to the CB-joint, can be calculated.

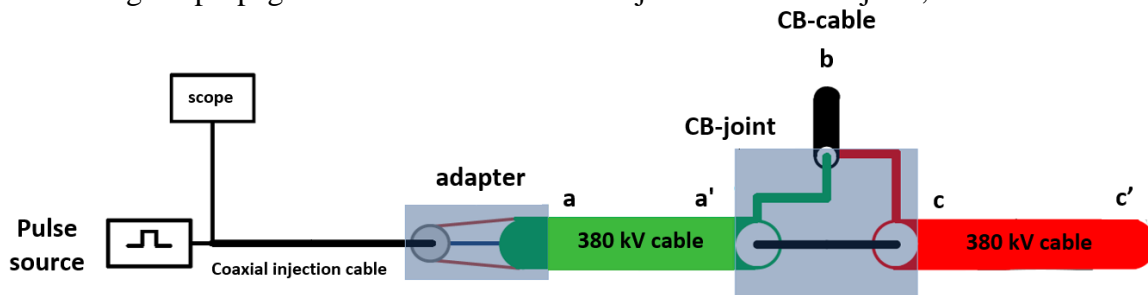


Figure 5.19 Measurement layout for pulse injection into CB-joint.

In Figure 5.20, the measured pulses are plotted. The green pulse is the injected pulse and the negative red pulse is caused by reflection at the 380 kV cable end at location a. The cyan pulse measured at 11.5  $\mu\text{s}$  is the reflection at the CB-joint. This time delay corresponds to the distance of the location of the CB-joint around 945 m away from the point of injection. The measured signals are transformed to the frequency domain in order to be able to calculate a value for the loop inductance of the CB-joint. This measurement resulted in an inductance of 860 nH.

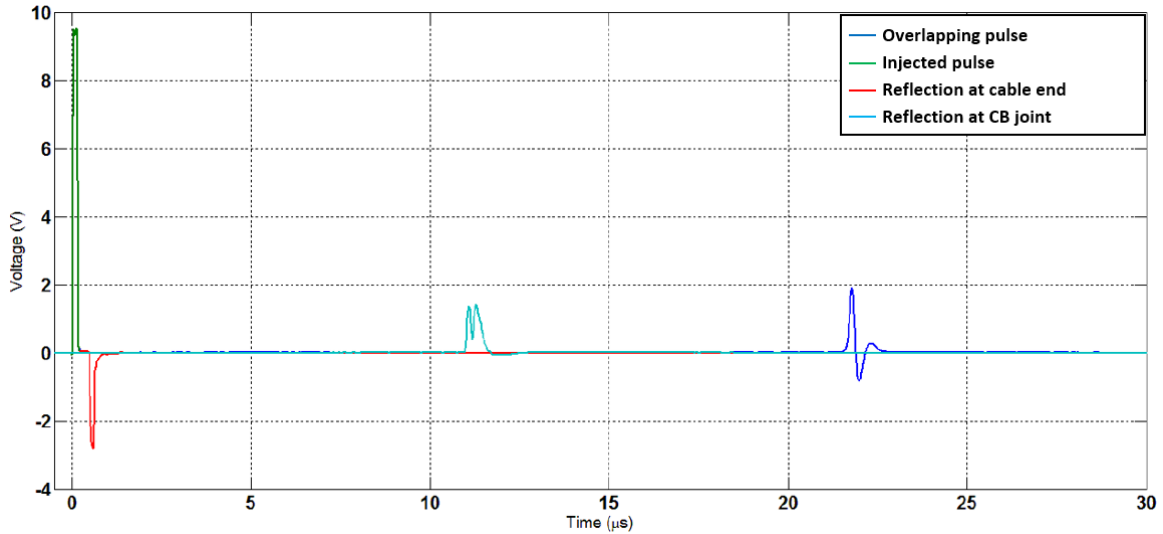


Figure 5.20 Measured pulses for the CB-joint measurement.

## 5.5 CONCLUSION

In this chapter, the modeling process was described for the 380 kV cable section, the cross-bonding (CB) cable, the overhead-line parts and the series reactor. A transient model was developed for the 380 kV cable section by using the Frequency Dependent Phase Model, available in the PSCAD software. It was proven by calculations that the mutual coupling between the cable circuits (2 circuits of 6 cables) in the section was quite small, which means that this coupling in this cable section can be neglected. This is an important conclusion for the grid operator for two reasons. The first reason is that neglecting the coupling between the cable circuits implies that the modeling work for such a cable system can be simplified when the grid operator wants to do transient calculations on cable sections, for instance for future planning studies. The second reason is that when we know that the coupling between the cable circuits is small, it is expected that when one circuit is out of service because of maintenance for instance, the induced voltage in that circuit by the other circuit is negligible. From safety point of view, this is very important.

Pulse measurements on the CB-cable were carried out and the measurement results were used for deriving appropriate lumped element models for the CB-cable, the CB-box and the CB-joint. The values for the lumped inductances of the CB-box and the CB-joint were calculated and are useful for modeling the total cable system and therefore, the models developed in this chapter are used for simulation studies for investigating switching



transients (Chapter 6) and lightning overvoltages (Chapter 7). The validity of the developed model is not only restricted to the cable parts in the Randstad 380 kV project, but the model is more general applicable to underground 380 kV systems in which cross-bonding is applied.

## CHAPTER 6

# SWITCHING OF MIXED 380 KV LINE-CABLE-LINE SECTIONS

### 6.1 INTRODUCTION

Switching actions in power systems are common and they are the origin of transient voltage and current oscillations, which occur in the grid. Switching actions occur when, for instance, a cable or a load is brought into operation or taken out of service. A switching action changes the topology of the network that results in a redistribution of the energy flows. The result of a switching action are oscillations in voltages and currents propagating as travelling waves through the power system. Attention should be paid to steep wave fronts that reach vulnerable power system parts like transformer windings. This chapter presents the results of a switching impact study on 380 kV mixed line-cable circuits. A switching transient produces voltage and current oscillations that play a role during energization of a mixed line-cable circuit. Knowing the resulting transient voltages and currents is important when new overhead lines and cables are being planned in an existing power system in order to be able to investigate the peak transient voltages will stay below the allowable limit during these switching actions (1040 kV for the 380 kV cable terminals) [30]. The severity of switching actions depends on the instant when the circuit breaker opens or closes. Switching surges are characterized by front times of several hundred microseconds with tail times up to of several milliseconds. Vacuum and SF<sub>6</sub> breakers can produce transient voltages with front times of nanoseconds.

The duration of the transient period is important, since a transient causes voltage and current oscillations affecting the steady state power voltage. PSCAD models of the overhead line and cable sections of the Randstad 380 kV connections in the Netherlands (see Chapter 5) are the bases for accurate transient studies. The objective of this chapter is to determine the amplitude and the duration of switching overvoltages under different switching conditions. To obtain representative simulation results, a suitable model for the circuit breaker is necessary. The power transformer model and the circuit breaker used in

this study are described in paragraph 6.2. In paragraph 6.3, the switching-in of both newly build 380 kV connections is analyzed under different operating conditions. In paragraph 6.4, the transient response of a charged cable is considered when it is being switched with opposite polarity to the power system voltage. Attention is paid to cable discharge currents in paragraph 6.5.

## **6.2 TRANSFORMER AND CIRCUIT BREAKER MODELING**

In Chapter 5, a transient simulation model for the new line-cable-line circuits in the Randstad has been developed. For a correct description of the transient behavior of the cable circuit, the simulation should have also a suitable model for the EHV transformer at the substation, including the shunt reactors, connected to the tertiary transformer winding. A simplified model of the transformer, containing lumped capacitances only, is sufficient for the calculations. During the transient phase, high frequency oscillations are dominated and the transformer windings must be modelled as transmission lines [70-72], since the wavelength of the oscillations is of the same order as the physical dimensions of the transformer. Hybrid modeling of the transformer winding, in which the winding is divided into sections, can be applied for calculating voltage transients in the winding [95]. In this model, each winding section is modeled as a single conductor transmission line to calculate the voltages at each end of that winding section. Thereafter, the section is modeled by a multi conductor transmission line to calculate the voltages at each turn of the winding section.

In the transmission line model of the winding, the capacitances between the primary and secondary windings and between the turns of the winding must be taken into account. At higher frequencies, the capacitances of the transformer winding play a dominant role, as the initial voltage distribution in the winding is mainly determined by these capacitances. For an appropriate transient model, all inter-turn capacitances and winding inductances must be taken into account together with the winding losses. Depending on the phenomena being observed, a simplified transformer model containing the equivalent winding capacitance can be enough for performing the study. In that model, the total transformer winding capacitance is represented as a lumped capacitance between the 380 kV primary winding and the ground, as is shown in Figure 6.1.

For the shunt reactor, being connected at the tertiary winding of the 380/150 kV transformer, a similar approach is made for the equivalent winding capacitance. The values for the equivalent lumped capacitance  $C_{eq}$  are taken from [79].

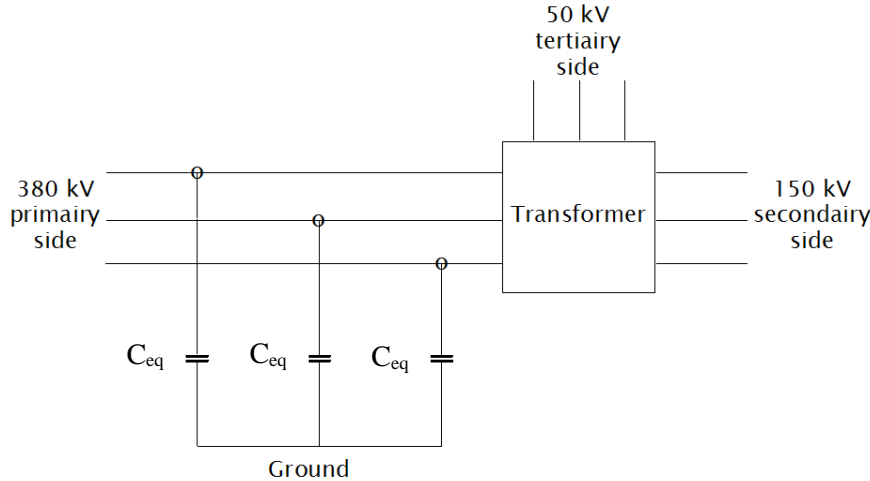


Figure 6.1. Transformer model with equivalent winding capacitance.

It depends on the loading condition whether the circuit breaker has to connect or disconnect the cable circuit during operation. Simulation of current interruption requires an accurate model of the circuit breaker. In the case of current interruption, an arc is formed between the breaker contacts after contact separation that conducts the current. At current zero, the arc is extinguished and the current is interrupted. After current interruption, the breaker contacts must withstand the Transient Recovery Voltage (TRV). Circuit breakers are distinguished by their extinguishing medium. In medium voltage systems, the vacuum circuit breaker is mostly applied. Current interruption can result in a reignition, giving high frequency current oscillations [73], [74]. For breaker modeling, the dielectric withstand voltage level and the critical current slope are important parameters.

In transmission systems, circuit breakers have SF6 as extinguishing medium [78] and that is why an SF6 breaker model is used for this study. Also reignition can occur in SF6 breakers and the breaker model used is based on the functionality of a 10 kV single phase vacuum breaker model [75]. To obtain a realistic model for the breaker to be applied in the 380 kV connections, the characteristics for a 400 kV SF6 breaker are implemented in the 10 kV simulation model and extended from single phase to three phase. This ensures that realistic values are used in the breaker's PSCAD simulation model to model the dielectric withstand characteristics and the breaker critical current slope. The breaker critical current slope is not easy to determine. The dielectric withstand voltage, being a function of the distance of the breaker contacts, forms a critical factor in controlling reignition overvoltages.

The breaker characteristics for the 400 kV SF6 breaker used in the model are taken from [76]. The locations of the circuit breaker (CB) in the cable circuit WTR-BWK are shown in Figure 6.4a.

### 6.3 CABLE SWITCHING-IN STUDY (ENERGIZATION)

Energization of the 380 kV cable circuit takes place when the cable is put into operation by closing the breaker. After switching, the cable circuit is supplied by the power system at 220 kV (phase to ground voltage). Switching actions results in transient voltages and currents in the network, depending on the circuit load condition. The energization of the cable is like switching a capacitance, with that difference that the cable capacitance is distributed.

After the cable is put into operation for the first time, the cable is in fact an uncharged capacitance and therefore a large capacitive inrush current is to be expected. In Figure 6.2, the block diagrams of the connections Waterningen - Bleiswijk and Bleiswijk - Beverwijk are drawn. To learn the impact of energizing the cable circuit under no-load condition, both terminals remain disconnected from the substation side.

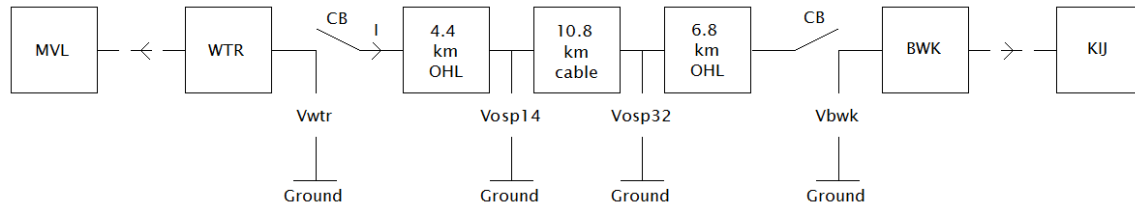


Figure 6.2a. Connection WTR-BWK.

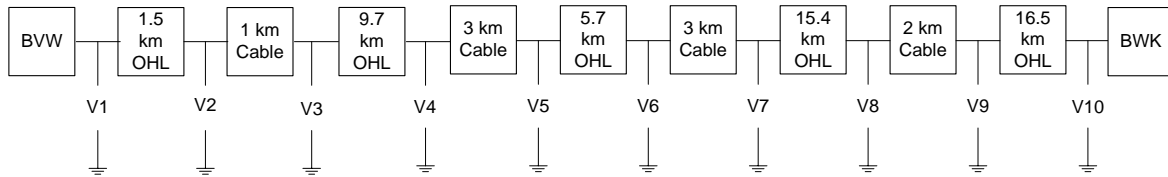


Figure 6.2b. Connection BWK-BVW.

To calculate the transient voltage response when the unloaded cable circuit is connected to the grid, the cable model, as it is described in Chapter 5, is used, including the (simplified) transformer- and the circuit breaker model. A step voltage function of 1 kV is switched-on to the network and represents a sudden change in the power frequency supply voltage. The result is an oscillating voltage response travelling along the connection and brings the peak value of which at the receiving open end is twice as high as the voltage level at the sending end.

The voltage peak value at the receiving end is the cumulative result of multiple reflections occurring at this location. When a lossless and distortion less cable is switched in, a sudden voltage change occur at the sending end resulting in a travelling voltage and current wave along the cable. The electromagnetic energy stored in the travelling wave has an electric

field component  $E$  and a magnetic field component  $H$  (Chapter 2). When the receiving open end is reached, the current wave drops to zero and the energy stored in the magnetic field component is transferred to the electric field component according to the relation of Equation (6.1). As a consequence, the peak value of the receiving open end voltage gets as high as 2 pu.

$$\frac{1}{2}Li^2 = \frac{1}{2}Cv^2 \quad (6.1)$$

where

$L$  is the line inductance [H/m]; and

$C$  is the line capacitance [F/m].

The resulting open end voltage can be found from the cable travelling time  $\tau$  and switching a unit step voltage function to the cable sending end at  $t = 0$ . When the starting voltage amplitude  $V_0$  is connected to the cable sending end, the open end voltage can be expressed as the time shifted unit step functions. From  $t = 0$  up to  $t = 7\tau$ , the receiving end voltage  $V_r$  is:

$$V_r = 2V_0u(t - \tau) - 2V_0u(t - 3\tau) + 2V_0u(t - 5\tau) - 2V_0u(t - 7\tau) \quad (6.2)$$

where

$\tau$  is the cable travelling time (s); and

$u(t)$  is the unit step voltage function.

From Equation (6.2), it becomes clear that the open end voltage jumps to  $2V_0$  after the first reflection. The open end voltage oscillates between  $2V_0$  and zero with an average value equal to  $V_0$ . In practice, the cable gives attenuation and distortion, and this results in a lower open end voltage peak value. The open end voltage after  $n$  reflections is calculated by the geometric series:

$$V_r = 2(k - k^3 + k^5 - k^7 + \dots k^{2n-1}) \quad (6.3)$$

In Equation (6.3),  $k$  is the attenuation factor as introduced and discussed in Chapter 5 for the 380 kV cable. The final open end voltage is reached when  $n \rightarrow \infty$  and equals:

$$V_{final} = \frac{2k}{k^2 + 1} \quad (6.4)$$

From Equation (6.4) we can see that for  $k=1$ , the final voltage is equal to the sending end voltage because there is no attenuation.

Figure 6.3 shows the calculated step voltage response at Bleiswijk after the cable is energized by a step voltage ( $V_{in}$  in the figure) with an amplitude of 1 kV at the Wateringen side. The receiving end voltage is  $V_{out}$  in the figure. From this figure, we can observe that the transient period is about 30 ms and the peak voltage is slightly higher than 2 pu. In Figures 6.4 and 6.5, the energization period of the connection Bleiswijk – Beverwijk is shown. From these figures, we learn that the transient period is significantly longer since the total length of the overhead lines in this connection is longer, and this means that the charging time is longer. We can also see that the oscillation period in Figure 6.4 is longer than the one in Figure 6.5 because compared to the WTR-BWK connection, this cable-line configuration contains more line-cable transition points causing a larger number of reflections that result in different voltage oscillation patterns. The damping, as it is observed from these figures, is coming from the cable and line attenuation, caused by their resistive losses. It is observed that the peak voltage at the receiving end exceeds the 2 pu, as it is shown in the Figures and in particular in Figure 6.5. This is the result of multiple reflections that occur between the line and cable sections.

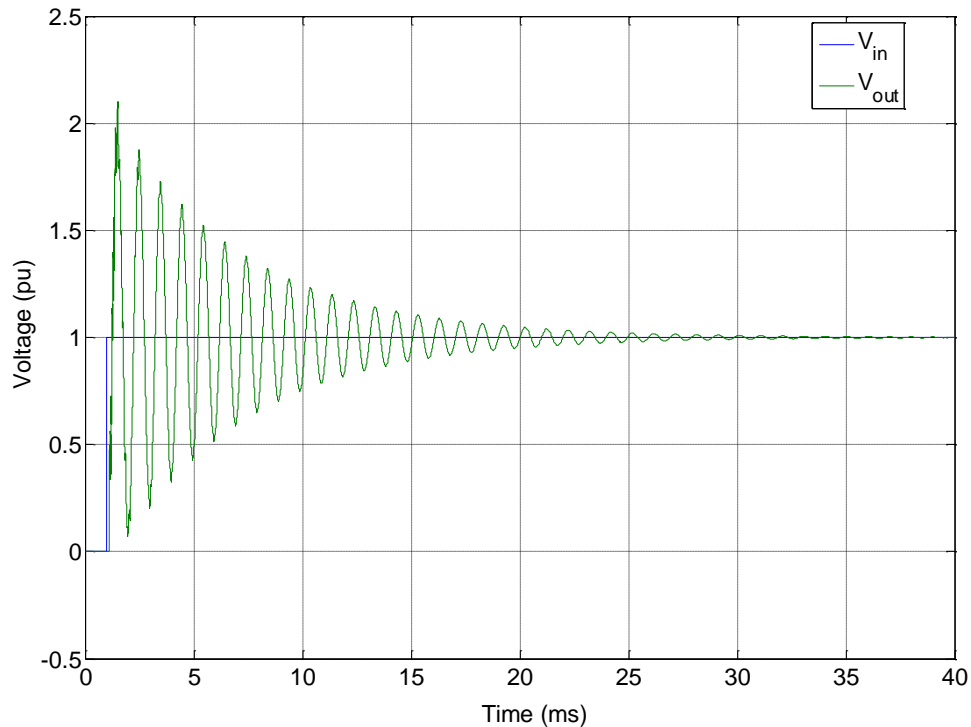


Figure 6.3. Step voltage response WTR-BWK when energized at Wateringen.

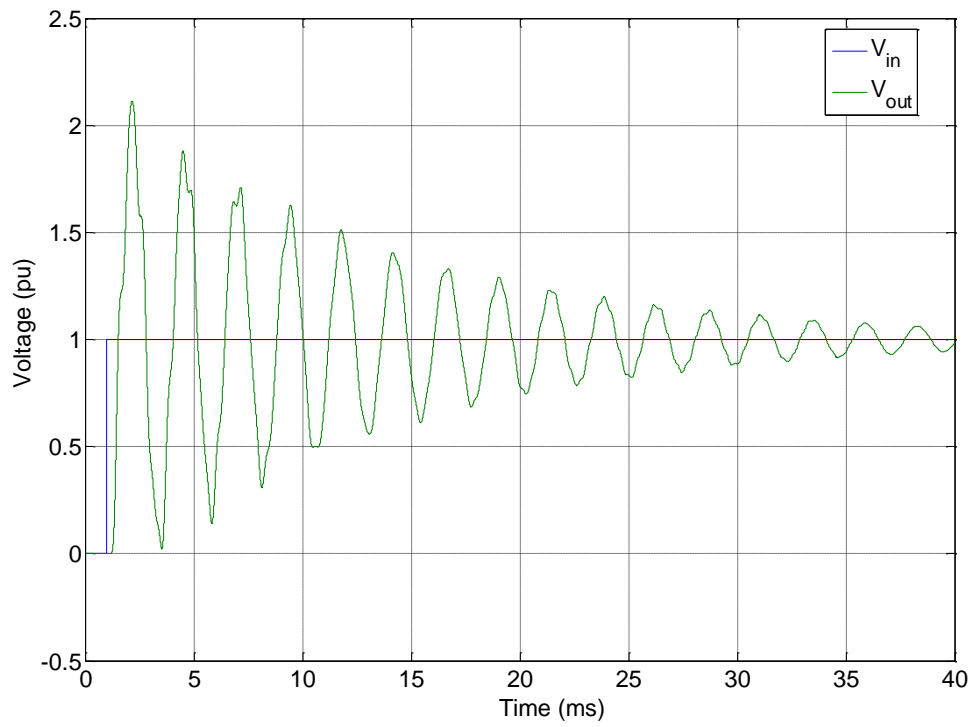


Figure 6.4. Step voltage response BWK-BVW when energized at Bleiswijk.

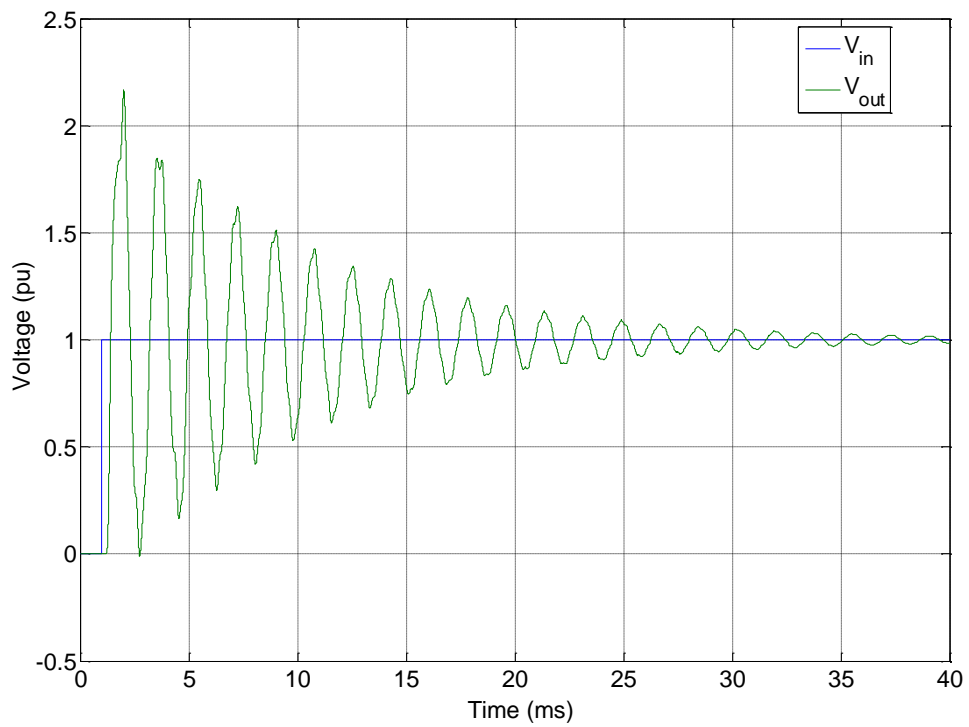


Figure 6.5. Step voltage response BWK-BVW when energized at Beverwijk.



In daily service, the mixed line-cable-line connection is a part of the power system and the origin of the energization transient comes from the power transformer in the substation and from the inductive shunt reactors. A simplified model to understand the process cable energization with a shunt reactor involved is drawn in Figure 6.6 [30].

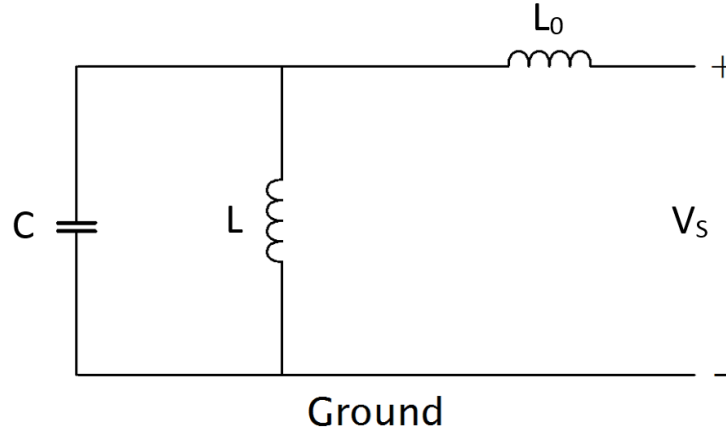


Figure 6.6. Equivalent circuit for cable energization with shunt reactor.

The parallel resonance frequency of this circuit can be calculated with:

$$f_0 = \frac{1}{2\pi} \sqrt{\frac{1}{LC} + \frac{1}{L_0 C}} \quad (6.5)$$

where

$L$  is the shunt reactor self-inductance (H);

$L_0$  is the equivalent source self-inductance (H); and

$C$  is the cable capacitance (F).

It is educational to look at the energization transient at both substations Wateringen and Bleiswijk, and at the cable-line transition points when the cable circuit is switched-on by the circuit breaker. The severity of the transient depends on the instant of switching. When switching-in an uncharged cable, a large capacitive inrush current flows, with a frequency mainly determined by the circuit inductance and cable capacitance. The capacitive inrush current can be calculated with Equation (6.6).

$$i(t) = \frac{V_{in}}{Z_0} \sin(\omega_0 t) \quad (6.6)$$

where

$\omega_0$  is the circuit natural frequency (Hz); and

$Z_0$  is the circuit characteristic impedance ( $\Omega$ ).

When we want to calculate the worst case scenario in relation to the voltage level, the line-to-line power voltage is taken to be 418 kV, since this is the maximum permissible steady state operating voltage level in the grid (see Chapter 4). This means that the phase to ground voltage peak value is in that case 341 kV.

In Figure 6.7, the voltages are shown at the Wateringen side for the case that the connection is switched-in at substation Wateringen at peak voltage of phase  $a$ , while the Bleiswijk side left open. The calculated amplitude of the steady state voltage is 341 kV. The switching instant is at  $t = 0.025$  ms. We note that the voltage peak is a bit above 500 kV in phase  $a$ , and there is a short voltage oscillation in the other two phases.

Figures 6.8 and 6.9 give the voltages for line-cable transition points OSP14 and OSP32 (indicated in Figure 6.2a) respectively. As can be seen from the figures, the voltages at the transition points have a similar response, but with a small time shift of a few microseconds by the travelling time of the cable.

Figure 6.10 shows the voltages at Bleiswijk side. Before the instant of switching, the voltage is zero for this location. We see that the peak voltage at this location for phase  $a$  is 550 kV, and this is slightly higher than at Wateringen. The voltage response is influenced by the cable dimensions and by the rest of the 380 kV network. The difference in peak voltage at both the locations is caused by the different impedances of the grid feeding in to the substations.

In Figures 6.11 and 6.12, the currents at the transition points OSP14 and OSP32 are plotted for the three phases after contact closing. As expected, the currents nearby the sending end are significantly higher in amplitude than at OSP32. Since for this case the connection at Bleiswijk is open, the final current value equals the cable charging current and the current value can be verified by Equation (6.7).

$$I_{cable} = \frac{V_{LN}}{X_{cable}} \quad (6.7)$$

where

$V_{LN}$  is the phase to ground operating voltage (V); and

$X_{cable}$  is the cable reactance ( $\Omega$ ).

In Chapter 5, we learned that the cable capacitance is equal to 0.23  $\mu\text{F}/\text{km}$ . Because there are two cable in parallel for each phase, the total capacitance for the 10.8 km cable section is nearby 5  $\mu\text{F}$ . Having a power frequency voltage of 230 kV phase to ground, the RMS value of the capacitive current, drawn by the cable at the sending end, is 345 A. The peak value of this current is 488 A, see Figure 6.11. The current at OSP32 is smaller compared to that at OSP14, since the capacitance at this location is less, and thus giving a smaller line charging current.

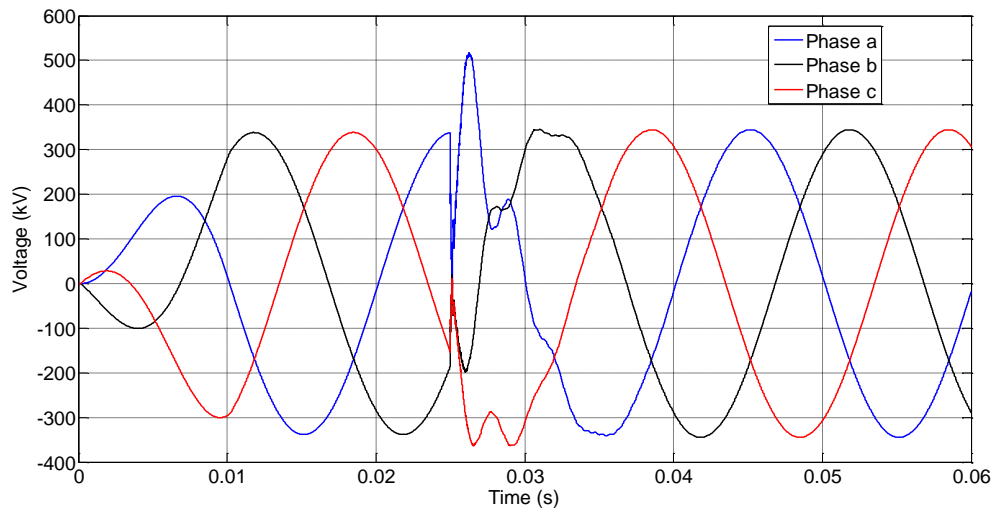


Figure 6.7. Voltage response at Watringen side.

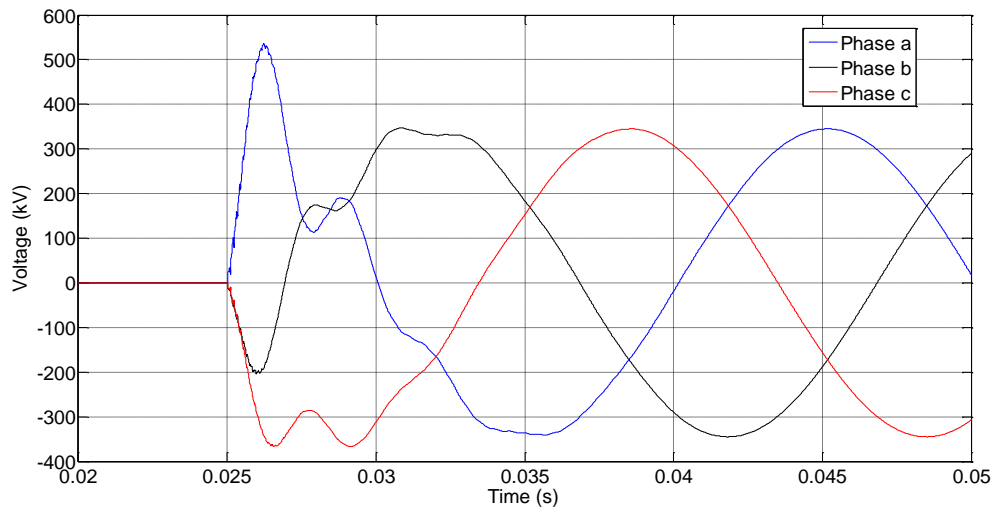


Figure 6.8. Voltage response at OSP14.

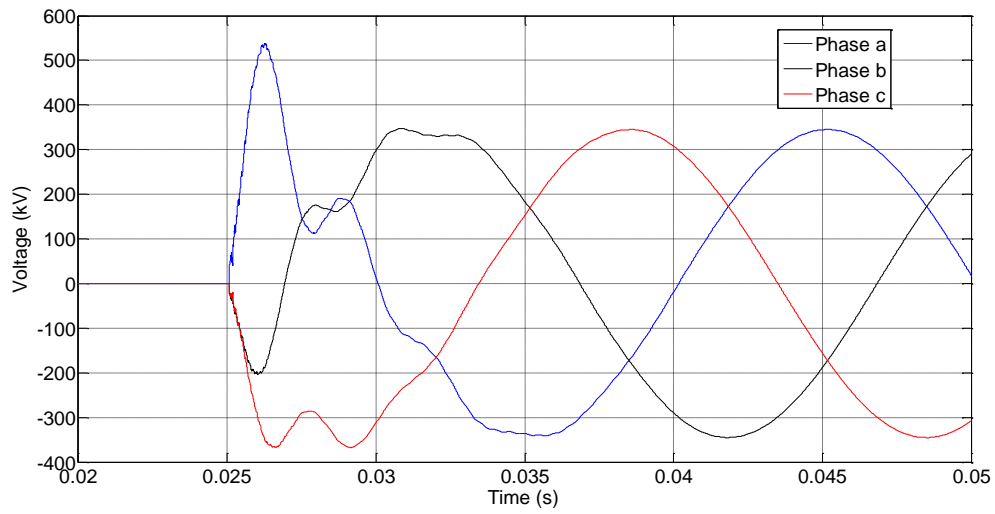


Figure 6.9. Voltage response at OSP32.

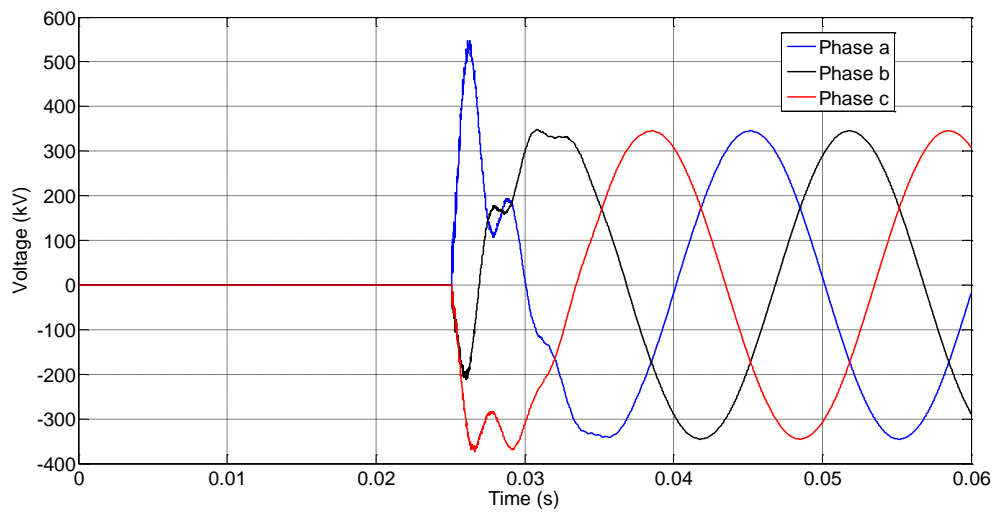


Figure 6.10. Voltage response at Bleiswijk side.

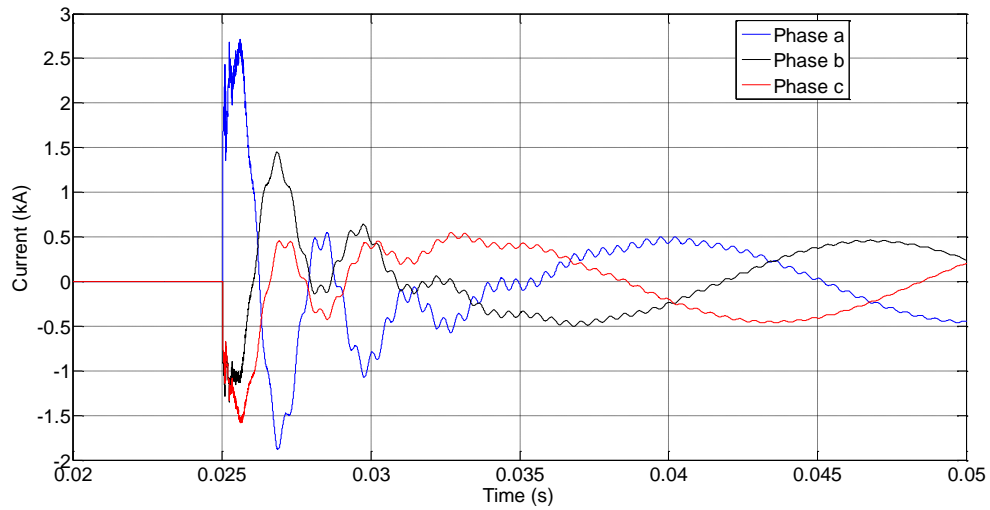


Figure 6.11. Currents at OSP14.

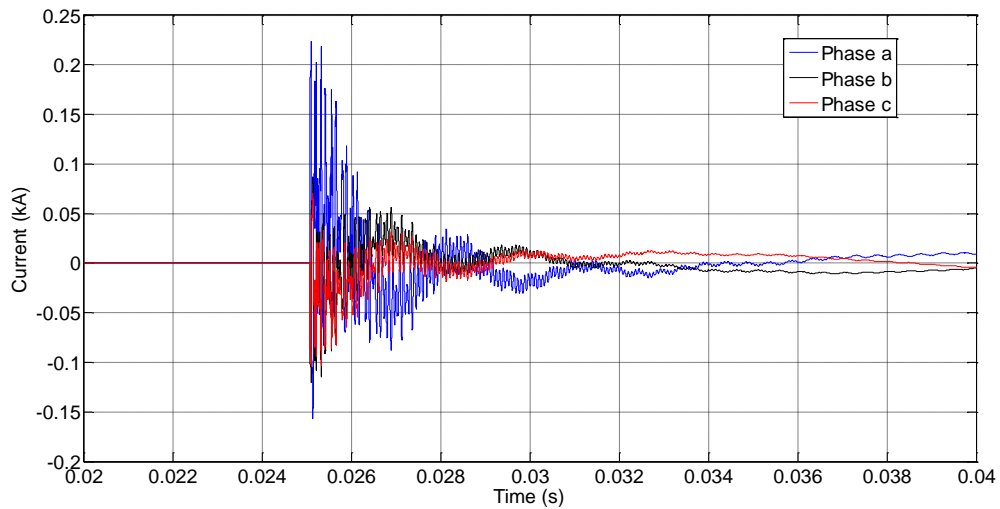


Figure 6.12. Currents at OSP32.

In a next situation, a similar switching action is considered, but with the connection switched from the Bleiswijk side, and Wateringen left open. Since the cable section is embedded between two sections of overhead line (having almost the same length), a similar voltage response is to be expected as in the previous situation. But as the grid impedances at the supply side of the substation differ, the voltage transients also differ. Figures 6.13 and 6.14 show the calculated voltage responses at Bleiswijk and Wateringen. The peak value of the voltage at the receiving open end at Wateringen exceeds 600 kV.

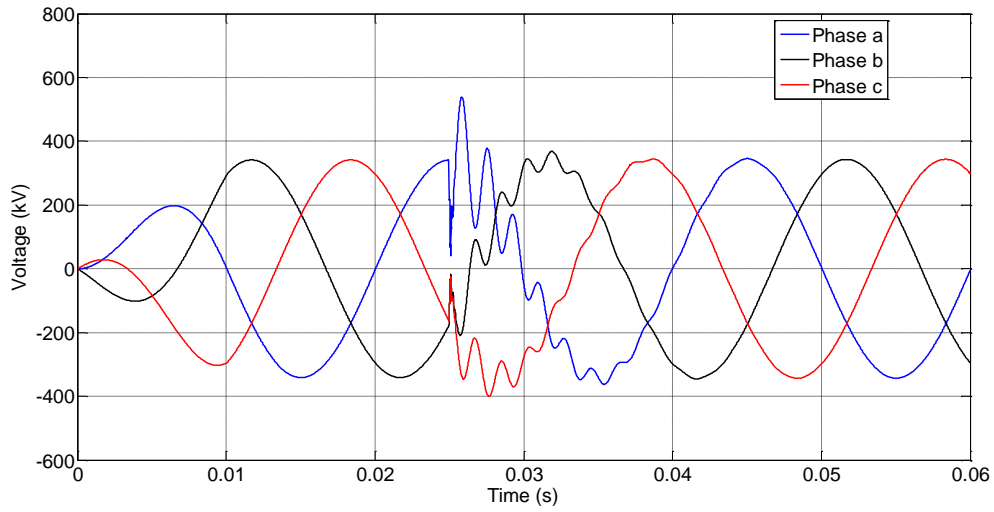


Figure 6.13. Voltage response at Bleiswijk side.

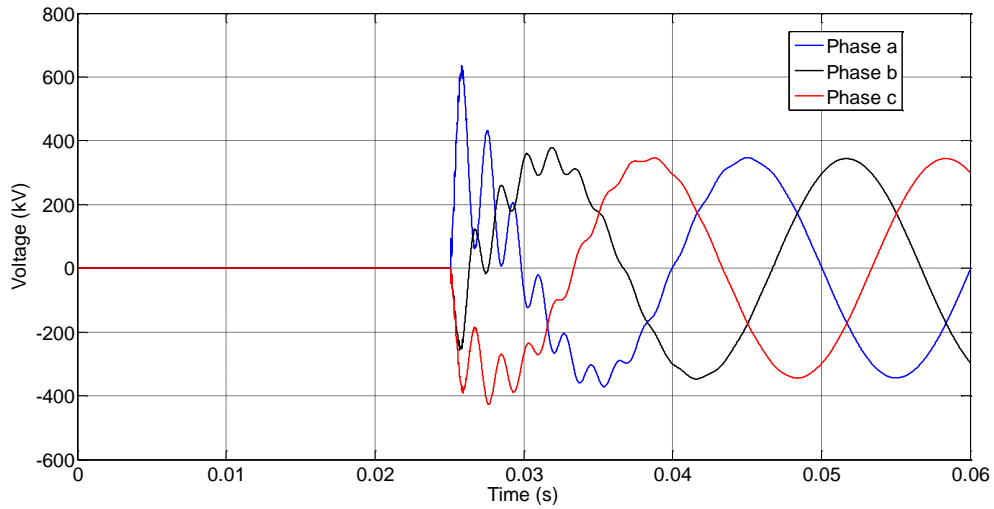


Figure 6.14. Voltage response at Wateringen side.

## 6.4 SWITCHING OF CHARGED CABLES

When cable circuits are disconnected from the network, a certain amount of charge remains trapped on the cable. In that case, the cable must be treated being an initially charged capacitance that is switched-in again. Depending on the instant of switching, this trapped charge has an impact on the transient voltage. Let us consider a fully charged cable, being disconnected from the grid. The worst case scenario is that a fully charged cable is re-connected to the grid when the supply voltage is at maximum opposite polarity. In

another case, the line-cable-line circuit is re-connected to the grid when the cable is charged to the peak value of the phase to ground supply voltage, being 341 kV. In Figure 6.15, the voltages are shown for Wieringen when the connection is switched-in with opposite polarity at  $t = 0.055$  s, and the receiving end at Bleiswijk left open. At the instant of switching, the steady state power voltage at phase  $a$  is of opposite polarity of the voltage of the cable at phase  $a$ .

The peak voltage is at Wieringen -700 kV, as it can be seen from the calculations. Figure 6.16 gives the voltages at the Bleiswijk side. The initial voltage is plotted till  $t = 0.055$  s. The peak value calculated at the open end at Bleiswijk is even higher, -750 V. In Figure 6.17 and 6.18, the voltages are shown for a similar switching action, but now the connection is switched-in at Bleiswijk, while it is left open at Wieringen. Like in the previous case, when the uncharged cable was switched, the difference in peak voltages is caused by the different impedances of the network feeding the substations. We can conclude that the peak value of the voltage transient during switching can exceed the theoretical maximum value of 2 pu, for energizing a cable.

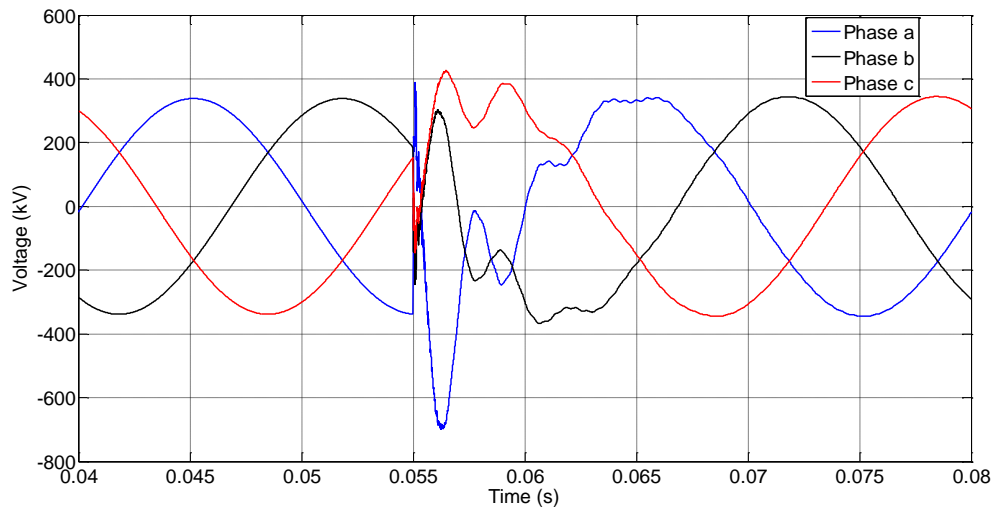


Figure 6.15. Voltage response at Wieringen side.

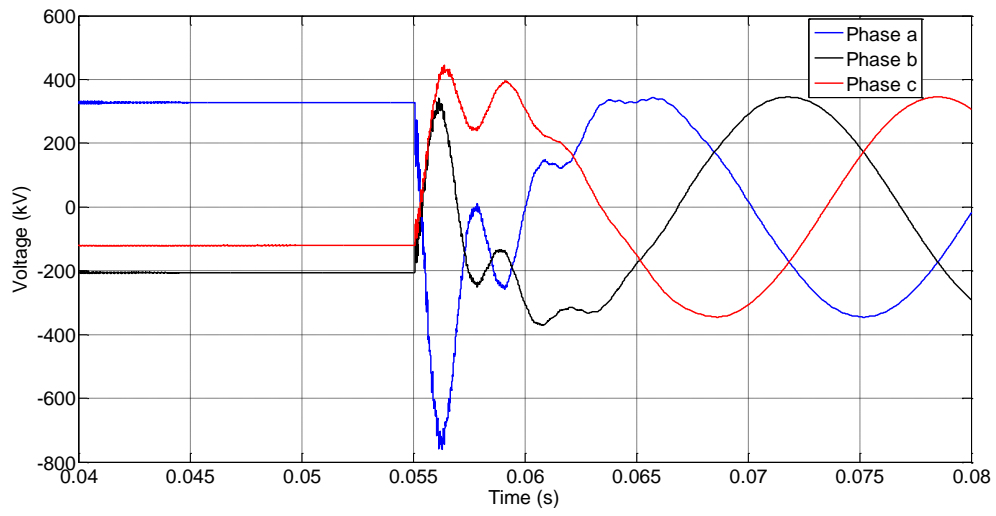


Figure 6.16. Voltage response at Bleiswijk side.

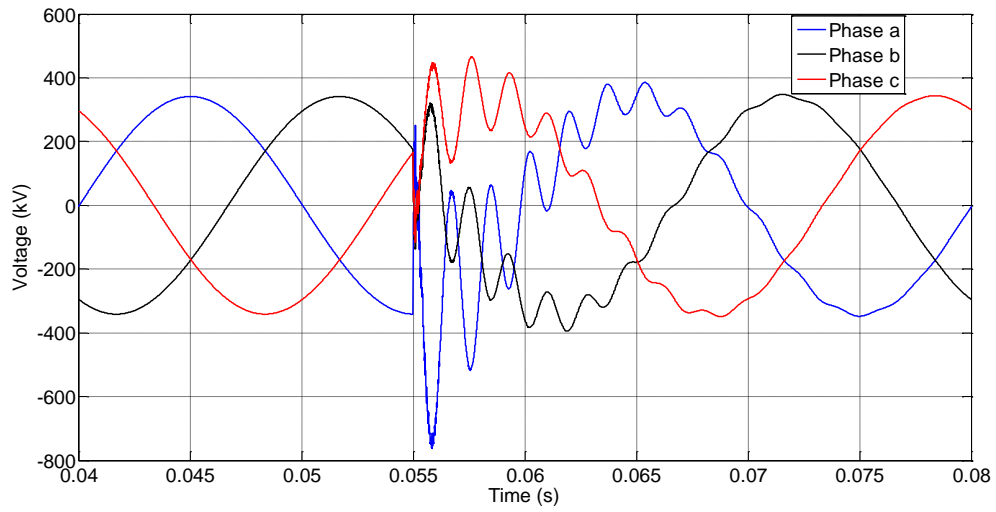


Figure 6.17. Voltage response at Bleiswijk side.



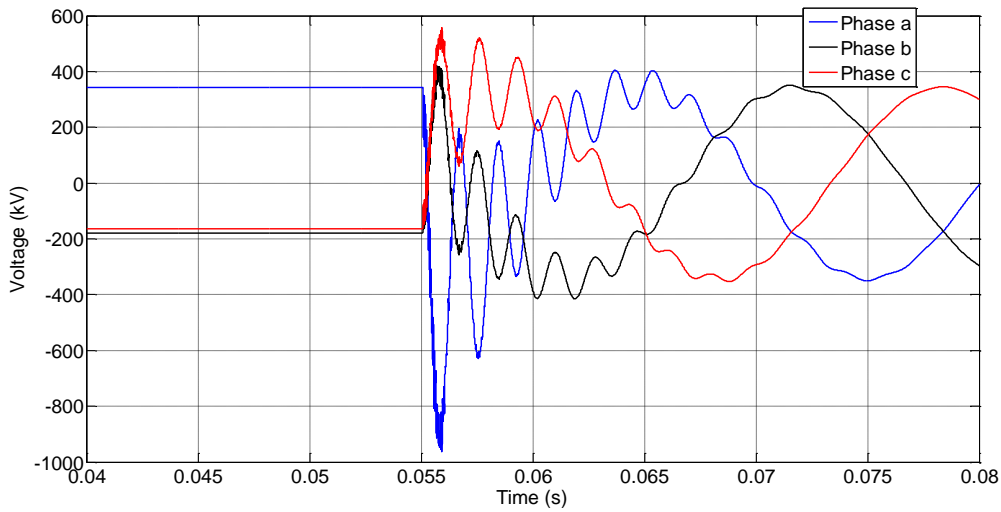


Figure 6.18. Voltage response at Wieringen side.

## 6.5 CABLE DISCHARGE CURRENTS

When the cable circuit is taken out of service, an amount of trapped charge can remain on the cable as discussed in the previous paragraph. Switching a charged cable, when the supply voltage is at opposite polarity, is the worst case scenario. It was demonstrated that switching an uncharged cable gives a lower transient overvoltage in comparison with switching with a cable with trapped charge. For safety reasons, the grid operator can discharge the cable before it is put into service. This is done by connecting the circuit terminals to ground potential by means of earthing switches. Important for the grid operator is what peak value of the discharge current is to be expected when the cable terminals are grounded. The current peak value during cable discharge is therefore an important parameter for the grid operator, as it has consequences for the dimensions of the ground rods to be installed in the substations [77].

In the next paragraph, the cable discharge current is calculated when the line-cable-line circuit is charged to the peak value of the power frequency voltage. The discharge currents are calculated for different cases and accounting for to the impedance of the grounding rods in the substations. In Figure 6.19, the location of the calculated discharge current  $I$  is shown in the schematic diagram of the connection Wieringen – Bleiswijk. The line-cable-line connection is disconnected from the substation when it is charged to the peak voltage value. When the switch closes, the current  $I$  is measured. Figure 6.20 shows the current flowing in the three phases with one terminal of the circuit being grounded at the Wieringen side. To simulate the worst case scenario, the impedance of the grounding rod is taken to be  $0 \Omega$ , because the maximum discharge current will flow in this situation. The discharge current has an sinusoidal shape with a peak of 10 kA in phase  $a$ , and decaying over time. We see that the oscillating period is similar for all three phases. The discharge

current is limited by the impedances of the overhead line sections at both sides of the cable. The inequality in current peaks at the instant of switching is caused by the mutual impedances between conductors. In Figure 6.21, the discharge currents are plotted when the connection is grounded at Bleiswijk side. This gives similar results compared with the previous case since the connection with the overhead lines at both sides of the cable are of almost equal length. The impedance of the grounding rods also influences the current peak value. Figures 6.22 and 6.23 show the discharge currents at Wieringen when the impedance is  $0.1 \Omega$  and  $0.5 \Omega$  respectively. We note that the influence of the ground rod impedance on the current peaks is rather small. The oscillation frequency of the discharge current is approximately 1.11 kHz.

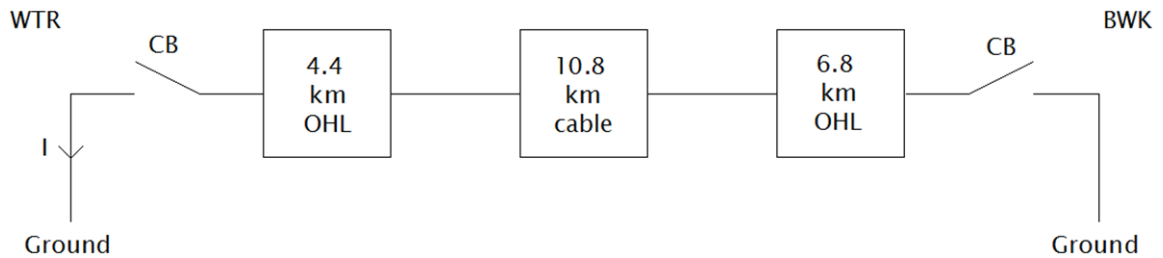


Figure 6.19. Location of the discharge current.

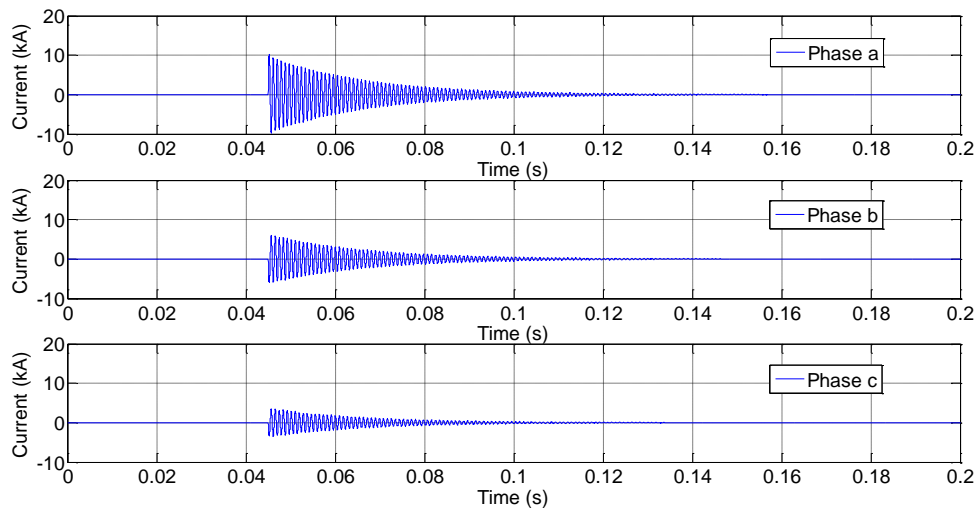


Figure 6.20. Discharge current when grounded at Wieringen.

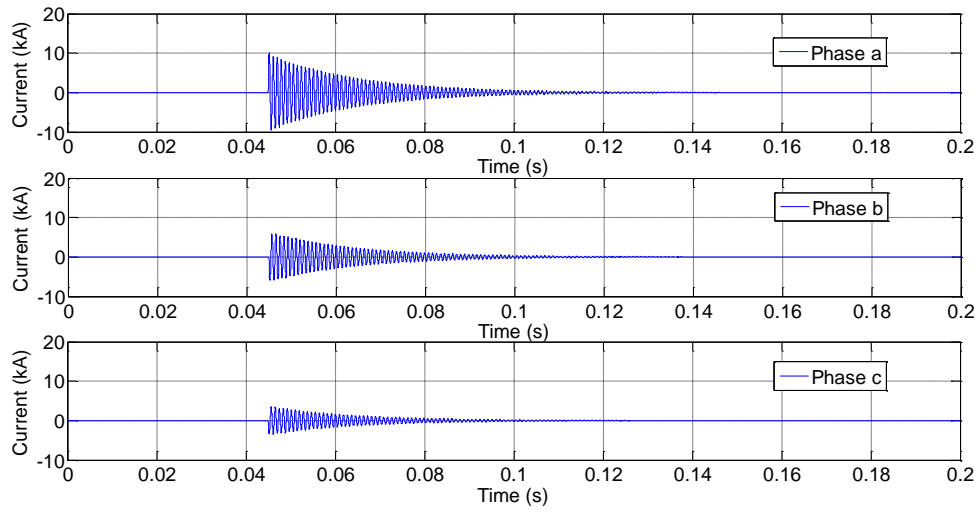


Figure 6.21. Discharge current when grounded at Bleiswijk.

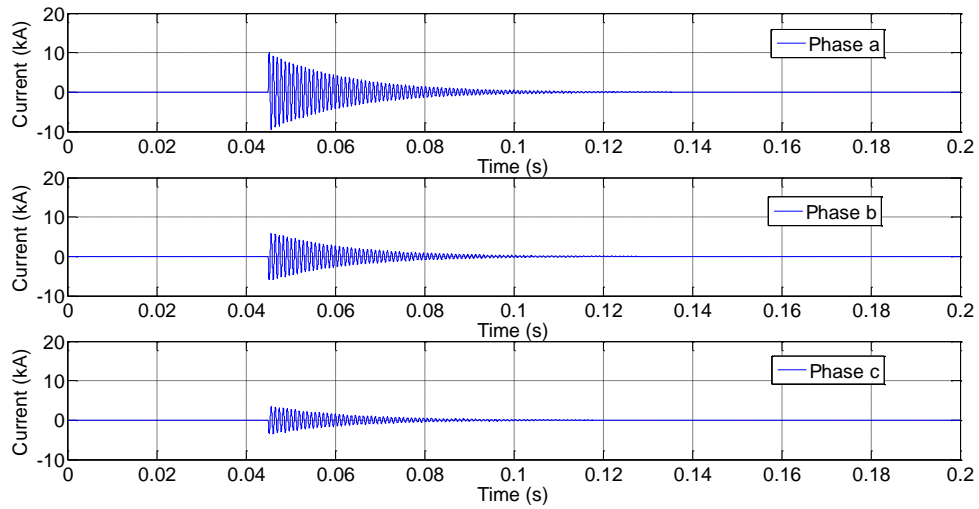


Figure 6.22. Discharge current at Watringen when grounded with 0.1  $\Omega$ .

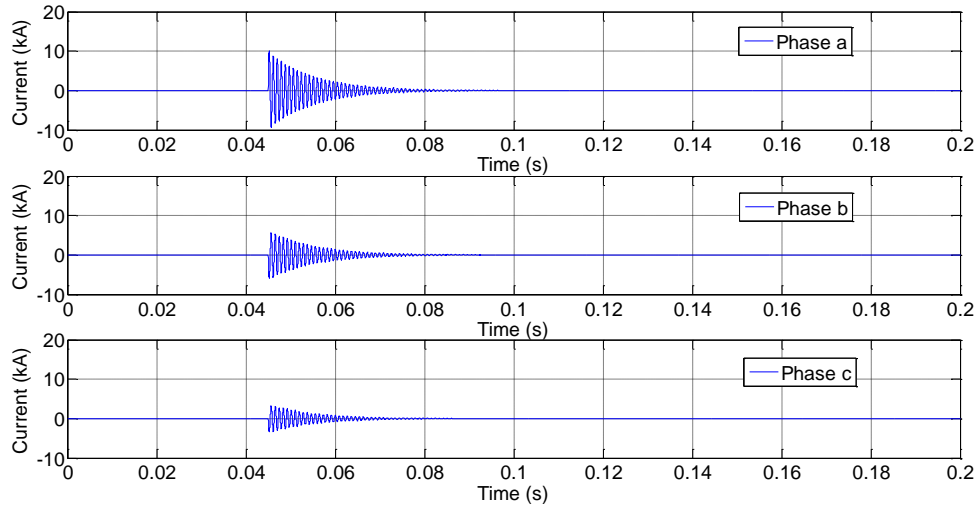


Figure 6.23. Discharge current at Watringen when grounded with 0.5  $\Omega$ .

The oscillating frequency of the cable discharge current can be verified by calculating the natural frequency of the system: take the overhead line section as a lumped inductance and the cable section as a lumped capacitance. In Chapter 5, we found that the cable capacitance is 0.23  $\mu\text{F}/\text{km}$  (specified by the manufacturer). This means that the total capacitance of the 10.8 km cable section is close to 5  $\mu\text{F}$ , because there are two cables in parallel for each phase. The line self-inductance is calculated by Equation (6.8).

$$L_{line} = \frac{\mu_0}{2\pi} \ln\left(\frac{D}{0.799r}\right) \quad (6.8)$$

where

$D$  is the distance between the phase conductors (m); and  
 $r$  is the conductor radius (m).

When we use the overhead line data from Chapter 5, the value for the line self-inductance becomes 1.13 mH/km. The natural oscillation frequency of the system can be calculated from on the line self-inductance and the cable capacitance, (by Equation 6.9). A frequency of 1007 Hz is found, which is close to the value from the calculated oscillation. The difference between the calculated oscillation frequency and the estimated value is due to the resistive cable losses that are not taken into account in Equation (6.9).

$$f_0 = \frac{1}{2\pi\sqrt{L_{line}C_{cable}}} \quad (6.9)$$

where

$L_{line}$  is the self-inductance of the overhead line (H/m); and

$C_{cable}$  is the cable capacitance (F/m).

## 6.6 CONCLUSION

This chapter gives the results of switching actions that were performed on the new 380 kV mixed line-cable-line circuits. Cable energization was analyzed in order to look at the voltage and current oscillation interval at the cable-line transition points and at the line ends under no-load condition. Transients voltages were calculated with the connection being energized from both sides in order to observe a difference in transient voltage peaks. The peak voltages depend on the impedance after the power system feeding into the substation. Attention was also paid to switching the cable with opposite power voltage polarity (the cable initially charged to the peak power voltage), to investigate voltage peaks to be expected at the receiving line end. The calculated results for cable energization proved that the highest peak transient voltage occurs at the Bleiswijk side, when the connection is switched-in at the Wateringen side. From this result, it can be concluded that the switching order is of importance when the cable connection is connected to the grid. The results implies that the peak voltage level after switching depends on the grid behind the substation as there is a difference in voltage level at the Bleiswijk side compared to the Wateringen side when switching under the same initial charging conditions. This means that modeling the grid impedance behind the substation is important when performing studies on a part of the grid. Special attention was given to the case when the cable is uncharged, after connecting the line ends to ground. From the calculated results shown in the figures, it is seen that the maximum peak current is 10 kA during discharging the cable. However, the dimension of grounding rods for instance, is not related to this type of discharge currents, but is based on IEEE standards for grounding. More research on cable discharge currents is advisable to determine the influence of parameters like the ground return impedance on the shape and the size of the discharge current.

## **CHAPTER 7**

# **LIGHTNING INDUCED OVERVOLTAGES IN 380 KV MIXED LINE-CABLE-LINE CIRCUITS**

### **7.1 INTRODUCTION**

Lightning induced overvoltages in the power system are the result of atmospheric discharges during a thunderstorm. Unlike the transient phenomena discussed in the previous chapter, the origin of lightning induced overvoltages can come from outside: during a lightning, large discharge currents can hit directly an overhead line conductor or a high voltage tower. Such a strike can be regarded as a large surge current injection into the power system. Depending on the location of the current injection and the amount of discharge, steep front end overvoltages with a large amplitude will propagate as travelling waves throughout the network and can damage power system components, like transformers, bushings etc. To prevent against those types of steep transient overvoltages, protection by applying surge arresters is necessary. This chapter describes the results of the impact study of lightning discharge currents on the transient overvoltage levels in 380 kV mixed line-cable-line configurations. The objective is to investigate whether the transient overvoltage levels will remain below the Basic Insulation Level (BIL) after a lightning stroke, being for 380 kV equipment 1425 kV. Studying power systems during lightning events is in general important, but in particular for mixed line-cable networks where high peak voltages have been reported at line-cable junctions when relatively short cable lengths are being applied [14], [80-82]. Therefore, the results of this overvoltage analysis presented in this chapter is of value for designing a protection strategy against large overvoltages in newly build 380 kV connections with short cable sections in mixed line-cable-line configurations. In the second paragraph of this chapter, the mechanism of lightning discharges will be explained shortly. The impact of lightning currents on the transient behavior of mixed line-cable circuits is investigated for the two new 380 kV connections in the Randstad, by applying the models that were described in Chapter 5. Paragraph 7.3 shows the results of the impact study for both 380 kV connections. Furthermore, the

influence of the applied cable length on the expected peak voltage is analyzed in paragraph 7.4. In paragraph 7.5, the peak value of the simulated transient overvoltages is verified by performing calculations and by applying lattice diagrams.

## 7.2 THE MECHANISM OF LIGHTNING DISCHARGE CURRENTS

When the temperature is high and the air humid, raindrops are formed caused by the temperature difference between the air at lower and higher altitudes. Lightning discharges are the result of raindrops that are polarized by the electric field that is present between the ionosphere and the earth surface. Most of the thunderclouds are negatively charged and are formed by space charge caused by negatively charged raindrops. This space charge creates locally a strong electric field inside the cloud and may reach values of about 10 kV/m. This strong electric field causes the negative ions to accelerate [33]. As a consequence, collision takes place between the air molecules and the negative ions and this result in new negative ions to accelerate. In this way, an avalanche takes place resulting in a strong electric field that causes negative discharges inside the cloud. These discharges reach the earth surface in steps of about 30 m. The main channel starts a discharge current and this paves the way for the main discharge. The main discharge current, also called the return stroke, is a positive discharge and can reach values of 100 kA or even more. The lightning stroke observed by the human eye consists of several of these discharges in a short time period. These strokes can hit transformer substations, high voltage towers and overhead transmissions lines. When considering the electric field strength caused by the charge and current in the vicinity of an overhead line conductor, the voltage that is induced in that conductor can be calculated. At any location in space, the total electric field strength associated with the charge and the current can be described by [79]:

$$\mathbf{E}_{total} = -\nabla\Phi - \frac{\partial\mathbf{A}}{\partial t} \quad (7.1)$$

In (7.1),  $\Phi$  is the scalar potential that is produced by the residual charge in the return stroke and  $\mathbf{A}$  is the vector potential produced by the return stroke current. The scalar potential is described by [79]:

$$\Phi(\mathbf{r}, t) = \frac{1}{4\pi\epsilon_0} \int \frac{\rho(\mathbf{r}', t - \sqrt{\epsilon_0\mu_0}|\mathbf{r} - \mathbf{r}'|)}{|\mathbf{r} - \mathbf{r}'|} dV \quad (7.2)$$

The vector potential is described by [79]:

$$\mathbf{A}(\mathbf{r}, t) = \frac{\mu}{4\pi} \int \frac{\mathbf{J}(\mathbf{r}', t - \sqrt{\varepsilon_0 \mu_0} |\mathbf{r} - \mathbf{r}'|)}{|\mathbf{r} - \mathbf{r}'|} dV \quad (7.3)$$

where

$\mathbf{r}, \mathbf{r}'$  - respectively the field and source points (m);

$\rho$  - charge density (C/m<sup>3</sup>);

$\mathbf{J}$  - current density (A/m<sup>2</sup>);

$t$  - time (s);

$\varepsilon_0$  - permittivity of free space (8.854 · 10<sup>-12</sup> F/m);

$\mu_0$  - vacuum permeability (4  $\pi$  · 10<sup>-7</sup> H/m); and

$V$  - volume on which is integrated.

Finally, when the total electric field is integrated over between 0 and the height  $h$  of the conductor above the ground, the induced voltage at the conductor is equal to [79]:

$$\mathbf{V}_{induced} = - \int_0^h \mathbf{E}_{total} \cdot d\mathbf{x} \quad (7.4)$$

### 7.3 LIGHTNING OVERVOLTAGE ANALYSIS FOR 380 KV MIXED LINE-CABLE-LINE CIRCUITS

Lightning discharge currents can enter the power system in different ways. During a lightning storm, moving charged clouds in the vicinity of an overhead line conductor can result in charge accumulation at the line conductor. A lightning stroke will remove the charge difference that exists between the clouds, and this has as result that the charge on the line conductor has to disappear in a very short time period. This sudden charge removal changes the energy state of the system and it should therefore be regarded as a transient phenomenon. The severity of such a discharge depends on both the magnitude of the discharge and the location of strike. A surge current that enters the line conductor will divert into directions. The corresponding voltage at the line phase conductor when a lightning surge current is injected into that line and in the case that there are no ground wires present between the towers, is equal to:

$$V = \frac{1}{2} I Z_0 \quad (7.5)$$



where

$Z_0$  - the characteristic impedance of the overhead line ( $\Omega$ ); and

$I$  - the magnitude of the injected current (A).

A lightning current can also directly strike on an high-voltage tower. The high-voltage towers are electrically connected to each other by ground wires. The ground wires are applied for protection of the phase conductors against a direct hit by a lightning surge current and are placed above the phase wires. In this way, a lightning current that comes near the earth surface will be caught by the ground wire before the phase conductor is reached. However, the probability that a lightning discharge current directly strikes on the phase conductor is relatively small as the striking distance of the lightning discharge depends on the amplitude of the current involved. The larger the current amplitude, the larger the striking distance and thus a larger probability that the ground wire is being hit before the current reaches the phase conductor. Besides protection against direct lightning strokes, the presence of those ground wires in the network cause several side effects [79]. In the case when a high-voltage tower is hit by lightning, the current will divide into three parts. One part will flow, through the conducting tower, to the ground. In this case, the tower acts as a transmission line and hence it has a characteristic impedance. The remaining part will be equally divided over the ground wires and will propagate as a travelling wave along the line in both directions. The total stroke current is equal to:

$$I = I_{tower} + I_{ground\ wire} \quad (7.6)$$

A drawing for the situation when a lightning current  $I$  strikes the high-voltage tower, is depicted in Figure 7.1 [79]. The figure shows a section of an overhead transmission system with three high voltage towers, connected to each other by the ground wires. The isolator strings between the line phase conductors and the high-voltage tower are connected at the tower top.

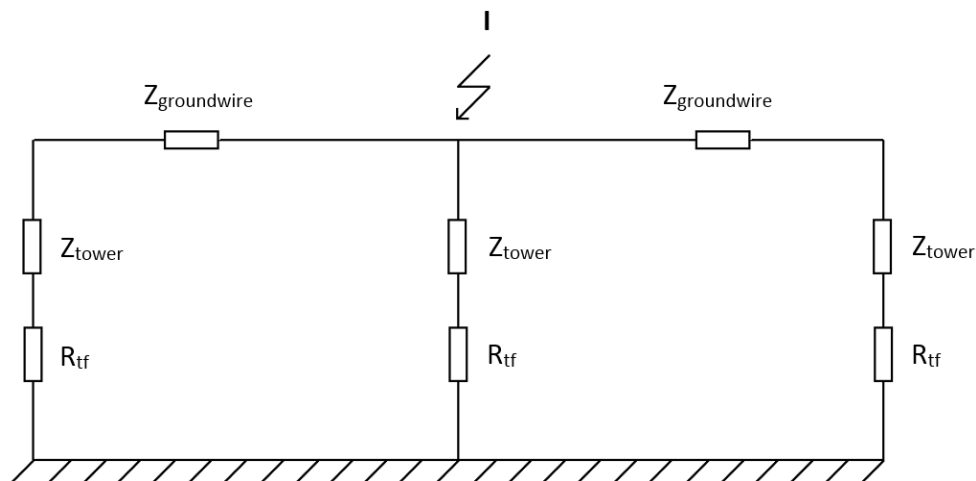


Figure 7.1. Drawing of the impedances of the tower and the ground wires.

In Figure 7.1:

$Z_{groundwire}$  - the characteristic impedance of the ground wires ( $\Omega$ );

$Z_{tower}$  - the characteristic impedance of the tower( $\Omega$ ); and

$R_{tf}$  - the tower-footing resistance ( $\Omega$ ).

The value for the tower characteristic impedance and for the tower-footing resistance depends on the shape of the tower and can be found in [79]. From Figure 7.1, we can calculate the equivalent characteristic impedance  $Z_{eq}$  seen by the injected current that is injected on the tower top:

$$Z_{eq} = \frac{Z_{groundwire} Z_{tower}}{Z_{groundwire} + 2Z_{tower}} \quad (7.7)$$

The initial voltage at the tower top is equal to:

$$V_0 = IZ_{eq} \quad (7.8)$$

The final tower-top voltage is the result of multiple reflections of the voltage wave against the tower-footing resistance, which is described in **Appendix C**.

When the lightning current strikes the phase conductor directly, a large surge current is injected into the system. The result is a surge voltage that propagates as a travelling wave in both directions along the line conductor. At the line-cable junction, the voltage wave sees a discontinuity because of the difference in characteristic impedance between line and cable. The characteristic impedance of the phase conductor is about 300  $\Omega$  and that of the cable is about 30  $\Omega$ . This means that when the wave propagates along the line towards the cable, reflection takes place at the line-cable junction point. One part will propagate back to the line while the remaining part will continue to the cable-line junction. When the cable section is embedded between two line sections, successive reflections will occur at these junctions, resulting in large voltage peaks in a short time period. In this paragraph, simulation results are presented for the case when the overhead line phase conductor of a mixed line-cable configuration is hit by a lightning discharge current.

The waveform of a surge current is characterized by its front time and tail time. The front time is defined as the rise time between 10% and 90% of the amplitude [83] and the tail time is the time needed to decay to 50% of the amplitude. Because of the stochastic nature of lightning discharges, there is a variation in both the steepness of the wave front and its peak value. The standardized wave shape used to represent lightning currents for testing purposes has been the 1.2/50  $\mu s$  surge, but in practice lightning surges can have a steeper

wave front. The standardized wave shape study with an amplitude of 10 kA is used in this impact study. The applied 1.2/50  $\mu$ s wave shape is shown in Figure 7.2.

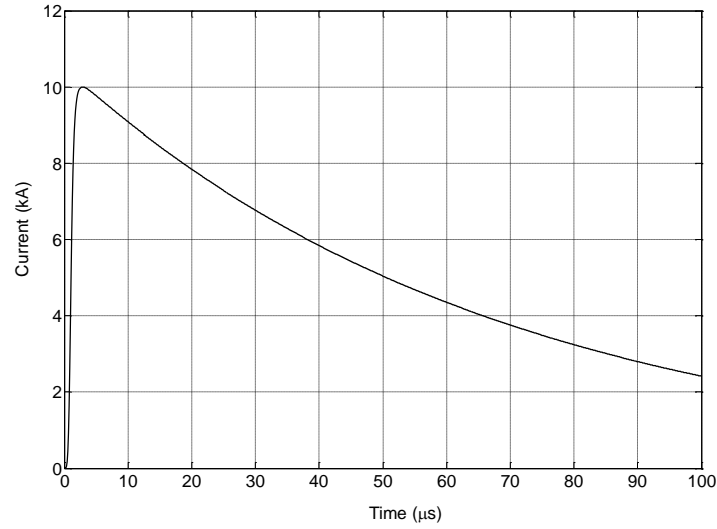


Figure 7.2. Wave shape of the 10 kA 1.2/50  $\mu$ s lightning surge current.

The wave shape of the lightning surge current can be mathematically described by the Heidler function [84] and is given by (7.9). For this study, the function makes part of the PSCAD program and is added to the existing models for the line and cable sections. The parameters for obtaining the 1.2/50  $\mu$ s wave shape are taken from [85].

$$i(t) = \frac{I_0}{\eta} \frac{(t/\tau)^n}{1 + (t/\tau)^n} \exp\left(-\frac{t}{\tau_1}\right) \quad (7.9)$$

where

$I_0$  - the peak value of the surge current (kA);

$n$  - determines the growth speed of the function;

$\eta$  - correction factor of the current peak value; and

$\tau$  and  $\tau_1$  - time constants to adjust the front time and tail time respectively (s).

In this impact study, the voltage levels in the newly build 380 kV connections are calculated when an overhead line phase conductor is being hit directly by a lightning impulse. In Figure 7.3, the considered 380 kV connection between substations Bleiswijk and Beverwijk is drawn (in which a lightning surge current will be injected).

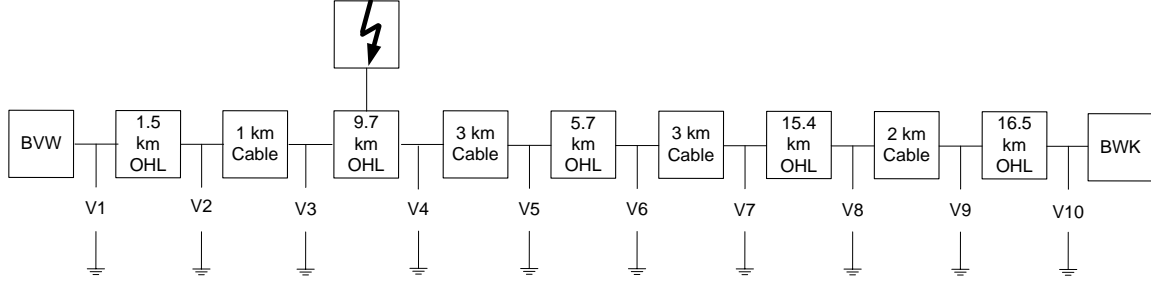


Figure 7.3. 380 kV connection BWK-BVW for lightning impulse studies.

During the lightning simulation, the connection is in a steady state operation condition. In the two high-voltage substations at the end, power transformers transform the voltage from 380 kV to 150 kV. The transformers have an influence on the transient behavior of the network. Since an accurate transient model of the power transformer is rather complicated, a simpler approach has been followed in order to keep the modeling work manageable. Therefore, the load is connected at 380 kV level at the substation BVW. The load is symmetric and has an active part  $P$ , modeled by a lumped  $R$  and a reactive part  $Q$  modeled by a lumped inductance  $L$ . The load impedance  $Z_{load}$  and its three phase load representation is shown in Figure 7.4. The power factor of the load is set at 0.95. When the connection is transmitting maximum power, 2600 MVA, the single phase active load equals 800 MW and is represented by a lumped resistor of 66  $\Omega$ . The reactive load part equals 200 MVar and is modeled by a lumped inductance of 0.84 H. The total load impedance  $Z_{load}$ , being a parallel connection of  $R$  and  $L$ , is equal to 64  $\Omega$  at 50 Hz power frequency. The three phase load for the phases  $a$ ,  $b$  and  $c$  are connected as is shown in Figure 7.4.

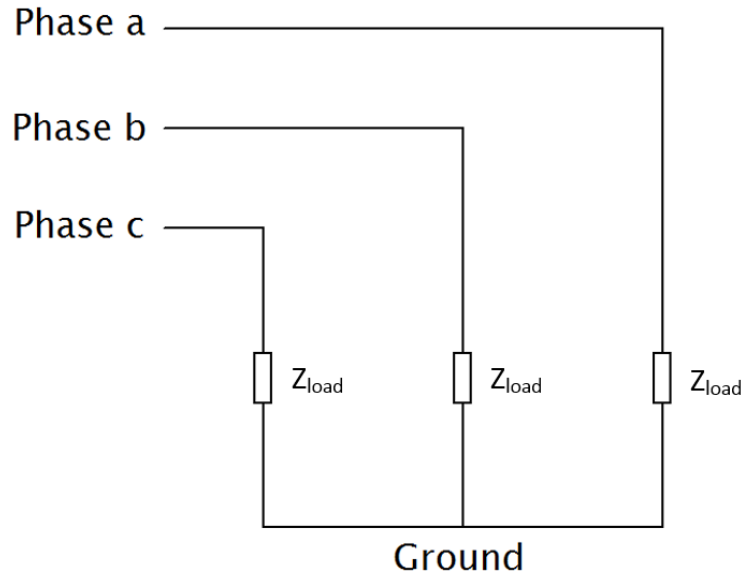


Figure 7.4. Representation of the three phase load connected at the 220 kV phase to ground voltage.

For substation BWK, the supply voltage is modeled by a 380 kV ideal voltage source with a Thevenin impedance that takes the remaining 380 kV grid behind the substation into account. At the line-cable junctions, surge arresters are placed to protect the cable terminals against large overvoltages. The main component of a surge arrester is the non-linear resistive element, (see Figure 7.5). The arrester has to act as an open circuit during steady state operation, but must provide a low impedance path to ground in case of a fast transient voltage, in order absorb the energy of the travelling wave. The arrester type in this 380 kV connection is a metal oxide arrester (MOSA, SBK 420/20.4-I) with a rated voltage of 420 kV and a continuous operating voltage of 336 kV. According to the specifications of the manufacturer, the residual voltage for a 1.2/50  $\mu$ s surge current with 10 kA amplitude is 1089 kV [86]. The values for the parameters  $C_a$ ,  $R_a$  and  $L_a$  of the arrester model are taken from [85], [87]. When these values are applied to the model shown in Figure 7.5, the calculated residual voltage is 1040 kV. This is close to the residual voltage specified by the manufacturer. Figure 7.6 shows the non-linear v-i characteristic of the arrester.

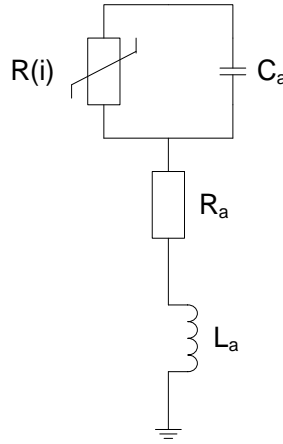


Figure 7.5. Surge arrester model.

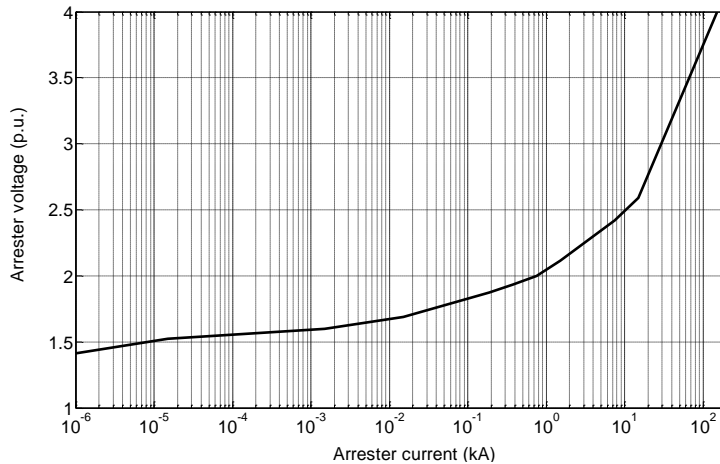


Figure 7.6. Non-linear v-i characteristic of the SBK 420/20.4-I surge arrester [86].

A lightning surge current with a peak value of 10 kA is injected into one overhead line phase conductor with the system in steady state operation. The peak values of the transient overvoltages at the cable-line junctions along the connection depend on the peak value of the injected current, the instant and location of injection and the circuit configuration. The peak value of the surge current is chosen to be 10 kA. A larger amplitude is not to be expected because there is large probability that a higher current hits the ground wires before the phase conductor is reached. Moreover, a current peak larger than 10 kA would result in a voltage peak higher than 1750 kV between the phase conductor and ground. The string insulator in the high voltage tower is able to withstand a maximum voltage of 1750 kV, and this means that a higher voltage level results in a flashover to ground. In that case, the injected surge current is short circuited to ground and the surge voltage disappears from the line immediately.

In order to simulate the worst case scenario with respect to the instant of injection, the surge current is injected when the A.C. voltage has reached its peak value: the phase-to-ground operating voltage is 220 kV, and the peak value is 311 kV. Furthermore, the location of injection will influence the peak values of the transient voltage responses. A lightning current can strike the phase conductors at several locations along the connection. If the lightning current hits the line far from a line-cable junction, for instance at midspan, the steepness and amplitude of the travelling wave is significantly reduced before it reaches the cable. In this case, lower overvoltages can be expected than when the current is injected close to the line-cable junction. Therefore, the current is injected into the 9.7 km line section, close to location V3 (see Figure 7.3). By this, the travelling voltage surge will reach the 1 km cable section almost immediately after injection. The transient voltages at the locations V1 to V5 are calculated for a time period of 500  $\mu$ s after the current injection. This simulation time is sufficiently long to observe the successive reflections of the voltage surges at the cable-line junctions. The voltages at V6 to V10 are not considered because these points are relatively far from the place of injection. The resulting transient overvoltages at these locations are therefore expected to be much lower. The calculation time step in this case is set at 0.1  $\mu$ s. To show the influence of the surge arresters on the peak values of the transient overvoltages, the calculations are done both with and without arresters. In Figure 7.7, the resulting calculated voltage responses are plotted for locations V1 to V5, when no surge arresters are connected at the line-cable junction points.

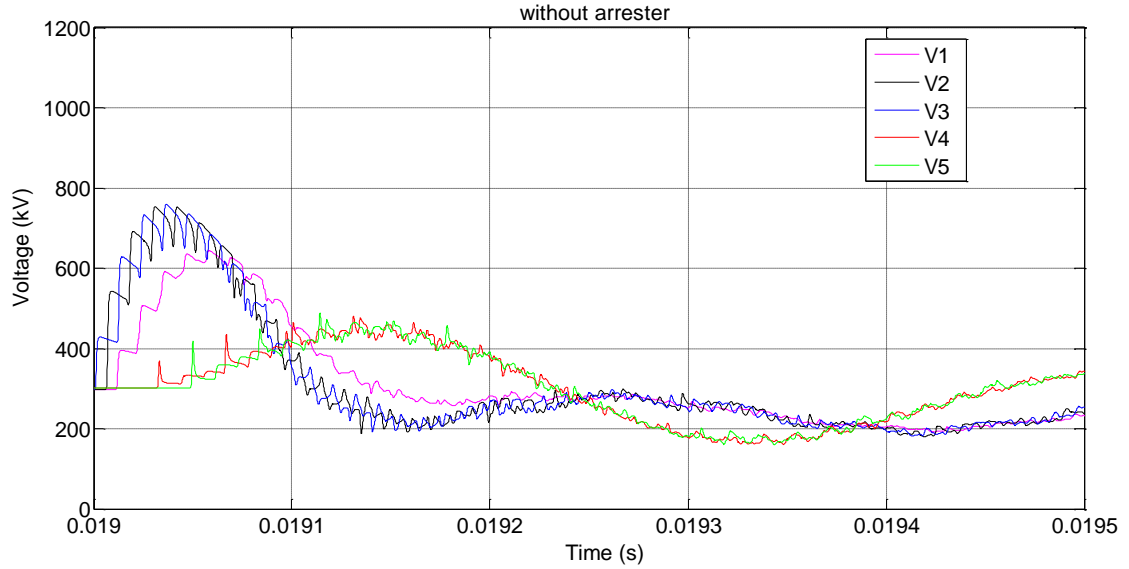


Figure 7.7. Voltages at locations V1 to V5 after 10 kA 1.2/50  $\mu$ s surge current injection without arresters.

From the calculation results, the propagation delay for each location can be estimated: the largest overvoltage is approximately 760 kV at locations V2 and V3, indicated by the black and blue plots respectively. The voltages result from multiple reflections in a relatively short time period at the cable-line junctions. The rise time of the reflected wave decreases over time under the influence of the transmission line parameters.

The calculated surge voltages at locations V4 and V5 have a significant lower amplitude, because they are further away from the striking location and the wave is more attenuated after reaching those locations.

Figure 7.8 shows the transient voltages for the same locations with surge arresters connected at the line-cable junctions. It turns out that for this case the peak voltages at V2 and V3 reach 685 kV, being a reduction of 10%. For V4 and V5, there is also a reduction, but less significant, since the amplitudes are lower because of the larger distance from the point of injection. To investigate the impact on the voltages of the location of the strike, the calculations are also done for a current injection into the 5.7 km line section. For this case, the voltage peak at V6 becomes more significant since it is closer to the point where the lightning strikes.

In Figure 7.9, the voltage responses are shown for locations V1 to V6 for the same time period as in the previous case. The highest voltage peaks occur at the terminals of the 3 km cable section, at locations V4 and V5. It can be seen that the voltages at V1, V2 and V3 are more attenuated compared with the previous case, as those locations are relatively far away from the point of injection.

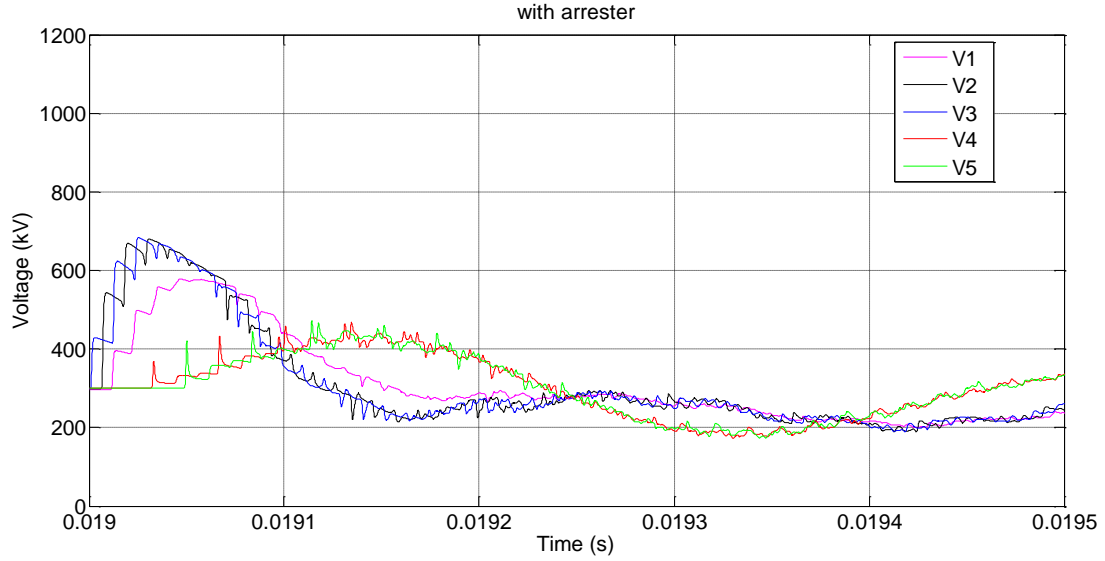


Figure 7.8. Voltages at V1 to V5 after 10 kA 1.2/50  $\mu$ s surge current injection with arresters.

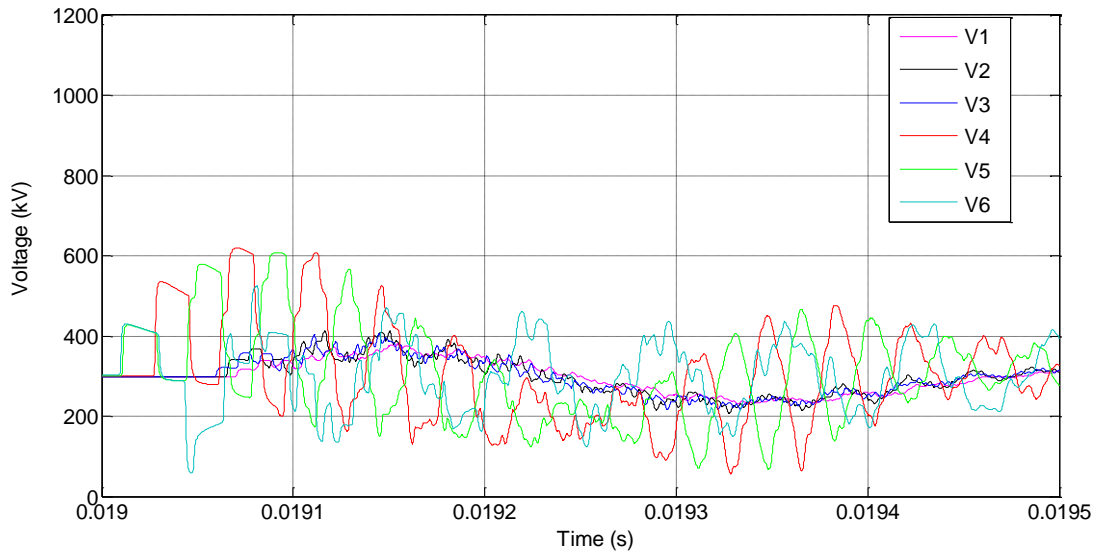


Figure 7.9. Voltages at V1 to V6 after 10 kA 1.2/50  $\mu$ s surge current injection into the 5.7 km line without arrester.

In Figure 7.10 the 380 kV configuration between the substations Wateringen and Bleiswijk is schematically drawn. The 1.2/50  $\mu$ s surge current with 10 kA amplitude is injected in the 4.3 km line section close to the line-cable junction. Like in the previous cases, the network is considered during lightning events when it is in steady state operation condition. The 380 kV power supply is modeled at the Bleiswijk side and the load, and is represented at Wateringen side. The resulting calculated transient voltage responses for the locations V2 and V3 are shown in Figure 7.11, without surge arresters. The largest peak value that is



found is 525 kV at V2, and this value is significantly lower than the values at locations V2 and V3 in the previous case.

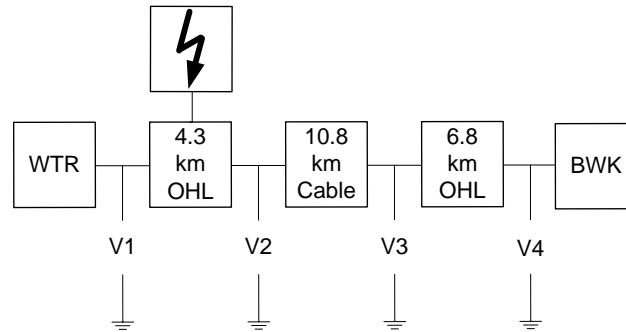


Figure 7.10. 380 kV connection WTR-BWK for lightning impulse studies.

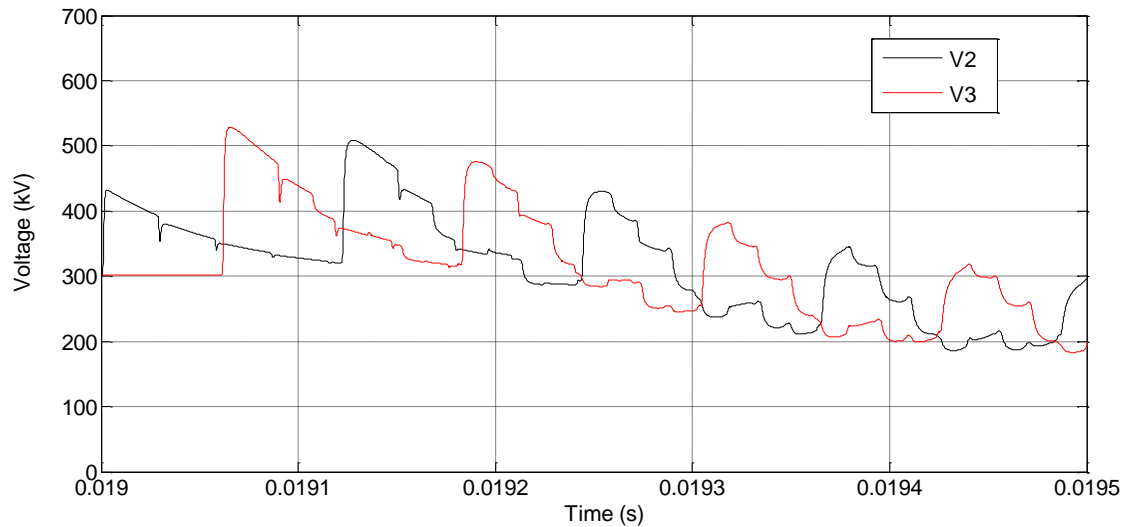


Figure 7.11. Voltages at V2 and V3 after 10 kA 1.2/50  $\mu$ s surge current injection into 4.3 km line without arresters.

From the calculation for both 380 kV mixed line-cable connections, we can conclude that the system configuration is important for the transient voltage level during lightning events. In the first configuration, four cable sections are embedded in between overhead lines, and this gives many reflection points, due to the difference in characteristic impedance, at the line-cable junctions. In the case shown in Figure 7.11, there is only one cable section with a total length of 10.8 km and the resulting voltage peak values at the line-cable junctions are considerably lower than in previous cases. Also, the location of injection is of importance, as it can be seen from the calculation plotted in the Figures 7.8 and 7.9. The largest peak voltage occurs at the terminals of the shortest cable section, when the surge current is injected into the line close to the cable terminal.

The voltage levels stay below the cable BIL for the considered cases. In theory, it is possible that several lightning currents with different amplitudes will hit the overhead

system at more locations simultaneously. In such a situation, the injected current could reach a higher value resulting in significant larger peak voltages at the line-cable junctions. Such peak voltages could even exceed the BIL, but the probability that such a lightning event occurs in practice is rather small and will therefore not be taken into account.

## **7.4 LIGHTNING OVERVOLTAGES VERSUS CABLE LENGTH**

In the 380 kV transmission system, short cable connections are sometimes applied to connect the overhead line terminal with the substation transformer. Because of the low cable characteristic impedance, a cable section between the overhead line and the transformer seems a good solution to reduce the surge slope that propagates towards the substations. When a surge voltage enters the cable, it gives a significant reduction of the surge voltage amplitude that reaches the transformer. However, short cables produce also successive reflections that result in high peak voltages, but they decrease the wave front [88]. In the previous paragraph, we learned from the figures that the highest peak value of the transient overvoltage appears at the terminals of the shortest cable length in the circuit. An important question that rises is what can happen when the length of the shortest cable section (1 km) is further reduced and how much it can be reduced in order to stay below the BIL. To give an answer to this question, the 380 kV connection shown in Figure 7.3 is looked at again, but now with the length of the cable section between locations V2 and V3 being reduced in several steps. The surge current is injected at the same location as it is shown in the figure. The circuit operates in steady state and under the same load condition. First, the length of the cable section is brought down from 1 km to 0.75 km.

The calculated transient voltage responses are shown in Figures 7.12 and 7.13 for the case without and with surge arresters connected. As it can be seen, the peak voltages at locations V2 and V3 are higher (850 kV instead of 760 kV) than in the case with 1 km cable length. The reason for this is that the shorter cable has a shorter travelling time and less damping. The shorter travelling time brings more reflections at the line-cable junctions in the same time period, adding up to a larger peak voltage. When the cable length is reduced further, the voltage peak will increase more, as can be seen from the Figures 7.14 to 7.17, which show the results when the cable length is reduced to 0.5 km and 0.3 km respectively. The largest peak value reached is 1025 kV, when the cable length is 0.3 km. The role of the surge arrester becomes more important when the voltage peaks increases. Table 7.1 gives an overview of the calculated peak voltages for locations V1 to V5, for four different cable lengths between V2 and V3. From these calculation results, we can conclude that the voltage levels do not exceed the BIL of 1425 kV during lightning events for the studied cases and network configurations. Based on this, the conclusion can be extrapolated: the peak voltages will be higher when the cable length is reduced further, but such a very short cable length in between two overhead line sections at 380 kV level will not be used in practice.

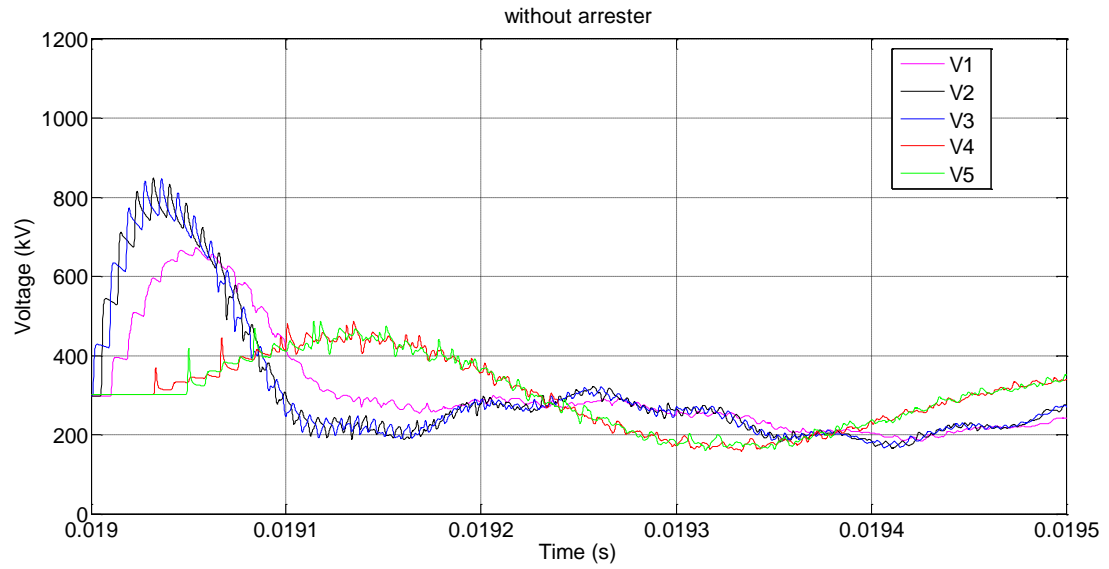


Figure 7.12. Voltages at V1 to V5 after a 10 kA 1.2/50  $\mu$ s surge current injection, with 0.75 km cable.

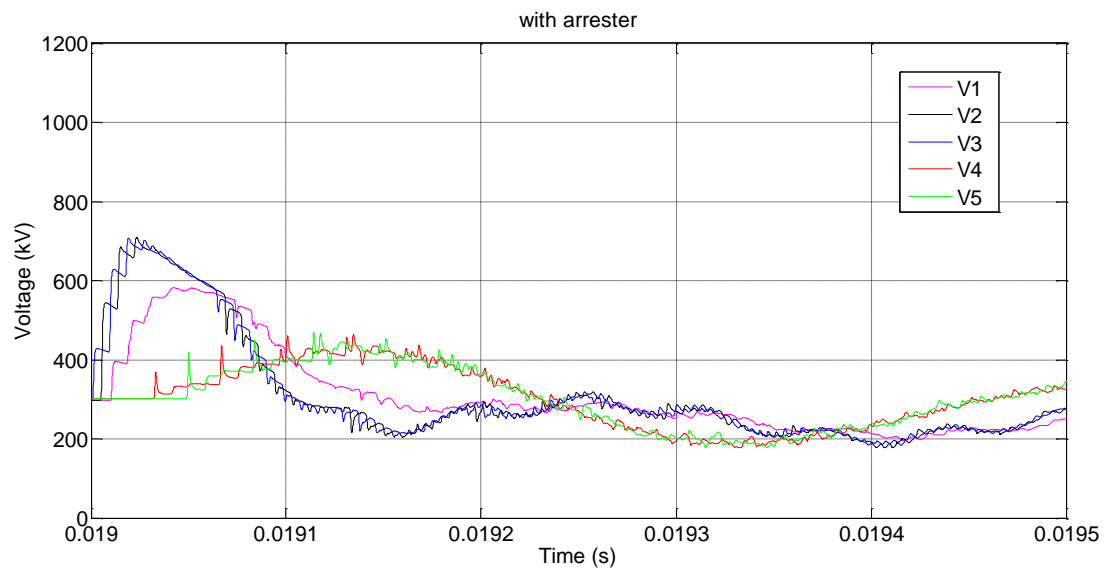


Figure 7.13. Voltages at V1 to V5 after a 10 kA 1.2/50  $\mu$ s surge current injection, with 0.75 km cable.

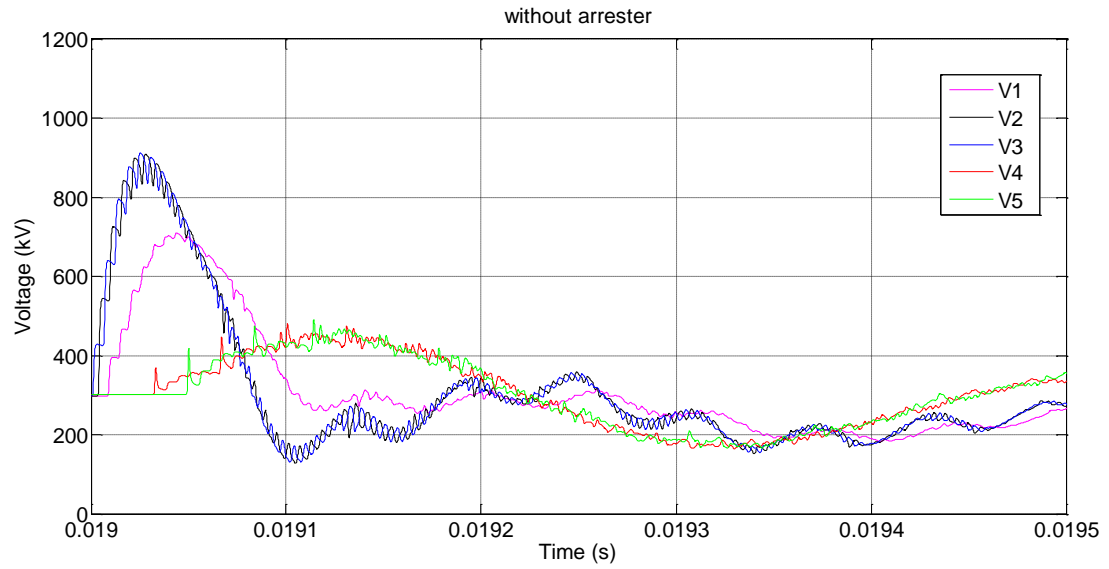


Figure 7.14. Voltages at V1 to V5 after a 10 kA 1.2/50  $\mu$ s surge current injection, with 0.5 km cable.

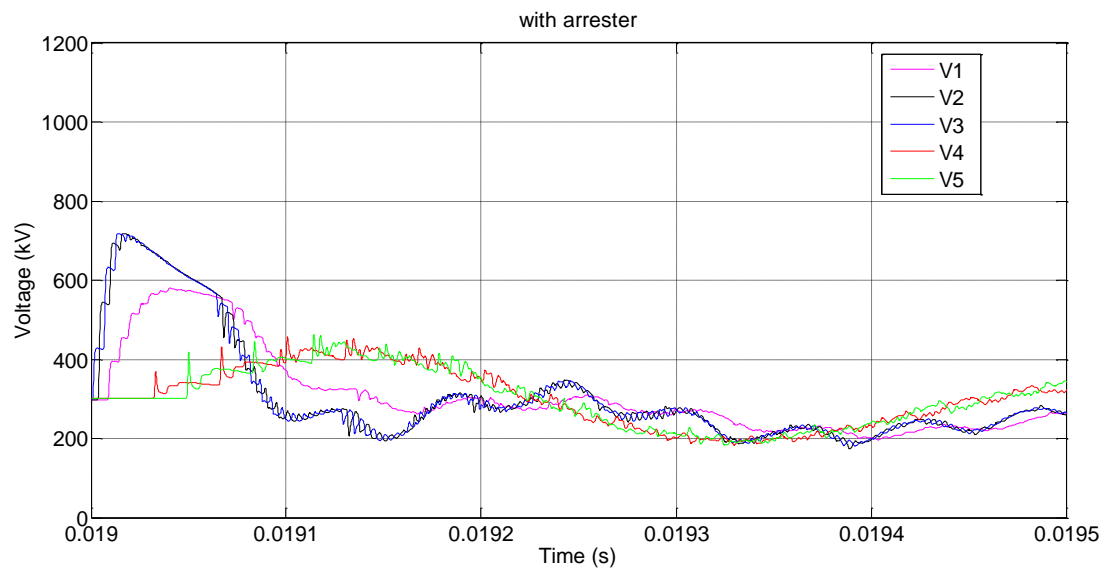


Figure 7.15. Voltages at V1 to V5 after a 10 kA 1.2/50  $\mu$ s surge current injection, with 0.5 km cable.

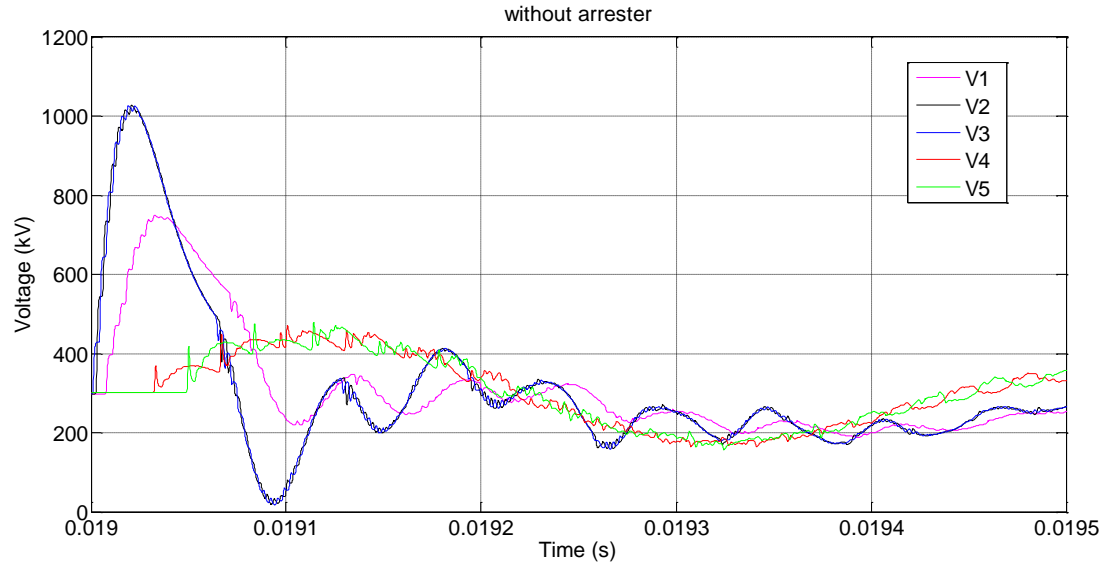


Figure 7.16. Voltages at V1 to V5 after a 10 kA 1.2/50  $\mu$ s surge current injection, with 0.3 km cable.

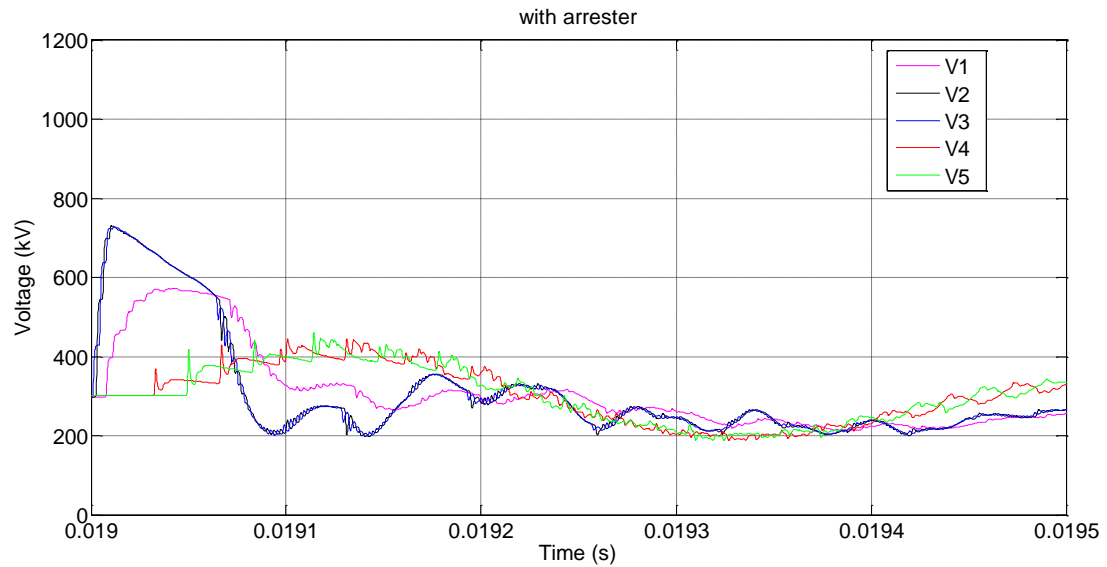


Figure 7.17. Voltages at V1 to V5 after a 10 kA 1.2/50  $\mu$ s surge current injection, with 0.3 km cable.

The results brought together in Table 1, make clear that surge arresters have more impact on the peak voltage when the cable length is reduced. The peak value of 1025 kV is reduced to 730 kV, being a reduction of about 29%.

Table 7.1. Overview of peak voltages, with and without surge arresters.

Cable length (km)	Arresters installed	Peak value of voltage (kV)				
		V1	V2	V3	V4	V5
1	No	645	760	760	490	490
	Yes	580	685	685	480	480
	$\Delta V$	<b>10%</b>	<b>10%</b>	<b>10%</b>	<b>2%</b>	<b>2%</b>
0.75	No	670	850	850	515	515
	Yes	580	710	710	490	490
	$\Delta V$	<b>13%</b>	<b>16%</b>	<b>16%</b>	<b>5%</b>	<b>5%</b>
0.5	No	710	910	910	515	515
	Yes	580	720	720	470	470
	$\Delta V$	<b>18%</b>	<b>21%</b>	<b>21%</b>	<b>9%</b>	<b>9%</b>
0.3	No	750	1025	1025	480	480
	Yes	580	730	730	458	468
	$\Delta V$	<b>23%</b>	<b>29%</b>	<b>29%</b>	<b>4.5%</b>	<b>2.5%</b>

## 7.5 BEWLEY LATTICE DIAGRAMS

Transient overvoltages stem from multiple reflections at line-cable junction points and can also be estimated from line and cable data. A Bewley lattice diagram draws the transmitted and reflected waves in a transmission system using the estimated reflection and transmission coefficients and the attenuation of the wave in the system [88], [89]. It is a time-space diagram with the distance of the transmission line on the horizontal axis and the time scale on the vertical axis. In this paragraph, the calculated peak value of the overvoltage by multiple reflections is verified with the Bewley lattice diagram. From the calculation results presented in the previous paragraph, it became clear that the highest overvoltage appears at the terminals of the shortest cable section. Therefore, the lattice diagram is drawn for this cable section, embedded between two line sections.

The line and cable sections are taken to be lossless, meaning that there is no attenuation of the waves. The lightning impulse current hits the overhead line section close to location V3. A small part of the wave travels through the cable. The calculated values for the voltages are given in per unit. When the characteristic impedance of the line is  $300 \Omega$ , the injected surge current of 10 kA produces a surge voltage between line and ground of 1500 kV and this value is taken as the base value of 1 pu. To construct the lattice diagram, the reflection and transmission coefficients at the locations V1 to V3 must be known. Furthermore, the propagation times of the line and cable sections are of importance. Based on the permittivity of the cable, the propagation speed is about 200 m/ $\mu$ s. For 1 km cable length, the travelling time becomes 5  $\mu$ s. The propagation speed of the overhead line is close to the speed of light, which is 300 m/ $\mu$ s. The 1.5 km line section has a travelling time

of 5  $\mu\text{s}$ . The line section of 9.7 km between V3 and V4 has a travelling time of approximately 30  $\mu\text{s}$ .

When the surge current hits the phase conductor, the first junction is at V3. The reflection coefficient at the line to cable junction is calculated by taking into account that there are two cables in parallel. The characteristic impedance of the line conductor is 300  $\Omega$  and from two parallel cables 15  $\Omega$ . The estimated reflection and transmission coefficient are calculated by Equations (7.10) and (7.11).

$$r_{lc} = \frac{Z_c - Z_l}{Z_c + Z_l} = \frac{15 - 300}{15 + 300} = -0.9 \quad (7.10)$$

$$\tau_{lc} = \frac{2Z_c}{Z_c + Z_l} = \frac{30}{15 + 300} = 0.1 \quad (7.11)$$

At V2, the wave propagates from the cable to the line section. For this location, the reflection and transmission coefficients are calculated by Equations (7.12) and (7.13). The larger part of the voltage will be reflected and a smaller part is refracted through the 1.5 km line section.

$$r_{cl} = \frac{Z_l - Z_c}{Z_l + Z_c} = \frac{300 - 15}{300 + 15} = 0.9 \quad (7.12)$$

$$\tau_{cl} = \frac{2Z_l}{Z_l + Z_c} = \frac{600}{300 + 15} = 1.9 \quad (7.13)$$

where

$r_{lc}$  - is the reflection coefficient from line to cable;

$r_{cl}$  - is the reflection coefficient from cable to line;

$\tau_{lc}$  - is the transmission coefficient from line to cable;

$\tau_{cl}$  - is the transmission coefficient from cable to line;

$Z_l$  - is the characteristic impedance of the overhead line ( $\Omega$ ); and

$Z_c$  - is the characteristic impedance of the cable ( $\Omega$ ).

When starting with unity voltage at the line-cable junction and knowing that the 1km cable traveling time is longer than that of the overhead line, the voltage at the cable-line junction V3 after three reflections equals:

$$V_{V_3} = k + r_{cl}k + r_{cl}^2k^3 + r_{cl}^3k^3 + r_{cl}^4k^5 + r_{cl}^5k^5 \quad (7.14)$$

with  $k$  being the cable attenuation factor.

When the voltage wave reaches the load at location V1, reflections occur at this location also. The load reactance increases with frequency, making the total load impedance frequency dependent. In the 1.2/50  $\mu$ s wave shape, the highest frequency involved is approximately 250 kHz. However, when the wave reaches the load, the front time is reduced and the highest frequency component is lower than 250 kHz. The characteristic impedance of the load is estimated, by taking the parallel connection of the lumped  $R$  and  $L$  and the worst case frequency of 250 kHz, being the expected maximum frequency during lightning strikes. The load impedance  $Z_{load}$  is approximately 64  $\Omega$ . This impedance value is used for calculating the reflection coefficient at location V1:

$$r_{load} = \frac{Z_{load} - Z_l}{Z_{load} + Z_l} = \frac{64 - 300}{64 + 300} = -0.65 \quad (7.15)$$

Substituting the values for the propagation times of the line and cable sections, the reflection and transmission coefficients, the lattice diagram can be drawn for the first 25  $\mu$ s after the instant of current injection, see Figure 7.18. At V3, 10% of the voltage will travel towards V2. The remaining 90% is reflected and this negative voltage propagates towards V4 (not in the figure). After this first reflection, the voltage at V3 equals the sum of the incident and the reflected wave. This results in a voltage of 0.1 pu. At V2, 90% of the incident wave is reflected and this part travels back to V3. After 10  $\mu$ s, two reflected waves meet at V3, meaning that the voltage level increases by the sum of 0.09 pu and 0.081 pu produced by the second reflection. After 20  $\mu$ s, three reflections have occurred and the voltage level at V3 is further increased by the addition of 0.071 pu and 0.064 pu. Multiple reflections increase the voltage level, but the contributions will lessens over time because the injected surge current has decayed to 50% of its amplitude after 50  $\mu$ s and after 60  $\mu$ s, the reflection at location V4, which has a negative polarity, will also contribute to the voltage peak at V3. This is not shown in the diagram but it will lower the voltage peak. The final voltage equals the sum of all the increments. At the instant where a reflection occurs, the voltage at the junction equals the sum of the incident voltage and the reflected voltage waves. In Figure 7.18, the values of the incident and the reflected voltage waves are given for the first three reflections reaching location V3. The peak voltage at location V3 after 60  $\mu$ s is the sum of the three increments:



$$V_{V_3} = 1 - 0.9 + 0.09 + 0.081 + 0.073 + 0.066 = 0.41 \text{ pu} \quad (7.16)$$

This value gives a peak value of 615 kV. To get the actual voltage peak, the phase to ground operating voltage peak of 311 kV should be added to this value. The result is a voltage peak of 926 kV. Since the cable attenuation is not taken into account in the lattice diagram, this voltage peak is significantly higher than the calculated value during simulation, which is 760 kV. It should be noted that the values used for the impedance of the line and cable are estimated and be different from the practical values. An estimation of the attenuation of the cable section can be acquired from the injection measurements in Chapter 5. For a propagating wave, the amplitude of the voltage  $V$  at any point  $x$  along the cable can be expressed as:

$$V_x = Ve^{-\gamma x} = Ve^{-(\alpha + j\beta)x} = Ve^{-\alpha x} e^{-j\beta x} \quad (7.17)$$

where

$V$  is the amplitude at the sending end (V);

$\gamma$  is the cable propagation constant;

$\alpha$  is the attenuation coefficient of the cable (dB/km); and

$\beta$  is the phase angle constant of the cable (rad/km).

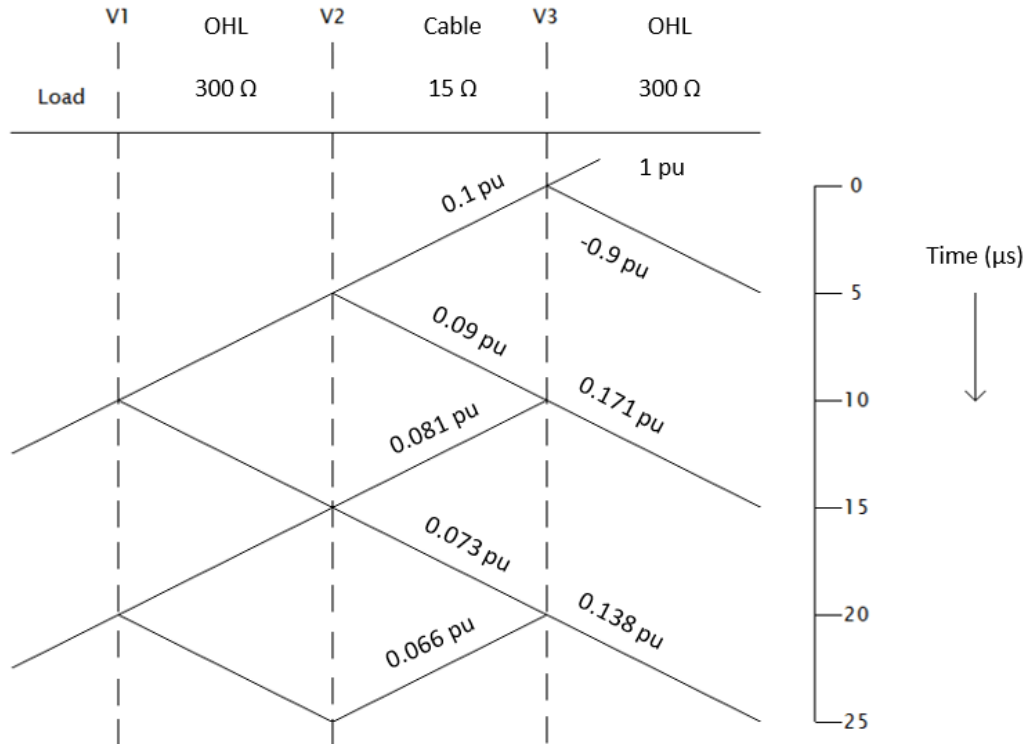


Figure 7.18. Lattice diagram for the voltage reflections at location V3.

To show the final voltage build up at the cable-line junction after a fast transient, a simple test simulation for the line-cable-line configuration with the same parameters is done to observe the voltage at the junction when applying a step voltage of 1 pu at the line. Figure 7.19 shows the building up of the voltage as a result of multiple reflections at the cable-line junction.

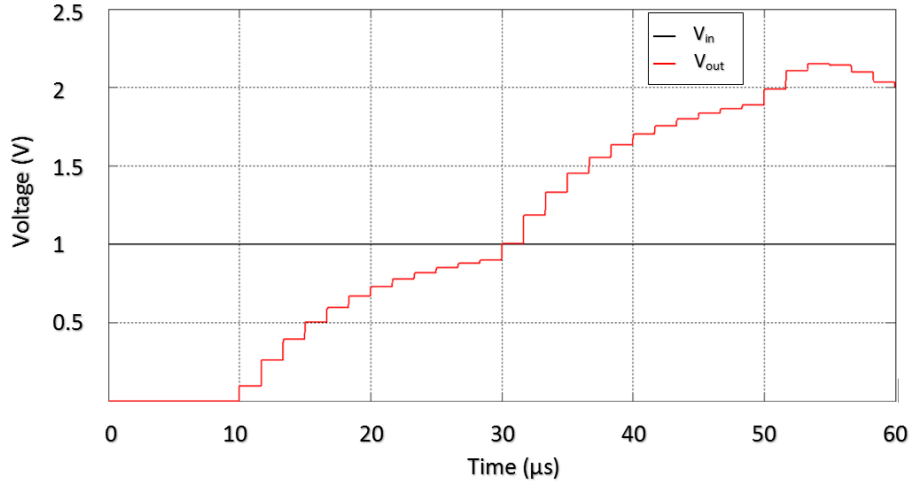


Figure 6.19. Building up of the voltage after energization by a step voltage.

For the 380 kV cable, the attenuation is approximately 0.86 dB/km (Chapter 5). This means that the attenuation coefficient for the 1 km cable section is about 0.91. When this value is used in the calculation, the peak value of the voltage after 60 μs equals:

$$V_{V_3} = 1 - 0.9 + 0.91^2(0.09 + 0.081) + 0.91^4(0.073 + 0.066) = 0.338 \text{ pu} \quad (7.18)$$

This value corresponds to a voltage peak of 507 kV with a total peak value of 818 kV when the power frequency voltage peak of 311 kV is added. This calculated voltage is more closely to the calculated value of 760 kV. There is however, still a difference, and this finds its origin by the assumptions made for the cable and line characteristic impedances. The calculation results prove that the values for the peak voltage can be verified by estimating the reflection pattern based on traveling times and characteristic impedances. A similar lattice diagram can be drawn for the connection Wateringen – Bleiswijk. The number of reflections is lower and so are the peak overvoltages and less severity is to be expected after lightning strokes in this particular connection.

## 7.6 CONCLUSION

This chapter gives the results and describes the background of lightning impact studies on 380 kV mixed line-cable-line circuits. The objective was to determine whether critical

overvoltages were to be expected in the network when short cable sections make part of that network. The simulation approach for this impact study was based on lightning strokes hitting directly the overhead line phase conductor. It turned out that the cable length in mixed configurations is an important parameter having a great influence on the transient voltage peak appearing at the cable terminals, as a result of multiple reflections at cable-line junctions. The shorter the applied cable section, the higher the transient voltage peak at the cable terminal. From the results obtained, we can draw the conclusion that the overvoltages in the analyzed cases will not exceed the Basic Impulse Level after a lightning stroke when the Randstad 380 kV mixed line-cable-line system is in steady state operation. Based on the calculated results, we can conclude that there is no necessity for installing surge arrestors at the line-cable junction points, as the voltage peak remain below the 1425 kV for the cable length that is being applied in the 380 kV network. The simulated peak voltages appearing after a surge current injection have been verified by calculation of multiple voltage reflections at the line-cable junction points, taking into account the cable attenuation. These results are important for situations where short cables are applied between components with relatively large surge impedance, like overhead lines, but also transformers in substations. This is the case when a cable connects the overhead line to the transformer. When a lightning currents would strike the overhead line close to the short cable part, the expected voltage peak at the terminals is high.

## **CHAPTER 8**

# **FIELD MEASUREMENTS FOR CABLE AND OVERHEAD-LINE MODEL VALIDATION**

### **8.1 INTRODUCTION**

Transmission line modeling and in particular underground cable modeling forms an important objective of this thesis. In Chapter 5, a transient model was developed for both the overhead lines and the underground cable sections of two new Dutch 380 kV connections between substations Wateringen and Bleiswijk and between Bleiswijk and Beverwijk. These models were used for several transient simulation studies, of which the results are presented and discussed in the Chapters 6 and 7. The verification of the developed models is done in order to confirm the validity of the those models for fast transient phenomena. Field measurements are very valuable for achieving model validation, because the results of those measurements can be used for comparison with simulated results. The transient modeling applied for an overhead line section is straight forward and the model has been successfully utilized over the years. Cable modeling is more complicated, as it was shown in Chapter 5. Field measurements have been used in cable studies to validate the cable model [90]. The main objective of this chapter deals with the validation of the transient cable model by comparing the results obtained by field measurement.

A transient cable model contains several parameters. Besides, checking the validity of the cable model, is important to determine its sensitivity, by varying the parameters. To achieve a good model validation, two types of measurements have been performed on the complete actual cross-bonded 380 kV cable system. Paragraph 8.2 describes the pulse injection measurement that was performed on the new 380 kV cable. To validate the cable modeling for fast transients, a step voltage function was applied to the cable core conductor. In paragraph 8.3, the results of the measurements are discussed. As for the cable, the same type of pulse injection measurement is applied for both the overhead line sections of this 380 kV connection. Using the measurement results, the validity of the transient line

model can be determined. The measured results obtained from both line sections are presented and discussed in paragraph 8.4. Furthermore, a detailed analysis of the measurement results of the cable, and the influence of changes in cable parameters on the simulation results are described in paragraph 8.5.

## 8.2 PULSE INJECTION MEASUREMENTS ON THE 380 KV CABLE

Since the 380 kV connection between substations Wieringen and Bleiswijk was under construction, it was a good opportunity to perform field measurements for the complete cross-bonded cable system. At the time when the measurement took place, the cross-bonded 10.8 km cable was disconnected from the overhead lines. A pulse injection measurement was applied to the cable system to measure its traveling time. The measured cable system contains two three phase circuits with 2 cables per phase. Pulse injection was applied at one cable of the circuit and the reflections of this pulse are measured at both the location of injection and at the receiving end of the cable. Since the mutual coupling between the cables is an important issue, the coupling between cables in the same circuit and between both circuits was also measured during pulse injection.

The pulse injection measurement is done at transition point where the cable is connected to the 4.3 km overhead line section to substation Wieringen. This transition point is referred to as OSP14. During this measurement, the cable receiving end at the location where the cable is connected to substation Bleiswijk was left open. This transition point is referred to as OSP32. In Figure 8.1, a picture of the measurement location and the KEMA measuring car containing the measurement equipment is shown. The measurement setup and the used equipment is shown in Figure 8.2. The arrangement of the 12 cables in the two circuits and a schematic overview of the measurement setup at OSP14 and OSP32 are shown in Figures 8.5a and Figure 8.5b respectively. The 12 cables terminals are indicated by the bullets in the figures, the numbers indicate the phase sequences of the cables. The black bullet in circuit ‘zwart’ gives the point of pulse injection. The grey bullets are the cables at which the resulting reflected pulses have been measured.



Figure 8.1a. Measurement location.



Figure 8.1b. KEMA measuring car.



Figure 8.2. Measurement setup in the measuring car.

Before the measurements are done, the coaxial measuring cables between the equipment in the car and the 380 kV cable end are calibrated. The used coaxial cables are of the type *RG 223*, with a length of 25 m and a characteristic impedance of  $50 \Omega$ . The calibration is performed by injecting a pulse into the short circuited coaxial cable, as it is depicted in Figure 8.3. A pulse with an amplitude of 50 V and a duration of  $1 \mu\text{s}$  is injected in the short circuited coaxial cable. The measured reflection pattern is shown in Figure 8.4. With a length of 25 m., the reflection time is expected to be 250 ns, as the propagation speed of this coaxial cable is approximately  $200 \text{ m}/\mu\text{s}$ . From the measurement, the reflection time is 240 ns. The amplitude of the injected pulse is 25 V, caused by the voltage division at  $50 \Omega$  output impedance of the pulse source. The calibration is done for all four coaxial cables that are used for this measurement.

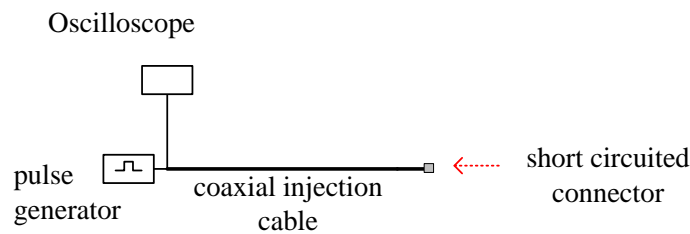


Figure 8.3. Calibration of a coaxial cable.

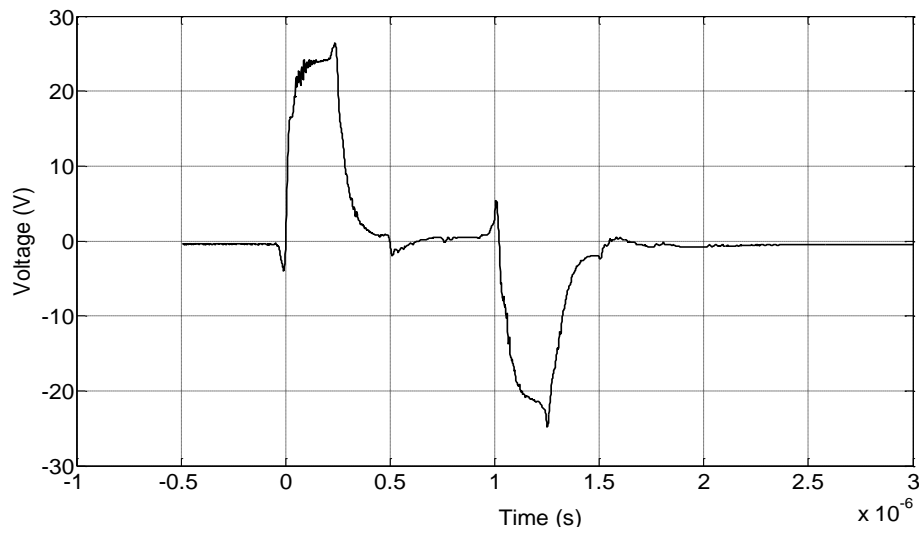


Figure 8.4. Measured reflection pattern.

A pulse with a 50 V amplitude and a duration of 1  $\mu\text{s}$  is injected via a coaxial measuring cable between the core conductor and the ground of cable 12, B6 of circuit ‘zwart’ at OSP14. The injected pulse propagates along the cable and pulse reflections occur at the cross-bonding locations, as it can be expected based on the theory and the measurements that were discussed in Chapter 5. At the cable receiving end that is left open, the pulse reflects and propagates back towards the sending end. This results in reflection patterns that are measured at both ends of the cable.

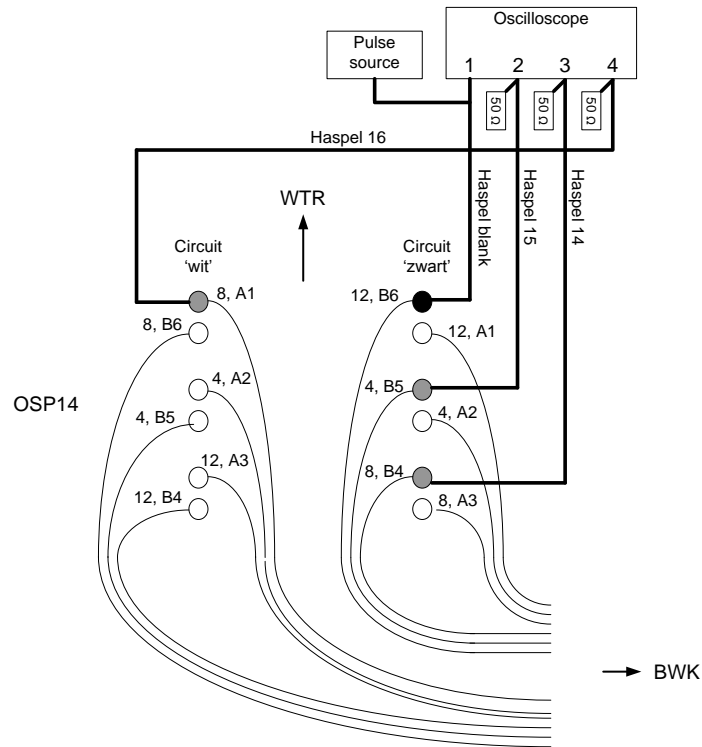


Figure 8.5a. Measurement setup at transition point OSP14.

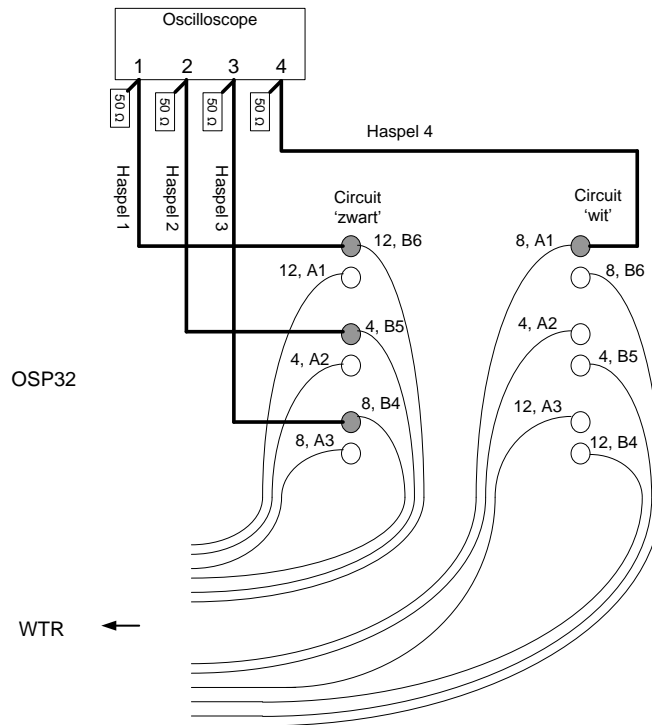


Figure 8.5b. Measurement setup at transition point OSP32.



The reflection patterns are recorded by a *Lecroy Wavejet 314* oscilloscope. The channels of the scope are terminated by a  $50\ \Omega$  impedance, as it is shown in the figures. Figure 8.6 shows the reflection patterns measured at the four cables as shown in the measuring setup. The blue colored line is the reflection pattern measured at the injected 380 kV cable. The impedance of the *MTSA* pulse source and the characteristic impedance of the measuring cable are both  $50\ \Omega$ , resulting in voltage division of the injected pulse. This means that the amplitude of the pulse that enters the 380 kV cable is 25 V, as it can be seen from the first peak in Figure 8.6. The injected pulse propagates along the cable and reflections occur at the cross-bonding locations and at the receiving open end of the cable. The first reflected pulse arrives after  $11\ \mu\text{s}$ . This is the location of the first cross-bonding point, at a distance of 900 m from the point of injection. At every 900 m, there is a cross-bonding point and a reflection occurs. The amplitude of the reflected pulses decreases rapidly at the bonding points further away from the point of injection, because of the attenuation of the cable itself and the small reflection coefficient of the cross-bonding location. At the receiving (open) cable end, the voltage pulse doubles. Given a total cable length of 10.8 km, together with the time of the first reflection at 900 m, this reflection is registered approximately  $132\ \mu\text{s}$  after pulse injection. In the figure, this point is observable around the negative peak in the responses. The green and the red lines are the reflected pulses measured at phase 4 and 8 of the circuit where the pulse was injected. These pulses result from the coupling between phases in the same circuit. The steepness of the measured waveforms decreases over time because attenuation and distortion.

The light blue line is the measured signal at the cable (8, A1) of circuit ‘wit’ that is nearest to circuit ‘zwart’ (Figure 8.6). There is no signal present, meaning that the mutual coupling between the two cable circuits is small. In Chapter 5, mutual coupling between cable circuits was discussed as part of the modeling work, because in the PSCAD program it is not possible to handle inductively coupled 12 cables. From the simulation results presented in Chapter 5, it can be seen that the coupling between the two cable circuits is negligible. The measurements confirm that the coupling between the two cable circuits is negligible indeed and that the cable modeling can be done with less complexity.

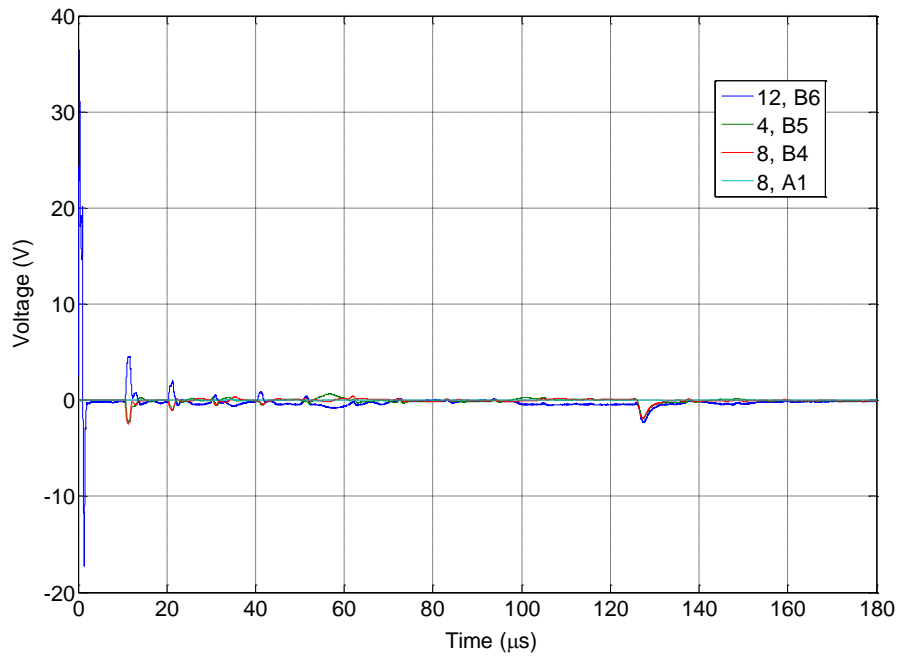


Figure 8.6. Reflection pattern measured at OSP14 after pulse injection.

The receiving (short circuited) end reflection is a negative pulse, as the incident voltage pulse will drop to zero because the impedance is zero at the short circuited cable end. In Figure 8.6, this negative pulse is clearly recognizable at 132  $\mu\text{s}$ . The propagation speed can be verified by using the corrected permittivity of the insulation material, which is 2.7. According to Equation (8.1), the propagation speed is approximately 182 m/ $\mu\text{s}$ . In order to compare the cable end reflection for the cases with open and short circuited termination, the measurement was done with open and with short-circuited cable end. In Figure 8.7, the measured reflection with open cable end is shown. At the open cable end, a positive reflected pulse is present because of the infinite impedance. From the measured reflection time, the propagation speed in the cable is about 169 m/ $\mu\text{s}$ .

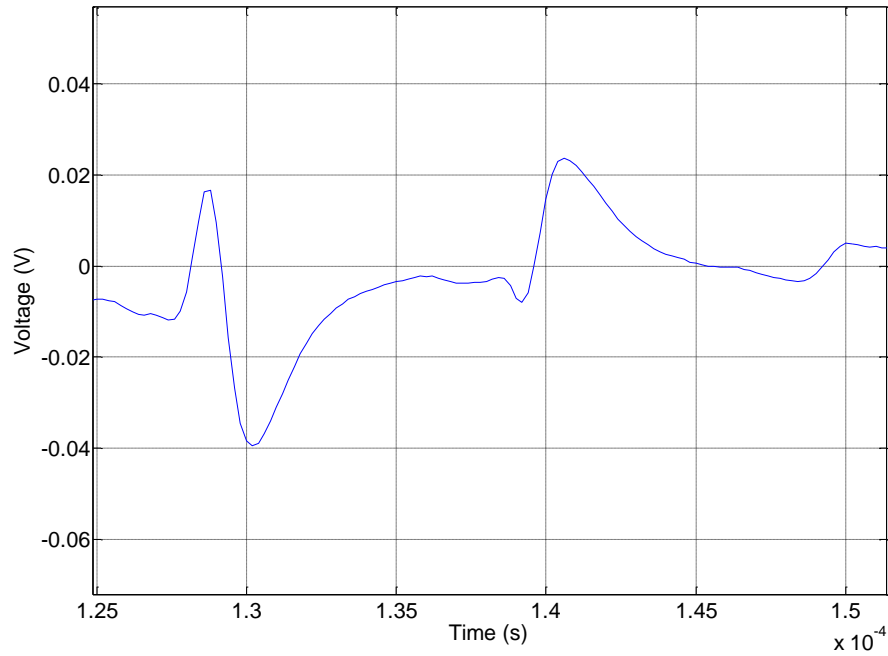


Figure 8.7. Reflection pattern with open cable termination.

$$v \approx \frac{c}{\sqrt{\epsilon_{corrected}}} \quad (8.1)$$

where

$v$  is the cable propagation speed (m/s);

$c$  is the speed of light ( $3 \cdot 10^8$  m/s); and

$\epsilon_{corrected}$  is the corrected cable insulation permittivity as introduced in Chapter 5.

In order to analyze the reflections at the first three cross-bonding points in more detail, they are shown in Figure 8.8 on a time scale of 50  $\mu$ s. The reduction of both amplitude and steepness of the reflected pulses is clearly visible and again it is confirmed that the coupling between the two cable circuits is small. At the receiving (open) cable end, the reflections are recorded as well and the results are shown in Figure 8.9 for the first 50  $\mu$ s after pulse injection at the sending end. From the measured waveforms in Figure 8.9, we see that the amplitude of the first peak is about 1.5 V, being 6% of the amplitude of the injected pulse.

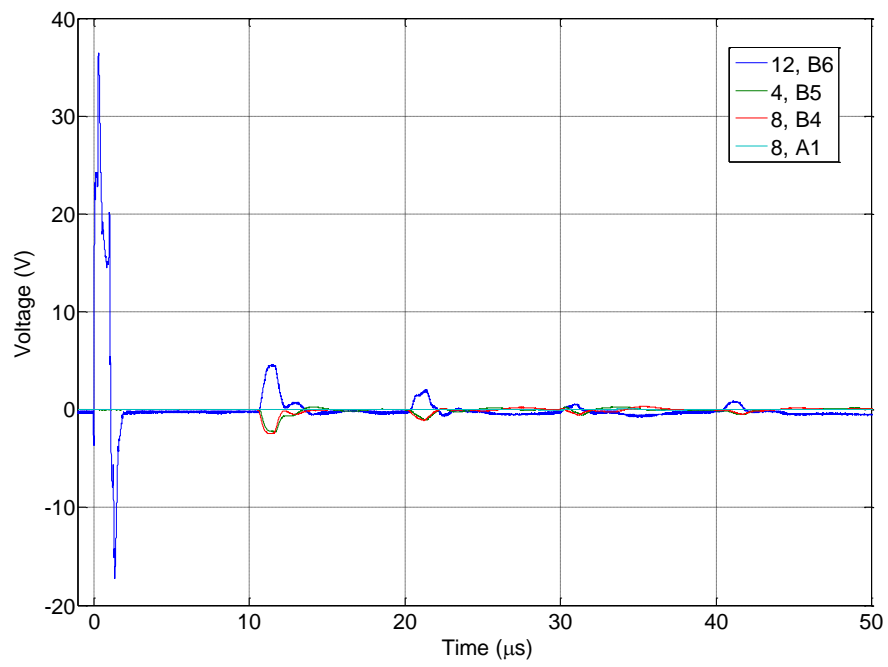


Figure 8.8. Reflection pattern measured at OSP14 for the first 50  $\mu\text{s}$ .

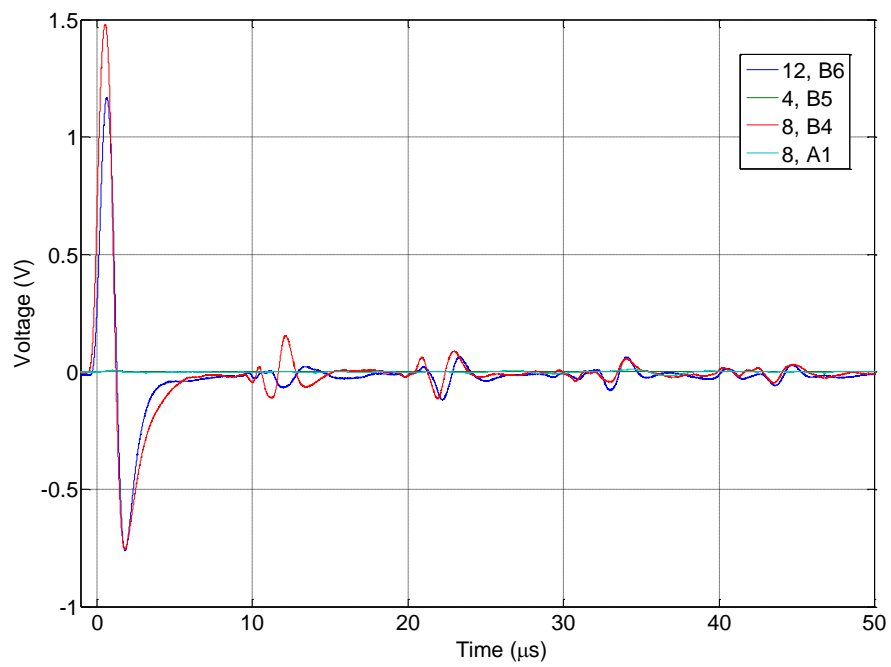


Figure 8.9. Reflection pattern measured at OSP32 for the first 50  $\mu\text{s}$ .

These measured results can be applied for model validation, for the simulated voltage reflections. In Figure 8.10, both the measured and the simulated reflection pattern are shown for the first 50  $\mu\text{s}$  for the case with pulse injection at (12, B6). The figure makes clear that there is a good agreement between measured and simulation results for the first and for the second reflection at the cross-bonding locations. After 25  $\mu\text{s}$ , there is more deviation between measurement and simulation. The measured cable propagation time can be calculated by taking length, characteristic impedance and capacitance, according to (8.2). In Chapter 5, we saw that the capacitance is about 0,2  $\mu\text{F}/\text{km}$ . For characteristic impedance of 30  $\Omega$ , the transmission time is 64.8  $\mu\text{s}$  and the estimated reflection time 129.6  $\mu\text{s}$ . This value is very close to the measured reflection time of 128  $\mu\text{s}$ .

$$\tau_{\text{cable}} = \ell Z_{\text{cable}} C_{\text{cable}} \quad (8.2)$$

where

$\tau_{\text{cable}}$  is the cable propagation time (s);

$\ell$  is the cable length (m);

$Z_{\text{cable}}$  is the cable characteristic impedance ( $\Omega$ ); and

$C_{\text{cable}}$  is the cable capacitance (F/m).

For higher frequencies, the cable losses are mostly in the semi conductive layers. The permittivity of the cable insulation is often modeled as constant value, but the permittivity is frequency dependent and should be taken as a complex number. The Frequency Dependent Phase Model (which is used for this simulation) does take into account the frequency dependent losses in the cable insulation material.

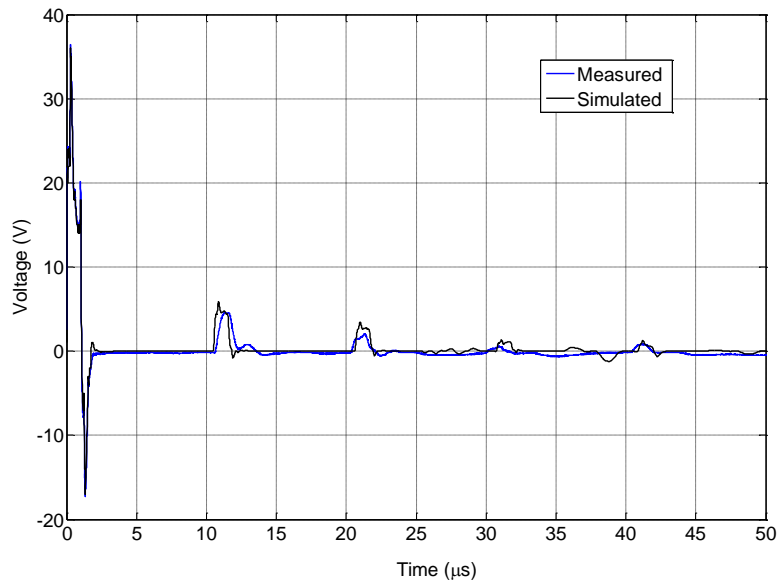


Figure 8.10. Measured and simulated results for the first 50  $\mu\text{s}$ .

### 8.3 STEP VOLTAGE MEASUREMENTS ON THE 380 KV CABLE

The step voltage measurement on the 10.8 km cross-bonded cable system is done at location OSP32, while the receiving cable end at OSP14 is left open. Figure 8.11 shows the measurement setup. The goal is to obtain the response of the 380 kV cable to a step voltage. The function generator used, is the *HP 33120A*, that is able to deliver a square wave with a rise time of about 20 ns. The internal impedance of the *HP 33120A* is 50  $\Omega$ .

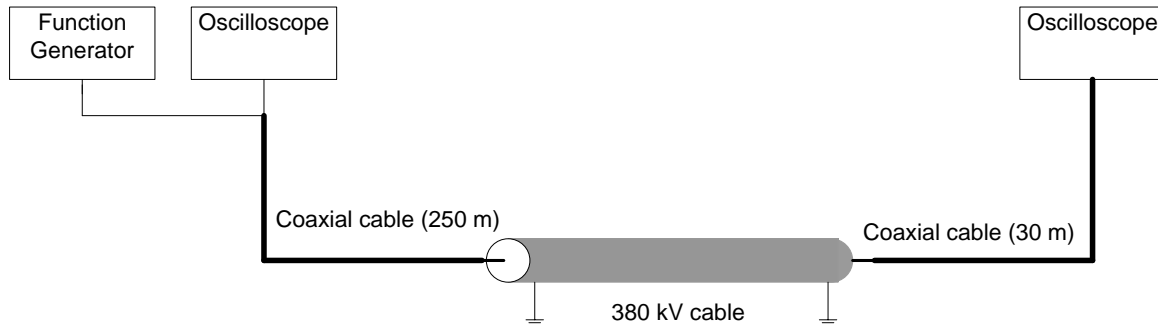


Figure 8.11. Measurement setup at OSP32 for step voltage measurement.

The *HP 33120A* generates a step voltage of 10 V amplitude via a 250 m long coaxial measuring cable to the 380 kV cable core conductor at location OSP32. The internal source voltage of the function generator is 20 V. Since both the internal impedance and the impedance of the coaxial measuring cable is 50  $\Omega$ , voltage division occurs and in this way, the function generator supplies a voltage of 10 V at the output terminals when it is loaded with an impedance of 50  $\Omega$ . At the near end of the measuring cable, the voltage is measured and recorded by the oscilloscope. The receiving end of the 380 kV cable is connected via a 30 m long measuring cable to the oscilloscope and measures the response voltage. The measurements at the sending and at receiving end are not synchronized, and thus the propagation time of the cable cannot be calculated from the results. But the propagation time was already calculated from the results of the pulse reflection measurement. In Figure 8.12, the voltage response measured at the sending end is shown for the first 4.5 ms. The oscillatory response caused by multiple reflections at the receiving open end can be clearly seen from the figure.

As can be seen in Figure 8.11, the measuring equipment at the sending end and at the receiving end is not directly connected to the 380 kV cable. The coaxial measuring cables do influence the measured step voltage response of the 380 kV cable and this should be taken into account for a correct interpretation of the results. This is achieved modelling the 380 kV cable including the measuring cable. Like the 380 kV cable system, the coaxial cables are modeled in PSCAD by making use of the universal line model. The geometric data required for the PSCAD model of the 50  $\Omega$  coaxial measuring cable are derived from its material properties. The cable consists of two concentric conductors with XLPE insulation, having a capacitance of 100 pF/m and this adds up to a total capacitance of 25

nF for this 250 m long measuring cable. The capacitance of the measuring cable, connected between the 380 kV cable receiving end and the oscilloscope, is 3 nF. Taking the relative permittivity to be 2.3 for the XLPE insulation and calculating the capacitance with Equation 8.3 for the capacitance, the ratio between the inner and outer radius of the conductors, indicated by  $a$  and  $b$  respectively, can be calculated. The ratio between  $b$  and  $a$ , has the value of 3.6 and this is used as input for modelling the measurement setup.

$$C_{coax} = \varepsilon_0 \varepsilon \frac{2\pi}{\ln\left(\frac{b}{a}\right)} = 100 \text{ pF/m} \quad (8.3)$$

where

$C_{coax}$  - coaxial cable capacitance (F/m);

$\varepsilon_0$  - vacuum permittivity ( $8.854 \cdot 10^{-12}$  F/m);

$\varepsilon$  - XLPE insulation relative permittivity (2.3);

$a$  - coaxial cable inner radius (m); and

$b$  - coaxial cable outer radius (m).

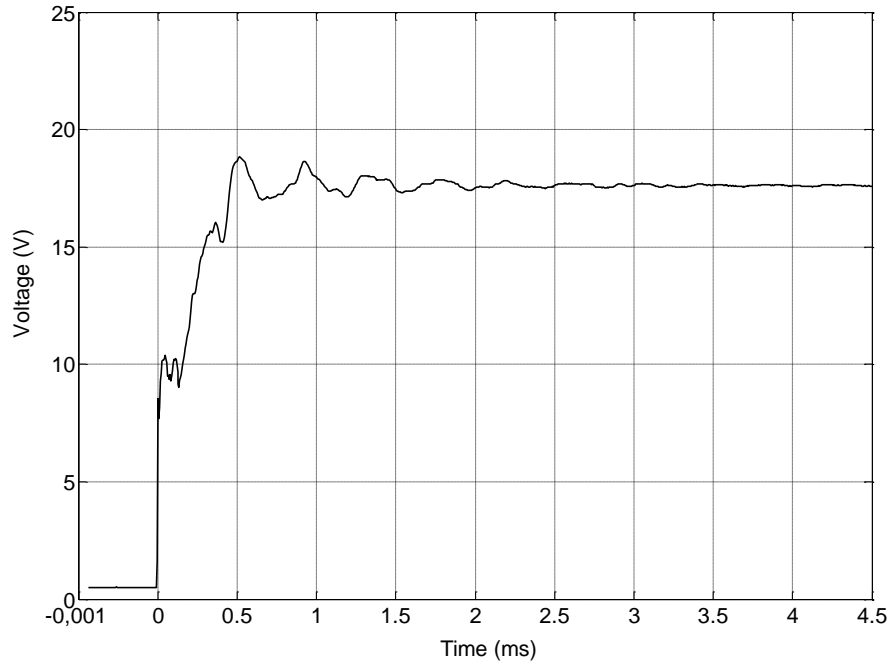


Figure 8.12. Measured voltage response at the sending cable end.

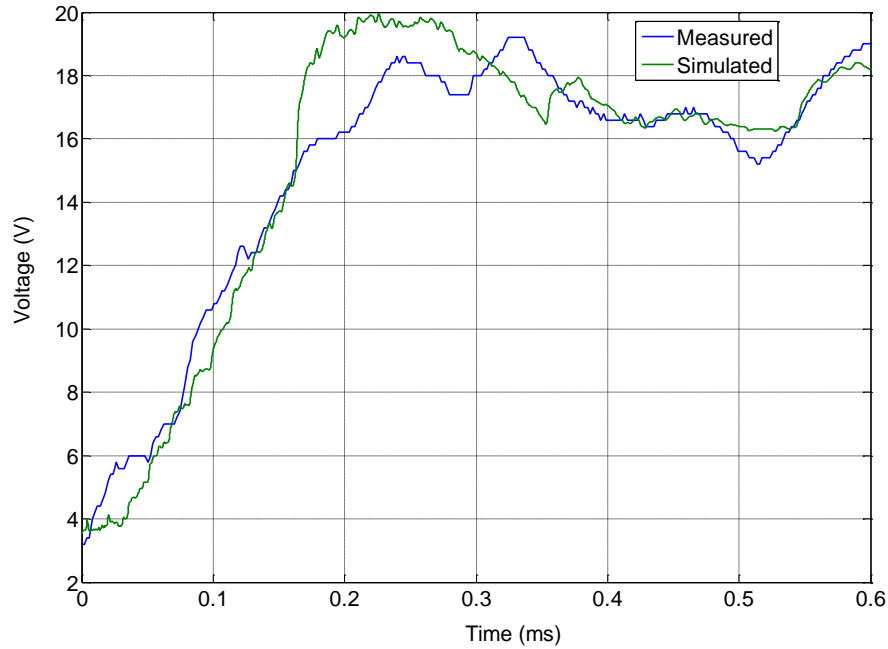


Figure 8.13. Measured and calculated voltage response at the receiving cable end.

Figure 8.13 shows the measured and calculated voltage response at the receiving open cable end. By comparing the two figures, there is a difference in rise times between the voltage at the sending and at the receiving end of the cable, caused by the charging of the  $2.5 \mu\text{F}$  cable capacitance for the total cable length of 10.8 km. The figure shows that the measured voltage response is in good agreement with the simulation up to 0.15 ms after pulse injection. After the first oscillation peak, the measured waveform resembles the simulated voltage wave rather well. When the cable is energized, the steady state voltage at the cable end will equal the voltage at the sending end, approximately 17 V.

For the cable model validation, it is important to know the sensitivity of the FDPM model for small cable parameters changes, as there is a certain mismatch during the first oscillation peak. An important parameter of the cable model that influences the measured results is the earth return resistance [27], as was already discussed in Chapter 3. The value of the earth return resistance strongly depends on the condition of the soil and this means that the weather conditions do influence the earth's return resistance. The step voltage measurement was carried out during a rainy period, resulting in wet soil and this has impact on the ground resistance. The earth return resistance is influenced by the specific resistance of the ground. To investigate the influence of this resistance on the step voltage response of the cable, calculations are done for different values of the specific resistance of the soil and compared with the default value in the PSCAD program, which is  $100 \Omega \cdot \text{m}$ . Figure 8.13 shows that the largest deviation lies between 0.15 and 0.3 ms. This period is observed in more detail by taking different values for the ground resistivity and by calculating the difference in voltage  $\Delta V$  with respect to the calculation with  $100 \Omega \cdot \text{m}$ . The results are depicted in Figure 8.14. It can be noted that the difference is not larger than 1%.



In [90], it was proven that the FDPM cable model was rather accurate till the first cross-bonding point of the cable. However further on, the model gives less accurate results due to intersheath waves propagating between the cable screens. The presence of several cross-bonding points in the studied 10.8 km cable also causes intersheath waves. This is the explanation for the deviation between the calculated results and the measurements during the first oscillation peak.

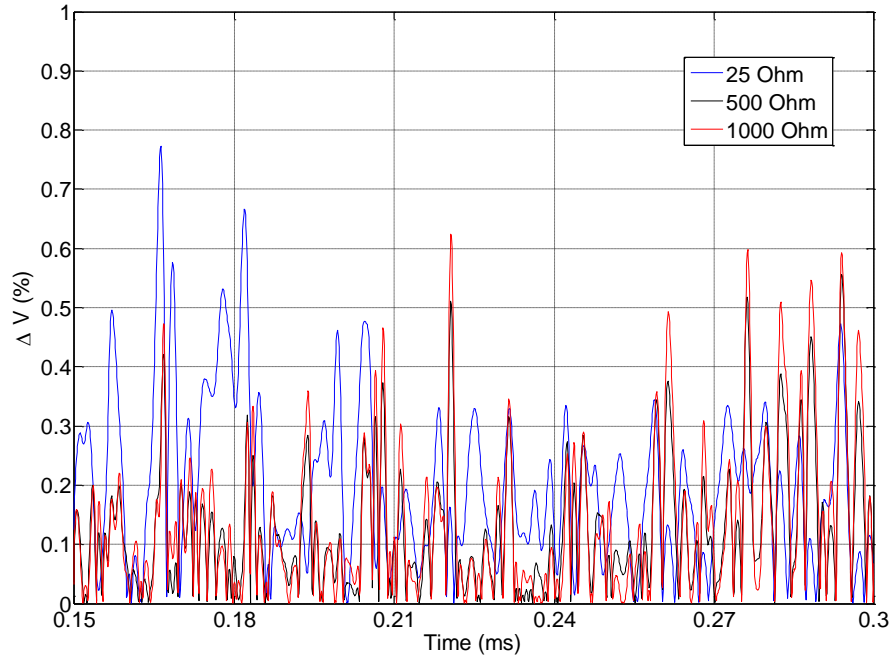


Figure 8.14. Voltage differences when the ground resistivity ( $\Omega m$ ) is changed.

Power system resonance find their origin in inductive and capacitive components, e.g. a cable capacitance oscillates with the inductive network. Several resonance analysis methods have been developed [91-94] and impedance plots are helpful tools to identify the cable resonance points. In PSCAD, an impedance scan of the cable is made. In Figure 8.15, the impedance plot of the 10.8 km cable section is shown for frequencies up to 1 MHz, for the situation that the receiving cable end is left open. Figure 8.16 shows a close up of this impedance plot and the corresponding phase shift for the frequency range from 0.1 to 1 MHz, in which the cable resonance points, being the peaks in the impedance plot, are clearly recognizable.

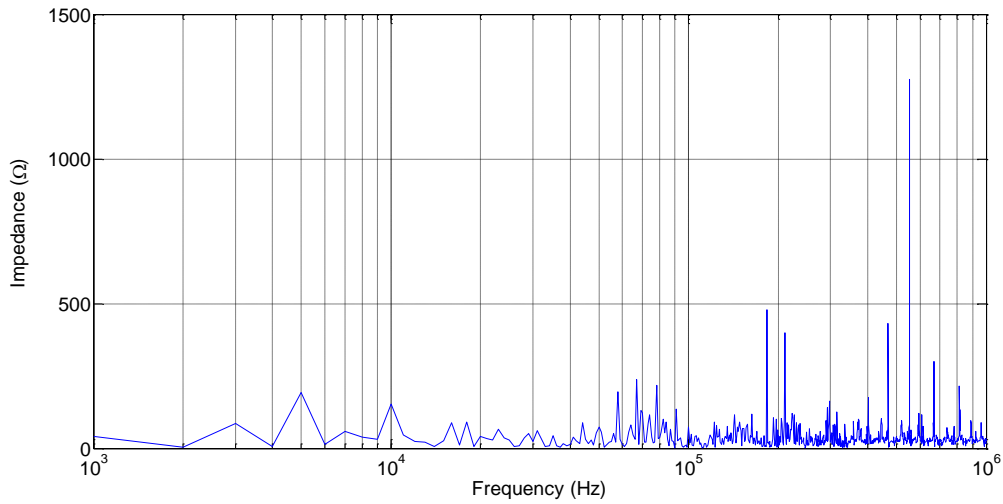


Figure 8.15. cable impedance plot from 1 kHz to 1 MHz.

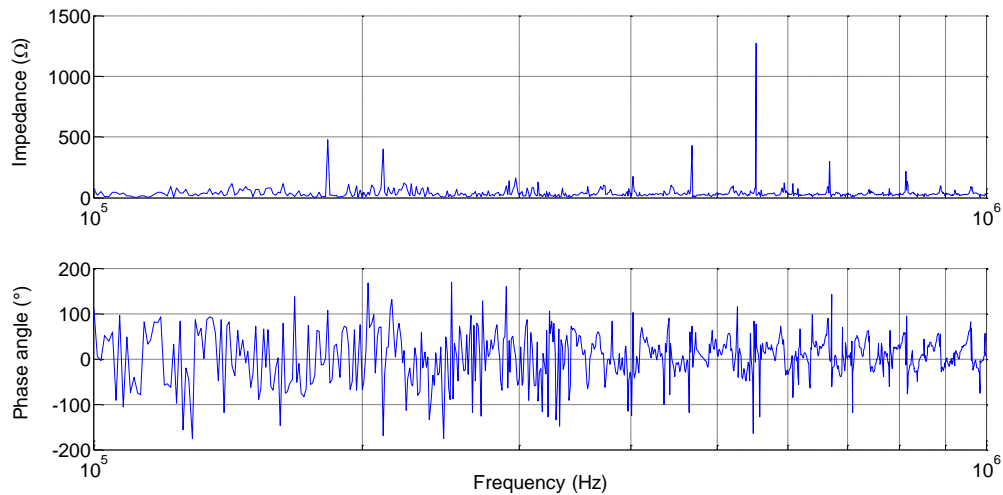


Figure 8.16. Frequency plot of the 10.8 km cable.

## 8.4 PULSE INJECTION MEASUREMENTS ON THE OVERHEAD-LINE SECTIONS

Validation of the Frequency Dependent Phase Model, that is also used for the overhead line conductors in the connection, is also done with field measurements on the overhead line sections. Pulse injection, as it was carried out for the cable, is also done for both line sections of the connection Wieringen - Bleiswijk in order to validate the transmission line model for fast electrical transients. In Chapter 5, the transient models of the line circuits were discussed and it was shown that the lines are positioned in two vertical planes in the new Wintrack tower design in order to reduce the magnetic field strength around the conductors. During the measurements, the lines were at both substations disconnected from the power transformers. In Figure 8.17, the measurement setup is shown for the pulse

injection that was performed for the 4.3 km line, that forms the overhead line section between substation Wateringen and the line-cable transition point. On both sides of the tower, 150 kV lines are positioned. For safety reasons and in order to avoid possible influence on the measurement results by inductive and capacitive coupling, the 150 kV lines were taken out of service during the pulse injection on the 380 kV lines.

In Figure 8.18, the measurement setup is outlined for the 6 km line section between the line-cable transition point and substation Bleiswijk. This measurement was done at the transition point while the line ends at Bleiswijk side are left open. In this line section, there are no 150 kV conductors in parallel with the 380 kV conductors. To protect the measuring equipment and the pulse source against a possible high overvoltage, a protective device is placed in between the oscilloscope and the coaxial measuring cables (indicated by the CP blocks in both figures).

Since the phase conductors of overhead lines are positioned rather close to each other, three different propagation modes for travelling waves exist [65]: a path between the three phase conductors and ground, a path between one phase and ground and a path between two phase conductors. When the propagation characteristics of the lines have to be determined unambiguously, all combinations should be measured but for validating the line model, the measurements are restricted to pulse injection between one phase conductor and ground only.

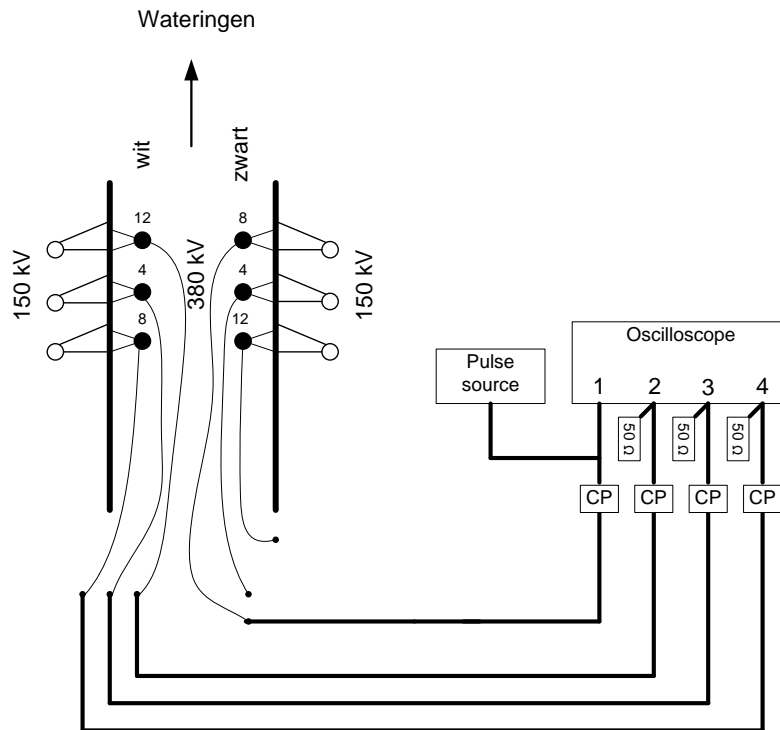


Figure 8.17. Measurement setup for pulse injection into the 4.3 km line.

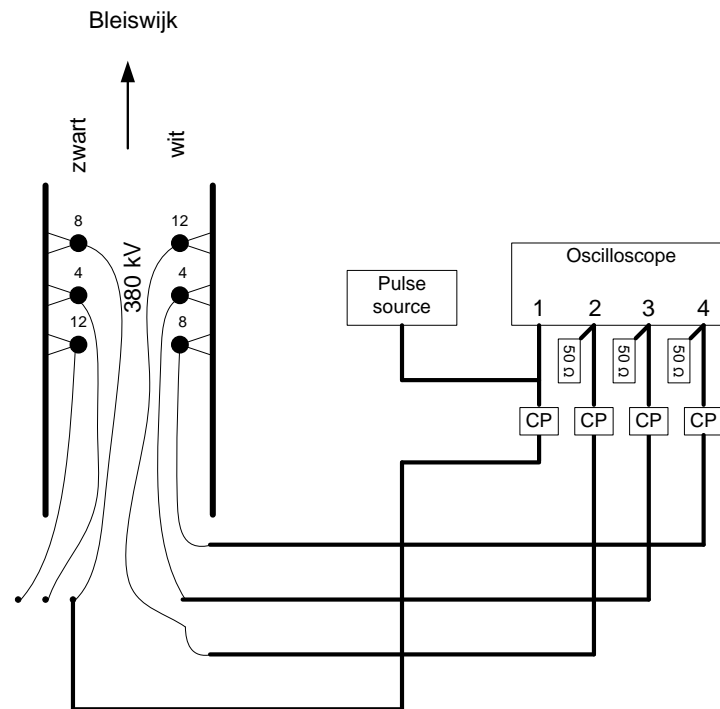


Figure 8.18. Measurement setup for pulse injection into the 6 km line.

A pulse with a 50 V amplitude and 1  $\mu$ s duration was injected via the coaxial cable into the phase conductor 8 of circuit 'zwart', as it is indicated in the figure. The receiving line ends at substation Wateringen are left open. At the point of injection, the reflection pattern was measured and recorded by the oscilloscope. Also, the mutual coupling from circuit 'zwart' to circuit 'wit' is being measured by recording the induced voltage waveforms at the line terminals of circuit 'wit'. In Figure 8.19, the measured reflections are shown till 160  $\mu$ s after the moment of pulse injection. The blue line is the measured pattern at the injected phase. The first maximum is the result of voltage division between the output impedance of the pulse source and the measuring cable, which have both the value 50  $\Omega$ . The second maximum is the reflection at the junction between the coaxial cable and the phase conductor. The peak that appears at about 32  $\mu$ s after pulse injection is the reflection at the open line end. The negative peak at about 62  $\mu$ s is caused by reflection when the wave arrives at the junction between the phase conductor and the coaxial cable. This resulted in the negative peak and reflection occurred at the open line end. It can be noted from the figures that the measured signals in circuit 'wit' are rather small. This means that the mutual coupling between the two circuits is weak and can therefore be neglected.

Figure 8.20, shows the measured reflection patterns for the 6 km line section. The shape of this reflection pattern looks similar to that of the 4.3 km section, except from the longer propagation time. The figure shows also a stronger coupling between the two circuits. This is not to be expected, since the arrangement of both line sections and the Wintrack tower are more or less similar.

In the Figures 8.21 and 8.22, the measured reflection patterns and the simulated results are shown in the same figure for both line sections for the first 100  $\mu$ s. There is a good

agreement between measured and calculated waveforms and the results prove the validity of the line model.

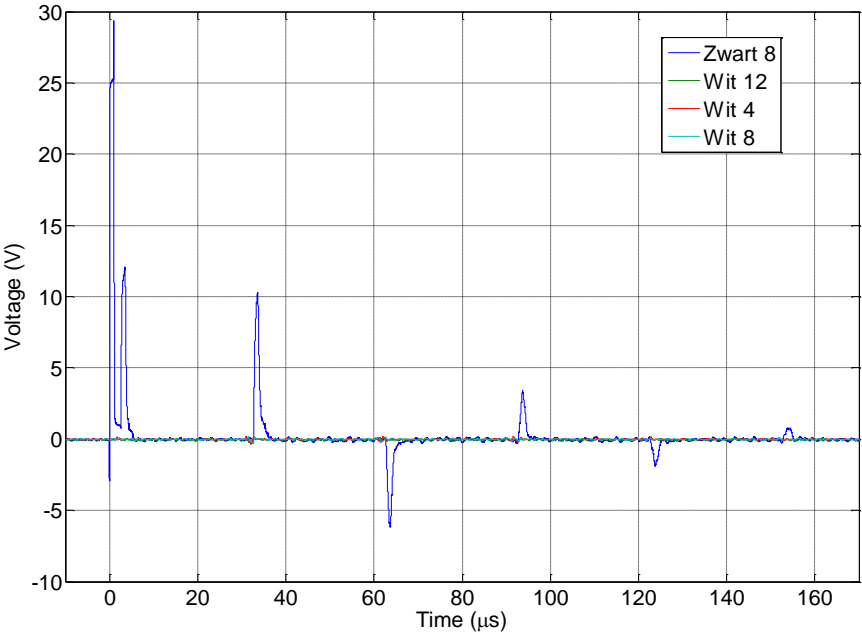


Figure 8.19. Measured reflections after pulse injection into the 4.3 km line.

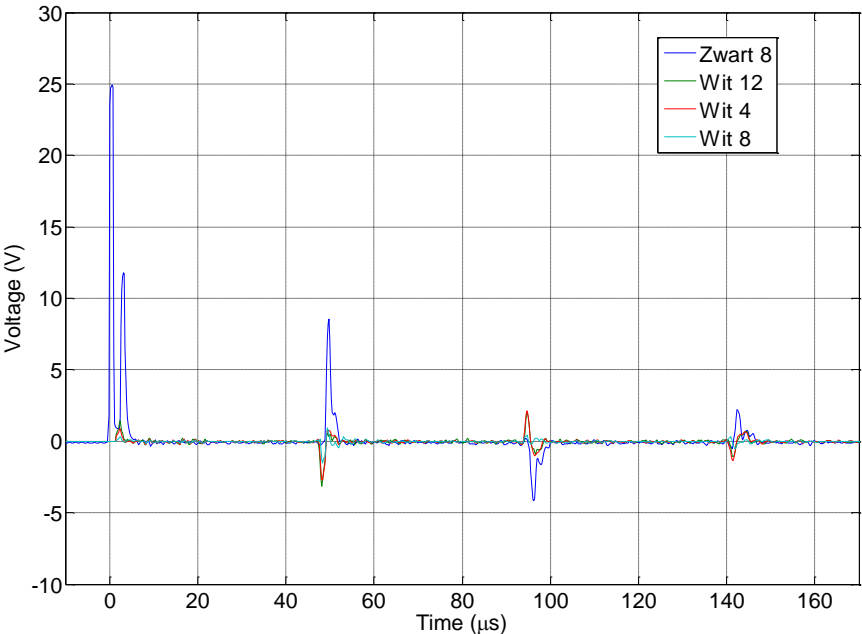


Figure 8.20. Measured reflections after pulse injection into the 6 km line.

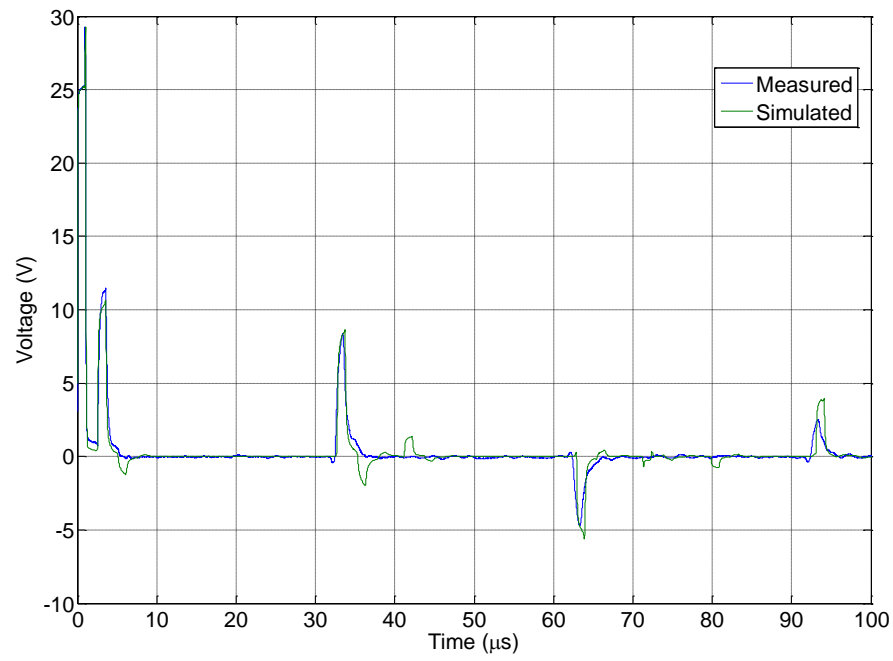


Figure 8.21. Measured and simulated reflections for the 4.3 km line.

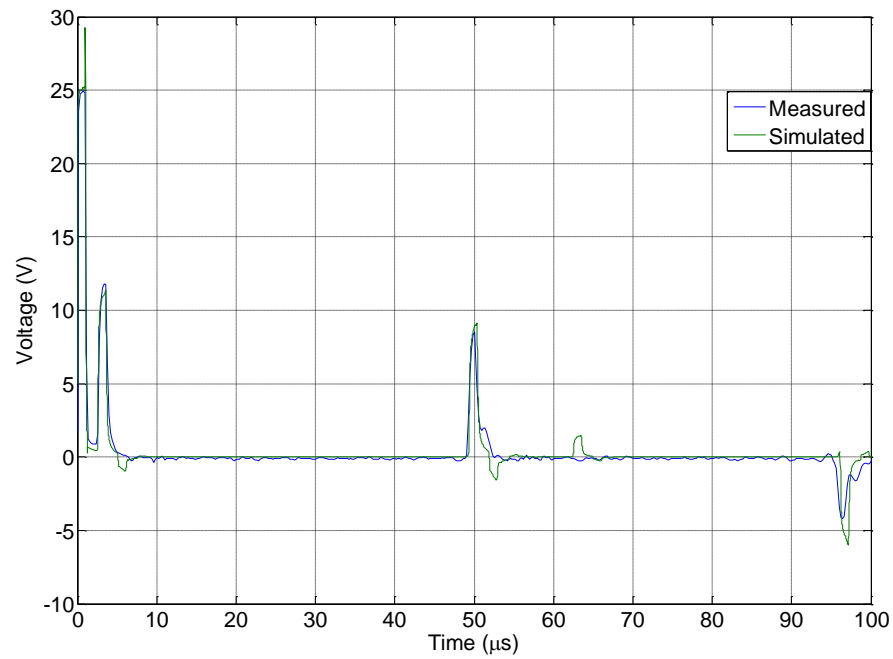


Figure 8.22. Measured and simulated reflections for the 6 km line.

## 8.5 CONCLUSION

This chapter describes the cable and overhead line model validation by using the results from field measurements on the actual cross-bonded 380 kV cable. For the 380 kV cable, a pulse injection was done to determine its propagation time. This measurement result is in good agreement with the calculated results, and this means that the cable propagation time is accurately determined from this measurement. This measurement also confirmed that the coupling between the two cable circuits is small, and this means that there is no necessity to take this coupling into account in the modeling work for a system with several 380 kV cables and that the modelling approach for the studied system is correct. The step voltage measurement on the 380 kV cable shows a good agreement with the calculations, but there is a deviation at the first oscillation peak, as was seen from the results. The origin for this difference lies in the sensitivity of the cable parameters. The earth return resistance is an important parameter that is influenced by the condition of the soil. Sensitivity analysis of the earth return resistance was done but it turned out that only small differences in the calculated voltage waveform occur when the specific ground resistance is varied. The smaller attenuation in the cable simulation model is also a reason for the larger oscillation peak. Frequency plots from 1 kHz to 1 MHz of the 380 kV cable clearly showed its resonance points, which are helpful for the grid operator for prediction of resonances in the network after cable switching. For the overhead line, the measurement confirmed the validity of the FDPM model for fast transients, as the measured results meet the calculated results quite well and this means that the transmission line model can be used for 380 kV overhead line and cable modeling for investigating transients in future 380 kV projects in which underground sections are applied.

## **CHAPTER 9**

# **CONCLUSIONS, RECOMMENDATIONS AND FUTURE WORK**

### **9.1 CONCLUSIONS**

The work presented in this thesis focused on the behavior of cables that are being applied in 380 kV grids. This work forms a part of a monitoring project that is managed by the Dutch transmission grid operator. In this monitoring program, the behavior of two new underground cable connections in the Dutch 380 kV grid are investigated. The research described in this thesis forms a contribution to the monitoring project in order to gain experience with cable application in the 380 kV grid. Unlike an overhead transmission line, a cable acts as a capacitance when it is in operation. In this thesis, different impact studies have been performed on the new Dutch 380 kV cable circuits located in the Randstad area. The results obtained from those impact studies will contribute to the answer the main research question in this monitoring project on how much cable can be applied in the Dutch 380 kV grid.

This thesis presented the steady state and transient modeling work for two new Dutch 380 kV mixed line-cable-line connections in the Randstad. The electromagnetic field theory that was described in Chapter 2, was used as a starting point on which this cable and line modeling work was based. These models were applied for performing transient studies on mixed line-cable-line circuits in order to increase insight in the behavior of such a circuit during steady state and transient phenomena.

In Chapter 3, cable modeling issues like mutual cable impedances and screen conductor cross-bonding were discussed in order to have a starting point for the transient cable modeling work.

The work presented in this thesis focused on steady state and transient behavior of 380 kV mixed line-cable-line circuits. The steady state performance studies performed on the 380



kV grid in which cables are applied contain the observation of the active and reactive power flows in the grid as well as monitoring the voltage levels at the 380 kV substations. Load flow studies were performed on the 380 kV grid in order to investigate the impact of shunt compensated cables in the Randstad on both the power flows and the voltage levels in the grid. Due to difference in impedance between overhead lines and cables, observation of the power flows was necessary to investigate whether overload will occur in the grid, when cables are applied.

One of the research goals was to evaluate whether the power flows and voltage levels in the 380 kV grid stay within the prescribed limits. From Chapter 4, it is known that the application of 20 km cable in the Dutch 380 kV grid have impact on both the power flows in the grid and the steady state voltage levels, since the amount of reactive power in the grid increases when cables are applied. Even outside the Randstad area, the impact on the power flow was visible, but no overloads were observed. Furthermore, the results obtained from  $n-1$  and  $n-2$  contingencies showed that there were no significant overloads observed in the grid during operation with cables. Moreover, the steady state voltage levels stayed within the allowable range prescribed by the transmission grid operator, which is 342 kV - 418 kV.

The transient modeling for the mixed 380 kV line-cable-line connections was discussed in Chapter 5. In Chapter 5, special attention was paid to the modeling work of the cable screen cross-bonding configuration. From the results obtained by pulse injection measurements that were performed on the cross-bonding cable, suitable values for the cross bonding cable parameters were found. Knowing these values for the cross bonding, a complete model for a cross bonded 380 kV cable system is created that makes use of an existing transmission line model. This complete model can be used for transient studies in similar cross bonded 380 kV cables.

The transient model for the new 380 kV connections were applied for performing switching and lightning impact studies, which were presented in respectively Chapter 6 and 7. The goal of the performed switching impact studies is to evaluate the severity of transients in the grid during energization of the cable circuit.

Another goal of this work was investigating whether the peak of the transient voltages at the cable terminals after lightning currents will stay below the Basic Insulation Level. The lightning impact studies in Chapter 6 showed that large transient voltage peaks can be expected when a lightning surge current directly hits the overhead line phase conductor. It turned out that the applied cable length in a mixed line-cable-line configuration is an important parameter that determines the peak overvoltages at the cable terminals during lightning currents. The shorter the cable section with respect to the overhead line length, the larger the transient voltage peaks at the cable terminals and this means that one should be careful when applying cable sections that are shorter than 1 km, which is the shortest length that is applied in the Noordring of the Randstad. The largest peak voltage that appears when 1 km cable is applied without surge arrestors is 760 kV and this is below the

BIL. The presented results of this lightning impact study could be helpful for the grid operator in taking decisions on overvoltage protection strategies, such as the installation of surge arrestors. From these results, it can be concluded that there is no protection equipment necessary for the Noord- en Zuidring in the Randstad.

Field measurements were performed on the actual cross-bonded 380 kV cable system. The results obtained from those measurements confirmed the validity of the applied Frequency Dependent Phase Model for both the 380 kV underground cable sections and the overhead line sections for fast transients. Although there are small deviations observed between measured and simulated results, it is shown that the simulated results matches the measured results pretty well. This means that the used existing cable model can be used for studying transient phenomena in future similar mixed line-cable projects.

Finally, coming back to the goal of the work as it was described in Chapter 1, one can conclude that no remarkable overvoltages occur during the studied steady state and transient situations.

## **9.2 RECOMMENDATIONS**

Although the research presented in this thesis provide clear results with respect to the power flows in the grid, there are still some aspects that need to be improved for doing further detailed analysis. As it was discussed in Chapter 4, assumptions were made for the load conditions and the power delivered by the production plants. Moreover, the presented load flow results are obtained by considering the 380 kV grid components only, meaning that the impact of cable application on the 150 kV side of the 380/150 kV transformer was not investigated. This restrictions makes further research desirable, by extending the grid model to the 150 kV side and application of more detailed data of the power plants and the load conditions to the foreign countries.

The cable monitoring program forms an important part of the Randstad 380 kV project. The results obtained from the measurements on the cable were used in this thesis for transient model validation. On-line measurements are being performed to monitor the behaviour of the mixed line-cable circuits during operation over a longer period of time. The measuring equipment, that is installed at cable-line transition points and at several other locations in the power system, record the voltages and currents. The results obtained from these measurements could be valuable for performance analysis when the system is subjected to a lightning strike or a switching action. The data collected by on-line measurements could also be valuable for additional grid model validation. The installation of such measuring equipment would also be valuable for the new connection Bleiswijk - Beverwijk, which is under construction at the moment. From the lightning impact study presented in Chapter 7, it turned out that large overvoltages can appear at cable-line junctions during fast transients. Therefore, collecting data at these locations during fast transients by performing similar online measurements would be very helpful for making decisions in the installation of protection equipment.

### 9.3 FUTURE WORK

In a subsequent PhD project, the impact of cables in the grid is further investigated. The work in that project focusses on the influence of increasing 380 kV cable length on the behavior of the Dutch 380 kV grid. In this thesis, the study was mainly focused on the impacts of further cabling by simulating a double-circuit mixed OHL-cable case study project in the future Dutch 380 kV grid.

This research investigates optimum shunt compensation allocation according to four sizing criteria for different cable lengths in the case study project. The study will be performed for different load-flow scenarios to determine the influence of both short-circuit and voltage levels on the optimum size and location of the reactors. In this work, investigation was done for two newly build 380 kV connections in the Randstad area in which there were fixed shunt reactors installed on the tertiary transformer winding. But for Dutch underground 380 kV cable projects in the future, the mixed-line configuration could differ from the Randstad 380 kV connections and this means that further investigation is desirable in order to find out whether there is an optimum with respect to both the shunt reactor size and the location of the installed reactors in the grid. In a subsequent research project, in which the complete Dutch 380 kV grid is considered during steady state operation, it will be investigated how the shunt reactor size is influenced by the mixed-line configuration. In this project, the complete Dutch 380 kV grid is considered for investigating the grid in order to find an answer to the question if there such an optimum can be found.

Frequency scan plots of the 380 kV cable section showed the impedance of the cable over a wide frequency range and this provides information about the cable resonance frequencies, which is important for predicting the resonance behavior of mixed line-cable circuits. The total applied cable length in the Randstad was limited to 20 km and it is interesting to investigate what would happen with the location of the resonance points when the applied cable length is increased. Therefore, in the new research project, the resonance behavior of mixed line-cable circuits is further investigated with the focus on the influence on the resonance points when the cable length is increased in the 380 kV grid. It will be figured out what the consequences are for both the order of the first harmonic resonance frequency and for the number of resonance points when having long cables in the grid. Moreover, switching transients related to energization, de-energization and re-energization of the mixed OHL-cable connection will be addressed by time-domain simulations. Different expected phenomena related to the switching actions will be investigated for increasing cable length in the grid. Several sensitivity analyses will be carried out to determine the best solutions to handle possible unwanted situations related to the operation of long cables.

## APPENDIX A

### CABLE MATRIX IMPEDANCE ELEMENTS APPROXIMATED BY BESSEL FUNCTIONS

The expressions for the two layer coaxial cable, of which the impedance matrix is presented in Chapter 3 (Figure A.1) can be approximated by Bessel functions. Figure A.1 shows the cross-section of the two-layer coaxial cable and Figure A.2 shows the impedances of the cable, that are present between the cable core conductor, the sheath and the earth [40].

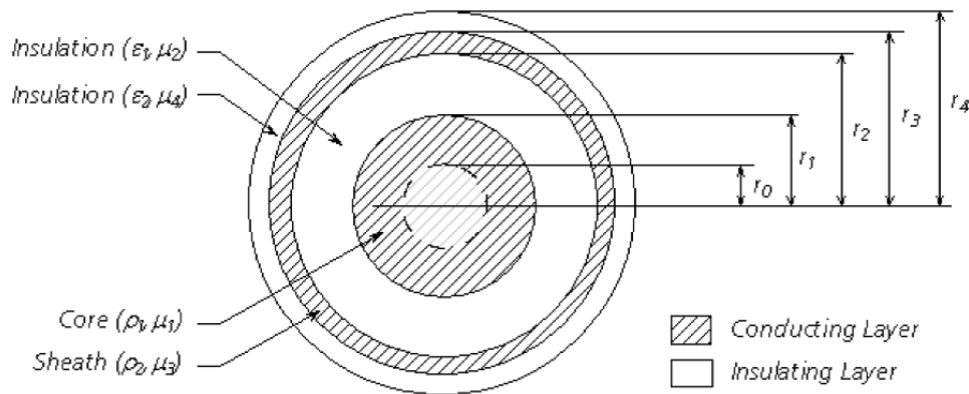


Figure A.1. Cross-section of a two-layer coaxial cable.

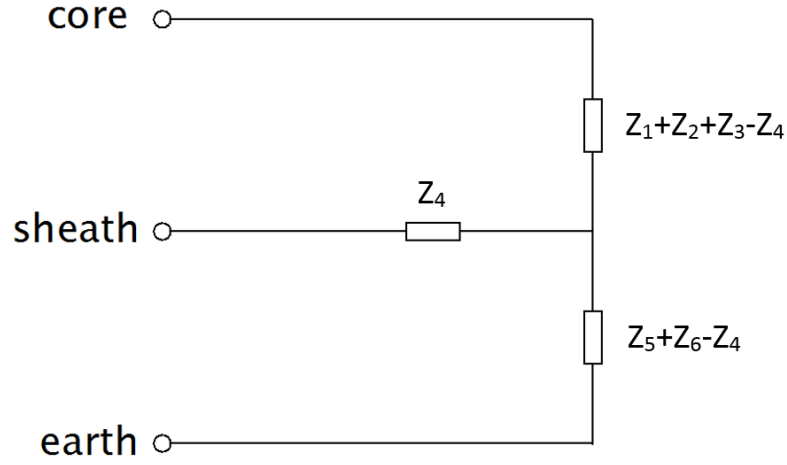


Figure A.2. Impedance elements of a two-layer coaxial cable.

The internal impedance of the cable core outer surface (solid cylinder) is:

$$z_1 = j\omega \frac{m\rho_1}{2\pi r_1} \frac{I_0(mr_1)}{I_1(mr_1)} \quad (\text{A.1})$$

The cable core outer insulation impedance is:

$$z_2 = j\omega \frac{\mu_0\mu_2}{2\pi} \ln\left(\frac{r_2}{r_1}\right) \quad (\text{A.2})$$

The internal impedance of the cable sheath inner surface:

$$z_3 = j\omega \frac{\mu_0\mu_3}{2\pi} \frac{1}{mr_2} \frac{I_0(mr_2)K_1(mr_3) + K_0(mr_2)I_1(mr_3)}{I_1(mr_3)K_1(mr_2) - K_1(mr_3)I_1(mr_2)} \quad (\text{A.3})$$

The cable sheath mutual impedance:

$$z_4 = \frac{\rho_2}{2\pi r_2 r_3} \frac{1}{I_1(mr_3)K_1(mr_2) - K_1(mr_3)I_1(mr_2)} \quad (\text{A.4})$$

The internal impedance of the sheath outer surface:

$$z_5 = j\omega \frac{\mu_0 \mu_3}{2\pi} \frac{1}{mr_3} \frac{I_0(mr_3)K_1(mr_2) + K_0(mr_3)I_1(mr_2)}{I_1(mr_3)K_1(mr_2) - K_1(mr_3)I_1(mr_2)} \quad (\text{A.5})$$

The cable outer insulation impedance:

$$z_6 = j\omega \frac{\mu_0 \mu_4}{2\pi} \ln\left(\frac{r_4}{r_3}\right) \quad (\text{A.6})$$

where:

$I_k(x)$  = Modified Bessel function of the first kind

$K_k(x)$  = Modified Bessel function of the second kind

$m = \sqrt{j\omega \frac{\mu_0 \mu_r}{\rho}}$ , which is the inverse complex depth of penetration

$\rho$  = resistivity [ $\Omega\text{m}$ ]

The equations for the internal potential coefficients are given in (A.7 and A.8).

The core potential coefficient:

$$P_{cj} = \frac{1}{2\pi\epsilon_{1j}\epsilon_0} \ln\left(\frac{r_{3j}}{r_{2j}}\right) \quad (\text{A.7})$$

The sheath potential coefficient:

$$P_{sj} = \frac{1}{2\pi\epsilon_{2j}\epsilon_0} \ln\left(\frac{r_{5j}}{r_{4j}}\right) \quad (\text{A.8})$$

## APPENDIX B

### THE FREQUENCY DEPENDENT PHASE MODEL

The Frequency Dependent Phase Model, also referred to as the Universal Line Model, directly fits all the cable parameters in the phase domain. The principle of the universal line model is to fit all the cable parameters directly in the phase domain. The cable terminal conditions are calculated by (B.1) and (B.2).

$$v_s(\omega) = v_r(\omega) \cosh(\gamma(\omega)l) - i_r(\omega) Z_{cable}(\omega) \sinh(\gamma(\omega)l) \quad (B.1)$$

$$i_s(\omega) = \frac{v_r(\omega)}{Z_{cable}} \sinh(\gamma(\omega)l) - i_r(\omega) \cosh(\gamma(\omega)l) \quad (B.2)$$

where

$v_s$  - cable sending end voltage (V)

$v_r$  - cable receiving end voltage (V)

$i_s$  - cable sending end current (A)

$i_r$  - cable receiving end current (A)

$Z_{cable}$  - cable characteristic impedance ( $\Omega$ )

$\gamma$  - cable propagation constant, containing the attenuation factor and the phase constant

When the cable parameters are fitted in the phase domain, the elements of the propagation matrix  $\mathbf{H}$  and the admittance matrix  $\mathbf{Y}$ , are fitted in the Phase Domain. Vector Fitting (VF), which is a least squares fitting routine, is used for fitting  $\mathbf{H}$  and  $\mathbf{Y}$  in the phase domain [29]. The Vector Fitting technique estimates the coefficients of a function  $f(s)$ , in such a way that the least squares approximation is found over a given frequency range. The function  $f(s)$  is given by:

$$f(s) = \sum_{n=1}^N \frac{c_n}{s - a_n} \quad (\text{B.3})$$

where

$a_n$  - poles for the function  $f(s)$

$c_n$  - residues for the function  $f(s)$

$N$  - number of poles

Each propagation mode  $i$  must be related in time by its time delay  $\tau_i$ , when the propagation matrix  $\mathbf{H}$  is being fitted in the phase domain. Since there are different inner and outer insulation layers in cables, there are different propagation speeds for each propagation mode [29]. The propagation function  $H$  for a specific mode, is given by:

$$H(\omega) = e^{-(\alpha + j\beta)l} \quad (\text{B.4})$$

where

$\alpha$  - modal attenuation constant

$\beta$  - model phase constant

As there are different propagation modes, there are also different travelling times for each mode. Therefore, each mode  $i$  is fitted as it is described by:

$$e^{s\tau_i} H_k^i(s) \sum_{k=1}^N \frac{c_k}{s - a_k} \quad (\text{B.5})$$

where

$\tau_i$  - time delay of mode  $i$

By applying (B.2), each element of the propagation matrix  $\mathbf{H}$  is calculated by:



$$h(s) = \sum_{i=1}^{N_g} \left[ \sum_{k=1}^N \frac{c_{ki}}{s - a_{ki}} \right] e^{-s\tau_i} \quad (\text{B.6})$$

where

$N_g$  - number of modes

$N$  - number of poles for each mode

$\tau_i$  - precalculated time constant for mode  $i$

When the propagation matrix  $\mathbf{H}$  is estimated by applying vector fitting, the cable admittance matrix  $\mathbf{Y}$  need to be fitted so that the conditions describe by (B.1) and (B.2) can be determined.

## APPENDIX C

### LIGHTNING OVERVOLTAGES AT HIGH VOLTAGE TOWER TOP

When the lightning current strikes the high voltage tower, the final tower top voltage is the result of multiple reflections between the tower-footing impedance, the grounding wire impedance and the tower impedance. The equivalent characteristic impedance seen by the lightning surge current as it strikes the high voltage tower top, is given by [79]:

$$Z_{eq} = \frac{Z_{groundwire} Z_{tower}}{Z_{groundwire} + 2Z_{tower}} \quad (C.1)$$

The initial voltage  $V_0$  at the high voltage tower top is equal to:

$$V_0 = IZ_{eq} \quad (C.2)$$

The voltage reflection and the transmission coefficient at the high voltage tower-footing resistance  $R_{tf}$ , are respectively given by:

$$a_{gr} = \frac{R_{tf} - Z_{tower}}{R_{tf} + Z_{tower}} \quad (C.3)$$

$$a_{gt} = 1 + a_{gr} \quad (C.4)$$

When the voltage is reflected at  $R_f$  travels back up the tower, a part will reflect back down the tower. The remaining part is transmitted to the grounding wire. The voltage coefficients are given by:

$$a_{tr} = \frac{Z_{groundwire} - 2Z_{tower}}{Z_{groundwire} + 2Z_{tower}} \quad (C.5)$$

$$a_{tt} = 1 + a_{tr} \quad (C.6)$$

Multiple reflections takes place along the grounding wire between the tower that is hit by the surge current and its adjacent towers. The reflection and transmission coefficients at the adjacent tower are given by:

$$a_{groundr}' = \frac{Z_{groundwire}}{Z_{groundwire} + 2Z_{tower}} \quad (C.7)$$

$$a_{groundt}' = 1 + a_{groundr}' \quad (C.8)$$

The coefficients at the tower that is hit are:

$$a_{groundr} = \frac{2Z_{tower} - Z_{groundwire}}{2Z_{tower} + Z_{groundwire}} \quad (C.9)$$

$$a_{groundt} = 1 + a_{groundr} \quad (C.10)$$

The final tower top voltage  $V_{tt}$  is the sum of all multiple reflections, given by:

$$V_{tt} = V_0(t)u(t) + a_{tt}a_{gr} \sum \left[ (a_{tr}a_{gr})^{n-1} V_0(t - 2n\tau_t)u(t - 2n\tau_t) \right] +$$

$$a_{groundt}a_{groundr}' V_0(t - 2\tau_s)u(t - 2\tau_s) \quad (C.11)$$

where

$V_0$  - initial tower top voltage (V);

$u(t)$  - unit step function;

$\tau_s$  - travel time of the span length (s);

$\tau_t$  - travel time of the tower length (s); and

$n$  - integer between 1 and  $t / 2\tau_t$ .

## BIBLIOGRAPHY

- [1] F. Noack: "Comparison between overhead lines (OHL) and underground cables (UGC) as 400 kV transmission lines for the Woodland-Kingscourt-Turleenan Project", *ASKON Consultinggroup, Ilmenau University of Technology, Germany*, September 2008
- [2] Cigre Working Group B1.10: "Update of service experience of EHV underground and submarine cable systems", *ISBN: 978-2-85873-066-7*, April 2009
- [3] Y. Ohki, S. Yasufuku: "The World's First Long-Distance 500 kV-XLPE Cable Line, Part 2: Joints and After-Installation Test", *IEEE Electrical Insulation Magazine*, May/June 2002-Vol. 18, No.3
- [4] C.F. Jensen: "Studies of transient overvoltage at the Horns Rev 2 wind farm EHVAC cable connection" *Aalborg University, Master Thesis*, January 2010
- [5] L. Colla, F.M. Gatta, A. Geri, S. Lauria and M. Maccioni: "Steady-state Operation of Very Long EHV AC Cable Lines", *In the Proceedings of IEEE Power Tech Conference*, Bucharest, June-July, 2009
- [6] F.M. Gatta and S. Lauria: "Very Long EHV cables and mixed overhead-cable lines. Steady-state operation", *In the proceedings of IEEE Power Tech Conference*, ST. Petersburg, June 2005
- [7] L. Colla, F.M. Gatta, F. Illiceto and S. Lauria: "Design and operation of EHV transmission lines including long insulated cable and overhead sections", *In the proceedings of IEEE International Power Engineering Conference*, Nov-Dec 2005
- [8] S. Lauria, F.M. Gatta and L. Colla: "Shunt compensation of EHV Cables and Mixed Overhead-Cable Lines", *In the proceedings of IEEE Lausanne Power Tech Conference*, July 2007

- [9] C.L. Bak, W. Wiechowski, K. Sogaard, S.D. Mikkelsen: "Analysis and simulation of switching surge generation when disconnecting a combined 400 kV cable/overhead line with shunt reactor", *In the proceedings of IPST conference, Lyon, France* June 2007
- [10] C.L. Bak, H. Baldursson, A.M. Oumarou: "Switching Overvoltages in 60 kV reactor compensated cable grid due to resonance after disconnection", *Institute of Energy Technology, Aalborg University, Denmark*
- [11] K. Burges, J. Bömer, C. Nabe, G. Papaefthymiou: "Study on the comparative merits of overhead electricity transmission lines versus underground cables", *Ecofys Germany GmbH*, May 2008
- [12] Tokyo Electric Power Company: "Joint Feasibility Study on the 400 kV Cable Line Endrup-Idomlund", Final Report, April 2008
- [13] Cigre Working Group B1.05: "Transient voltages affecting long cables", April 2005
- [14] F. Massaro, G. Morana, R. Musca: "Transient Behavior of a "Mixed" Overhead-Cable EHV Line under Lightning Events", *IEEE Proc. International Power Engineering Conference*, September 2009
- [15] F. Faria de Silva, C.L. Bak, U.S. Gudmundsdottir, W. Wiechowski, M. Randrup: "Methods to Minimize Zero-Missing Phenomenon", *IEEE Transactions on Power Delivery*, Vol. 25, No. 4, October 2010
- [16] F. Faria de Silva, C.L. Bak, U.S. Gudmundsdottir, W. Wiechowski and M.R. Knardrupgard: "Use of a Pre-Insertion Resistor to Minimize Zero-Missing Phenomenon and Switching Overvoltages", *IEEE Power Eng. Soc, General Meeting, Calgary, AB, Canada*, July 2009
- [17] J.R. Marti: "Accurate Modelling of Frequency-Dependent Transmission Lines in Electromagnetic Transient Simulations", *IEEE Transactions on Power Apparatus and Systems*, Vol. PAS-101, No. 1, January 1982
- [18] L. Marti: "Simulation of Transients in Underground Cables With Frequency-Dependent Modal Matrices", *IEEE Transactions on Power Delivery*, Vol.3, No.3, July 1988
- [19] T. Noda, N. Nagaoka, A. Ametani: "Phase Domain Modeling of Frequency-Dependent Transmission Lines by Means of an ARMA Model", *IEEE Transactions on Power Delivery*, Vol.11, No.1, January 1996

- [20] A. Morched, B. Gustavsen, M. Tartibi: "A universal model for accurate calculation of electromagnetic transients on overhead lines and underground cables", *IEEE Transactions on Power Delivery*, Vol.14, No.3, July 1999
- [21] T. Yu, J.R. Marti: "A Robust Phase-Coordinates Frequency-Dependent Underground Cable Model (zCable) for the EMTP", *IEEE Transactions on Power Delivery*, Vol.18, No.1, January 2003
- [22] A. Ametani: "A general formulation of impedance and admittance of cables", *IEEE Transactions on Power Apparatus and Systems*, Vol. PAS-99, no.3, pp. 902-910, May/June 1980
- [23] A. Ametani, Y. Miyamoto, N. Nagaoka: "Semiconducting Layer impedance and its Effect on Cable Wave-Propagation and Transient Characteristics", *IEEE transactions on Power Delivery*, Vol.19, No.4, October 2004
- [24] Y. Yin, H.W. Dommel: "Calculation of Frequency-Dependent Impedances of Underground Power Cables With Finite Element Method", *IEEE Transactions on Magnetism*, Vol.25, No.4, July 1989
- [25] R.A. Rivas, J.R. Marti: "Calculation of Frequency-Dependent Parameters of Power Cables: Matrix Partitioning Techniques", *IEEE Transactions on Power Delivery*, Vol.17, No.4, October 2002
- [26] F.A. Uribe: "Accurate Modeling of Underground Cable Earth Impedances for Electromagnetic Transients", *IEEE Power Engineering Society General Meeting*, October 2006
- [27] F.A. Uribe, J.L. Naredo, P. Moreno, L. Guardado: "Algorithmic Evaluation of Underground Cable Earth Impedances", *IEEE Transactions on Power Delivery*, Vol.19, No.1, January 2004.
- [28] F.A. Uribe: "Assessing Closed-Form Approximations for Underground Cable Earth Impedances", *IEEE Power Engineering Society General Meeting*, July 2003
- [29] U.S. Gudmundsdottir: "Modeling of long High Voltage AC Cables in Transmission Systems", *PhD Thesis, Aalborg University, Denmark*, May 2010
- [30] Cigre Working Group C4.502: "Power system technical performance issues related to the application of long EHVAC cables", January 2011
- [31] EPRI. Palo Alto: "Transmission Line Reference Book 345 kV and Above", USA, 1975
- [32] D. Quak, A.H.M. van Roermund and L. van der Sluis: "EMC in Theorie en Praktijk", *Lecturenotes 2001-2002*

- [33] L. van der Sluis: "Transients in Power Systems", John Wiley & Sons, 2001
- [34] Agilent Technologies: "Practical characterization and analysis of lossy transmission lines", USA, april 10, 2002
- [35] F.L. Neerhoff: "Elektrische circuits, model structuur en dynamica", deel 1, 1997
- [36] F.L. Neerhoff: "Elektrische circuits, model structuur en dynamica", deel 2, 1996
- [37] P.N.M. Gockel: "Steady state voltage profile and reactive power balance for EHV AC cable systems in the Randstad380 project", Master Thesis, Delft University of Technology, April 2009
- [38] San-Yi Lee: "A cable configuration technique for the balance of current distribution in parallel cables", Journal of Marine Science and Technology, Vol. 18, No. 2, pp. 290-297, 2010
- [39] A.A. Ghandakly and R.L Curran: "A model to predict current distributions in heavy current parallel conductor configurations", IEEE Transactions on Industry Applications, Vol. 30, No. 2, pp. 240-244, 1993
- [40] Manitoba EHVDC Research Centre: "EMTDC™ user's guide", Canada 2010
- [41] E. Peschke and E. Von Olshausen: "Cable systems for high and extra high voltage", Pirelli, 1999. ISBN 3-89579-118-5
- [42] S. Ansorge, B. Arnold: "Jointing of High voltage cable systems", PFISTERER IXOSIL AG, 2005
- [43] P.H. Schavemaker, L. van der Sluis: "Electrical Power System Essentials", John Wiley and Sons, 2008
- [44] G.W. Brown and R.G. Rocomora: "Surge propagation in three-phase pipe-type cables, Part 1-Unsaturated pipe", IEEE Transactions on Power Apparatus and Systems, 95(1), 89-95, January/February 1976
- [45] G.W. Brown and R.G. Rocomora: "Surge propagation in three-phase pipe-type cables, Part 2-Duplication of field tests including the effects of neutral wires and pipe saturation", IEEE Transactions on Power Apparatus and Systems, 96(3), 826-833, May/June 1977
- [46] J.R. Carson: "Wave propagation in Overhead Wires with Ground Return", Bell Syst. Techn. J., Vol. 5, pp. 539-554, 1926



- [47] A. Deri, G. Tevan, A. Semlyen, A. Castanheira: "The Complex Ground Return Plane – A Simplified Model for Homogeneous and Multi-Layer Earth Return", IEEE Transactions on Power Apparatus and Systems, Vol. PAS-100, No. 8, pp. 3686-3693, August 1981
- [48] F. Pollaczek: "Sur le champ produit par un conducteur simple infiniment long parcouru par un courant alternatif", Revue Gen, Elec., 29, pp. 851-867, 1931
- [49] L.M. Wedepohl, D.J. Wilcox: "Transient Analysis of Underground Power-transmission Systems. System Model and Wave-propagation Characteristics", Proc. IEE, 120, (2), pp. 253-260, 1973
- [50] F.A. Uribe-Campos: "Numerical Infinite Series Solution of the Ground-Return Pollaczek Integral", Departamento de Mecánica Eléctrica División de Ingenierías, Universidad de Guadalajara, May 2013
- [51] A. Greenwood: "Electric Transients in Power Systems", John Wiley & Sons, 1<sup>st</sup> Edition, 1971
- [52] M.V. Escudero, M. Redfern: "Effects of transmission line construction on resonance in shunt compensated EHV lines", IPST05-109, June 2005
- [53] Position Paper: "Verantwoord en innovatief ondergronds", TenneT, Arnhem, The Netherlands, 2009
- [54] J.J. Meeuwsen: "Reliability evaluation of electric transmission and distribution systems", PhD Thesis, Delft University of Technology, December 1998
- [55] Kwaliteits- en Capaciteitsplan 2008-2014, TenneT, Arnhem, The Netherlands, 2007
- [56] L. van der Sluis, M. Popov, J.J. Meeuwsen, G. Hoogendorp, R.A.M. van Amerongen: "Leveringszekerheid in het kader van het project Randstad 380", Technische Universiteit Delft/D-Cision, 2009
- [57] PSS<sup>TM</sup>E 31.0 User's Manual: Siemens Power Transmission & Distribution, Inc Power Technologies International, December 2007
- [58] John J. Grainger, William D. Stevenson, Jr.: Power System Analysis, McGraw-Hill, Inc, 1994
- [59] CIGRE WG 33.02: "Guidelines for Representation of Network Elements when Calculating Transients", CIGRE Brochure no. 39, 1990.

- [60] A. Gole, J.A. Martinez-Velasco and A. Keri (Eds.): “Modeling and Analysis of Power System Transients Using Digital Programs”, IEEE Special Publication TP-133-0, IEEE Catalog No. 99TP133-0, 1999.
- [61] B. Gustavsen and A. Semlyen: “Rational approximation of frequency domain responses by vector fitting”, *IEEE Transactions on Power Delivery*, vol. 14, no. 3, pp. 1052-1061, July 1999
- [62] B. Gustavsen, J.A. Martinez, D. Durbak: “Parameter determination for modeling system transients – part ii: insulated cables”, *IEEE Transactions on Power Delivery*, vol. 20, no. 3, pp. 1045-2050, July 2005
- [63] I. Tannemaat, C.S. Engelbrecht: “Supplemental transient studies for 380 kV oil immersed series reactors in the connection Maasvlakte-Westerlee”, KEMA Consulting, 2009
- [64] B. Gustavsen: “A study of overvoltages in high voltage cables with emphasis on sheath overvoltages”, Trondheim, Norway: PhD Thesis, NTH, 1986
- [65] J.J. de Regt: “Identification of Overvoltages in Earth Screens of Cross bonded 400 kV Underground Power Cables”, Graduation paper, Eindhoven university of Technology, 2012
- [66] P. Wagenaars: “Integration of Online Partial Discharge Monitoring and Defect Location in Medium-Voltage Cable Networks”, PhD Thesis, Department of Electrical Energy Systems, Eindhoven University of Technology, March 2010.
- [67] P. Wagenaars, P.A.A.F. Wouters, P.C.J.M. van der Wielen and E.F. Steennis: “Measurement of transmission line parameters of three-core power cables with common earth screen”, *IET Science on Measurement and Technology*, Vol. 4, No. 3, pp. 145-155, August 2008.
- [68] Clayton R. Paul: “Inductance: Loop and Partial”, New Jersey: wiley, 2010, pp. 126-130
- [69] A.G. Heaton: “Transients response of cross bonded cable systems”, *Proceedings IEE*, Vol. 117, No. 3, March 1970.
- [70] L.F. Blume, A. Boyajian, G. Camilli, T.C. Lennox, S. Minneci and V.M. Montsinger: “Transformer Engineering”, Chapter 17, second edition. John Wiley & Sons, 1951
- [71] M. Popov, L. van der Sluis, G.C. Paap, H. de Herdt (2003). “Computation of Very Fast Transient Overvoltages in Transformer Winding”, *IEEE, Transactions on power delivery*, Vol.18, No. 4, 1268 – 1274

- [72] M. Popov, L. van der Sluis, R.P.P. Smeets, J. Lopez Roldan (2007). "Analysis of Very Fast Transients in Layer-Type Transformer Windings", *IEEE, Transactions on power delivery*, Vol. 22, No. 1, 238-247
- [73] Mietek T. Glinkowski, Moises R. Guterrez, Dieter Braun: "Voltage Escalation and Reignition Behaviour of Vacuum Generator Circuit Breaker During Load Shedding."
- [74] G.P. Slade: "Vacuum Interrupters: The New Technology for Switching and Protecting Distribution Circuits", *IEEE Trans. On Power Delivery*, vol 8, No 4.
- [75] O. Karlén: "Vacuum Circuit Breaker model in PSCAD/EMTDC".
- [76] Z. Ma: "An Investigation Of Transient Overvoltage Generation when Switching High Voltage Shunt Reactors by SF6 Circuit Breaker", *IEEE Trans. on Power Delivery*, Vol. 13, No. 2, April 1988, pp 472-479
- [77] M. Popov: "Power System Grounding", Delft University of Technology, Power systems laboratory.
- [78] René Smeets, Lou van der Sluis, Mirsad Kapetanović, David Peelo, Anton Janssen: "Switching in Electrical Transmission and Distribution Systems", John Wiley & Sons, Ltd, 2015
- [79] P. Chowdhuri: "Electromagnetic Transients in Power Systems", John Wiley & Sons Inc., 1996
- [80] L. Colla, F.M. Gatta, A. Geri, S. Lauria: "Lightning Overvoltages in HV-EHV "Mixed" Overhead-Cable Lines", *IPST Lyon, France*, June 2007.
- [81] A. Geri, F.M. Gatta, S. Lauria and L. Colla: "Lightning performance of long mixed overhead-cable EHV lines", in *Proc. 28th International Conference on Lightning Protection (ICLP 2006)*, Kanazawa, Japan, September 2006.
- [82] F.M. Gatta, A. Geri and S. Lauria: "Simulation of lightning response of a long mixed overhead-cable EHV line", in *Proc. International Conference on Grounding and Earthing (GROUND'2006)*, Maceio, Brazil, 2006.
- [83] D. Kind, K. Feser: "Hochspannungs-Versuchstechnik", Friedr. Vieweg&Sohn Verlagsgesellschaft mbH, Braunschweig/Wiesbaden, 1995, ISBN 3-528-43805-3
- [84] O. Hevia: "Sources of Type Impulse in the ATP", *European EMPT User Group (EEUG) News*, November 1998.

- [85] M. Popov: "Switching Three-Phase Distribution Transformers with a Vacuum Circuit Breaker", PhD Thesis, Delft University of Technology, The Netherlands, November 2002.
- [86] TRIDELTA Überspannungsableiter GmbH: Prospectus no. 1387 e/d Hermsdorf, Germany.
- [87] M. Popov, L. van der Sluis: G. C. Paap: "Investigation of the Circuit Breaker Reignition Overvoltages Caused by No-load Transformer Switching Surges", *European Transactions on Electric Power (ETEP)*, Vol. 11, No. 6, November/December 2001, pp. 413-421.
- [88] L.V. Bewley: "Traveling Waves on Transmission Systems", second edition, Dover Publications, New York, 1951
- [89] Cigre Working Group 01: "Guide to procedures for estimating the lightning performance of transmission lines", October 2001
- [90] U.S. Gudmundsdottir and et. al., "Field test and simulation of a 400 kV cross bonded cable system", *IEEE Transactions on Power Delivery*.
- [91] K.N. Md Hasan, K. Rauma, A. Luna, J. Ignacio Candela and P. Rodriquez: "Harmonic Resonance Study for Wind Power Plant", Technical University of Catalonia, C/Colom 1 0822, Terrassa, Spain
- [92] Modeling and Simulation Of The Propagation Of Harmonics in Electric Power Networks, Part I: "Concepts, Models and Simulation Techniques, Task Force on Harmonics Modeling and Simulation", *IEEE Transactions on Power Delivery*, Vol.11, No. 1, January 1996
- [93] S. Mark Halpin, Paulo F. Ribeiro and J.J. Dai: "Frequency-Domain Harmonic Analysis Methods", [http://www.calvin.edu/~pribeiro/IEEE/ieee\\_cd/chapters/pdf/c6pdf.pdf](http://www.calvin.edu/~pribeiro/IEEE/ieee_cd/chapters/pdf/c6pdf.pdf), 2007
- [94] W. Xu, Z. Huang, Y. Cui and H. Wang: "Harmonic Resonance Mode Analysis", *IEEE transactions on Power Delivery*, vol. 20, no. 2, April 2005
- [95] G. Hoogendorp, M. Popov and L. van der Sluis: Application of hybrid modeling for calculation of interturn voltages in transformer windings, *IEEE Transaction on Power Delivery*, Vol. 24, No. 3, pp. 1742-1744, July 2009.

# ACKNOWLEDGMENT

After finalizing this thesis, I would like to thank many people, as this work would not have been finished without the effort and cooperation of many people around me. First off all, I want to thank my promotor prof.ir. Lou van der Sluis for offering me the opportunity to apply for a PhD project, after my Master of Science graduation. Special thanks to my co-promotor and daily supervisor dr.ir. Marjan Popov. Without the daily discussions I had with them regarding the progress of the work and the direction of the project, the work would not have reached the final stage.

Special thanks to the colleagues from TenneT, in particular to ir. Jan de Jong, for his technical guidance during the project and the regular progress meetings and the valuable feedback during the informal meetings we had. Furthermore, I want to thank dr. Robert Kuik, for managing the Randstad 380 kV project and organizing and chairing the valuable regularly progress meetings. I want to thank Nela Nenadovic and Jorrit Bos for their guidance and their help during the steady state modeling work for the 380 kV grid.

I want to thank drs. ir. Robert van Amerongen, for his guidance during the prior stage of the project and his fruitful advises and interest in the project with respect to the load flow studies and contingency analysis.

Furthermore, my thanks goes to the colleagues from KEMA: prof.dr.ir. Fred Steennis, for chairing the measurement campaign and his fruitful advices and recommendations during the last stage of my project when the fields measurements on the 380 kV cable system were performed. I would also like to thank ir. André Cuppen for his guidance during the field measurements.

Special thanks to my former office made and friend Freek Baalbergen, for the fruitful talks and discussions during our PhD projects. Also thank's to my new office made Romain Thomas for his willingness to discuss all kind of problems. I want to thank my colleague and former neighbor for the nice talks and dinners we had. Furthermore, I want to thank my colleagues from TU/e Lei Wu and Jos de Regt for the fruitful discussions regarding cable modeling issues and their participation during the measurement campaign. Also

thank's to ing. Paul van Nes from the TU Delft high-voltage laboratory, for giving me advises regarding the measurement set-up for doing measurements on the cross-bonding cable in the lab.

Last but not least, I want to thank my girlfriend Xandra, our children Luuk, Remmelt and Milou for their understanding and patience during the weekends and holidays when I had to work on finalizing my thesis.

## **CURRICULUM VITEA**

Gerben Hoogendorp was born on 27<sup>th</sup> of October in 1980, in The Hague, the Netherlands. After finishing the high school, he started the Bachelor course on Electrical Engineering at the Delft University of Technology in September 2002. In 2007, he joined the Power Systems Group for doing his master thesis in the field of transients in power transformer windings. After finishing his master thesis, he started a prior study to the application of 380 kV cables in the Randstad380 kV project, commissioned by TenneT. In June 2009, he received his MSc degree in Electrical Power Engineering from that university.

In November 2009, he started his PhD project in the Power Systems Group at the Delft University of Technology.

From November 2013 to August 2015, he has worked as a teacher/researcher at the Hogeschool van Amsterdam and since September 2015, he is a teacher/researcher in the field of Electrical power Engineering at the Haagse Hogeschool in Delft.

## LIST OF PUBLICATIONS

- [1] G. Hoogendorp, M. Popov and L. van der Sluis: Application of Underground 380 kV AC cables in Power Systems, Young Researchers Symposium, Delft University of Technology, 16-17 April 2012
- [2] G. Hoogendorp, M. Popov, L. van der Sluis: Lightning induced overvoltages in mixed 380 kV line-cable-line connections, IPST 2013: International Conference on Power Systems Transients, Vancouver, Canada, 18-20 July 2013
- [3] J.J. de Regt, G. Hoogendorp, P. Wagenaars, P. Wouters, M. Popov, L. van der Sluis, E.F. Steennis: Cross-bonding cable and box model based on pulse reflection measurements, *IET Science, Measurement and Technology*, pp. 1-8, September 2014.
- [4] G. Hoogendorp, M. Popov, L. van der Sluis: Field Measurements for Model Validation of a new Cross-bonded 380 kV Cable System. This paper will be submitted to the *Transactions on Power Delivery*.